Assessing the composition and timing of Late Quaternary volcanic eruptions in southern South America using tephra layers from lacustrine and peat sequences



Rebecca Elizabeth Smith

St Edmund Hall

Research Laboratory for Archaeology and the History of Art,

University of Oxford

A thesis submitted for the degree of Doctor of Philosophy in Archaeological Science

Trinity Term 2019

Assessing the composition and timing of Late Quaternary volcanic eruptions in southern South America using tephra layers from lacustrine and peat sequences

Rebecca Elizabeth Smith
St. Edmund Hall | D.Phil. in Archaeological Science | Trinity Term 2019

Abstract

Volcanic ash (tephra) deposits from large, explosive events travel great distances and can form visible or invisible (cryptotephra) layers in sedimentary archives. These layers have unique chemical (glass) compositions which are useful for stratigraphic correlations; correlating tephra over wide regions can provide temporal constraints on varying magma chemistry, eruption style, frequency and magnitude. Eruptive behavior has been proposed as partially controlled by ice-unloading at the end of the Last Glacial Maximum, ~18 ka. This thesis aims to compile detailed eruption records from southern South America over the last 80 ka to improve event frequency datasets, facilitate stratigraphic correlations, and enable the evaluation of climatic influences, particularly ice-unloading, on explosive volcanism.

The visible tephra layers of two sedimentary archives, Lago Puyehue (Chile) and Laguna Potrok Aike (Argentina) were examined. Tephra componentry (via microscopy), and geochemical characterisation of glass-shards (via WDS-EPMA major elemental analysis) were used to investigate temporal changes in the frequency and composition of tephra deposits. A reference chemistry database was developed by analysing glass-shards from proximal deposits to produce robust tephrocorrelations. These records provide evidence for numerous eruptions in southern South America over the past 80 ka. The records do not show any systematic changes in eruption composition or frequency over time, suggesting the effect of changing ice loads is limited in this context. These records often have tephra layers that appear to be primary but are actually reworked, with low glass concentrations, rounded minerals, and/or heterogenous glass compositions. This reworking is likely caused by wind, basin morphology, and tephra loading.

Cryptotephra records from three Falkland Islands peat archives were also examined to better understand the dispersal of Andean volcanic deposits. Moreover, extensive age-modelling was undertaken in this thesis to refine the ages of 49 explosive Quaternary eruptions from southern South America. The eruption stratigraphies of particular volcanoes were also modelled using novel Kernel Density Estimates to better constrain temporal variation in frequency and the age-uncertainties.

For everyone who thinks they can't and to all who think that they won't ever be good enough: you can and you already are.

I>AV&;



Osorno volcano from Petrohué Falls

Acknowledgements

My PhD has been fun, horrible, difficult, challenging, enjoyable, exciting and pretty much every other emotion possible. I've been pushed to every edge and stretched in every way. A lot has happened in four years – it seems like a long period of time when you're 22, but it's gone quickly. In four years, great stuff has happened: I've been on a few holidays, I went on fieldwork to Chile and sampled sediment in Germany. I also went to conferences across the globe, had three peer reviewed papers published, got engaged to my best friend, was awarded funding for an insulin pump and continuous blood glucose monitor, *and* completed this thesis on a subject I am passionate about. However, this four years has also been filled with personal difficulties: my Dad nearly died, I was also ill *a lot*, both physically and mentally, and it has been difficult to maintain normality, let alone continuous, productive output at times. However, during all of this, my **family, friends and fiancé, Dan**, have stood by my side and offered their unwavering support. I could not have completed this, let alone continued with life, without them: their belief, encouragement and brilliance can never be underestimated. Thank you. Thank you for everything.

Thank you also to my supervisors, **Dr. Victoria Smith, Dr. Karen Fontijn and Prof. Stefan Wastegård**. As I've said, it's been fun as well as difficult – the PhD is always referred to as being full of highs and lows. But the challenges, or the lows, have always been made easier by my supervisors continued support, be it academic or emotional. My supervisors have put in relentless hours to ensure that this project worked, and always with my best interests at heart – they've always been keen that I not only learn about volcanism and tephra, but that I enjoy it, and ultimately produce the best science possible. I cannot express how much I appreciate their enthusiasm, support and commitment to the project.

Dr. Catalina Gebhardt, Prof. Chuck Stern, Dr. Victoria Cullen, Dr. Richard Staff, Prof. Christopher Bronk Ramsey, Dr. Paul Albert, Prof. Bernd Zolitschka, Prof. David Pyle, Dr. Sebastien Bertrand and **Dr. Christian Ohlendorf** must also be thanked for sharing their experience and in-depth knowledge of subjects ranging from age-modelling to sedimentology; this has been so much appreciated and massively improved my research. This thesis could also not have been completed without the generous collaboration and sharing of samples from **Dr. Gill Plunkett, Dr. Christoph Mayr, Dr. Sebastien Bertrand, Prof. Bradley Singer,** and **Prof. Charles Stern**. Thank you also to **Prof. David Pyle and Dr. Gill Plunkett** for an engaging viva (and of course for reading the work in so much detail)!

I would also like to thank **Dr. Sarah Leung**, the **GP's at 28 Beaumont Street**, and the **NHS** more generally for their support and for making me at the least moderately healthy enough to complete this work! I would also like to thank **Victoria Forth**, **Claudia Azevedo, Diane Baker** and **Barbara Morris** for their administrative support.

Finally, I must thank the many funding bodies that have made this research possible. The **Natural Environment Research Council** (NERC) funded this research and training through the **Doctoral Training Partnership grant: NE/L002621/1.** I also obtained funding from: **St Edmund Hall** (**Postgraduate College Grant** 2016, 2017, 2019; **50th Anniversary Grant** 2016), **The Walter Gordon Bequest** (for disabled students; 2016), the European Association of Geochemistry (**EAG**), the International Association of Volcanology and Chemistry of the Earth's interior student grant (**IAVECI**; 2017), the Scientific Committee on Antarctic Research student grant (**SCAR; AntVolc subgroup**; 2018), and the International Union for Quaternary Research student grant (**INQUA**; 2019).

Acronyms

Ant	Antillanca (volcanic complex)
AP	Alpehue Pumice
AVZ	Austral Volcanic Zone
BA	Back-arc
BSE	Back-scattered electron
CabHuel	Caburgua-Huelemolle
Cha	Chaitén
CLD	Chilean Lake District
CLV	Carrán-Los Venados (volcanic complex)
COR	Corcovado (volcano)
DRE	Dense Rock Equivalent
EC	Event corrected
EDS-SEM	Electron Dispersive Spectroscopy-Scanning Electron Microscopy
EMP	Electron Microprobe
FB	Fox Bay
H	Hudson (volcano)
HUA	Huanquihue (volcanic group)
IRSL	Infrared Stimulated Luminescence
KDE	Kernel Density Estimate
LGM	Last Glacial Maximum
LP	Llaima Pumice
LPA	Laguna Potrok Aike
m-cd	Metres-composite-depth
MAC	Macá (volcano)
MB	Mt Burney (volcano)
MC	Mocho-Choshuenco (volcanic complex)
MCMC	Markov Chain Monte Carlo
MEL	Melimoyu (volcano)
MEN	Mentolat (volcano)
MIC	Michinmahuida (volcano)
NHT	Nahuel Huapi Tephra
NSVZ	Northern Southern Volcanic Zone
OVC	Okataina Volcanic Complex
PBN	Playas-Blanca Negra
PCC	Puyehue-Cordón Caulle (volcanic complex)
PDC	Pyroclastic Density Current
PDF	Probability Density Function
PFPDC	Pampa Frutilla Pyroclastic Density Current
PHP	Poncho Hill Pass
PUII	Lago Puyehue, site 2
Quet	Quetrupillán (volcano)
R	Reclus (volcano)
SC	Stanley Common
SE	Secondary electron
SSVZ	Southern Southern Volcanic Zone
SVZ	Southern Volcanic Zone
TAS	Total Alkali-Silica (diagram)
TSVZ	Transitional Southern Volcanic Zone
TVC	Taupo Volcanic Centre
VEI	Volcanic Explosivity Index
WDS-EMP	Wavelength Dispersive Spectroscopy-Electron Microprobe
YAN	Yanteles (volcano)

Table of contents

Chapter 1: Introduction **1**

1.1. An overview and context 1
1.1.1. The principles of tephrochronology 2
1.1.2. Bayesian age modelling 3

1.2. Research aims and strategy 4

1.3. The Andean volcanic arc: history and context 6
1.3.1. The Southern Volcanic Zone (SVZ; 33-46°) 10
1.3.1.1. Geology 10
1.3.1.2. Tephra preservation and chemical composition 11
1.3.2. The Austral Volcanic Zone (AVZ; 49-55°) 17
1.3.2.1. Geology 17
1.3.2.2. Tephra preservation and chemical composition 17
1.3.3. The Pali Aike Volcanic Field (PAVF) 20

1.4. Regional and local setting 20

1.5. The coupled relationship between deglaciation and volcanic activity 22

1.6. Site Selection 25
1.6.1. Lago Puyehue 27
1.6.2. Laguna Potrok Aike 34
1.6.3. Poncho Hill Pass, Stanley Common, and Fox Bay in the Falkland Islands 40

1.7. Summary 42

Chapter 2: Materials and Methods **44**

2.1. Sediment collection and laboratory treatment 44
2.1.1. Lago Puyehue 44
2.1.2. Laguna Potrok Aike 45

2.2. Tephra preparation and analysis 46
2.2.1. Tephra extraction 47
2.2.1.1. Lago Puyehue 47
2.2.1.2. Laguna Potrok Aike 47
2.2.1.3. Falkland Islands 48
2.2.1.4. Proximal tephra analysis 49
2.2.2. Sieving and isolating tephra 50
2.2.3. The production of resin stubs 51

2.3. Visual analysis of glass-shards and/or minerals 52
2.3.1. Glass-shard abundance 52
2.3.2. Glass-shard morphology and colour 53

2.4. Compositional analysis of tephra 54
2.4.1. Overview of EDS-SEM and WDS-EMPA 54
2.4.2. EDS-SEM theory 54
2.4.3. EDS-SEM operating conditions and methodology 56

2.4.4. Wavelength Dispersive Spectroscopy-Electron Microprobe Analysis (WDS-EMPA) theory 57
2.4.5. WDS-EMP operating conditions and methodology 58
2.5. Distinguishing secondary deposits from primary deposition events 59
2.6. Bayesian age modelling in OxCal 4.3 60
2.6.1. Age-depth (depositional) models in OxCal 4.3 61
2.6.2. Phase models in OxCal 4.3 62
2.6.3. Kernel Density Estimations in OxCal 62
2.6.3.1. Eruptive flux calculations 63
2.6.4. Conditions for OxCal age models used in this thesis 64
2.6.4.1. Lago Puyehue 64
2.6.4.2. Laguna Potrok Aike 65
2.6.4.3. Poncho Hill Pass, Stanley Common, and Fox Bay in the Falkland Islands 65
2.6.4.4. Mocho-Choshuenco 65
2.6.4.5. Okataina Volcanic Complex (OVC) and Taupo Volcanic Centre (TVC) 66
2.6.4.6. Mount Mazama and the Crater Lake Region 66
2.6.4.7. Regional Age Model 67
Chapter 3: Investigating the tephra record of Lago Puyehue, Chilean Lake District 68
3.1. Introduction 69
3.2. Age-depth model for Lago Puyehue 72
3.2.1. Sensitivity analysis of Model 2 73
3.2.1.1. Additional dates 73
3.2.1.2. Event correction 74
3.2.1.3. Outlier modelling 75
3.2.1.4. Radiocarbon offsets 76
3.2.1.5. Age-depth model selection 76
3.3. The tephrostratigraphy of Lago Puyehue 81
3.3.1. The frequency of eruptive deposits in Lago Puyehue 90
3.4. The chemical composition of tephra deposits identified in the Lago Puyehue sedimentary sequence 93
3.4.1. Contamination 94
3.4.2. Heterogeneous deposits in Lago Puyehue 96
3.4.3. Llaima volcano (38°41’ S; 71°43’ W) 100
3.4.4. Caburgua-Huelemolle (39°15’ S; 71°42’ W) 101
3.4.5. Puyehue-Cordón Caulle (40°35’ S; 72°07’ W) 103
3.4.6. Calbuco (41°19’ S; 72°37’ W) 104
3.4.7. Chaitén (42°49’ S; 72°38’ W) 106
3.5. Regional marker horizons 106
3.5.1. Regional marker horizons in the Lago Puyehue sedimentary record 106
3.6. Temporal variation in the composition and frequency of volcanic units identified in the Lago Puyehue sedimentary record 113
3.7. Conclusions 118

Chapter 4: Developing a better understanding of past eruptive frequency through the application of Kernel Density Estimations in OxCal 120

4.1. Introduction 121
4.1.1. KDE statistical analysis 123

4.2. Case studies: the application of KDE in OxCal and its relevance and importance to volcanology and tephrochronology 124
4.2.1. Lago Puyehue and Mocho-Choschuenco, southern South America 124
4.2.1.1. An overview of activity in southern South America 125
4.2.1.2. The Lago Puyehue and Mocho-Choschuenco record and background 126
4.2.1.3. Interpretation of Lago Puyehue and Mocho-Choshuenco KDE and its usefulness 127
4.2.2. Taupo Volcanic Centre and Okataina Volcanic Complex, New Zealand 130
4.2.2.1. An overview of activity in New Zealand 130
4.2.2.2. Records of TVC and OVC volcanism from Kaipo Bog and terrestrial outcrops 131
4.2.2.3. Interpretation of TVC and OVC KDE and its usefulness 133
4.2.3. Mount Mazama and the Crater Lake region, Oregon, USA 135
4.2.3.1. An overview of activity in the Mount Mazama and Crater Lake region 135
4.2.3.2. Records of volcanism from terrestrial outcrops in Mount Mazama and the Crater Lake region 136
4.2.3.3. Interpretation of the Mount Mazama and Crater Lake KDE and its usefulness 136

4.3. Discussion and Conclusions 138

Chapter 5: Refining the Late Quaternary tephrochronology for southern South America using the Laguna Potrok Aike sedimentary record 141

5.1. Introduction 142
5.1.1. Records of volcanism in southernmost South America 143
5.1.2. Laguna Potrok Aike and previous tephra work 146

5.2. Results 147
5.2.1. Glass chemical composition of proximal deposits 147
5.2.1.1. Hudson 149
5.2.1.2. Mt Burney 150
5.2.1.3. Reclus 151
5.2.1.4. Lautaro/Viedma 151
5.2.1.5. Aguilera 152
5.2.2. Tephra units from Laguna Potrok Aike and their glass chemical composition 152
5.2.2.1. Group 1 tephra 156
5.2.2.2. Group 2 tephra 158
5.2.2.3. Group 3 tephra 158
5.2.2.4. Group 4 tephra 159

5.3. Interpretation and discussion 160
5.3.1. Chemical fingerprints and tephra correlations 160
5.3.1.1. Hudson volcano 161
5.3.1.2. Mt Burney 162
5.3.1.3. Reclus and NAVZ centres 165
5.3.2. Temporal changes in volcanic activity 168
5.3.3. Reworking of tephra deposits 171
5.3.4. Changes in eruptive activity in relation to climate 176

5.4. Conclusions 178

Chapter 6: Distal cryptotephra from southern South America in the Falkland Islands 180

6.1. Introduction 181
6.1.1. Site Background 184
6.1.2. Chronological constraints 186

6.2. Results and interpretation 186
6.2.1. Geochemical results and interpretation 186
6.2.1.1. Poncho Hill Pass 188
6.2.1.1.1. 18-20 cm 188
6.2.1.1.2. 20-25 cm 189
6.2.1.1.3. 82-83 cm 189
6.2.1.2. Stanley Common 190
6.2.1.2.1. 17-19 cm 192
6.2.1.2.2. 20-21 cm 192
6.2.1.2.3. 24-27 cm 192
6.2.1.2.4. 73-74 cm 193
6.2.1.2.5. 90-92 cm 193
6.2.1.2.6. 98-100 cm 193
6.2.1.3. Fox Bay 194
6.2.1.3.1. 30-35 cm 195
6.2.1.3.2. 60-65 cm 196
6.2.2. Chronology of Stanley Common 196

6.3. Discussion 198
6.3.1. Primary tephra layers 199
6.3.2. Tephra remobilisation 200
6.3.2.1. Site-specific taphonomy 200
6.3.2.2. Aeolian reworking 202
6.3.2.3. Alternative explanations 203

6.4. Conclusions 205

Chapter 7: Refining the age of large, explosive volcanic events in southern South America: development of southern South America's tephrochronological model using Bayesian age modelling 207

7.1. Introduction 208

7.2. Methodological background 211

7.3. Results and discussion 218
7.3.1. Eruptive dates from the Central-Southern SVZ 218
7.3.2. Eruptive dates from the southernmost SSVZ 222
7.3.3. Eruptive dates from the AVZ 225
7.3.4. Expansion of the tephrochronology 232

7.4. Conclusions 237

Chapter 8: Discussion and summary 238

8.1. Discussion 238
8.1.1. Aim 1: Identify widespread isochronous markers 238

8.1.2. Aim 2: Determine whether there is a relationship between eruption frequency and/or magma composition through time 243
8.1.3. Aim 3: Develop a well-defined chronicle of explosive events 245
8.2. Summary 247

Bibliography **250**

List of figures

Chapter 1: Introduction **1**

1.1. Map of southern South America, including different volcanic zones 7
1.2. Ash dispersal map of widespread units identified in the Chilean Lake District 12
1.3. Total Alkali versus Silica diagram of volcanic deposits from the Southern Volcanic Zone 14
1.4. Felsic enclave in mafic bomb identified at Casablanca volcano, Antillanca volcanic complex 14
1.5. Regional tephrochronology from Fontijn et al (2016) 16
1.6. Glass compositions of tephra deposits from volcanoes in the Austral Volcanic Zone 19
1.7. Summary of the explosive history from Mocho-Choshuenco since deglaciation 24
1.8. Map of Lago Puyehue, Chilean Lake District 28
1.9. Age-depth model for the sediments of Lago Puyehue 30
1.10. Schematic diagram of Lago Puyehue sedimentary sequence 31
1.11. Illustration of Lago Puyehue and nearby volcanoes 33
1.12. Map of Laguna Potrok Aike 35
1.13. Schematic diagram of Laguna Potrok Aike sedimentary sequence 37
1.14. Age-depth model for the sediments of Laguna Potrok Aike 39
1.15. Map of Falkland Islands 42

Chapter 2: Materials and Methods **44**

2.1. Illustration of the preparation and procedure for mounting visible tephra samples 52
2.2. Semi-quantitative abundances (in percent) of material 53
2.3. Schematic representation/classification guide of tephra/mineral componentry 53
2.4. Schematic diagram illustrating typical EDS-SEM system 56
2.5. Schematic diagram illustrating a typical WDS-EMPA system 57

Chapter 3: Investigating the tephra record of Lago Puyehue, Chilean Lake District **68**

3.1. OxCal age-depth model (Model 2D) for Lago Puyehue sedimentary sequence 78
3.2. Tephra deposits identified in the Lago Puyehue sedimentary sequence 82
3.3. Schematic diagram of Lago Puyehue sedimentary sequence listing tephrocorrelations 83
3.4. Photographs of tephra morphologies preserved in Lago Puyehue sedimentary sequence 85
3.5. Tephrostratigraphy illustrating tephra horizons identified in Lago Puyehue 92
3.6. Frequency histogram representing number of volcanic deposits preserved in the Lago Puyehue sedimentary sequence 93
3.7. BSE images of basaltic andesite shards with microphenocrysts identified from Lago Puyhue 95
3.8. Tephra chemistry of layers which have indiscriminate chemical composition and likely from nearby centres 99
3.9. Tephra chemistry of PUII_445 101

3.10. Tephra chemistry of PUII_851, PUII_1078 and PUII_1117 102
3.11. Tephra chemistry of layers most likely associated with Puyehue-Cordón Caulle volcanism 104
3.12. Tephra chemistry of PUII_130 and PUII_899 105
3.13. Tephra chemistry of layers identified as correlatable to regional marker horizons 108
3.14. Temporal variability in tephra chemistry and frequency of tephra deposits identified from the Lago Puyehue sedimentary sequence 115

Chapter 4: Developing a better understanding of past eruptive frequency through the application of Kernel Density Estimations in OxCal 120

4.1. *KDE_Plots* of Lago Puyehue and Mocho-Choshuenco volcanism in association with climatological variations (δ18O) 129
4.2. Map of central and northern North Island, New Zealand 131
4.3. Volumes and ages of TVC and OVC highly-silicic-only volcanism 133
4.4. *KDE_Plots* of eruptive deposits from OVC and TVC 134
4.5. *KDE_Plots* of pre-Mazama and Mount Mazama volcanism 137

Chapter 5: Refining the Late Quaternary tephrochronology for southern South America using the Laguna Potrok Aike sedimentary record 141

5.1. Map of southernmost South America 143
5.2. Glass-shard geochemistry from regional marker horizons 148
5.3. Logarithmic scale of tephra thicknesses 154
5.4. Variation diagrams of glass-chemical data for tephra identified in the Laguna Potrok Aike sedimentary sequene 155
5.5. Variation diagrams of glass-chemical data for tephra deposited via primary ash-fall 161
5.6. Illustration of reworked tephra deposits in the Laguna Potrok Aike sedimentary sequence 172
5.7. Images of volcaniclastic deposits illustrating diagnostic features of primary and reworked tephra in the Laguna Potrok Aike sedimentary sequence 173
5.8. Plenary diagram for tephra changes in tephra chemistry in deposits identified in the Laguna Potrok Aike sedimentary sequence 177

Chapter 6: Distal cryptotephra from southern South America in the Falkland Islands 180

6.1. Schematic illustration of cryptic glass-shard distribution profiles 182
6.2. Distribution of volcanic glass-shards in three peat bog localities in the Falkland Islands 185
6.3. Chemical data for Andean volcanic centres and glass-shards from sites investigated in the Falkland Islands 187
6.4. Age-depth model for Stanley Common 197

Chapter 7: Refining the age of large, explosive volcanic events in southern South America: development of southern South America's tephrochronological model using Bayesian age modelling **207**

7.1. Schematic showing criteria of acceptance for transferring ages of tephra into other sequences for age modelling 212
7.2. Map of southern South America and extra-Andean Islands 218
7.3. Schematic illustration of the synchronicity between archives of widespread tephra deposits in southern Chile, Argentina, the Falkland Islands and the South Georgia Islands 236

List of tables

Chapter 1: Introduction **1**

1.1. List of volcanic centres in southern South America (Chile and Argentina) 8
1.2. Already established correlations to widespread tephra layers identified in the Laguna Potrok Aike sedimentary sequence 40

Chapter 2: Materials and Methods **44**

2.1. Widespread (proximal) tephra samples from the Austral Volcanic Zone 49

Chapter 3: Investigating the tephra record of Lago Puyehue, Chilean Lake District **68**

3.1. Comparison between age model inputs 73
3.2. Table of radiocarbon data for selected OxCal (2D) and CLAM 2.2 age-depth model (1) 79
3.3. Dates for regional marker horizons identified in Model 1, 2D and the literature 80
3.4. Description of all tephra deposits identified in the Lago Puyehue sedimentary sequence 86
3.5. Glass-shard geochemistry of tephra identified at 804 cm depth 95
3.6. Glass-shard geochemistry of PUII_81 (Mil Hojas) 109
3.7. Glass-shard geochemistry of PUII_226.2 (PCC4) 110
3.8. Glass-shard geochemistry of PUII_632.7 (Cha1) 111
3.9. Glass-shard geochemistry of PUII_1036.5 (PCC1) 112

Chapter 5: Refining the Late Quaternary tephrochronology for southern South America using the Laguna Potrok Aike sedimentary record **141**

5.1. Glass-shard geochemistry of widespread eruptive deposits 150
5.2. Glass-shard geochemistry of different groups of tephra identified in the Laguna Potrok Aike sedimentary sequence 157
5.3. Glass-shard geochemistry for primary tephra layers identified in the Laguna Potrok sedimentary sequence 163

Chapter 6: Distal cryptotephra from southern South America in the Falkland Islands **180**

6.1. Glass-shard geochemistry of cryptotephra deposits identified in Poncho Hill Pass 188
6.2. Glass-shard geochemistry of cryptotephra deposits identified in Stanley Common 191
6.3. Glass-shard geochemistry of cryptotephra deposits identified in Fox Bay 195
6.4. Calibrated ages for Stanley Common age-depth model 197

Chapter 7: Refining the age of large, explosive volcanic events in southern South America: development of southern South America's tephrochronological model using Bayesian age modelling 207

7.1. Table showing which widespread tephra units, from what sequences, were included in age models 214
7.2. New modelled ages of widespread marker horizons identified in the SVZ and AVZ, ordered by median age 228

Chapter 1
Introduction

1.1. An overview and context

Volcanic eruptions can cause disruption to society and economy, and can additionally cause loss of life (Brown et al., 2017; Oppenheimer et al., 2003; Wisner et al., 2003). With population growth, the risks associated with eruptive activity increases. To better understand these threats we must obtain detailed records of past volcanic behaviour, including eruptive frequency and the controlling mechanisms of volcanism. Typically, the impacts from large explosive events (i.e., Volcanic Explosivity Index >5; VEI; Newhall and Self, 1985) are more widespread and extensive than those from effusive events, such as lava flows, or dome-forming events (e.g., Brown et al., 2017; Cassidy et al., 2018).

Volcanic ash (tephra) from large explosive events is able to travel over great distances and subsequently form either visible or crypto-tephra (ash that is not visible to the naked eye) layers in terrestrial outcrops, sedimentary archives (e.g., peat bogs, marine and lacustrine cores) and ice cores. Fingerprinting common layers through the use of glass-shard geochemistry (e.g., Shane, 2000) may enable stratigraphic correlations between a number of archives (e.g., Bronk Ramsey et al., 2015). These correlations can help constrain the chronology of archives through the use of relative and absolute dating, as well as provide temporal constraints on variations in magma chemistry, and the eruption style, frequency and magnitude which may or may not be controlled by external forcings, such as deglaciation (e.g., Fontijn et al., 2016; Rawson et al., 2016; Kutterolf et al., 2019).

Tephra deposits in lake and peat environments with high accumulation rates provide detailed records of volcanism. These deposits can not only provide data including grain size and deposit thickness which details information on past volcanism, but they are also less prone to erosion than their terrestrial counterparts (e.g., outcrops). The most complete reconstruction of

past volcanic activity is often formed when records of volcanism from terrestrial outcrops and sedimentary archives are combined (e.g., Fontijn et al., 2016; Albert et al., 2018).

1.1.1. The principles of tephrochronology

This thesis utilises tephrochronology to produce correlations, and hence the principles are here explained. Tephra is a term for unconsolidated, fragmented, volcanic ejecta, and deposits are composed of minerals, crystals and glass. The unique characteristics of the layer (e.g., glass composition) may enable the production of isochronous horizons across archives in which it is found, including sediment sequences (marine, lacustrine, peat bogs), terrestrial outcrops, and/or ice cores, when robust chemical fingerprints are able to be established. This is principally because the glass chemical composition of tephra deposits reflect the composition of the melt at the time of the volcanic eruption, and this is typically unique, and thus provides a chemical fingerprint (e.g., Thorarinsson et al., 1959). The composition of the glass is invaluable to identifying chronostratigraphic markers in archives.

The collective term for identifying, correlating, and using tephra layers to improve dating of Quaternary sedimentary archives is: tephrochronology. Tephrochronology rests on the principle that tephra layers are the result of direct atmospheric fallout immediately after a volcanic eruption. Tephra fallout occurs geologically instantaneously, producing isochrons on extremely short time scales (e.g. a few days), despite the vast distances that it travels; the eruptive column of explosive eruptions can reach several tens of kilometers, and the volcanic ash can also travel hundreds-thousands of kilometres (Bursik, 1998; Woods, 1998). To exemplify, the ash veil from the VEI ≤5 Puyehue-Cordón Caulle eruption in Chile circumnavigated the Earth, impacting aviation in Australia. In addition, tephra horizons in eastern North America have been sourced to Alaska and the Pacific northwest (Rose and Durant, 2011; Pyne-O'Donnell et al., 2012; Klüser et al., 2013), and the VEI 7 Campanian Ignimbrite deposit from Italy has deposited tephra across much of Eastern Europe and the central Eastern Mediterranean Sea, with ultra-distal tephra identified >1500 km from the vent (Pyle et al., 2006). Tephra is particularly useful as it can be

utilised for relative dating, whereby the date of a tephra in one archive allows the numerical age to be transferred to other sites (Wagner, 1998). In some cases, it can also be used for absolute dating, whereby the deposit is directly dated (e.g., K/Ar and $^{39}Ar/^{40}Ar$ dating; Bacon and Lanphere, 2006; Mark, 2011).

Tephrochronology is a powerful tool and is frequently used in many disciplines, including, for example, archaeology (e.g., Lowe et al., 2012), palaeoecology (e.g., Langdon and Barber, 2004) and volcanology (e.g., Dugmore, 1989). In the case of archaeology, it can be highly valuable to constrain the age of the archive in which it is found; this can be useful to better refine the timing of cultural changes (e.g., Machida et al., 1982; Bolender et al., 2011). In the case of volcanology, it contributes vastly to understanding changes in the magnitude and frequency of eruptions through time, compositional changes, and assessing the robustness of the age data (e.g., Gerlach et al., 1988; Lowe, 2011; Rawson et al., 2016; Fontijn et al., 2016; Albert et al., 2018).

1.1.2. Bayesian age modelling

Bayesian age modelling is relied on heavily throughout this thesis and therefore background information is supplied here. Robust age models can be developed using Bayesian statistics (i.e., probability expressed as a degree of belief in the occurrence of event), and these allow archaeologists to fully investigate both relative and absolute chronological information – this is something that frequentist statistics (i.e., probability expressed as the limit of its relative frequency in a large number of trials) cannot achieve (Buck and Juarez, 2017). Bayesian models utilise all information available, and can additionally adapt as new information is supplied; the model outputs express the likelihood that any one sample has a particular age which is called a probability density function (PDF; Bronk Ramsey et al., 2009a).

Within archaeology, Bayesian statistics are used mostly to combine scientific (absolute) dates with relative or absolute prior knowledge, such as stratigraphic information (i.e., the sequential or absolute depth of a tephra identified in a sequence; Buck and Juarez, 2017). This relative information is referred to as the Prior, while the calendar date information is expressed

as the likelihood (Bronk Ramsey, 2009a). Used in this way, Bayesian statistics can constrain the chronology of the archive being investigated.

Age-modelling is often used to constrain the timing of volcanic events (e.g., Bronk Ramsey et al., 2015; Rawson et al., 2015; McLean et al., 2016) as most likely eruptive dates can be derived from well-constrained age-models. This technique has been used in the Chilean Lake District (CLD) to refine the timing and sequence of eruptive events in the form of a tephrostratigraphy (Fontijn et al., 2016). High chronological precision of both archives and tephra deposits is sought because it is useful for the production of robust comparisons between different Late Quaternary stratigraphical proxy records. For example, a study by Lane et al. (2013) identified time-transgressive climate shifts in Europe by correlating high-temporal resolution sedimentary archives, Meerfelder Maar and Kråkenes, using the Vedde tephra layer from Icelandic volcano, Katla.

Many Bayesian age-modelling packages are available, such as OxCal (Bronk Ramsey, 2009a), Bacon (Blaauw and Christen, 2011), Bchron (Haslett and Parnell, 2008) and CLAM (Blaauw, 2010), and all can i) calibrate radiocarbon dates, and ii) be used to constrain the timing of events. Now, Kernel Density Estimations (KDE) which allow visualisation of the shape of data can also be applied to age models in OxCal; this well-used statistical method is novel when used in OxCal since it allows estimations of PDF's while accounting for the age-uncertainties of the age-data, and this could be useful to look at volcanic event-frequency (Chapters 2, 4).

1.2. Research aims and strategy

This thesis predominantly aims to develop a more comprehensive understanding of past volcanic activity in southern South America by analyzing the compositions and timing of deposits. It furthermore sets out to evaluate this data and determine whether post-deglacial ice unloading influences volcanic behaviour in continental arcs.

The overall aims and objectives of this thesis are:

1. Identify which are the widespread isochronous markers that can assist future stratigraphic correlations across wide geographic distances, including for example, proximal volcanic stratigraphies, and extra-Andean archives. These will be invaluable for palaeoenvironmental studies.
    - Laguna Potrok Aike and Lago Puyehue will be sampled for visible tephra. The frequency of deposits will be catalogued and glass chemical compositions and tephra componentry will be used to correlate the tephra to other units that are documented in the published literature; where there is insufficient glass-chemistry in existence for known units, the glass chemical compositions will be established on proximal deposits. These findings will be integrated into the existing regional framework. Extra-Andean chemical comparisons will be attempted using cryptic tephra deposits identified in Falkland Islands: Stanley Common, Poncho Hill Pass, and Fox Bay.

2. Analyse whether there is a relationship between eruption frequency and/or magma composition through time using the detailed eruption records of Lago Puyehue and Laguna Potrok Aike in addition to KDE analysis of different resolution records across the globe.
    - An analysis of the literature will be undertaken to establish regional and local changes in climate. Thereafter, compositional and temporal trends in the frequency of volcanic eruptions, will be evaluated against climatological changes. The novel application of KDE in OxCal may prove useful to analyse the timing of volcanic deposits while also representing the age-uncertainty of units.

3. Provide a well-refined chronicle of explosive eruptions that will improve upon the existing knowledge (e.g., frequency of events and distribution of ashfall) of the regional volcanic history of southern South America. In doing so, we attempt to extend and refine the existing southern South American tephrostratigraphic framework (see Fontijn et al., 2016).

- The ages of widespread tephra layers will be modelled to determine the most refined age possible.

1.3. The Andean volcanic arc: history and context

Volcanism in the Andean Cordillera, a >7,500 km continuous mountain chain, is the result of plate convergence in the western margin of South America. There are four separate segments in the Andean volcanic arc system: the Northern Volcanic Zone (5°N-2°S), Central Volcanic Zone (14-27°S), Southern Volcanic Zone (SVZ; 33-47°S), and the Austral Volcanic Zone (AVZ; 49-55°S; Stern, 2004). Within this Andean volcanic arc system as a whole, there are >200 Quaternary volcanoes which are potentially active (Stern, 2004). This thesis focuses on the SVZ and the AVZ (Figure 1.1), as within this region, there have been numerous eruptions during the Late Quaternary (Table 1.1).

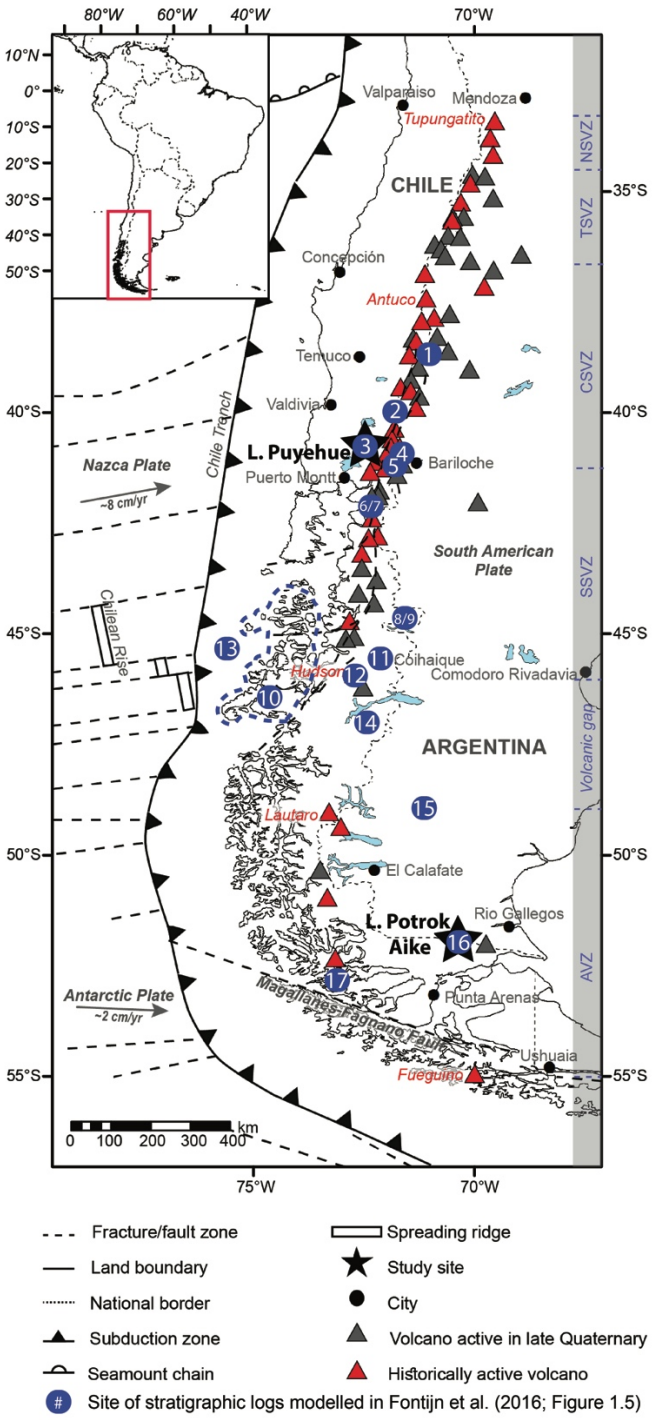


Figure 1.1. Site map demonstrating regional features, tectonic plates, boundaries and volcanoes, as well as sub-sections for the Southern Volcanic Zone (i.e., Northern SVZ (NSVZ; 33-34.5°S), Transitional SVZ (TSVZ; 34.5-37°S), Central SVZ (CSVZ; 37-41.5°S), Southern SVZ (SSVZ; 41.5-46°S)), the volcanic gap (46-49°S), and the Austral Volcanic Zone (AVZ; 49-55°S) (as per Stern, 2004). Selected towns and study sites are additionally highlighted. Blue circles represent sites that were modelled for the regional tephrochronology in Fontijn et al. (2016; Figure 1.5); 1=Icalma; 2=Mocho-Choshuenco; 3=L. Puyehue; 4=El Treból; 5=Hualaihue; 6=L. Teo; 7=Chaitén-Michinmahudia; 8=L. Shaman; 9=L. Embudo; 10=Chonos-Taitao peninsula; 11=Coyhaique; 12=Hudson; 13=MD07-3088; 14=Cochrane; 15=Cardiel; 16=Potrok Aike; 17=Lago Chandler; L.=Lago. Geographical data is obtained from Natural Earth (naturalearthdata.com).

Table 1.1. List of volcanic centres in southern South America (Chile and Argentina). This demonstrates both Holocene and Quaternary volcanism. Table modified after Siebert et al. (2010) and Fontijn et al. (2014). *Viedma is not yet confirmed as a volcano (cf. Blampied et al., 2012; Suarez et al. 2019).

Volcano	Latitude ºS	Longitude ºW	Elevation	Last activity (year AD)	Known large eruptions (VEI/M >5)
Northern Southern Volcanic Zone					
Tupungatito	33.4	69.8	6000	1987	
San José	33.78	69.9	5856	1960	
Maipo	34.16	69.83	5264	1912	
Transitional Southern Volcanic Zone					
Palomo	34.61	70.3	4860	Holocene	
Caldera del Atuel	34.65	70.05	5189	Holocene	
Tinguiririca	34.81	70.35	4280	1994	
Infiernillo	35.14	69.83	2045	Holocene	
Planchón-Peteroa	35.24	70.57	4107	2010	
Calabozos	35.56	70.5	3508	Holocene	
Descabezado Grande	35.58	70.75	3953	1933	
Cerro Azul	35.65	70.76	3788	1967	1932
San Pedro-Pellado	35.99	70.85	3621	Holocene	
Laguna del Maule	36.02	70.58	3092	Holocene	
Nevado de Longaví	36.19	71.16	3242	Holocene	
Lomas Blancas	36.29	71.01	2268	Holocene	
Payun Matru	36.42	69.2	3680	Holocene	
Resago	36.45	70.92	1890	Holocene	
Cochiquito Volcanic Field	36.77	69.82	1435	Holocene	
Nevados de Chillán	36.86	71.38	3212	2018	
Central Southern Volcanic Zone					
Tromen	37.14	70.03	3978	1822	
Antuco	37.41	71.35	2979	1869	
Copahue	37.85	71.17	2997	2013	
Callaqui	37.92	71.45	3164	1980	
Laguna Mariñaqui	38.27	71.1	2143	Holocene	
Tolguaca	38.31	71.64	2806	Holocene	
Lonquimay	38.38	71.58	2865	1990	
Llaima	38.69	71.73	3125	2009	Llaima Pumice; Curacautín 1,2
Sollipulli	38.97	71.52	2282	1240	Alpehué Pumice
Laguna Blanca	39.02	70.37	1700	Holocene	
Caburgua-Huelemolle	39.25	71.7	1496	Holocene	

Volcano	Latitude ºS	Longitude ºW	Elevation	Last activity (year AD)	Known large eruptions (VEI/M >5)
Villarrica	39.42	71.93	2847	2015	Pucón Ignimbrite; Licán Ignimbrite
Quetrupillan	39.5	71.7	2360	1872	
Lanín	39.63	71.5	3747	Holocene	
Huanquihue Group	39.88	71.58	2139	1750	
Mocho-Choshuenco	39.93	72.03	2422	1937	Pirehueico; Neltume Pumice
Carrán-Los Venados	40.35	72.07	1114	1979	
Puyehue-Cordón Caulle	40.59	72.12	2236	2011	Mil Hojas; Pr2/Pht
Pantoja, Cerro	40.77	71.95	2024	Holocene	
Antillanca Group	40.77	72.15	1990	Holocene	An-A/RA; Nahuel Huapi Tephra
Puntiagudo-Cordón Cenizos	40.97	72.26	2493	1850	
Osorno	41.1	72.49	2652	1869	
Tronador	41.16	71.88	3491	Holocene	
Cayutué-La Viguería	41.25	72.27	506	Holocene	
Calbuco	41.33	72.61	2003	1972	Ca8; Ca1
Cuernos del Diablo	41.4	72	1862	Holocene	
Southern Southern Volcanic Zone					
Yate	41.75	72.4	2187	Holocene	
Hornopirén	41.87	72.43	1572	Holocene	
Apagado	41.88	72.58	1210	Holocene	Ap1
Crater Basalt Volcanic Field	42.02	70.18	1359	Holocene	
Huequi	42.38	72.58	1318	1907	
Minchinmávida	42.79	72.44	2404	1835	MIC1; Amarillo Ignimbrite
Chaitén	42.83	72.65	1122	2010	Cha1; Cha1
Corcovado	43.18	72.8	2300	Holocene (?)	COR3
Yanteles	43.5	72.8	2042	Holocene	YAN1
Palena Volcanic Group	43.78	72.47	1449	Holocene	PalRF
Melimoyu	44.08	72.88	2400	Holocene	MEL1
Puyuhuapi	44.3	72.53	524	Holocene	na
Mentolat	44.7	73.08	1660	1710	MEN1
Cay	45.06	72.98	2090	Holocene	na
Maca	45.1	73.17	2960	Holocene	MAC1
Cerro Hudson	45.9	72.97	1905	2011	1991; H2/T5; H1/T2; Ho
Austral Volcanic Zone					
Lautaro	49.02	73.55	3607	1979	
Viedma*	49.36	73.28	1500	1988	
Aguilera	50.33	73.75	2546	Holocene	A1

Volcano	Latitude ºS	Longitude ºW	Elevation	Last activity (year AD)	Known large eruptions (VEI/M >5)
Reclus	50.96	73.58	1000	1908	R1, R2, R3
Palei-Aike Volcanic Field	52	70	282	Holocene	
Monte Burney	52.33	73.4	1758	1910	MB1, MB2
Fueguino	54.95	70.25	150	1820	

1.3.1. The Southern Volcanic Zone (SVZ; 33-46°)

1.3.1.1. Geology

The SVZ is formed as a result of subduction of the oceanic Nazca plate underneath the continental south American plate. Subduction along this 1,400 km-long continuous arc segment occurs at a rate of approximately 7-9 cm/yr (Stern, 2004). The region has been active for the past 1.1 Ma and there are at least 60 potentially active centres in Chile and Argentina (Stern, 2004). Volcanic features include monogenetic spatter and cinder cones, lava flows, and several large composite volcanoes. Volcanic centres that have been particularly productive or active during the Late Quaternary include Villarrica, Puyehue-Cordón Caulle, and Hudson (Fontijn et al., 2016; Van Daele et al., 2014).

The SVZ is divided into four sub-sections; the northern (33-34°S), transitional (34-37°S), central (37-41.5°S) and southern (SSVZ; 41.5-46°S; Figure 1.1). The CLD is located in the SSVZ at 40-43°S. The Northern-most end of the SVZ coincides with the southern end of the Chile Rise and the subducting Juan Fernández Ridge, while the southernmost end is marked by Hudson volcano (45°45'S; 72°58'W) which rests on the border of the volcanic gap (an area where no Benioff zone or seismic activity exists; Gutiérrez et al., 2005; Stern, 2004). A dextral strike-slip fault termed the Liquiñe-Ofqui Fault Zone runs 1000-1200 km N-S through the southern and central SVZ. This structural feature controls the location of some of the small Holocene monogenetic centres and larger stratovolcanoes that lie in this region (López-Escobar et al., 1995; Stern, 2004).

1.3.1.2. Tephra preservation and chemical composition

Overall, tephra is not well preserved in terrestrial sites in this region as the winds are typically strong and the semi-arid climate means there is sparse vegetation and little soil development, resulting in easily eroded tephra. Even though strong climatic gradients exist in the region, with the west being more wet and the east being more arid, there is limited evidence of variable weathering processes, soil formation or vegetation cover affecting tephra preservation in the region. This is despite the fact that Dugmore et al. (2018) and Cutler et al. (2018), who utilised historical tephra deposits from the 1985 Mount St. Helens eruption in Washington, USA and the 1947 Hekla eruption from Iceland, showed that differences in vegetation cover can alter the thickness of tephra preserved in terrestrial sequences by as much as 36 %, and biocrust formation can additionally stabilise thin (0-10 cm thick) tephra units. Such work is yet to be conducted in the Andes but pre-existing research indicates that in the Andes, even in areas where vegetation is thick and soil accumulation rates are high, the topography tends to be steep which can result in erosion/remobilisation of the tephra (Brown et al., 2014; Fontijn et al., 2014; McNamara et al., 2019).

Despite the difficulties in tephra preservation that exist in the region, the analysis of tephra deposits preserved in lacustrine and terrestrial environments across the SVZ and AVZ has not only informed on the frequency and magnitude of events, but has also enabled reconstructions of the dispersal patterns of large (VEI ≥5) Late Quaternary eruptions (Figure 1.2). While some deposits within the SVZ have a northward dispersal (e.g., Neltume pumice from Mocho-Choshuenco volcano), the majority are heavily influenced by the strong prevailing westerly winds which predominantly carry tephra fallout from eruptions in the SVZ towards the east, across Chile and into the Argentinean Patagonian steppe (e.g., Pucón Ignimbrite fall from Pucon volcano; Figure 1.2; Rawson et al., 2015; Fontijn et al., 2016).

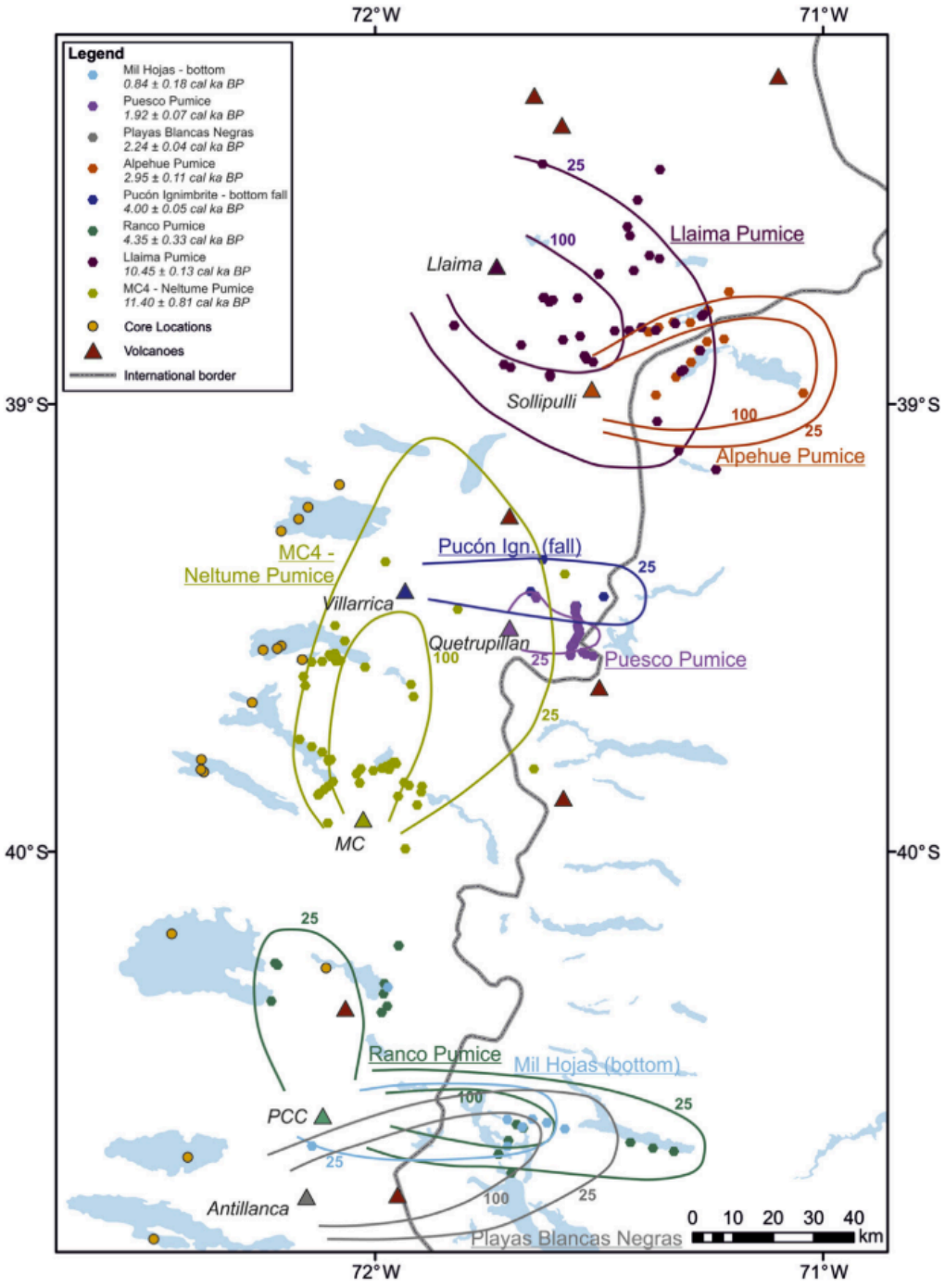


Figure 1.2. Ash dispersal map of widespread units identified in the Chilean Lake District illustrated by 100 and 25 cm isopach contours of largest known eruptions in the last 16.71 ka cal BP, from Fontijn et al. (2016) age model (excludes deposits from non-Chilean Lake District volcanoes, e.g., Cha1 from Chaitén). There is a predominant Eastward dispersal. MC = Mocho-Choschuenco; PCC = Puyehue-Cordón Caulle. Source: Fontijn et al. (2016).

Tephra deposits from volcanoes in the SVZ have a wide range of glass chemical compositions (Figure 1.3), but regionally dispersed deposits are usually dacitic to rhyolitic in composition (e.g., Alpehue pumice from Sollipulli volcano, and Cha1 from Chaitén; Fontijn et

al., 2016). Basaltic-andesitic tephra from this region has also been described (e.g., Pucon Ignimbrite from Villarrica). These mafic products are typically microphenocryst-rich, which makes it difficult to analyse the groundmass glass with standard electron microprobe (EMP) settings (e.g., Fontijn et al., 2016).

Bimodal glass compositions within single eruption deposits have recently been documented in the Andean sector, and are likely more common than currently acknowledged (e.g., Geoffroy et al., 2018). For example, glass from Hudson volcano deposits show a wide range of compositions on an evolutionary trend, from basaltic-andesite through to rhyolite, and the Llaima pumice, from Llaima volcano at 10.34-10.59 cal ka BP, is also compositionally heterogeneous with a dacitic pumice component and an andesitic scoria component (Fontijn et al., 2016). Antillanca has also erupted deposits with heterogeneous chemistries (e.g., NHT/PBN), and volcanic bombs with silicic enclaves have been identified at Casablanca volcano (Antillanca volcanic complex) which are indicative of magma mingling (Figure 1.4).

Bimodal compositions can be a result of magma mingling whereby mafic magma replenishes a felsic reservoir (Sparks et al., 1977); the magma injected is denser than the felsic magma and a stratified system can develop. A density inversion is usually produced as a result of crystallisation which can produce overturning, and this results in the associated mixing or mingling, dependant on the viscosity difference (Sparks et al., 1977; Huppert et al., 1984; Laumonier et al., 2014). Bimodal compositions can also occur as a result of different magma bodies being stored separately (Laumonier et al., 2014). However, most deposits are homogenous (e.g., PCC1 from Puyehue-Cordón Caulle; Fontijn et al., 2016).

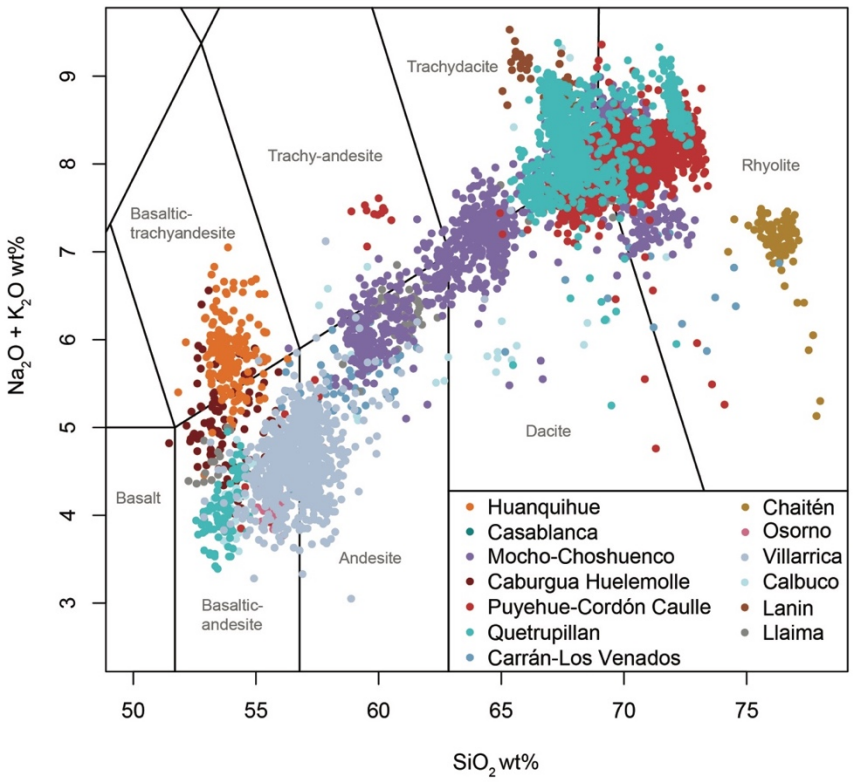


Figure 1.3. Total Alkali versus Silica (TAS) diagram illustrating the glass major element composition of different major volcanic centres in the Southern Volcanic Zone which are known to have had large Late Quaternary eruptions. Each coloured symbol represents an individual analysis; different colours represent different centres/volcanoes (see Key at bottom right of figure; Casablanca is a volcano in the Antillanca volcanic complex; volcanoes in Key can be located on map shown in Figure 1.8; the dispersal patterns of some eruptions can be identified in Figure 1.2; data sourced from Fontijn et al., 2016 and reproduced here).



Figure 1.4. Felsic enclave in mafic bomb identified at Casablanca volcano in the Antillanca volcanic centre. The melts in the bombs are vesiculated and show that they are likely mingled, as opposed to being xenoliths. Eruption unknown.

Fontijn et al. (2016) identified a number of regionally-dispersed tephra units with well constrained chemical compositions and was able to refine the age estimates for these, including for example, the 10.45 ± 0.13 cal ka BP andesitic-dacitic Llaima Pumice from Llaima volcano,

and the 0.84±0.18 cal ka BP rhyodacitic Mil Hojas layer from Puyehue-Cordón Caulle. In Fontijn et al. (2016), tephra correlations were produced in the SVZ and placed within a regional postglacial tephrostratigraphic framework (Figure 1.5); tephra correlations produced include the Mil Hojas tephra from Puyehue Cordón Caulle volcano which is tentatively located in Lago Villarrica (39°15′S; 72°05′W), Lago Calafquen (39°31′S; 72°08′W), Lago Riñihue (39°50′S; 72°17′W), and Lago Puyehue, and the northerly dispersed Cha1 (9.90±0.25 cal ka BP) tephra from Chaitén which is located in Hualaihue, Chaitén-Michinmahuida, and other outcrops across the SSVZ (Naranjo and Stern, 2004; Watt et al., 2011; Amigo et al., 2013; Watt et al., 2013b; Fontijn et al., 2016; Figures 1.1, 1.8). With more work, further tephra correlations could be produced; for example, the Cha1 tephra from Chaitén is speculated to be present in Lago Puyehue and Lago Teo (Fontijn et al., 2016). These correlations could additionally expand the tephrostratigraphic framework beyond the Chilean Lake District. The VEI 5 Alpehue Pumice from Sollipulli volcano at 3.0±0.1 cal ka BP has been correlated to tephra in Laguna Cabeza de Buey (36°29′S; 61°18′W; Tonello, Fontijn et al., unpublished), and sub-Antarctic South Georgia, 3000 km from the original source (54°S, 36°W; Oppedal et al., 2018), demonstrating the potential of correlation on a regional scale far beyond the CLD.

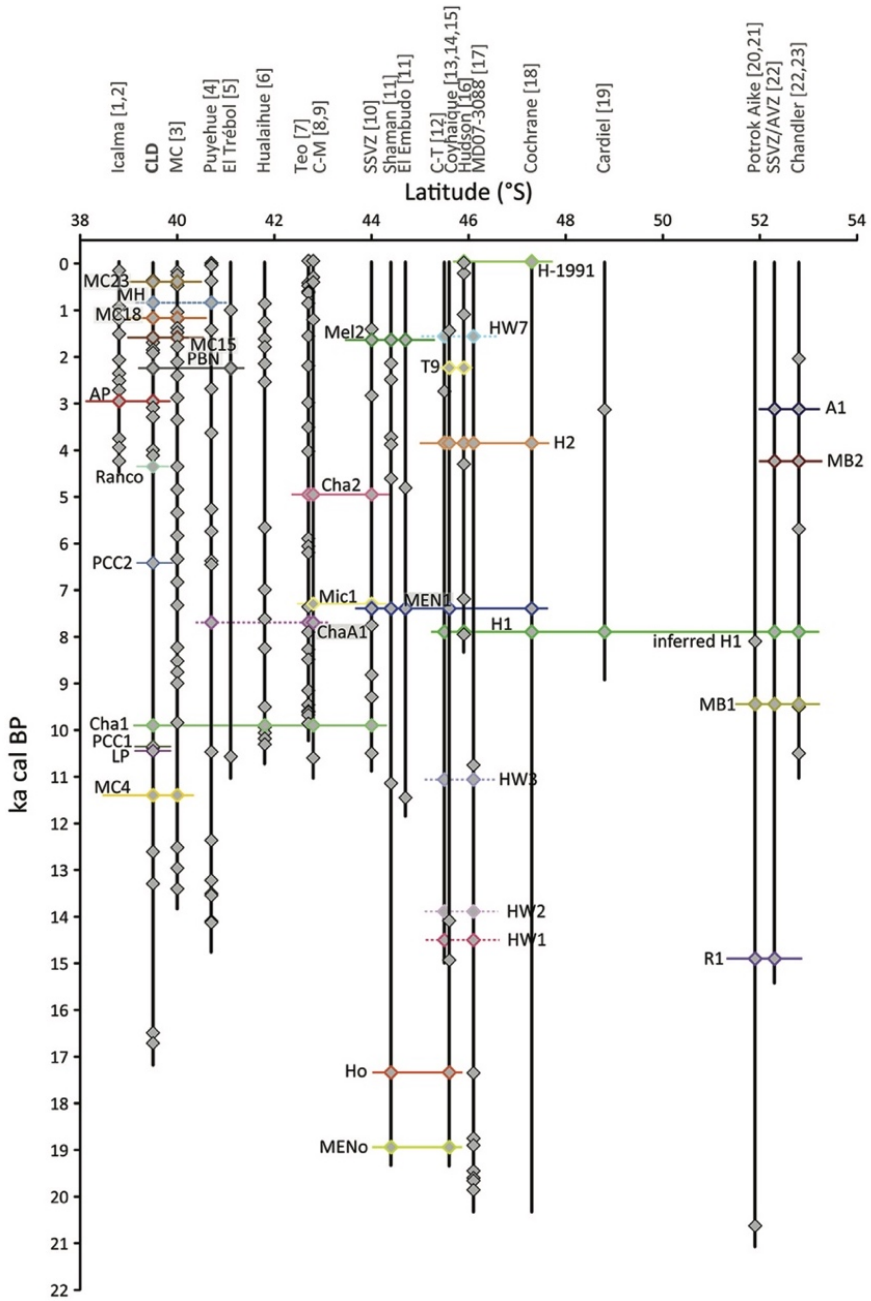


Figure 1.5. Schematic illustration of the widespread tephra deposits and their correlations in southern Chile and Argentina (~39-53°S). Logs represent either individual lake sequences, or compiled stratigraphic sequences from terrestrial exposures (locations in Figure 1.1). Tephra deposits are represented by diamonds; those in grey are uncorrelated, while those in colour are correlated using glass chemistry. Logs are scaled to depositional age of tephra using either Watt et al. (2013a), Fontijn et al. (2016) or calibrated ages in the literature (cf. Fontijn et al., 2016). Only studies with chemical data and prescribed ages are shown in this illustration and therefore this may under-represent the abundance of tephra layers in the region. Dashed lines indicate that a correlation should exist between the two archives, but more chemical analyses are required. H_1 is inferred in the PASADO sedimentary sequence of Laguna Potrok Aike, but identified in the SALSA sedimentary sequence (Haberzettl et al., 2007). Tephra names are taken from the literature; MH: Mil Hojas; PBN: Playas Blancas Negras; AP: Alpehue Pumice; LP: Llaima Pumice; H/HW: Hudson tephras. Several key units within the Lake District are expected to be widespread and have a strong potential as chronological markers (Ranco, PCC2, PCC1 and

Llaima Pumice). To illustrate the potential of regional-scale tephrochronology in southern Chile and Argentina, sections south of Chaitén are shown, despite not being age-modelled. CLD: Chilean Lake District; MC: Mocho-Choshuenco; CeM: Chaitéen-Michinmahuida; SSVZ: Southern Southern Volcanic Zone; C-T: Chonos-Taitao; AVZ: Austral Volcanic Zone. References: [1] Juvigné et al., 2008; [2] Bertrand et al., 2008a; [3] Rawson et al., 2015; [4] Bertrand et al., 2008b, only thickest tephras shown; [5] Villarosa et al., 2006; [6] Watt et al., 2011; [7] Moreno et al., 2015a; [8] Amigo et al., 2013; [9] Watt et al., 2013b; [10] Naranjo and Stern, 2004; [11] Stern et al., 2015; [12] Haberle and Lumley, 1998; [13] Weller et al., 2014; [14] Weller et al., 2015; [15] Van Daele et al., 2016; [16] Naranjo and Stern, 1998; [17] Carel et al., 2011; [18] Stern et al., 2016; [19] Markgraf et al., 2003; [20] Haberzettl et al., 2009; [21] Wastegård et al., 2013; [22] Stern, 2008; [23] Kilian et al., 2003. Source: Fontijn et al (2016).

1.3.2. The Austral Volcanic Zone (AVZ; 49-55°)

1.3.2.1. Geology

The AVZ lies to the south of the SVZ, beyond the volcanic gap, and is the result of subduction of the dense oceanic Antarctic plate beneath the less dense continental South American plate and Scotia microplate (Stern, 2004). Along this 800 km volcanic arc segment there are a complex of Holocene domes and flows on Cook Island, and five stratovolcanoes on the Chilean mainland: Aguilera, Lautaro, Viedma, Reclus and Mt Burney (Stern, 2004, 2008).

1.3.2.2. Tephra preservation and chemical composition

Lautaro, Viedma and Aguilera are the three most northerly volcanoes in the AVZ (Figures 1.1 and 1.12) and are referred to as the Northern Austral Volcanic Zone (NAVZ) volcanoes (Stern, 2004). Tephra from these centres have very similar bulk and glass chemistries (Mayr et al., 2019; Naranjo and Stern, 1998; Stern, 2004; Wastegård et al., 2013). However, in general, the deposits from these centres are difficult to access and poorly preserved and thus, not particularly well characterised. More deposits from these volcanoes should be chemically fingerprinted to aid tephra correlations to source. For example, there has been no analysis of proximal deposits from the ice-covered Viedma volcano due to lack of samples, and it is simply speculated that Lautaro and Viedma share a similar chemical signature (e.g., Mayr et al., 2019). It should also be noted that Viedma has been argued by some to be a nunatak rather than a volcanic centre (e.g., Blampied et al., 2012; Suarez et al., 2019).

Stern (2008) indicated that the whole rock deposits from Lautaro, Viedma and Aguilera are compositionally variable within individual deposits. However, glass-shard chemical analysis of tephra layers identified in the Laguna Potrok Aike sedimentary record that are from the same centres (Latuaro, Viedma and Aguilera) are compositionally similar (Wastegård et al., 2013; Figure 1.6). This is possibly a consequence of high mineral content in the tephra deposits, and an artefact of bulk chemical analysis.

Whole-rock data cannot be used for tephra correlations because the content of the denser mineral phases in the deposits varies with distance from the vent and thus the whole-rock composition for the same unit is different in proximal and distal locations. As such, individual grain glass-shard geochemistry provides the most accurate approach to fingerprint the composition of tephra deposits over wide areas, and secure robust tephrocorrelations (e.g., Tomlinson et al., 2015; Fontijn et al., 2016; Del Carlo et al., 2018). Many of the AVZ tephra layers (both proximal and distal) have been characterised using whole rock chemistry (e.g., Naranjo and Stern, 1998; Stern, 2008; Stern et al., 2016; Weller et al., 2015, 2017, 2018). Some glass compositional data exists for some of the AVZ ash layers (e.g., Stern, 1990, 1992, 2008; Kilian et al., 2003; Stern et al., 2016; Wastegård et al., 2013; Del Carlo et al., 2018; Mayr et al., 2019) and these data can be used for correlation.

Using glass-shard geochemistry, Wastegård et al. (2013) have found that the NAVZ centres display higher K_2O contents of ~2.7-3.9 wt%, and more constrained SiO_2 concentrations of 76-78 wt% than bulk geochemical analyses from Stern (2008). Mt Burney and Reclus volcano are the two southerly centres in the AVZ, and they have the most distinctive chemistries. Glass compositions of tephra from Mt Burney have relatively low K_2O/SiO_2 ratios compared to the volcanoes further north (Wastegård et al., 2013) and this is due to their position relative to the arc front.

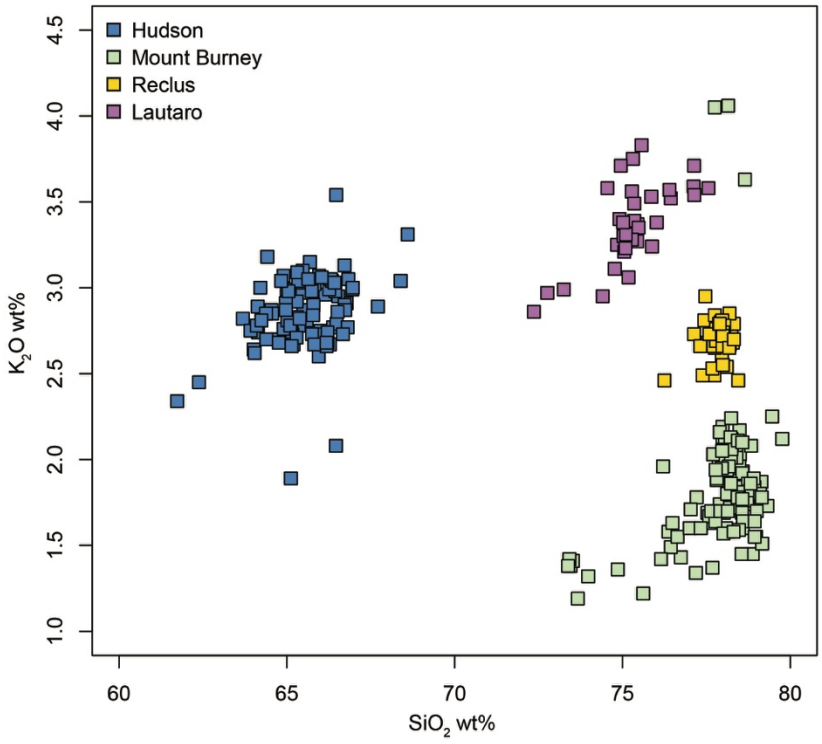


Figure 1.6. Glass compositions of tephra deposits from volcanoes in the AVZ, notably Reclus, Lautaro, and Mt Burney. Compositional data from Hudson volcano is also shown for comparison. Data used is obtained from Haberle and Lumley (1998; Hudson), Del Carlo et al. (2018; Hudson, Reclus and Mount Burney) and Mayr et al. (2019; Lautaro).

Tephra from Hudson and Mentolat volcanoes, located in the SSVZ, are relatively widespread across the AVZ. For example, the H_1, H_2, H_3, (Hudson volcano), and MEN1 (Mentolat volcano) regional marker horizons are identified around the town of Coihaique (Stern et al., 2016; Figure 1.1). Mt Burney tephra is additionally widespread in the AVZ. For example, its dacitic, 18 mm thick, MB_1 tephra layer is observed in Laguna Potrok Aike; this early Holocene layer is of interest because it is not well constrained independently (Wastegård et al., 2013). It has most recently been prescribed an age of 10.2-8.9 cal ka BP (Wastegard et al., 2013), but has previously been reported as 9.9-8.9 cal ka BP (Stern, 2008) and 9.2-9.0 cal ka BP (Kilian et al., 2003). The MB_2 tephra from Mt Burney at ~4.2 cal ka BP (Kilian et al., 2003) is also found in numerous locations in the AVZ including for example, Tierra Del Fuego, Dawson Island, Peninsula Brunswick and Peninsula Munoz Gamero (cf. Stern, 2008). Also of interest is the A_1 marker horizon from Aguilera volcano at ~3.5 cal ka BP (Kilian et al., 2003) that has been observed in Lago Argentino, Cordillera Baguales, Torres Del Paine and Peninsula Brunswick (cf.

Stern, 2008). There is therefore potential for these layers to be preserved in the Laguna Potrok Aike sedimentary sequence, which would allow it to be correlated to others records in the AVZ and improve the robustness of the eruptive age.

1.3.3. The Pali Aike Volcanic Field (PAVF)

The Pali Aike Volcanic Field (PAVF) lies in the back-arc at ~52°, and is a ~4,500 km^2 wide area within the Santa Cruz province, Argentina (Mazzarini and D'Orazio, 2003; Kliem et al., 2013a). Satellite imagery and field surveys have identified up to 467 volcanic cones at the region. Three units, defining the volcanic formations, have been identified: 1) plateau-like lava flows with a maximum exposed thickness of 120 m, located at the base of the sequence; 2) eroded scoria and spatter cones, tuff rings, maars and related lava flows; and 3) the youngest activity includes monogenetic cones, maars and lavas (Mazzarini and D'Orazio, 2003).

K/Ar and $^{40}Ar/^{39}Ar$ ages of the volcanic products at the Pali Aike volcanic field indicate activity spanned 3.78 to 0.17 Ma, with a trend to increasing frequency toward the present day (Mazzarini and D'Orazio, 2003). Magmas erupted from this region have an alkali basaltic/basanitic composition and commonly contain mantle xenoliths.

1.4. Regional and local setting

The Strait of Magellen in southernmost South America (53–55°S) was heavily glaciated from ~31.7 cal ka BP (Clappterton, 1994), until a first deglaciation phase began at 17.50-17.15 cal ka BP, followed by a second phase at 15.65-15.35 cal ka BP (McCulloch et al., 2000). Further North (40-46°S), the first deglaciation phase began at ~18.0±0.14 cal ka BP and accelerated at ~17.77±0.13 cal kyr BP (Moreno et al., 2015b; Bendle et al., 2019). Tephra deposited on land before or during deglaciation was destroyed during ice melt or as a result of the significant erosion that ice melt caused, and subsequently often only postglacial deposits are available for analysis. These postglacial deposits are often affected by preservation issues, predominantly because the region is dry, strong prevailing winds result in little sediment accumulation, poor vegetation

growth and soil instability (e.g., McConnell et al., 2007; Brown et al., 2014; Fontijn et al., 2014). Deposits can also be difficult to access, particularly in glaciated regions of South America such as Patagonia.

In the SSVZ, historical records are only available for the last 100-200 years (Siebert et al., 2010; Fagel et al., 2017). The analysis of tephra in natural archives therefore extends and enhances the historical record by, at the very least, informing on the frequency of past events. Previous work reveals that the SSVZ and AVZ are highly volcanically active; 74 volcanic centres erupted in the postglacial period, and a minimum of 21 of these centres had one or more large explosive eruptions during the Late Quaternary (Fontijn et al., 2014). Tephra from these large, explosive eruptions are often identified in multiple records, providing marker layers that can be used to correlate records in the region with those further afield, such as those on distant islands, marine records or ice-cores from Antarctica (Section 1.1.1; Figure 1.5).

The tephra deposits from many of the large eruptions that have occurred in the SVZ and AVZ have distinctive chemical compositions, and with further glass-shard chemical fingerprinting it may be possible to produce robust correlations across numerous archives, including extra-Andean archives such as marine records, sedimentary archives, or Antarctic ice cores. The potential for such work is demonstrated in southern South America by Monteath et al. (2019) who have identified widespread cryptotephra layers in an exposed peat cliff section at Hookers Point (51°42′S; 57°47′W) in the Falkland Islands, and by Oppedal et al. (2018) who identified cryptotephra layers in Diamond Bog on South Georgia (54°S; 36°W). In addition, Narcisi et al. (2012) correlated cryptotephra layers in the EPICA-Dome C Antarctic ice-core to eruptions from southern South America but this is disputed as there is insufficient chemical evidence for the correlations (e.g., Koffman et al., 2011; Del Carlo et al., 2018). Such extra-Andean tephra correlations provide additional information on the dispersal of past eruptions in the region, and therefore the magnitude and tempo of past eruptive behaviour. Moreover, the finding of isochronous layers linking regions in southern South America and extra-Andean records can help validate the chronologies of the respective archives, and provide the possibility of identifying phased relationships between climate records (e.g., Lane et al., 2013).

1.5. The coupled relationship between deglaciation and volcanic activity

A magmatic response to ice-unloading (e.g., Huybuers and Langmuir, 2009; Rawson et al., 2016), sea level change (e.g., Crowley et al., 2015) and erosion (e.g., Sternai et al., 2016) has been recorded in numerous environments, but is particularly well-documented in areas where enhanced melt is produced as a result of decompression melting (e.g., oceanic ridges such as Iceland; Jull and McKenzie, 1996; Crowley et al., 2015). To exemplify, a theoretical model analysing global changes in ice volume, produced by Jellinek et al. (2004), indicates that glacial unloading may influence dyke formation by reducing the confining lithostatic stress and crustal residence times. Using Iceland as a case study, Jull and McKenzie (1996) calculated melt production rates based upon changes in volcanic parameters (notably non-hydrostatic stress field and viscous flow) and determined that if an ice sheet 2 km thick melted over a 1 ka period, the average volcanic-melt production rate would increase by 30 times. Similarly, Maclennan et al. (2002) noted that, in Iceland, eruption rates were 30-50 times higher after the deglaciation (~18 kyr BP) than during the Holocene period. Likewise, Sigvaldason et al. (1992) also reported an increase in magma production in Iceland between 10.0 and 4.5 ka of at least 20 and 30 times greater than the past 2.9 kyr.

Increases in eruptive activity in areas of decompression melting are speculated to result from increased mantle melting, the tapping of magma chambers, the release of pooled magma (e.g., Sigvaldason et al., 1992, 2002; Maclennan et al., 2002) and shorter crustal residence times (Gee et al., 1998; Jellinek et al., 2004). Jull and McKenzie (1996) have proposed that after ice unloading, melt rapidly reaches the surface (within ~1 ky). Maclennan et al. (2002) and Watt et al. (2013a) have additionally reported that this increase in activity lasts for ~2 ky after ice-unloading. Even small changes in ice mass have been associated with changes in volcanism in Iceland; small increases in ice mass occurred at ~5.5-4.5 kyr BP following an ~600 year change in atmospheric circulation patterns, and during this short time, eruptive activity in Iceland decreased. However, following a return to normal atmospheric and glacial conditions, activity returned to baseline levels (Swindles et al., 2018).

The coupled relationship between deglaciation and increased volcanism in continental arc-settings (e.g., Chile) is, however, more contentious (Watt et al., 2013a; Schindlbeck et al. 2018; Kutterolf et al., 2019). The controlling mechanisms behind any such coupled relationship are thought to be different in continental arc-settings, and the evidence is less pronounced (e.g., Watt et al., 2013a; Rawson et al., 2015, 2016; Fontijn et al., 2016). In arc-settings mantle melt is hypothesised to pool and fractionate as a result of compression, but there is no evidence of an increase in mantle melting post-deglaciation as per decompression settings (e.g., Singer et al., 2008; Tuffen, 2010; Watt et al., 2013a; Rawson et al., 2016).

Chemical analysis of glass-shards from tephra deposits in Chile indicate that there are significant changes in the composition of magmas post-deglaciation, possibly in response to changes in ice-overburden (Fontijn et al., 2016; Rawson et al., 2016). This is hypothesised to be due to the storage and release of magma. This detailed record, from Mocho-Choschuenco volcano (site location shown in Figure 1.2), shows a tripartite pattern of volcanic activity post-deglaciation, formed from distinct groups of time-averaged eruptive fluxes, sizes, compositions, and temperature ranges; these are phase 1 at 13-8.2 cal ka BP, phase 2 at 7.3-2.9 cal ka BP, and phase 3 at 2.4 cal ka BP-present (Rawson et al., 2016). Phase 1 is typified by eruptions with large magnitudes (~VEI 5), high eruptive fluxes (>0.9 km^3/ky dense rock equivalent (DRE)) and evolved deposits of low frequency (1.9 eruptions/ky). During phase 2, eruptions and eruptive fluxes are low magnitude (~VEI 3; 0.01 km^3/ky DRE). Deposits in this phase (2) are composed of intermediate compositions (i.e., basaltic andesite melts) and are deposited infrequently (2.0 eruptions/ky). Finally, phase 3, is characterised by an increase in activity, with a variety of eruption magnitudes (~VEI 3-5) and a high eruptive flux of 1.0 km^3/ky DRE. Eruptive frequency in phase 3 is also high (6.3 eruptions/ky; Rawson et al., 2016; Figure 1.7).

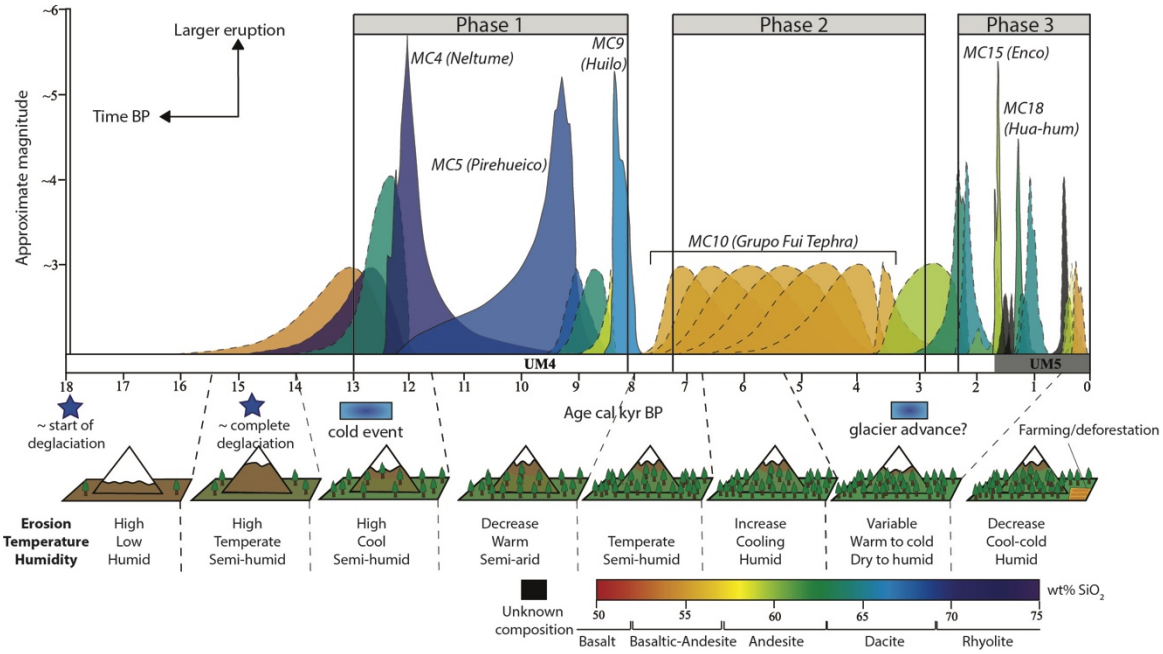


Figure 1.7. Summary of the explosive history from Mocho-Choschuenco since deglaciation at ~18 ka. Each unit is represented by its age probability distribution which is determined by Bayesian analysis of radiocarbon data; the height corresponds to the approximate magnitude (dashed lines are used where the magnitude is poorly constrained). Colour corresponds to the average SiO_2 glass composition. Magnitude = $\log_{10}$[eruption mass (kg) -7] (as per Pyle, 2000). The erosion rates, temperature, humidity, climate, and vegetation densities are inferred from interpretations made on the Lago Puyehue core ~90 km south of Mocho-Choschuenco (Bertrand et al., 2008a; Vargas-Ramirez et al., 2008). After: Rawson et al. 2015.

The aforementioned changes reflected in the Mocho-Choschuenco eruption deposits have been tentatively related to ice-unloading. At this site, there is a ~5 ka lag in the response post-deglaciation (Rawson et al., 2016). This is longer than the lag typically observed in areas of decompression melting, but likely holds true since a similar trend has been noted in tephra deposits from across the CLD (Fontijn et al., 2016). The time lag may also be related to the composition of the deposits, with silicic and basaltic magmas with lags of 3.2±4.2 and 11.2±2.3 kyr at a site of decompression melting (Jellinek et al., 2004). Alternative explanations for such a delayed response include i) poor tephra preservation due to the lack of soil development and sparse vegetation cover (i.e., the lag is inaccurately recorded), and/or ii) the timing of deglaciation is poorly constrained at Mocho-Choshuenco.

A similar, albeit less obvious trend in the scale and tempo of the volcanism, and composition of the magma erupted, has been observed in the tephra deposits at Puyehue-Cordón Caulle, a volcanic centre in the Chilean Lake District that is close to Mocho-Choschuenco (Singer

et al., 2008). Singer et al. (2008) noted more siliceous tephra post-deglaciation between 7 and 5 ka BP. However, this trend is not recorded in the tephra deposits in the nearby lacustrine sediments of Lago Puyehue which are thought to predominantly preserve eruptive events from Puyehue-Cordón Caulle (Bertrand et al., 2008b). As such, further analysis is needed regarding the compositional variation of the volcanic deposits preserved in the Lago Puyehue sedimentary archive.

Evidence of synglacial volcanism in Chile, and other arc settings, is limited. This is predominately because deglaciation at the end of the Last Glacial Maximum (LGM) removed deposits from the landscape. Preserved records are typically restricted to subglacial lavas that only reflect effusive volcanism, and such deposits have only been studied at a few volcanoes (e.g., Puyehue-Cordón Caulle; Singer et al., 2008). Medial to distal tephra records are likely to preserve the most complete record of volcanism but these have currently not been fully studied in the SVZ; if there is a relatively simple relationship between ice-unloading and volcanism then it is expected that the analysis of such complete records would show a decline in eruptive frequency during the glacial period, when ice mass is at its fullest extent (e.g., Jellinek et al., 2004). Long-term, synglacial records, such as Laguna Potrok Aike, could be beneficial in determining whether there is a relationship between ice-unloading and volcanic activity (both in frequency and composition).

1.6. Site Selection

Firstly, lacustrine and peat archives were targeted as they typically have rapid sediment accumulation and, consequentially often preserve tephra layers very well (e.g. Bertrand et al., 2014; Lane et al., 2014; Davies, 2015; McLean et al., 2018). As such, they provide an ideal opportunity to study more complete records of volcanism than terrestrial records alone. In this thesis, two long lake sediment sequences are identified as having good tephra records which could be analysed and provide evidence to meet the aims and objectives of this thesis. These are: i) Lago Puyehue, located in the SVZ and ii) Laguna Potrok Aike, located in the back-arc of the

AVZ. Both records preserve numerous tephra layers which have previously been catalogued (Lago Puyehue = Bertrand et al., 2008a; Laguna Potrok Aike = Haberzettl et al., 2008; Wastegård et al., 2013). However, studies on the tephra layers have not been conducted in sufficient detail to permit a thorough reconstruction of past volcanism; Lago Puyehue is located in such a position that it should capture tephra from both large regional eruptions as well as small eruptions from numerous local volcanoes (Chapter 3, 4). Laguna Potrok Aike is located downwind of major productive centres and should subsequently provide an excellent history of explosive volcanic events. Additionally, all records in the region which seek to better understand whether a relationship exists between climate and volcanism are postglacial (e.g., Fontijn et al., 2016; Rawson et al,. 2016). Because Laguna Potrok Aike is one of the longest lacustrine archives available in southern South America, extending well into the last glacial period with basal sediments of ~80 cal ka BP, this aim can be investigated in great detail for the first time (e.g., Zolitschka et al., 2009; Buylaert et al., 2013; Kliem et al., 2013b; Gebhardt and Ohlendorf, 2019; Chapter 5). The only other known records in existence which extend into the glacial period are marine records which are already rather well-studied (e.g., Siani et al., 2010; Carel et al., 2011).

This thesis also focuses on three peat archives from the Falkland Islands: Stanley Common, Poncho Hill Pass, and Fox Bay. The tephra at these sites have been investigated previously and indicate that ash from the Andes is preserved, but only a small amount of data is published (Holmes et al., 1999; Hall et al., 2001). The tephra record from these archives thus provide an opportunity to determine how far Andean tephra from Holocene eruptions is capable of travelling, in addition to assessing Andean tephra preservation and concentration in the extra-Andean locations.

Finally, three case studies formed using literary data from five different sites are investigated using the KDE function in OxCal to analyse temporal changes in volcanism (Section 2.6.3). These sites were selected based on the excellent chronological control of the record in addition to the resolution of the archive. The records studied include: (1) Lago Pueyhue and Mocho-Choshuenco volcano in the SVZ, Chile, and (2) Taupo Volcanic Centre and Okataina Volcanic Zone in New Zealand. (3) Mount Mazama and the region around Crater Lake, USA.

1.6.1. Lago Puyehue

Lago Puyehue (40°, 42'S; 72°, 27'W) is a moraine dammed lake, located in the Chilean Lake District, SVZ (Figure 1.8). It sits at an elevation of 185 m a.s.l, at the foot of the Andes with a water volume of 12.6 km^3, surface area of 165.4 km^2, catchment area of 1,510 km^2 and a maximum water depth of 122 m (Campos et al., 1989; De Batist et al., 2008; Bertrand et al., 2008a, 2014). The lake is thermally stratified from December to March and circulates once a year, during the austral winter (July to September). There are several inflows to Lago Puyehue, including the Río GolGol and Río Lícan to the east of the lake; the main outflow is Río Pilmaiquén to the west. Annual precipitation varies from ~2000 mm/yr at the lake edge to ~5000 mm/yr at the summit of the volcano (Bertrand et al., 2008b). Wind speeds and precipitation are significantly reduced during El Niño years (De Batist et al., 2008).

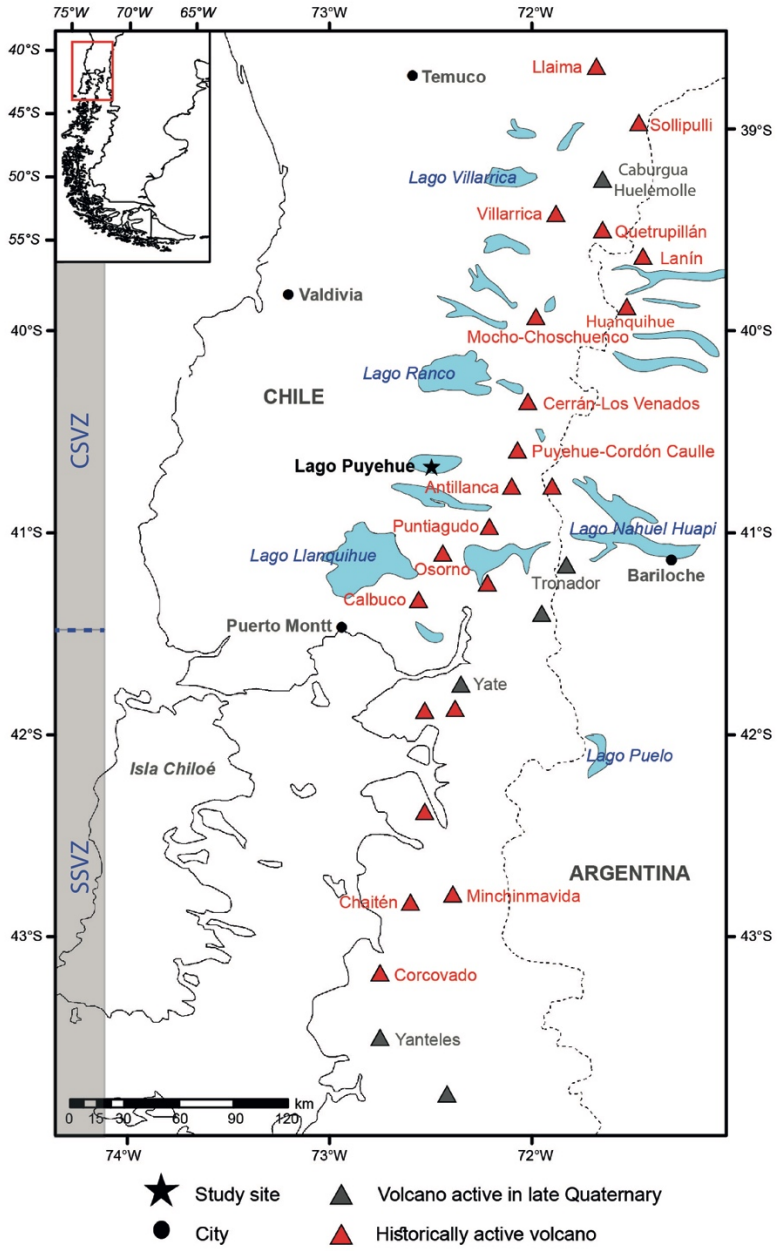


Figure 1.8. Map showing Lago Puyehue, Chilean Lake District, and the volcanoes that have been active in the Quaternary. Triangles = volcanoes (grey = active in Quaternary; red = historically active); circles = towns; star = site location.

In the austral summer of 2001-2002, a seismic assessment enabled the identification of steep slopes, sub-basins and faults (Charlet et al., 2008). This data indicated that the eastern and southern parts of the basin were ideal study sites for palaeoclimate (e.g., palynology), since they were continuously infilled and uninterrupted, away from mass wasting and turbidite deposits; the western sub-basin showed a number of unconformities, making the sequence less ideal for tephra

analysis, though ideal for the analysis of turbidites as a proxy for palaeoearthquakes (Charlet et al., 2008).

Sediment samples from these ideal regions (i.e., East and South of the basin) were obtained during the same summer (2001-2002). Long sediment cores, totalling a depth of 1122 cm, were obtained with a UWITEC piston corer, while six short cores, totalling a depth of 236 cm, were obtained with a UWITEC gravity corer. The sediment cores have since been analysed in studies on palaeoclimatology, tephra, tephra chemistry and radiocarbon dating (Bertrand et al., 2008b), diatom (Sterken et al., 2008), pollen (Vargas-Ramirez et al., 2008), sedimentology and bulk sediment geochemical analysis (Bertrand et al., 2008a).

When waters become rich in dissolved calcium carbonates, they can cause radiocarbon ages to appear too old. In most cases, this is because old limestone weathered to bicarbonate has no radioactive carbon and it dilutes the lake activity, resulting in a ^{14}C depletion (Philippsen, 2013). As a result, the lake has a different ^{14}C reservoir than that in the biosphere and thus requires a radiocarbon correction to be applied. This is termed the hard-water effect, or is called a radiocarbon reservoir. While the hard-water effect at Lago Puyehue has been deemed to be negligible, there is a reported age-discrepancy whereby sediments appear older than their true age and this is believed to be a consequence of old carbon remaining from post-glacial volcanic lakes (Blaauw et al., 2011; Bertrand et al., 2012). The age-offsets in the Lago Puyehue sedimentary sequence were calculated by Bertrand et al. (2012) to be between 307 and 1080 years. A new version of the age model has been created by S. Bertrand (pers comms) using CLAM 2.2 (Blaauw, 2010) after Bertrand et al. (2012) and this has provided ages for the entire sequence (i.e., an age per cm of sediment; See Figure 1.9). The 11.2 m sequence spans ~15.5 cal ka BP (S. Bertrand, pers comms). An age-depth chronology for Lago Puyehue is published, and makes use of 16 calibrated radiocarbon dates, 20 ^{210}Pb measurements, ^{137}Cs measurements, varve counts, and historical ages (see Bertrand et al. (2008b, 2012) for a fuller description).

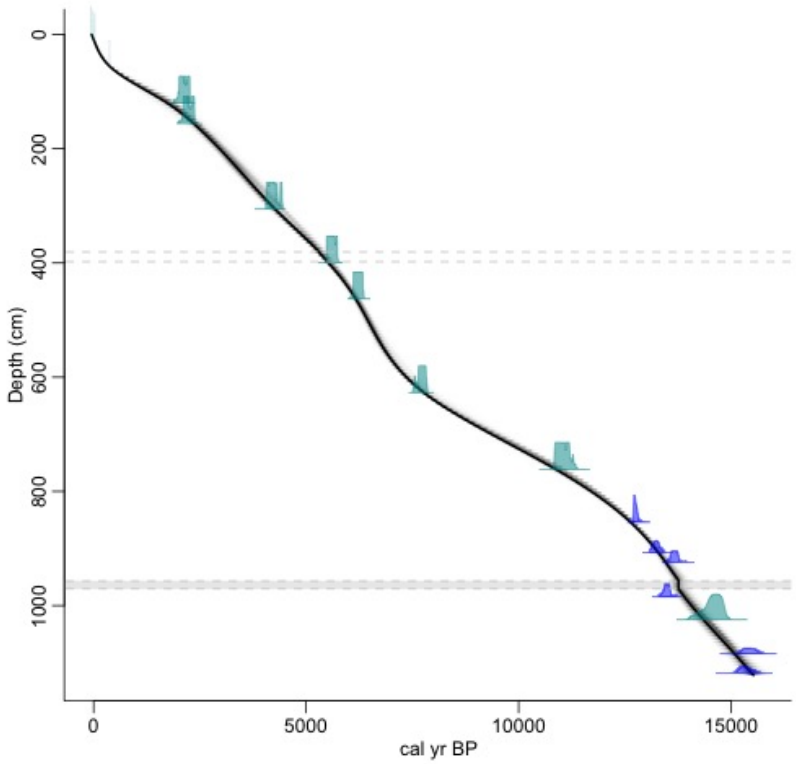


Figure 1.9. Age-depth model for the sediments of Lago Puyehue derived from CLAM 2.2 (Blaauw, 2010). The grey-dashed lines represent turbidites and are considered instantaneous deposits in this model adapted by S. Bertrand (unpublished) from Bertrand et al. (2012); the model is corrected for these three turbidite events. It is not corrected for tephra events as taking into account the thickness of these layers made no difference to the ages produced. Green probability density functions were calibrated manually and include, for example, historic tephra dates, and radiocarbon dates needing to be corrected for old carbon input (i.e., reservoir effects). Blue probability density functions represent ages calibrated within CLAM 2.2; these were not calibrated manually since the samples of organic matter were aquatic, and during the deglaciation it is considered that there was no old carbon (Bertrand et al., 2012). Model sourced from Bertrand (unpublished) and modified.

A full sedimentological description of the long, continuous sequence, PUII, can be obtained from Bertrand et al. (2008b) and is summarised in Figure 1.10. The sequence is typical for calm, open-water environments and is composed of predominantly silty sediments, which include diatoms, amorphous clays, organic matter, crystalline materials and tephra (Bertrand et al., 2008b). Bertrand et al. (2008b) observed 78 sandy layers, 1-75 mm thick, and suggested that these are tephra layers (Figure 1.10).

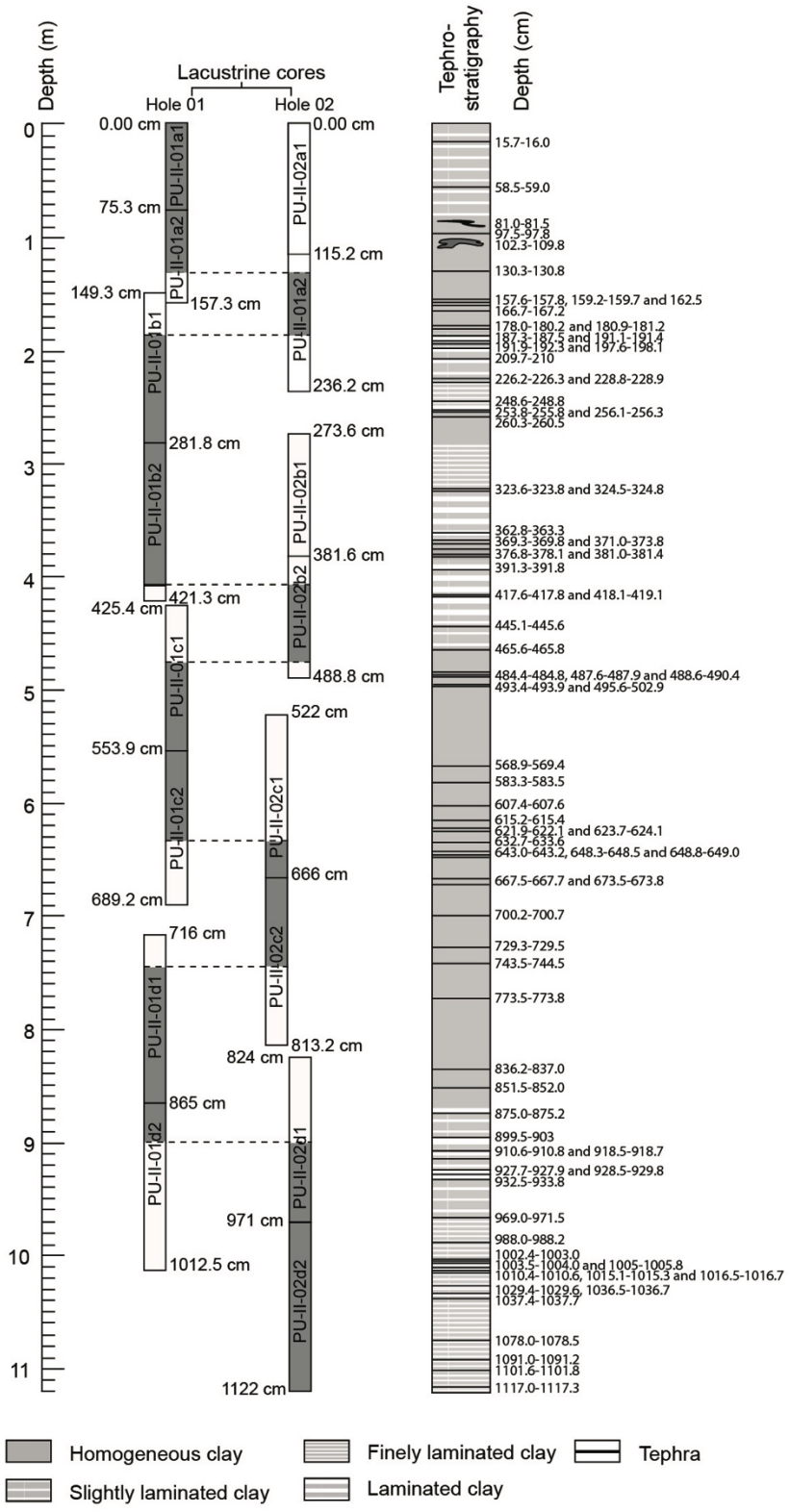


Figure 1.10. Schematic diagram of Lago Puyehue demonstrating the correlations between the 3 m long sections from different boreholes, enabling the production of the composite sequence. The dark grey sections within 3 m long sections represent the parts used to produce the composite log (middle). The composite log is drawn in accordance to macroscopic descriptions (this study; far right). After: Bertrand et al. (2008b).

Within close proximity of Puyehue Lake, there are five volcanic complexes/volcanoes which are considered to be possible sources of tephra units, including, Carrán-Los Venados, Puyehue-Cordón Caulle, Antillanca, Puntiagudo, and Osorno (Bertrand et al., 2008b, Siebert et al., 2010; Figure 1.11; Table 1.1). Most of the tephra deposits identified in the sediments of Lago Puyehue are likely to have originated from these aforementioned complexes or volcanoes due to their proximity to the lake. Puyehue-Cordón Caulle volcanic complex is expected to be the largest contributor as it has been frequently active in the Late Quaternary, and its close proximity and the abundance of inlets feeding the lake from the base of the volcano (Bertrand et al., 2008b; De Batist et al., 2008; Singer et al., 2008).

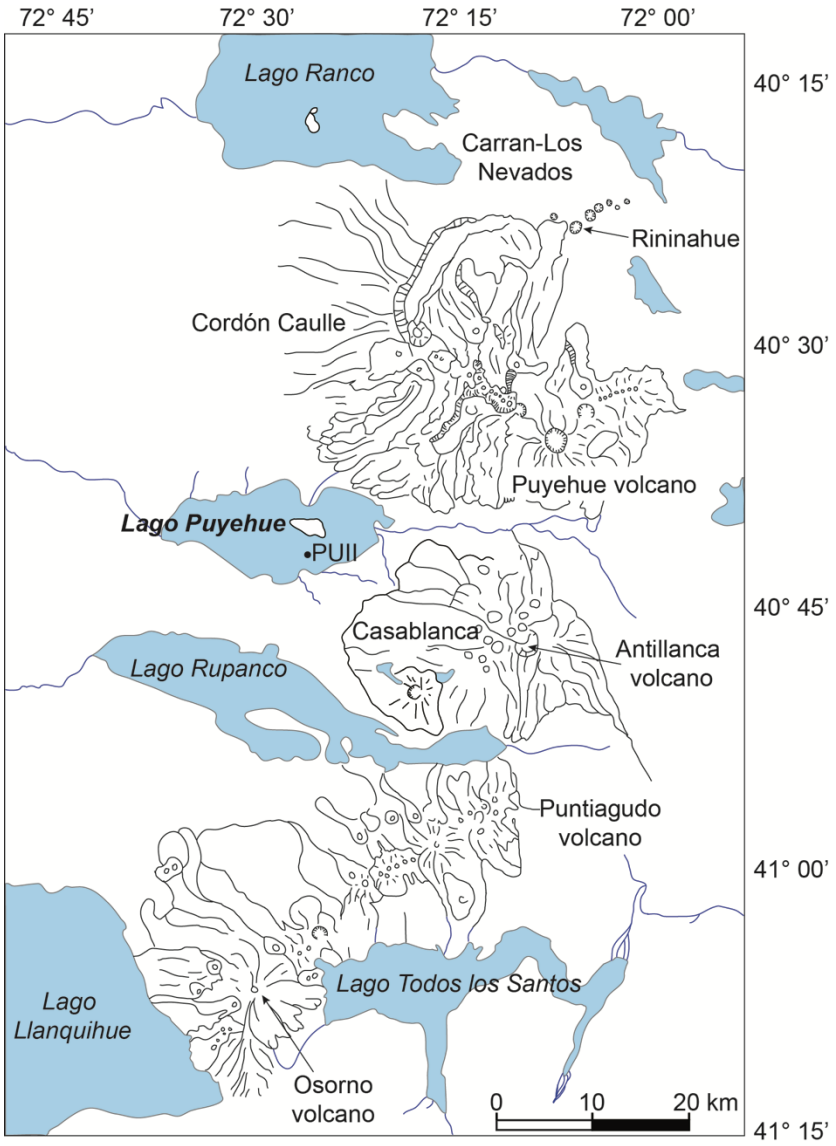


Figure 1.11. Illustration of Lago Puyehue and nearby volcanoes, their explosive eruptions may be persevered as tephra in the Lago Puyehue record. Note the close proximity of Puyehue-Cordón Caulle, as well as the Antillanca volcanic group. Lakes are shown in blue; lake inlets and outlets are shown in dark blue; volcanoes and volcanic features are outlined in black. PUII coring site is labelled. After: Bertrand et al. (2008b).

An investigation of the 2011 Cordón Caulle tephra deposits by Bertrand et al. (2014) at different types of lakes in the CLD illustrated that tephra in Lago Puyehue can be deposited via fluvial inwashing immediately following the eruption; these deposits are still useful for reconstructing the frequency, and establishing the tephra composition of past volcanic events, despite their depositional pathway (e.g., Bertrand et al., 2014). Fluvial inwashing via the Golgol and Lícan rivers, may be particularly likely to occur with eruptive deposits from nearby volcanic centres (e.g., Puyehue-Cordón Caulle, Osorno, Carrán-Los Venados, Antillanca), whose ash is

typically carried East by the wind regime, and may fall directly over the lake, or into its catchment, and thus be washed into Lago Puyehue (e.g., Bertrand et al., 2014; Chapron et al., 2007). As a result of this mechanism of deposition and its ideal location in the CLD (see Section 1.3.1), Lago Puyehue provides an excellent archive of different sized volcanic events throughout the entirety of the Holocene, which are not all preserved in the terrestrial realm due to their limited dispersal range, and their relatively poor preservation potential.

Bertrand et al. (2008b) analysed the PUII sedimentary sequence and suggested four tephra correlations to historical eruptions based on the mineralogy and geochemistry of the deposits:

- AD 1960 - Puyehue-Cordón Caulle
- AD 1921–22 - Puyehue-Cordón Caulle
- AD 1907 - Rininahue maar (tentative)
- AD 1575 – Osorno

Bertrand et al. (2008b) also chemically analysed a limited selection of older tephra but were unable to produce any correlations and some of the data obtained had poor analytical totals, or the layers were not characterised. This record has been revisited to better establish the frequency and chemical composition of the events in Lago Puyehue.

1.6.2. Laguna Potrok Aike

Laguna Potrok Aike (51°1, 57'S; 70°, 22'W) is located in the back-arc, southernmost Patagonia (Argentina; Figure 1.12). The lake sits at an elevation of 113 m a.s.l, in the western part of the Pliocene-Quaternary PAVF (Mazzarini and D'Orazio, 2003; Section 1.3.3). The water depth of Laguna Potrok Aike reaches 100 m in depth at the centre and its diameter is 3.5 km (Recasens et al., 2012). The lake is sub-saline (salinity of 2.2 %, pH of 8.8), and annually there is <300 mm of precipitation in the region as a result of the rain shadow effect in the Patagonian Steppe (Mayr et al., 2007; Recasens et al., 2012). Because of strong westerly winds, there is limited lake stratification (Haberzettl et al., 2007; Zolitschka et al., 2009). Laguna Potrok Aike

was probably not covered entirely by the Patagonian ice sheet during the Last Glacial Maximum (between ~26.5 and ~18 cal ka BP; Moreno et al., 2015b), or prior to this, and therefore the sediments are one of the only synglacial/glacial records from the region (Zolitschka et al., 2006).

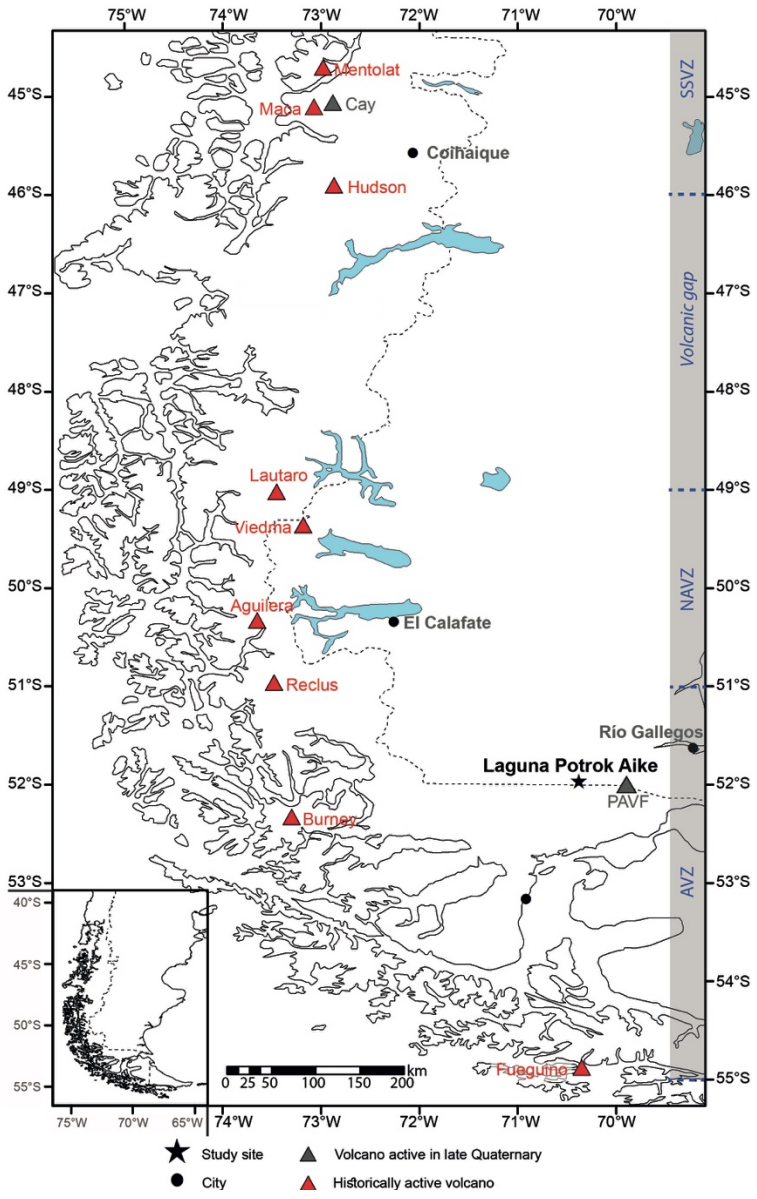


Figure 1.12. Site map shows Laguna Potrok Aike and the nearby volcanoes active in the Quaternary. Triangles = volcanoes (grey = active in Quaternary; red = historically active); circles = towns; star = site location.

At present, the lake is fed by groundwater and has no outflows or tributaries, although deep gullies have formed in the surrounding terraces as a result of ephemeral/episodic runoff

(Haberzettl et al., 2007; Mayr et al., 2007; Zolitschka et al., 2009; Kliem et al., 2013b), and analysis of the lacustrine sediments and terrestrial tephra deposits indicate that at ~17 ka BP and ~52 cal ka BP there was lake overflow (Kliem et al., 2013a; date changed to reflect that of the updated age-model of Gebhardt and Ohlendorf, 2019).

Laguna Potrok Aike and nearby Laguna Azul were investigated between 2002 and 2005 in the South Argentinian Lake Sediment Archives and modelling (SALSA) project (Zolitschka et al., 2006). A more constrained project focusing solely on Laguna Potrok Aike was developed after the SALSA sediments were analysed. In the austral spring of 2008, the Potrok Aike Maar Lake Sediment Archive Drilling Project (PASADO) began, using a hydraulic piston corer, to obtain a long sediment core as part of an International Continental Scientific Drilling Project (ICDP; 5022). A composite profile was produced, and labelled 5022-2CP. The 5022-2CP profile is 106.09 m long and comprises of 101.02 m of sediment. There are 24 gaps, totalling 5.06 m, in the composite sequence as a result of ineffective core catchers, broken liners and a lack of sedimentary features permitting core correlation (Kliem et al., 2013b; Figure 1.13). The sediments of this composite profile have been extensively studied for palaeoenvironmental reconstructions using multiple proxies, including for example, stable isotopes, diatoms, pollen, rock magnetism, geochemistry, radiocarbon dating, tephra and tephra chemistry (e.g., Mayr et al., 2007; Gogorza et al., 2012; Recasens et al., 2012; Jouve et al., 2013; Kliem et al., 2013b; Wastegård et al., 2013; Hahn et al., 2014).

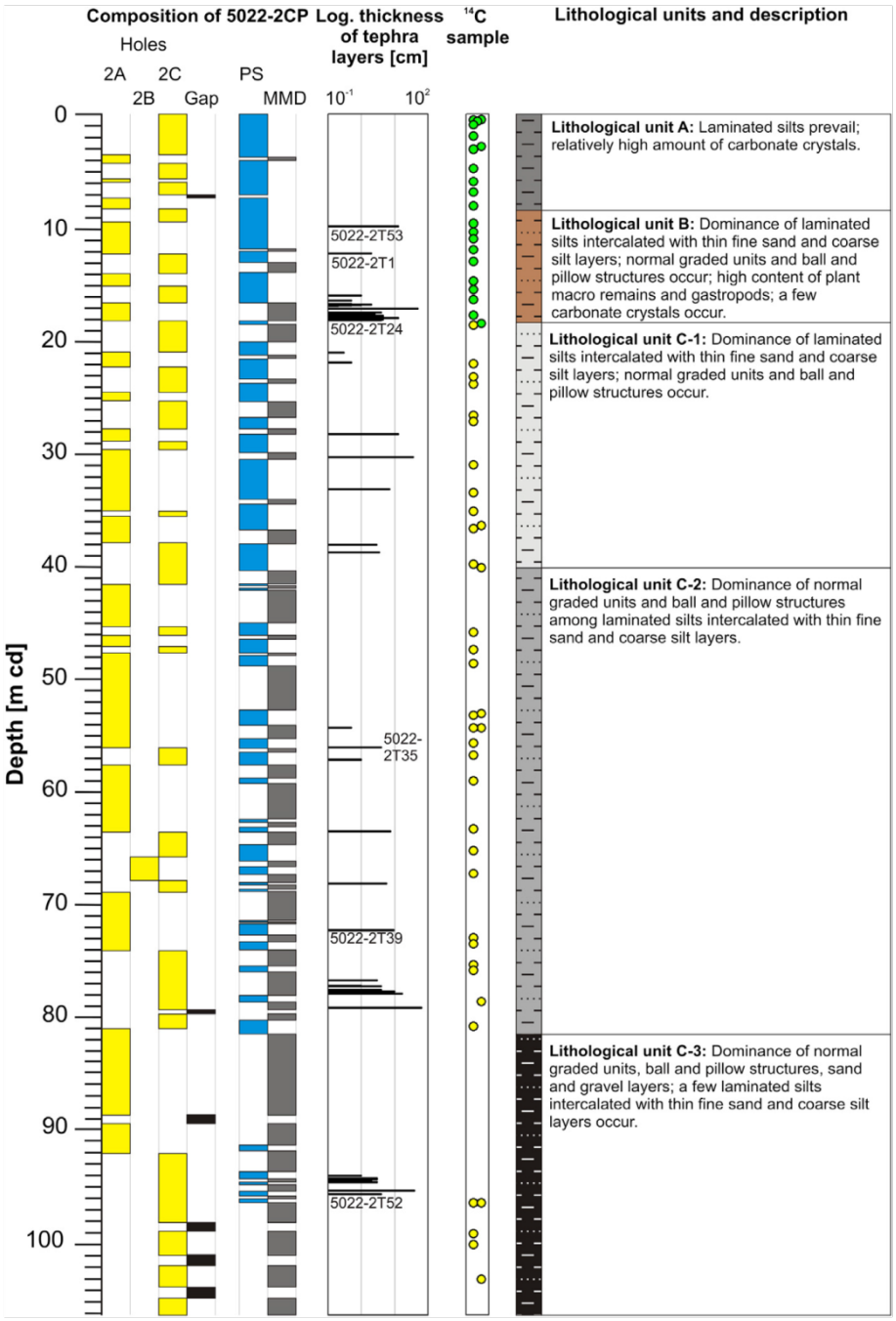


Figure 1.13. Composition and lithology of the composite profile from site 2 (5022-2CP; used in this study). 2A, 2B and 2C refer to the holes used to obtain sediment; gap = missing sediment from coring process (must be >10 cm); PS = pelagic sediment; MMD = mass movement deposit (e.g., turbidite). Tephra layers are shown according to average depths. Green radiocarbon samples are correlated ages from SALSA core PTA03/12 + 13 (as per Haberzttl et al., 2007); yellow are directly obtained from PASADO core 5022-2CP. Source: Kliem et al. (2013b). Note: Gebhardt and Ohlendorf (2019) have made minor alterations to the sediment classification.

A total of 58 radiocarbon dates were produced using carbonates, organic macrofossils, and bulk sediments; 21 dates were obtained between 0 and 18 m-cd (metres composite depth;

present-14.5 cal ka BP) and 37 dates were obtained between 18 and 106 m-cd (80-14.5 ka BP) of 5022-2CP (dates derived from Gebhardt and Ohlendorf, 2019; Kliem et al., 2013b). From the top 18 m-cd, three dates were omitted because they were interpreted as being reworked (i.e., not in stratigraphic order; Haberzettl et al., 2007), and from beneath 18 m-cd, three dates were omitted near the base of the core as they returned infinite ages due to having low ^{14}C values (Kliem et al., 2013b).

The chronology of the top 18 m-cd is derived by transferring ^{14}C dates obtained from the earlier acquired (2002 campaign) PTA03/12+13 (SALSA) record to the composite 5022-2CP (PASADO) record, using magnetic susceptibility and lithological features (Kliem et al. 2013b). Plant macrofossil remains of aquatic mosses from the 5022-2CP sedimentary sequence were used to determine radiocarbon ages (Kliem et al., 2013b). These analyses were performed at the Poznan Radiocarbon Laboratory, Poland, and the measurements were calibrated using the SHCal13 curve for the southern hemisphere (Hogg et al., 2013) and CLAM v.2.2 (Blaauw, 2010). Analysis of the lacustrine sediments indicate that there is no hard-water effect at the site (Haberzettl et al., 2005, 2007).

Unfortunately, the core cannot be dated using the $^{40}Ar/^{39}Ar$ technique for the sediments as the tephra do not contain potassium feldspar (Kliem et al., 2013b). However, Infrared Stimulated Luminescence (IRSL) measurements were obtained by Buylaert et al. (2013) on Site 1, which extend back to ~65 ka (non-composite core 1D). To transfer the ages obtained from IRSL measurements to the composite record (5022-2CP), correlation between site 1 and 2 was carried out using distinct layers, including volcanic ash layers, clay caps of turbidites and sand layers (Gebhardt and Ohlendorf, 2019). IRSL measurements were excluded if correlations were unclear (Gebhardt and Ohlendorf, 2019; See Figure 1.14).

Three visible tephra layers are identified in the upper part of the sequence and used to refine the age model: H_1 (Hudson; this thesis), Mount Burney (MB_1; Wastegård et al., 2013) and Reclus (R_1; identified in Wastegård et al., 2013, re-located in this study, see Chapter 5). Refined ages of these eruptions were acquired from the regional compilation of eruptive ages by Fontijn et al. (2016) using over- and/or underlying radiocarbon ages, and these ages have been

applied to the age model to further constrain the chronology. Tuning of relative palaeointensity between Laguna Potrok Aike and the Sint-800 stack was also conducted to confirm the chronology beyond 30 ka (Gebhardt and Ohlendorf, 2019; Chapter 2).

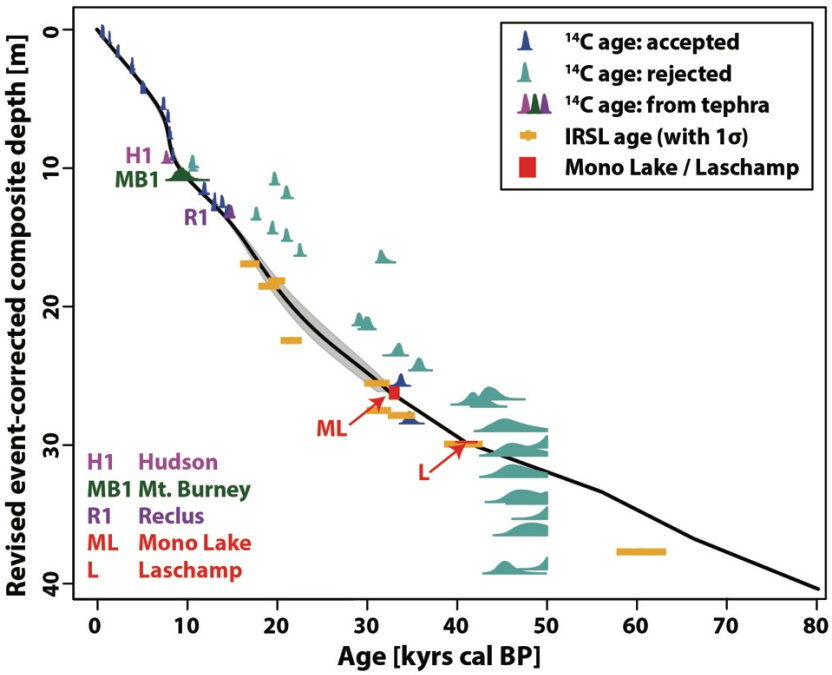


Figure 1.14. Age-depth model of 5022-2CP composite Potrok Aike sediment core, which utilises additional data from non-composite site 1 and palaeointensity data. Dates of three tephra layers (H_1, MB_1, and R_1) are used within the age model. Sourced from Gebhardt and Ohlendorf (in prep).

Forty-seven visible ash layers have been observed in the composite record, 5022-2CP, and 18 of these were chemically analysed (Kliem et al., 2013b; Wastegård et al., 2013). These tephra layers are up to 50 cm thick, often with coarse bases, and contain both light and dark coloured grains. These horizons are comprised of glass shards, amorphous clasts, pumice, minerals and microphenocrysts (Kliem et al., 2013b). Tephra chemistry observed in the Potrok Aike PASADO core thus far shows that the deposits originate from Mt Burney, the volcanoes in the NAVZ (Lautaro, Viedma, or Aguilera), and Reclus (Wastegård et al., 2013; Table 1.2).

Some of the lithology is reworked, with increasing abundance of sediment mobility downcore (Kliem et al., 2013b; Gebhardt and Ohlendorf, 2019), and seven of the 18 tephra layers that have been analysed in detail are classed as reworked (Wastegård et al., 2013).

Table 1.2. Table showing the already established correlations to widespread tephra layers identified in the Laguna Potrok Aike sedimentary sequence (PASADO and SALSA). Data from: 1=Haberzettl et al. (2007), 2=Kliem et al. (2013b), and 3=Wastegård et al. (2013). Composite depth refers to PASADO sequence depth (Kliem et al., 2013b).

Tephra Sample	Composite depth (m)	Thickness (mm)	Age (cal BP), 2σ range	Source Volcano	Tephra Correlation	Remarks	Reference
5022-2T53	-	-	-	Hudson	H_1	SALSA core only	1,2
PAS-2T1	12.32-12.34	18	9,545 (8,851-10,238)	Mt Burney	MB_1	-	3
PAS-2T2	16.04-16.05	10	-	Reclus	R_1	Reworked	3
PAS-2T3	16.48	4	-	Reclus	R_1	Reworked	3
PAS-2T4	16.78-16.79	5	16,379 (15,780-16,978)	Reclus	R_1	Upper part of R_1, or reworked	3

The evolved SiO_2 rich, distal, eruptive products that we may expect to identify in the Laguna Potrok Aike sedimentary record differ significantly from the PAVF's eruptive products which are primitive. Deposits from the PAVF typically have alkaline basalt and basanite compositions, accompanied with minor olivine basalt (D'Orazio et al., 2000); the event frequency of the PAVF is poorly established as a consequence of preservation (e.g., D'Orazio et al., 2000; Coronato et al., 2013). Currently, no tephra from local PAVF eruptions have been observed in Laguna Potrok Aike; it is argued that dominating westerly winds may have prevented tephra from younger, Holocene eruptions that are from vents east of Potrok Aike from accumulating in this sequence (Kliem et al., 2013b).

1.6.3. Poncho Hill Pass, Stanley Common, and Fox Bay in the Falkland Islands

The Falkland Islands (Islas Malvinas) are located ~500 km due East from the South American mainland, and no volcanic centres are located on it. The Islands are comprised of two main landmasses: the West and East Falkland Islands, and together span a total of ~250 km from East to West. Notably, the islands are well located for the analysis of tephra because they lie

below the central jet of the Southern Westerly Winds (50-55ºS) and are located downwind of the SVZ and AVZ. Ash from the 1991 Hudson volcano eruption (~1100 km distance) caused irritation to livestock and people on the island, and thus distally travelled deposits are likely to be found in archives across the Islands (Wilson et al., 2011).

Cryptotephra (ash not visible to the naked eye) was identified on the Islands in primitive studies by Holmes et al. (1999) and Hall et al. (2001), and more recently by Monteath et al. (2019). Work by Holmes et al. (1999) and Hall et al. (2001) on the concentrations of cryptotephra identified in vertically exposed peat bogs at three sites: Poncho Hill Pass (51°36'S; 59°49'W), Stanley Common (51°42'S; 57°49'W) and Fox Bay (51°36'S; 59°49'W; Figure 1.15) indicated potential for tephra correlations between mainland South America. Geochemical analysis in these studies was rudimental, and research surrounding the technique has advanced significantly since these initial publications (e.g., Blockley et al., 2005). Thus, we re-investigate the chemistry of tephra layers in the prospect of broadening knowledge with regards to what tephra from the Andes is preserved, and how far it may have travelled. Recent work by Monteath et al. (2019) on Hookers Point (51°42′S; 57°47′W; Figure 1.15) in the Falkland Islands has identified the widespread layers: MB_1 and R_1 from Mt Burney and Reclus volcano, respectively.

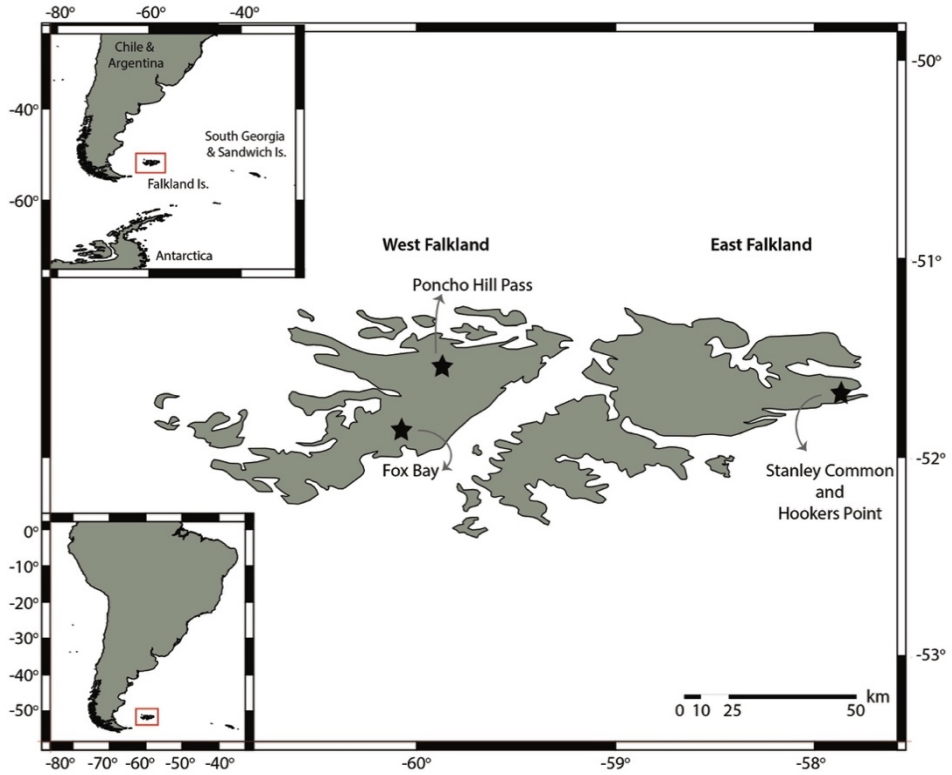


Figure 1.15. The Falkland Islands and locations of the studied sites. Inset map (bottom) shows South America; inset map (top) shows southernmost South America with sub-Andean islands. The Falkland Islands is highlighted in red in both inset maps. Stars = site locations; note that Stanley Common is geographically similar to Hookers Point, the site of Monteath et al.'s (2019) research.

1.7. Summary

This thesis aims to significantly develop the current understanding of past eruptive history in southern South America, including determining which volcanoes were erupting at what time, and whether event frequency and glass chemical compositions are affected by post-deglacial ice unloading in continental arcs.

The chapters in this thesis are presented as research articles, with abstracts at the beginning. **Chapter 1** has outlined the necessary background literature to enable a good understanding of the following chapters. **Chapter 2** represents the methods used in the articles of this thesis, including age-modelling techniques and tephra preparation. **Chapter 3** focusses on the sedimentary sequence of Lago Puyehue. It presents a new age-model for the Lago Puyehue sediments, and additionally provides a thorough overview of the visible tephra record preserved at the site and possible tephrocorrelations that may exist. **Chapter 4** investigates best practices

in representing the temporal distribution of volcanic frequency by using KDE in OxCal. Information from the literature is obtained for five well-dated tephra records of different resolution and used to form three case-study analyses of the temporal changes in volcanism at these different sites: (1) Lago Pueyhue and Mocho-Choshuenco volcano in the SVZ, Chile; (2) Taupo Volcanic Centre and Okataina Volcanic Zone in New Zealand; and (3) Mount Mazama and the region around Crater Lake, USA. A detailed tephra study of the Laguna Potrok Aike lacustrine sequence is presented in **Chapter 5** and has also been published after peer-review in Quaternary Science Reviews (Smith et al., 2019). This work also builds upon the chemical compositions of widespread events through the use of proximal deposits, allowing source information for numerous deposits in the sequence to be identified. In this chapter, ways to classify the tephra deposits depositional mechanism (i.e., reworked or primary) are also discussed. **Chapter 6** investigates the capabilities for widespread Andean tephra to be dispersed and preserved in extra-Andean localities by analysing cryptic ash layers in peat records from the Falkland Islands. In **Chapter 7**, the ages of 49 explosive and widespread volcanic eruptions across Chile are refined in a revised regional tephrochronology which utilises a very accurate approach to age-modelling. This chapter will shortly be submitted to Quaternary Geochronology. Finally, **Chapter 8** provides a discussion of the previous chapters in relation to the wider literature. It also provides a summary of the thesis which recaps on the key findings presented herein. Ultimately, this work will fill significant gaps in knowledge, and will be useful for better understanding the behaviour of Andean volcanoes.

Chapter 2
Materials and Methods

2.1. Sediment collection and laboratory treatment

2.1.1. Lago Puyehue

In the austral summer of 2001-2002, a seismic reflection study identified steep slopes, sub-basins and faults in the Lago Puyehue basin (Charlet et al., 2008). A lack of irregular reflections on the eastern and southern parts of the basin indicated that these parts of the lake were continuously infilled, uninterrupted, and away from mass wasting and turbidite deposits, and therefore ideal target locations to core from in order to obtain lacustrine sediment samples for palaeoenvironmental analysis (Charlet et al., 2008).

Sediment cores were obtained later that summer from the area (2001-2002). A UWITEC piston corer was used to obtain long sedimentary cores, and these totalled a depth of 12.22 m. Six short cores were also obtained with a UWITEC gravity corer, and combined these extend to a depth of 236 cm. Samples from the sediment cores have since been analysed for radiocarbon dating, tephra componentry and composition (Bertrand et al., 2008b), pollen (Vargas-Ramirez et al., 2008), granulometry and geochemistry (Bertrand et al., 2008a). Recent radiocarbon dates indicate that the basal sediments in the cores are ~15.5 cal ka BP in age (Bertrand, unpublished).

The Lago Puyehue sediment samples for this study were provided by Dr. Sébastien Bertrand of Ghent University, Belgium, in March and April of 2016. Contiguous 1 cm samples for the entire 12.22 m sequence were sent to the University of Oxford. The samples from Lago Puyehue are labelled for clarity using the lake record name (PUII) followed by the depth. For example, PUII_100 refers to the tephra identified in the Lago Puyehue long sedimentary record at 100 cm depth. Layers that contained visible tephra as described in Bertrand et al. (2008a) were selected for more detailed analysis than previously undertaken. This includes a coarse tephra

layer at 11.17 m depth, which was not originally reported in Bertrand et al. (2008b), but is documented in Bertrand's personal notes.

It is important to note that the 1 cm contiguous samples of the core, which were sent to Oxford, were amalgamated and therefore, samples often include lacustrine sediment. This limits the ability to undertake descriptive analysis of the individual tephra layers, including semi-quantitative analysis (e.g., abundance of differing components, including minerals, lithics and glass-shard types). However, ash from the 2011 Puyehue-Cordón Caulle eruption was deposited in Lago Puyehue via the fluvial systems reaching the lake; this layer was deposited instantaneously, and looks similar to others identified earlier in the sequence (Bertrand et al., 2014). In light of this, and because semi-quantitative analysis cannot be accurately undertaken on deposits from the Lago Puyehue sedimentary record, all tephra layers must be hypothesised to be primary ashfall and thus possible time-synchronous markers.

2.1.2. Laguna Potrok Aike

In the austral spring of 2008, the Potrok Aike Maar Lake Sediment Archive Drilling Project (PASADO) begun, using a hydraulic piston corer to obtain a long sediment core as part of an International Continental Scientific Drilling Project (ICDP; ICDP-5022). A composite profile was produced from cores obtained from site 2, labelled 5022-2CP. The 5022-2CP sequence is comprised of 101.02 m of sediment and is 106.09 m in length. There are 24 gaps, totalling 5.06 m, in the composite sequence as a result of ineffective core catchers, broken liners and a lack of sedimentary features permitting core correlation (Kliem et al., 2013b).

This composite profile has been extensively studied using a multi-proxy strategy; analysis includes, for example: stable isotopes, diatoms, pollen, rock magnetism, geochemistry, radiocarbon dating and tephra composition (e.g., Mayr et al., 2007; Gogorza et al., 2012; Recasens et al., 2012; Jouve et al., 2013; Kliem et al., 2013b; Wastegård et al., 2013; Hahn et al., 2014). Twenty-four visible ash layers were observed in the 5022-2CP composite record, and eighteen of these were chemically analysed (Kliem et al., 2013b; Wastegård et al., 2013). These

tephra units were up to 50 cm thick, often having coarse bases, and containing both light coloured and black clasts. Kliem et al. (2013b) found that these horizons contained glass shards, amorphous clasts, pumice, and minerals.

Fifty-eight samples of carbonates, organic macrofossils, and bulk sediments throughout the composite sequence have been radiocarbon dated (Kliem et al., 2013b). Modern aquatic plants were radiocarbon dated to determine if there was a hard-water effect (Chapter 1), but these were not contaminated with old carbon, and there are also no carbonates in the catchment; as such, it is deemed that there is no hard-water effect at Laguna Potrok Aike (Haberzettl et al., 2005). Infrared Stimulated Luminescence (IRSL) age-measurements were obtained by Buylaert et al. (2013), but these were from the non-composite record (site 1, core 1D) and difficult to transfer to the composite sequence and these were therefore not used in the initial age model. Most of these IRSL measurements have subsequently been transferred to the composite core via correlation of distinct layers (ash layers, clay caps of turbidites and sand layers) and are used in a new age model by Gebhardt and Ohlendorf (2019). This new age-depth model for the entire Potrok Aike sequence includes a combination of age-data to constrain the sedimentary archive, including IRSL measurements, known eruptive ages for tephra deposits, and tuning of magnetic susceptibility data between Laguna Potrok Aike and the Sint-800 stack (a globally stacked record of 33 geomagnetic field palaeointensity variations over the past 800 kyr; Guyodo and Valet, 1999) (Gebhardt and Ohlendorf, 2019). This new age model places the base of the sequence at ~80 kyr BP (Gebhardt et and Ohlendorf, 2019).

2.2. Tephra preparation and analysis

Tephra layers were prepared using procedures outlined below, and are only slightly different for the different sequences studied.

2.2.1. Tephra extraction

2.2.1.1. Lago Puyehue

Samples obtained from the top 100 cm of the lake core were treated in accordance to the soil Food and Environment Research Agency (FERA) license held by the Research Laboratory of Archaeology and the History of Art (RLAHA), University of Oxford. These sediment samples were placed in a 15 ml conical test tube, placed in a fume cupboard, and covered in 10 % Hydrochloric (HCl) acid. The samples were left for 2-4 hours and then were agitated. If there was still any reaction (effervescence), up to 5 ml more of HCl was added and the sample left for another 2 hours. The sample was considered to be sterile when the reaction had stopped, and at this point, tephra extraction began. During this process, all equipment used was cleaned using demineralised water and lint-free tissues, and any disposables with sample material attached was placed into clinical waste for incineration. Sterile samples were subsequently treated as per all visible tephra units in this thesis (See Sections 2.2.2 and 2.2.3).

In addition to this, three samples of lacustrine sediment at 292-293 (nearest tephra above: 260.5 cm, nearest tephra below: 323.6 cm), 781-782 (nearest tephra above: 773.8 cm, nearest tephra below: 836.2 cm), and 804-805 (nearest tephra above: 773.8 cm, nearest tephra below: 836.2) cm depth were investigated to determine the concentration of glass-shards in the background sediments. The samples were prepared as per Sections 2.2.2 and 2.2.3.

2.2.1.2. Laguna Potrok Aike

At the onset of this project, it was intended to investigate the invisible ash layers (cryptotephra) of the Laguna Potrok Aike sequence. As such, in 2016, L-channels were collected from the Laguna Potrok Aike sedimentary sequence, stored at Bremen University in Germany, so as to preserve the integrity of sediments. During this trip, numerous speculative visible tephra layers were observed across the 11 sediment cores obtained; these layers were collected using a spatula and/or scalpel before being placed in labelled plastic sample bags. The identification of many speculative visible tephra that had not previously been identified caused concern for a

cryptotephra based analysis of the Laguna Potrok Aike sediments, and thus it was decided to instead focus on fully investigating the visible tephra record to establish a record of volcanism for the archive.

During a second trip to Bremen University in 2017, 67 core sections (core 1: 2C-1H-1A to core 67: 2C-22H-1A) were opened and assessed for the presence of visible tephra. Visible tephra layers, or samples that had the characteristics of a visible tephra (e.g., particularly coarse or fine grained material and sediment with notable colour changes), were processed as per the speculative visible tephra obtained during analysis of cores in 2016. Every speculative visible tephra layer from the Laguna Potrok Aike sequence was subsequently processed as per Section 2.2.2. All tephra layers are referred to as LPA_m-cd with the composite depth (cd) quoted in metres and representing the uppermost boundary of the horizon.

2.2.1.3. Falkland Islands

Glass-slides that contain volcanic glass-shards from Poncho Hill Pass, Stanley Common and Fox Bay were obtained from Dr. Jane Holmes, via Dr. Gill Plunkett of Belfast University, Northern Ireland, to further investigate the tephra that were documented in published research (Holmes et al., 1999; Hall et al., 2001). The samples mounted on the slides provided do not necessarily relate to the highest glass-shard concentrations identified in Hall et al. (2001) and Holmes et al. (1999); it is not clear why the highest concentrations were not selected for detailed chemical analysis (i.e., mounting) by Hall et al. (2001) and Holmes et al. (1999), but it is likely that all shards were prepared for analysis to determine whether glass-shards were reworking of an isochron or evidence of low-level concentration cryptic tephra being deposited over the islands.

The glass-slides were re-polished using increasingly finer grades of diamond suspensions (3 and 1 μm). To avoid contamination, the glass-slides were cleaned in a beaker filled with demineralised water which was placed in a sonic bath for several minutes between each polishing-stage. Finally, the glass-slides were placed in a beaker filled with Petroleum Ether which was

inserted into a sonic bath for five minutes to thoroughly clean them; they were dried with lint-free tissue before being coated in carbon (Figure 2.1). They were subsequently chemically analysed as per Section 2.4.5.

2.2.1.4. Proximal tephra analysis

Terrestrial tephra samples were obtained from 14 sites across southernmost South America (Table 2.1; Chapter 5). These samples were supplied by Prof. Charles Stern of Colorado University, USA. These samples had previously been analysed for bulk chemical composition and the sources of these tephra layers were already established and in most cases published (Table 2.1). However, because bulk chemical compositions cannot easily be compared with individual grain glass-shard chemical compositions, the glass-shards were analysed using techniques described in Section 2.4. The samples were prepared as per Section 2.2.2.

Table 2.1. Widespread tephra samples analysed in this thesis. See Figure 5.1 for site location on map.

Volcano	Marker horizon or age (AD)	Label	Site	Location	Archive	Thickness (cm)	Reference	Previous geochemical analysis	Reference in Figure 5.1
Aguilera	A_1	93-03	Lago Roca	50º22'S; 72º45'W	Bog peat	10	Stern, 2008	Bulk and glass EMPA major elements/ Trace elements	1
	MB_2	90-16	Altos de Boquero n (TDF)	53º17'S; 70º10'W	Bog peat	2	Stern, 1992; Stern, 2008	Bulk trace elements	2
	MB_2	93-07(-2)	Lago Parillar	53°26′S; 71°05′W	River sediment	4	Stern, 2008	Bulk trace elements	3
Burney	MB_1	BF-370cm	Rio Rubens	52º02'S; 71°57'W	Barking Fox bog core	10	Markgraf (pers comms) in Stern, 2008		4
	MB_1	Laguna Tom Gold	Laguna Tom Gold (TG1)	52º09'S; 69º56'W	Site excavatio n	5-10	Massone, 1989; Stern, 2008	Bulk trace elements	5
	MB_1	93-21W	Chico river (TDF)	53º33'S; 68º42'W	Bog peat	1	Stern, 2008		6
	MB_1				Unknown	4			NA

Volcano	Marker horizon or age (AD)	Label	Site	Location	Archive	Thickness (cm)	Reference	Previous geochemical analysis	Reference in Figure 5.1
Reclus	R_1	90-06 R1-RioTurbio	Pampa Alegre (Rio Seco)	53º04'S; 70º51'W	Fluvial-glacial sediment	6	Stern, 1992; Stern, 2008	Bulk trace elements	7
	R_1		Rio Turbio	51ºS; 72ºW	River sediment	Unknown	Unreported		8
	R_1[1]	90-01	Rio Tres Brazos (PB)	53º16'S; 71º02'W	Bog peat	1	Stern, 1992; Stern, 2008	Bulk trace elements	9
	R_1				Unknown 1				NA
	R_1				Unknown 2				NA
	R_1				Unknown 3				NA
Hudson	H_2	H2_Q_60-85	Lago Quijada	45°43'S; 71°54'W	Lacustrine sequence	24	Weller et al., 2014, 2015	Bulk trace elements	10
	H_2	H2_E_0-30	Lago Espejo	45°52'S; 72°1'W (Chile)	Lacustrine sequence	53	Weller et al., 2015	Bulk trace elements	11
	H_1	93-21G	Chico River (TDF)	53º 33'S; 68º42'W	Bog peat	20	Stern, 2008		6
	H_1	RI-16II	Río Ibáñez, Aisén	46°19'S; 71°54'W	River sediment	Unknown	Stern, 2008		12
Lautaro	1959/60?	VT1	Laguna Verde	49°20'S; 72°98'W	Lacustrine	5	Mayr et al., 2019	Glass EMPA major elements	13
	1933?	VT2	Laguna Verde	49°20°S; 72°98'W		3			13
	1876/78?	VT3	Laguna Verde	49°20°S; 72°98'W		6			13
	1536-1669[2]	VT4	Laguna Verde	49°20°S; 72°98'W		1			13
	1959/60?	GT2	Laguna Gemelas	49°39'S; 72°90'W		4			14
	1876/78?	GT3	Laguna Gemelas	49°39'S; 72°90'		5			14
Viedma?	1963/1964?	GT1	Laguna Gemelas	49°39'S; 72°90'W		5			14

[1] Sample R1-90-01 was reported as A_1 (Aguilera) in Stern (2008), but this was a geochemically unconfirmed correlation.

[2] Extrapolated age

2.2.2. Sieving and isolating tephra

Visible tephra samples from lacustrine sediments were wet-sieved using 25 μm nylon mesh and demineralised water. Tephra samples from proximal (terrestrial) environments were

gently crushed with a pestle and mortar before being wet sieved using 80 μm nylon mesh and demineralised water.

Newly identified tephra layers from Laguna Potrok Aike only were additionally processed using heavy density extraction methods due to a relatively low abundance of glass-shards in some samples. This method involves using a heavy density liquid, Sodium Polytungstate ($Na_6[H_2W_{12}O_{40}]$), to firstly remove organic material and then to isolate the glass-shards, using the densities: 2.0 g cm^3 and 2.5 g cm^3 for each step, respectively. Typically, material is firstly digested in 10 % HCl, but the samples were not particularly organic-rich, and this step was thus not deemed necessary; the full method is outlined in Blockley et al. (2005).

2.2.3. The production of resin stubs

After sieving/extracting, tephra samples were oven-dried at 50 °C and stored in labelled 5 ml storage tubes before being mounted on blocks capable of holding several samples (e.g., Froggatt and Gosson, 1982; Lowe, 2011). Struers SpeciFix 20 or EpoFix 20 Epoxy resin was used to backfill the holes and the blocks were cured for 24 hours. The shards in the block were sectioned by hand in order to expose the fresh surfaces using progressively finer Silicon Carbide grinding paper (P1200, P2500, and P4000). The resin block was then machine-polished on a Logitech PM2A using increasingly finer grades of diamond suspensions (3 and 1 μm). To avoid contamination, the block was cleaned in a beaker filled with demineralised water placed in an ultrasonic bath for several minutes between each polishing stage. Blocks were finally placed in a beaker filled with Petroleum Ether which was placed in a sonic bath for five minutes in order to thoroughly clean them; they were dried with lint-free tissue before being coated in carbon (Figure 2.1).

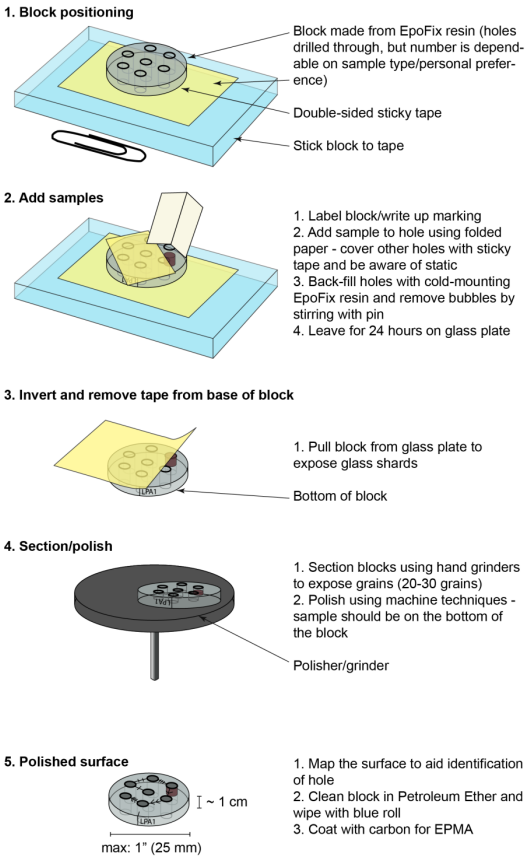


Figure 2.1. Illustration demonstrating preparation and procedure for mounting visible samples of glass shards in Epofix resin blocks for analysed by EMP (after Lowe 2011).

2.3. Visual analysis of glass-shards and/or minerals

To better understand the extracted tephra samples and their componentry, they were studied using binocular microscopy to assess the various constituents outlined in the sections below.

2.3.1. Glass-shard abundance

The abundance of glass-shards, minerals, lithics, and organic material was classified using semi-quantitative techniques as per Figure 2.2. Since the Lago Puyehue core samples were taken from contiguous 1 cm samples and included both tephra and sediment (Section 2.1.1), this step was only undertaken on material sampled from the Laguna Potrok Aike cores (Section 2.1.2).

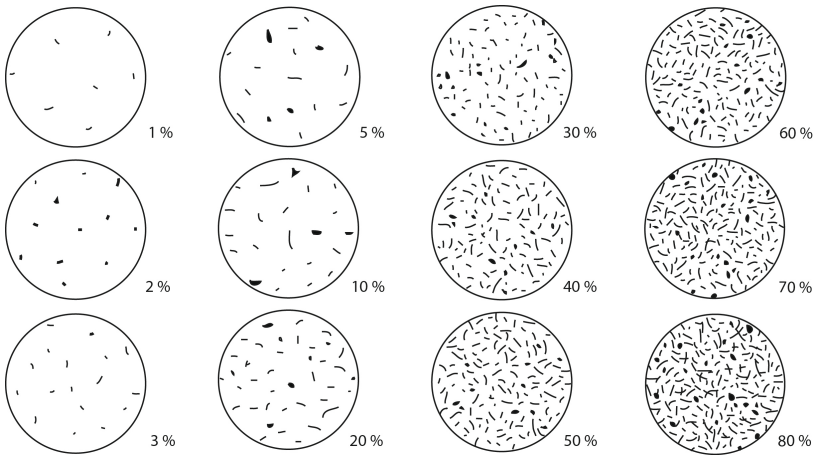


Figure 2.2. Percentages and approximate material appearance for semi-quantitative analysis of samples (after Terry and Chilingar, 1955).

2.3.2. Glass-shard morphology and colour

Glass-shard morphology and colour was described in order to better characterise the tephra layer and assess variations between eruptions and volcanic sources (Figure 2.3). The data was also intended to provide further information regarding the depositional nature of the tephra (e.g., primary or reworked), with occurrences of different glass-shard morphologies from underlying layers being particularly indicative of primary ashfall.

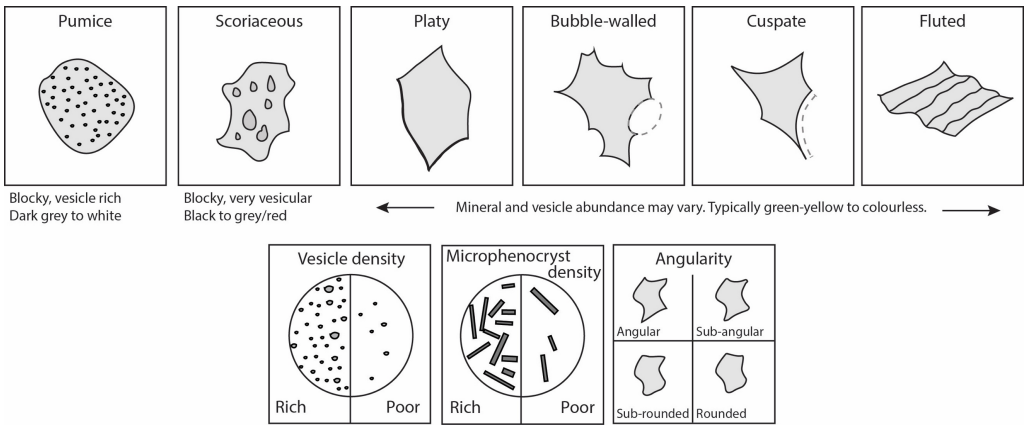


Figure 2.3. A schematic representation/classification guide of the glass-shard morphologies, microphenocryst and vesicle content, and angularity identified during investigation.

2.4. Compositional analysis of tephra

2.4.1. Overview of EDS-SEM and WDS-EMPA

Determining the chemical composition of volcanic glass-shards is essential to fingerprint individual tephra deposits and to subsequently determine the eruptive source. This analysis is typically undertaken using Wavelength Dispersive Spectroscopy-Electron Microprobe Analysis (WDS-EMPA), but it can also be undertaken using Electron Dispersive Spectroscopy-Scanning Electron Microscopy (EDS-SEM).

In both methods elemental analysis is obtained by the collection of characteristic X-rays that are generated when an electron beam bombards a sample (Reed, 2005). This primary electron beam causes the atoms in the sample material to be ionised by exciting and ejecting electrons from the inner shells of the atoms. Atom stability is regained by electrons from the outer shells refilling the inner shell vacancies. This process is associated with the emission of electromagnetic radiation in the form of X-rays. The energy of these characteristic X-rays is determined by the energy difference between the electron shells, electron spin, and the number of protons in the nucleus of the atom and is therefore dependent on atomic number and the specific shells involved in the electronic transition. The main difference between methods is therefore the X-ray spectrometer type: one collects the energy spectrum (EDS), while the other collects specific X-rays (WDS).

In this thesis, EDS-SEM analysis was used to ground-truth visual mineral identification undertaken through binocular microscopy while WDS-EMP was used to quantitatively analyse the chemical composition of individual glass-shards. Back-scattered electron and secondary electron (BSE and SE) images of both glass-shards and minerals were also taken. This section describes the theory behind EDS-SEM and WDS-EMPA, and the conditions used during analysis.

2.4.2. EDS-SEM theory

A tungsten filament located in the electron gun is heated, and this causes the filament to emit electrons. A fine-focussed beam is produced by the acceleration of electrons through the

column using a 5 to 30 kV accelerating voltage, and the electrons are focussed towards the sample through a series of electromagnetic lenses. The fine-focussed beam bombards the sample, and the final beam diameter is typically 1 micron.

Various forms of radiation are formed by the interaction of the electron beam with the sample. These include secondary electrons, characteristic X-rays, auger electrons (i.e., electron bombardment causes energy to be transferred to an electron in the outer shell, ejecting it from the atom), backscatter electrons, and ‘‘bremsstrahlung’’ X-rays (i.e., continuous/background X-rays); the characteristic X-rays are dependent on the chemical composition. The energy dispersive X-ray spectrometer records X-rays of all energies simultaneously, producing output plots of photon energy versus intensity.

SEM images, which provide a representation of the surface morphology of the sample, are produced by the collection of the secondary electrons generated when this internal electron beam scans across the sample. By contrast, BSE images allow for the observation of compositional differences in the sample since they are the result of atomic number contrast; brighter images indicate a heavier atomic number (Welton, 2003; Reed, 2005).

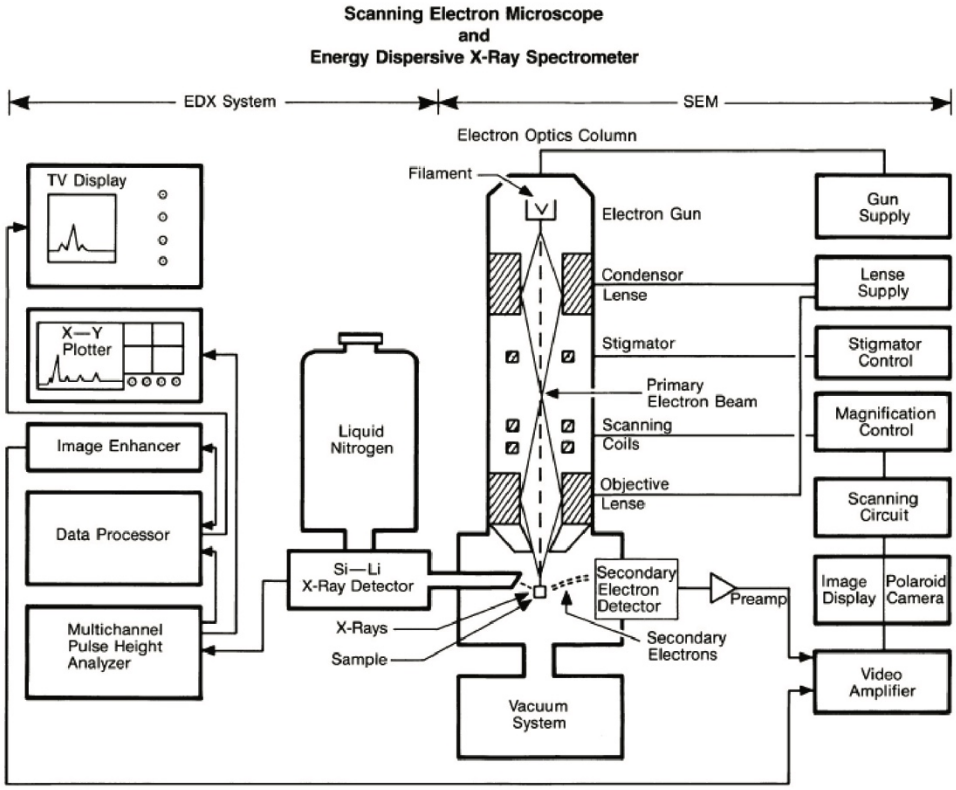


Figure 2.4. Schematic diagram illustrating a typical EDS-SEM system. Source: Welton (2003).

2.4.3. EDS-SEM operating conditions and methodology

Samples for SEM analysis were prepared as per Section 2.2.3. Prepared samples were placed into the sample chamber of the instrument, which was then evacuated to a high vacuum (~$2x10^{-6}$ Pa) for analysis. Factors which affect analysis include dead-time (defined as the time interval after the arrival of a pulse, after which the detector is unresponsive to further pulses, resulting in lower than actual count-rates; Reed, 2005), specimen topography, detector geometry and sample coating; these factors were all taken into account during instrument set-up.

All EDS-SEM analysis in this study was undertaken using an JEOL JSM-5910 SEM with INCA software. An accelerating voltage of 15 kV for the analysis of tephra and minerals was used, with a count time of 100 s to acquire sufficient X-rays of the major elements. A deadtime of lower than 30 % was achieved at all times during analysis and was typically ~15 %. A working distance of 11 mm was set during analysis, allowing the most X-rays to be captured.

All resin blocks were coated in carbon to an optimum thickness of ~20 nm prior to analysis (section 2.2.3) and secured in the sample holder with carbon putty. Small amounts of carbon tape were added to the top of the blocks adjoining the metal holder to prevent sample charging. Calibrations were not performed as the SEM was used for mineral identification and imaging (BSE) only.

2.4.4. Wavelength Dispersive Spectroscopy-Electron Microprobe Analysis (WDS-EMPA) theory

Wavelength-dispersive spectrometers use synthetic crystals (e.g., LiF, TAP, PET) with well-defined spacing (d) in the crystal lattice to diffract X-rays emitted from the sample (Figure 2.5). This diffraction follows Bragg's law ($n\lambda = 2d \sin\theta$), which describes the scattering (angle of incidence, θ) of X-rays of a given energy and thus wavelength (λ). Moving the position of the crystal within the spectrometer changes the angle of incidence (θ) and therefore enables the analysis of different elements emitting X-rays with a certain wavelength (λ) (Reed, 2005).

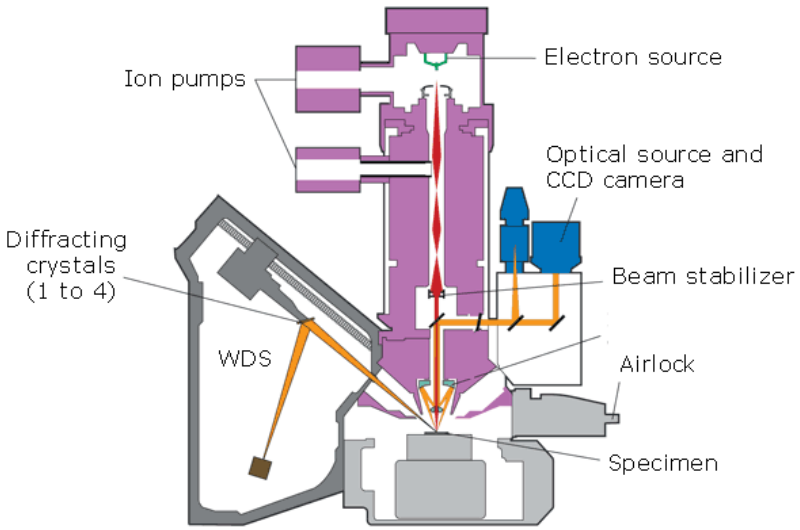


Figure 2.5. Schematic diagram illustrating a typical WDS-EMPA system. Source: Heath (2015).

The accuracy of WDS-EMPA can reach ±1 % (relative) for major elemental analysis and detection limits down to tens of parts per million (by weight) can be obtained, and this is considerably better than analysis via EDS (Reed, 2005). In order to determine the measurement

of error in the instrument, it is essential to undertake calibrations; the ratio of the intensity of X-rays in the unknown sample to that of the intensity of the standard should be (approximately) equal to the ratio elemental concentration in the unknown to that of the standard (Goldstein et al., 1992). Primary standards that are of a similar composition to the unknowns, or are very well characterised, should be used in order to avoid large extrapolations.

The process of calibrating becomes complicated when dealing with samples more than a few microns thick and containing multiple elements. Matrix corrections are utilised to overcome this. The ZAF matrix correction is commonly used, whereby *Z* refers to processing atomic number effects, *A* refers to the absorption correction applied, and *F* refers to fluorescence (Goldstein et al., 1992). In this thesis we used a modified ZAF matrix correction called PAP (Pouchou and Pichoir, 1991). Secondary standards were also used to calibrate the microanalytical technique and permit analytical quality checks. In this thesis, MPI-DING reference glasses were used; chemical analyses of the reference glasses fall within two standard deviations of the preferred values reported in Jochum et al. (2006).

2.4.5. WDS-EMP operating conditions and methodology

In this thesis, the major element composition of glass-shards was obtained using the same method throughout. Glass-shards were analysed at the Research Laboratory for Archaeology and the History of Art, University of Oxford, using a wavelength-dispersive JEOL JXA-8600 electron microprobe (EMP) equipped with four spectrometers, and an accelerating voltage of 15 kV. Shards were predominantly analysed with a low beam current of 6 nA and a 10 μm beam diameter; very small shards were analysed with a 5 μm beam, and a 4 nA current. Thirty shards were analysed for each sample where possible.

Sodium (Na) was analysed first to minimise element loss due to migration. Elemental peaks were collected for a total of 60 s (P), 50 s (Cl), 40 s (Mn), 30 s (Si, Ca, K, Al, Ti, Fe, Mg), or 12 s (Na) and for half of the total peak time on each of the background positions on either side of the peak. Prior to analysis, the EMP was calibrated for each element using primary mineral

standards. To verify the calibration, Max Planck Institute reference glasses (MPI-DING) were used as secondary standards; StHs6-80/G, ATHO-G, and GOR132-G (Jochum et al., 2006) were analysed at the beginning, during and at the end of all sample runs. The averaged values of these lie within two standard deviations of the preferred values (see Jochum et al., 2006).

Preferable total values for unknown samples are ≥95-100.5 wt% (e.g., Shane, 2000; Lowe, 2011; Fontijn et al., 2016). To maximise the retention of analyses where devitrification has started to occur, lower total values of >94-100.5 wt% are considered acceptable (Shane, 2000; Fontijn et al., 2016). Microphenocrysts, vesicles and resin were avoided during analyses. To account for variable secondary hydration, data was normalised to 100 wt%. Individual glass-shard chemical analyses are shown as biplots, particularly using SiO_2/K_2O, as potassium is the most distinguishing element of SVZ and AVZ deposits due to along-arc variations in the potassium composition of the melt (Kilian et al., 2003; Stern, 2008; Wastegård et al., 2013).

2.5. Distinguishing secondary deposits from primary deposition events

Determining how tephra is deposited is important because reworked tephra horizons should i) not be used as regional marker horizons, and ii) over-thickening or multiple units of a single eruption deposit can give erroneous estimations of the past frequency and/or magnitude of eruptions.

Samples from Laguna Potrok Aike were analysed under a binocular microscope prior to chemical analysis to evaluate the relative abundance of glass-shards, organic and detrital material. Glass-shard morphology, angularity (Figure 2.3), and colour were also described. The dominant minerals present were additionally noted, including whether minerals predominantly had preserved or degraded glass-coatings. These data (in addition to chemical analyses; Section 2.4) were used to provide detailed further information on the depositional nature and help distinguish between primary or reworked events (e.g., McLean et al., 2018) in Laguna Potrok Aike. The glass chemical composition of deposits, including for example normalised compositional totals and unusual abundances of certain elements, such as overly high silica and depleted sodium, may

indicate aeolian reworking; unaltered glass-shard chemistry may indicate erosional reworking (e.g., Monteath et al., 2019).

Notably, the distinction between primary and reworked tephra layers was determined using a point-based criteria. Points relate to indicators of reworking, and deposits which had three or more points relating to reworking characteristics (below) were considered as reworked. Before concluding the classification, these deposits were also considered as a whole afterwards (e.g., appearance in lithology, including contact, and previous reports on layer). The criteria that were used are as follows, and deposits received one point for each of these characteristics identified:

- minerals in the sample are rounded or sub-rounded;
- minerals have no glass coating, or glass-coating is degraded;
- glass-shard abundance is low (≤60 %);
- high abundance of organic material (≥5 %);
- high abundance of detrital material (≥10 %);
- chemistry of glass-shards is the same as those in the tephra layer/s below.

2.6. Bayesian age modelling in OxCal 4.3

In this thesis, OxCal 4.3 (Bronk Ramsey, 2009a) is selected as an age-modelling tool. OxCal is chosen because of its easy-to-use interface, regular updates and good chronological constraints (e.g., Trachsel and Telford., 2017). In general, age-models have a number of possible outcomes to consider, and thus Markov Chain Monte Carlo (MCMC) methods are often used; OxCal is no exception; each iteration of the MCMC provides a possible solution of all the model parameters, resulting in the most likely age-estimates (Bronk Ramsey, 2009a). OxCal allows for the production of different types of models, and chiefly these are: age-depth (or depositional), and phase. The former is typically used in instances where both age and depth data are available, such as a lacustrine sequences. Phase models are typically used in instances whereby the age of deposits may be known, but only data on their stratigraphic position is available, such as

stratigraphic outcrops or archaeological sequences. For the purposes of this thesis, we utilise both types of model in OxCal.

2.6.1. Age-depth (depositional) models in OxCal 4.3

When producing a depositional model in OxCal, the type of depositional process needs to be selected:

- uniform sedimentation (*U_Sequence*);
- variable sedimentation (*P_Sequence*); or
- processes used only where there is an age gap between two points, for example, varved sediments or tree rings (*V_Sequence* - varves; *D_Sequence* - tree rings)

The use of the *P_Sequence* allows interpolation of the sedimentation rate along the sequence and is the recommended method for age-depth modelling of lacustrine sediments since a minority of these archives have linear deposition; this Bayesian function follows Poisson law and subsequently assimilates sedimentation as a random process (Bronk Ramsey, 2009a). Sedimentation regularity is subsequently determined by the *k* parameter whereby the higher the *k* parameter, the more linear the deposition is along the sequence. The *k* parameter is typically 1.

To generate an age-depth model in OxCal, one must add data in the form of commands, including for example: uncalibrated ^{14}C ages (*R_date*), OSL dates (*C_date*), and/or historical dates; each of these inserted commands will also require a corresponding depth (*Position*), and this is ideally event-free (i.e., turbidities and tephra deposits are removed). The model determines the calibrated age of each uncalibrated date following the regularity of the sedimentation (Pouderoux et al., 2012) with associated probability ranges: 68.2 % and 95.4 %. Once the dates are returned, an agreement index for individual radiocarbon ages is produced. This is calculated from the Probability Density Function (PDF) of the calibrated radiocarbon age and the PDF of the modelled ages at the same depth - if the probability density of both aspects is simultaneously high, then A (Agreement) is typically >100 %; if it is not simultaneously high, then A is typically

<100 %. An individual agreement index is calculated (called $A_{overall}$), in addition to an overall agreement index for the age-depth model (called A_{model}) and this is a calculation of the geometric mean of the agreement of individual dates (Trachsel and Telford, 2016); A_{model} is preferred (Bronk Ramsey, 2009a). In essence, the A_{model} is a measurement of the agreement between the model and the observational data that has been included as a percentage (Bronk Ramsey, 2009a). Typically the A_{model} should be >60 %. This can, however, be ignored entirely if a model is run with outlier analysis since using outlier analysis means that dates that do not conform with the rest of the model are downweighted; the modelled results thus form an average between a model whereby the measurement/s (outlier/s) are accepted and one in which they are rejected (Bronk Ramsey, 2009b).

2.6.2. Phase models in OxCal 4.3

Phase models are used to constrain the timing of events in a sedimentary archive where the deposition rate is unknown and where there are multiple dates for single events. Typically phase models are distributed uniformly (e.g., bounded by a start and end boundary), but other boundaries are available (e.g., Tau, Sigma and Zero) which may be more useful if the frequency of events is variable at the start or end (Bronk Ramsey, 2009a). The coding within a phase model can produce phases which are: contiguous, sequential, or overlapping, and the flexibility of these model options allow for event timings to be well-constrained when modelling the ages of cultural transitions, or a sequence of eruptive deposits, for example.

2.6.3. Kernel Density Estimations in OxCal

Both frequency histograms and Kernel Density Estimations (KDE; data smoothing) are non-parametric tests, which is to say that the data's distribution is not pre-assumed in the analysis. However, unlike a frequency histogram, KDE generate a PDF (i.e., the expression of the likelihood of the sample) of random variables which produces data smoothing on a finite population dataset (e.g., Parzen, 1962; Chapter 4). KDE statistics were recently introduced to the age modelling programme, OxCal; the use, mathematics surrounding, and application of

KDE_Plot is discussed in Bronk Ramsey (2017). In essence: KDE is a frequentist approach (i.e., the probability is expressed as the limit of its relative frequency in a large number of trials) which can now be applied within a Markov Chain Monte Carlo (MCMC; i.e., methods for sampling from probability distributions) simulated Bayesian framework (i.e., the probability is updated as more information/data is supplied). In archaeology, the application of KDE in OxCal can be useful to research the timing or emergence of a particular society, for example. In this thesis, KDE is utilised to investigate best practises in investigating the timing of volcanic events. Because the method allows the calculation of temporal changes in eruptive frequency while acknowledging the statistical spread of eruptive ages, it may be more beneficial than other frequency analysis functions. For this work (Chapter 4), three case studies of data from five records are selected for KDE analysis; these represent different temporal records and have excellent chronological data associated with them (Section 1.6).

The command used in OxCal to conduct KDE analysis is: *KDE_Plot.* This can be used to provide the probability distribution of the OxCal model in instances where there are dates of event/s which is/are unknown. The *KDE_Plot* function can be used within both phase and age-depth models (Bronk Ramsey, 2017). In this thesis, KDEs are applied to determine the probability distribution of volcanic events per year to better understand eruptive frequency. *KDE_Plot* can be inserted after the *P_Sequence* in the case of age-depth models, or after *Sequence* in the case of phase models (Section 1.1.2). Tephra of interest in the *KDE_Plot* can then be cross-referenced to the tephra listed in the *P_Sequence* or *Sequence* (i.e., the age-model) to permit statistical analysis (i.e., the KDE). Furthermore, events that cannot to be inserted into the age-model because of insufficient information (e.g., depth or age) can still be inserted into the *KDE_Plot* by adding a *Sequence()* within a *KDE_Plot*; the tephra need not be cross-referenced, but a prerequisite is knowledge of relative stratigraphic position.

2.6.3.1. Eruptive flux calculations

Eruptive flux calculations were determined by summing the effusive and explosive masses in 0.5 ky bins, using deposit volumes and age probability distributions, as per Rawson et

al. (2016). Magma densities were assumed based on deposit composition, with ~1500 kg/m^3 for deposits of mafic (basaltic andesite) composition, and ~1000 kg/m^3 for silicic (dacite-rhyolite) deposits. Masses for deposits from Mocho-Choshuenco were obtained from Rawson et al. (2015) while masses for deposits from New Zealand events (from Okataina and Taupo Volcanic Complex) were obtained from Smith et al. (2005). The erupted mass was calculated by using the calculation: erupted mass (kg) = DRE (m^3) * magma density (kg/m^3).

Finally, to fully calculate eruption flux:

1. The age of each tephra was described as a PDF from Bayesian analysis, and the probabilities (i.e., area within the curve) all sum to one.
2. For each tephra deposit, the area of the probability distribution was scaled to the deposit mass.
3. The flux was smoothed by dividing the scaled area into 0.5 kyr bins for each deposit.
4. The areas (mass/kyr) for all deposits were then summed within each 0.5 kyr bin, and a curve drawn through the midpoint value for each bin, providing the approximate magma flux.

2.6.4. Conditions for OxCal age models used in this thesis

The parameters selected for age modelling should be tailored to the environment that is under investigation. This section describes the conditions used in OxCal models through this thesis, and the rationale behind this.

2.6.4.1. Lago Puyehue

The chronology of Lago Puyehue is outlined fully in Chapter 3 (Supplementary Data S.1). Sensitivity analysis was conducted in OxCal 4.3 to develop the most effective model. An age-model for the sediments produced by S. Bertrand was compared with five age-depth models produced in these thesis. These included variable parameters, including the i) removal of obvious

outliers, ii) application of age offsets as defined by Bertrand et al. (2012) and S. Bertrand (pers comms), iii) application of event-corrected ages, iv) outlier analysis, v) application of ^{210}Pb dates, vi) the application of historical tephra dates. In Chapter 4, Kernel Density analysis was applied to the age-model using the *KDE_Plot()* function, and tephra units were cross-referenced to their positions in the age-model (Supplementary Data S.2.1).

2.6.4.2. Laguna Potrok Aike

The chronology of the Laguna Potrok Aike sedimentary sequence was derived from Gebhardt and Ohlendorf (2019*;* see Section 2.1.2; Chapter 5). KDE was not applied to this sedimentary sequence.

2.6.4.3. Poncho Hill Pass, Stanley Common, and Fox Bay in the Falkland Islands

Due to insufficient chronological data, an independent age-depth model could not be produced for the sites of Poncho Hill Pass, or Fox Bay. A crude age-depth model was produced for Stanley Common in OxCal 4.3 (Bronk Ramsey, 2008; Supplementary Data S.4.1). This was created using a *P_Sequence* and placing boundaries at the 'top' and 'bottom' which were representative of the uppermost and lowermost identified sediment. The most well-regarded ages of the widespread volcanic ash layers identified in Stanley Common were then imported using the *Date()* function (e.g., Date("H2",N(calBP(3920),50))). Outlier analysis was applied at 0.05 likelihood (i.e., 5 % likelihood that the age information supplied was an outlier). This permitted an approximation of the sediment accumulation rate (Chapter 6).

2.6.4.4. Mocho-Choshuenco

The (phase) age-model for Mocho-Choshuenco was derived from Rawson et al. (2015). Kernel Density analysis was subsequently applied to this phase model by using the *KDE_Plot()* function at the bottom of the age-model script and by using the cross-referencing function (=),

allowing the 32 tephra units in the age-model to be outputted as a KDE plot (Supplementary Data S.2.2).

2.6.4.5. Okataina Volcanic Complex (OVC) and Taupo Volcanic Centre (TVC)

To develop a *KDE_Plot* that shows the frequency of volcanism from the TVC and OVC over the past 50 ky, a composite model was produced using data from the Kaipo Bog sedimentary sequence (Lowe and Hogg, 1986; Lowe et al., 2013), and terrestrial sequences (Froggat and Lowe, 1990; Smith et al., 2005). In both the age-model for TVC and OVC, tephra layers were inserted into the model using the *Sequence()* function of OxCal (35 layers for TVC and 26 for OVC). Kernel Density analysis was subsequently applied to this age-model by using the *KDE_Plot()* function at the bottom of the age-model. Occurrences of tephra units in the age-model which had individual dates were cross-referenced (=) in the *KDE_Plot* (Supplementary Data S.2.3, S.2.4).

2.6.4.6. Mount Mazama and the Crater Lake Region

Data for Mount Mazama and the Crater Lake region was obtained from Bacon and Lanphere (2006). This was separated into pre-Mazama volcanics (<420 ka) and Mount Mazama volcanics (i.e., >420 ka) based on the eruptive periods defined by Bacon and Lanphere (2006). This separation is made because the pre-Mazama volcanics do not represent eruptive deposits from Mount Mazama, and rather show activity that occurred before the development of the Mazama edifice (Bacon and Lanphere, 2006). Bacon and Lanphere (2006) also describe eruptive deposits that are not from Mount Mazama, but from other cones and centres in the region (regional volcanics); these units could not be modelled here because there are insufficient chronologic or stratigraphic constraints.

The pre-Mazama and Mount Mazama volcanic datasets were modelled together using the *KDE_Plot* tool. Similarly to Sections 2.6.4.4 and 2.6.4.5, the data involved in the KDE was cross-referenced (=) to data utilised in the age model. Some deposits did not have chronological

information, and thus were constrained only by stratigraphy. The Mount Mazama volcanic dataset was also modelled separately to better determine subtle variations in the temporal distribution of deposits on a shorter time-series (Supplementary Data S.2.5).

2.6.4.7. Regional Age Model

A regional age model was developed using a sequential phase model in OxCal 4.3 (Bronk Ramsey, 2008). This is further explained in Chapter 7 (Supplementary Data S.5).

Chapter 3

Investigating the tephra record of Lago Puyehue, Chilean Lake District

Abstract

This chapter outlines the chronology of the Lago Puyehue sedimentary record and the detailed methods behind this; the selected age-depth model for the sedimentary sequence is ran on the calibration programme OxCal 4.3 (Bronk Ramsey, 2009a) using event-corrected depth, outlier analysis, ^{210}Pb measurements, and historical tephra layers. Seventy-nine tephra layers from the Lago Puyehue sedimentary sequence are described, and where possible, their chemical signature is used to determine their source affinity. In many instances, the overlapping, complex compositional fields of deposits from the Southern Volcanic Zone, in addition to the overall heterogeneity of deposits identified in Lago Puyehue, complicates tracing units to source. Four tephra units have been associated with regional marker horizons: PCC1, PCC4 and Mil Hojas from Puyehue-Cordón Caulle; and Cha1 (also called Chana) from Chaitén volcano. We identify no obvious relationship between climate and temporal changes in the composition of melt and/or frequency of events at Lago Puyehue despite the local and regional trends being observed by Rawson et al. (2016) and Fontijn et al., (2016).

3.1. Introduction

Sites in Chilean Patagonia are generally regarded as having a poor tephra preservation potential due to, for example, humid temperatures and high rainfall (~2,000 mm/yr at Lago Puyehue lake edge) which can lead to remobilisation, erosion, and chemical alteration (Fontijn et al., 2014). This can particularly affect tephra deposits in the terrestrial realm (e.g., soil-tephra alternations) which may also be difficult to access. However, small eruptions are often well preserved in lacustrine sequences, especially ones that are very proximal to volcanoes (e.g., Bertrand et al., 2008b, 2014; Van Daele et al., 2014). For example, Bertrand et al. (2008b) identified numerous tephra in the Lago Puyehue sedimentary sequence and suggested these were likely from the nearby centres, including for example, Puyehue-Cordón Caulle. In addition, Bertrand et al. (2014) identified that tephra in Lago Puyehue can be deposited via fluvial inwashing nearly instantaneously after an eruption which allows for the preservation of time-synchronous event markers that may not typically be dispersed toward Lago Puyehue, and this provides a more complete archive of past volcanic activity than many terrestrial outcrops (Chapter 1). For these reasons, the Lago Puyehue sedimentary record was selected to reconstruct a detailed record of past volcanic activity in the central Chilean Lake District (CLD; ~37-41°; Chapter 1; Figure 1.8, 1.11).

The CLD is volcanically a highly active region, consisting of 29 centres. Of these, 15 have erupted during the historical past. The CLD is situated in the Southern Volcanic Zone (SVZ; 33-47°S), and, based on previous tephra investigations of Lago Puyehue, Bertrand et al. (2008b) described the SVZ as being consistently active through the Holocene. However, the eruptive frequency at individual centres in the CLD have been noted to be more variable (e.g., Mocho-Choshuenco; Rawson et al., 2016), and regionally, temporal changes have been observed in large, explosive events from the analysis of deposits from numerous volcanic centres in the CLD (Fontijn et al., 2016).

Many of the deposits observed in the Lago Puyehue record will come from local, predominantly mafic centres that are close to the lake, including Puyehue-Cordón Caulle, Antillanca, Mocho-Choshuenco, and Carrán-Los Venados, which are likely to be from relatively

small events (i.e., <VEI 3). Puyehue-Cordón Caulle is expected to be the largest source of deposits in Lago Puyehue because i) it is located proximally to Lago Puyehue (~30 km from source), and ii) a significant proportion of the Lago Puyehue catchment covers the western flanks of the volcanic complex (e.g., Bertrand et al., 2008a). There is relatively little known about the frequency of small-medium Quaternary Holocene eruptions at Puyehue-Cordón Caulle (Lara et al., 2006; Lara and Moreno, 2006; Singer et al., 2008; Naranjo et al., 2017).

The modern Puyehue stratovolcano was built over the past 69 kyr, while the Cordón Caulle fissural zone formed over the past ~16.5 kyr (Singer et al., 2008). The most recent eruptive activity at the Puyehue stratovolcano occurred at ~1.1 cal ka BP, but the Cordón Caulle complex remains active, and there has been frequent historical activity (e.g., 2011). The whole-rock major and trace elemental compositions of deposits from the different vents within the complex are similar, suggesting they are fed by the same source (Singer et al., 2008). In the historical record, repose times at Cordón Caulle are on the order of a few decades (e.g., Siebert et al., 2010).

Large deposits from the Puyehue-Cordón Caulle complex include the PCC1 (10.46-10.30 cal ka BP; VEI 4), PCC2 (6.60-6.27 cal ka BP; VEI 5), Ranco Pumice (4.68-4.10 cal ka BP; VEI 5), PCC4 (3.26-3.00 cal ka BP; VEI ~4), and Mil Hojas events (1.02-0.67 cal ka BP; VEI 5; Fontijn et al., 2016). Based on volcanological studies including historical records, ash from this centre is typically dispersed away from the lake and to the south and south-east (e.g., Klüser et al., 2013; Bertrand et al., 2014; Fontijn et al., 2016; Koffman et al., 2017). However, since ash can be deposited in the lake via the catchments numerous inlets, deposits from both large and small events are likely to be observed in the lacustrine sequence (e.g., Bertrand et al., 2014; Chapter 1).

Tephra deposits identified in Lago Puyehue may also originate from other volcanoes surrounding the catchment: Antillanca, Carrán-Los Venados, Osorno and Mocho-Choschuenco (Figures 1.8, 1.11). Mocho-Choschuenco is the best studied volcano of these, with a high-resolution tephrostratographic record for the postglacial (Rawson et al., 2015). The highly active centre has erupted ~75 times since 18 cal ka BP, including a large pyroclastic density current

(PDC) dominated, sub-Plinian event (Enco) and three Plinian eruptions (volume ≥1 km^3; Neltume, Pirehueico and Huilo; Rawson et al., 2015).

Two eruptive deposits are recorded from Antillanca to date: (1) a distinct, white rhyodacite with sharp transition to basaltic andesitic scoria in the top ~15-20 %, called the Playas Blanca Negra (PBN), that occurred at <2.88 cal ka BP (this unit is referred to as the Nahuel Huapi Tephra (NHT) in and prior to Villarosa et al. (2006)), and (2) a lithic-rich, brown coloured pumice and scoria fall deposit called the NHT that occurred at <1.93 cal ka BP (e.g., Villarosa et al., 2006; Watt et al., 2013a; Fontijn et al., 2016; Naranjo et al., 2017; this unit is referred to as Ant2 in Fontijn et al., 2016). An additional unit called the Pampa Frutilla Pyroclastic Density Current (PFPDC), that occurred at 1.93 cal ka BP, has been described by Naranjo et al. (2017), but is more likely a soil formation event and is not considered here.

There is very little known about the Holocene succession of the Carrán-Los Venados group, located 52 km north of the lake. The group consists of ~70 Pleistocene and Holocene basaltic scoria cones and maars (López-Escobar and Moreno, 1981). Three historic eruptions are recorded: AD 1907 Riñinahue maar, AD 1955 Carrán (or Ñilahue maar), and the AD 1979 Mirador scoria cone (Gerlach et al., 1988; López-Escobar and Moreno, 1981).

Little is also known about pre-historical events from Osorno volcano. It is a mafic centre and basaltic-andesite deposits have been identified and attributed to an AD 1575 eruption which is hypothesised to be associated with the December 16th AD 1575 Valdivia earthquake (magnitude 8.5; Chapron et al., 2007; Bertrand et al., 2008b). Deposits of basaltic-andesite affinity have also been recorded and associated with effusive Osorno activity in AD 1790 and 1835 (González-Ferrán, 1994; Bertrand et al., 2008b; Boës and Fagel, 2008).

Infrequent but explosive events from more distal centres such as Calbuco and Chaitén (~73 and ~240 km distance from Lago Puyehue, respectively) are also expected to be identified in the lake sequence. Calbuco erupts a range of chemical compositions, while Chaitén volcano predominantly only erupts high-silica products. Fontijn et al. (2016) speculated based on preliminary chemical data from Bertrand et al. (2008a) that a tephra identified at 633 cm depth in the Lago Puyehue sedimentary sequence would correlate to Chaitén volcano, and specifically

a tephra called ChaA1 (also referred to as Puma Verde by Alloway et al., 2017a). The ChaA1 tephra occurs between 8 and 8.3 cal ka BP (Alloway et al., 2017a) and has been observed as a 1 cm thick ash in the Lago Espejo sedimentary sequence (Alloway et al., 2017a), ~62 km east from Lago Puyehue and ~255 km north from Chaitén volcano. Another marker horizon from Chaitén volcano, and which may be preserved in Lago Puyehue (possibly at 633 cm depth), is the felsic Cha1 (also referred to as Chana by Alloway et al., 2017a) widespread tephra from Chaitén, that occurred at ~9.7 cal ka BP. This unit is the only deposit from this centre that is known to have been dispersed northward (Watt et al., 2011; Fontijn et al., 2016). It has been observed 400 km from source, including in Lago Villarrica (Fontijn et al., 2016) and therefore could also occur in Lago Puyehue.

Calbuco was particularly highly active in the early Holocene and may too have deposited ash across the region (Watt et al., 2011; Fontijn et al., 2016). Many of these deposits are speculated to have travelled to the east and south-east based on isopach mapping of proximal deposits (Watt et al., 2011). However, there have been at least 13 eruptions since the post-glacial (Watt et al., 2011), and at least three historical eruptions from Calbuco (including the AD 1920, AD 1860, and AD 1775) have been associated with deposits identified in the Nahuel Haupi Lake (Daga et al., 2008; ~85 km south-east from Lago Puyehue). The 2015 Calbuco tephra indeed travelled north-east based on isopach mapping (Castruccio et al., 2016; McNamara et al., 2019).

3.2. Age-depth model for Lago Puyehue

As described in Chapter 1, an age-depth model for the sediments of Lago Puyehue has been created by S. Bertrand (*unpublished*; after Bertrand et al., 2012) in CLAM 2.2 (Blaauw, 2010) using 16 calibrated radiocarbon dates, ^{210}Pb and ^{137}Cs measurements, varve counts, and historical ages for distinct eruptions (Bertrand et al., 2008b; 2012). This age-model has provided ages for the entire sequence (i.e., an age per cm of sediment; Figure 1.9), and the sequence spans ~15.5 cal ka BP. However, this sequence comprises a proportionally large number of tephra layers and three turbidite layers, and the calculations for the aforementioned age-depth model are not produced using event-corrected depths. Therefore, this section of the chapter examines whether

the unpublished age-model by S. Bertrand, produced in CLAM 2.2, is more effective than an event-corrected version produced for this thesis in OxCal 4.3 (Bronk Ramsey, 2009a). In doing this, different modelling parameters can be tested to produce the most robust age-depth model possible, including outlier modelling, radiocarbon offsets, and different dating methods (Section 3.2.1). The two model types will hereafter be called Model 1 (in reference to the unpublished age-depth model by S.Bertrand produced in CLAM 2.2) and Model 2 (in reference to the age-depth model produced in this thesis using OxCal 4.3). Since we test the sensitivity of the model, there are variations of Model 2 (2A-2E). In Section 3.2.1.5, the most fine-tuned age-model is selected and described.

3.2.1. Sensitivity analysis of Model 2

Sensitivity analysis is conducted on Model 2 (i.e., Model 2A-E) and results are compared with Model 1. An overview of the model inputs are presented in Table 3.1.

Table 3.1. Quick view comparison between inputs of Model 1 (CLAM 2.2; Bertrand, unpublished) and Model 2A-E (this study; OxCal 4.3). [1]Bronk Ramsey et al. (2009a); [2]Blaauw (2010); *See Table 3.2; †^{210}Pb and ^{137}Cs measurements were used in Model 1 to confirm ages of historical tephra, but calculated ^{210}Pb dates were not inserted into Model 1. In Model 2A-2E, the ^{210}Pb ages are used directly in the model to constrain the ages; ΨAll outlier models are analysed as a 'General Outlier Model' at 0.05 probability.

Model	SHCal13 calibration curve	Number of ^{14}C dates inputted*	Number of ^{14}C dates removed*	Age-offset applied	Fully event-corrected	Outlier Model Ψ	^{210}Pb	Historical tephra
1[2]	**Y**	**16**	**2 (725.5, 1012.0 cm)**	**Y**	**N**	**N**	**N†**	**Y**
2A[1]	Y	16	0	N	N	N	Y	Y
2B[1]	Y	16	0	N	Y	N	Y	Y
2C[1]	Y	16	0	N	N	Y	Y	Y
2D[1]	**Y**	**16**	**0**	**N**	**Y**	**Y**	**Y**	**Y**
2E[1]	Y	16	0	Y	Y	Y	Y	Y

3.2.1.1. Additional dates

Lead (^{210}Pb) measurements are reported for the Lago Puyehue sequence at 4.0, 10.5 and 13.0 cm depth. Both ^{210}Pb and continuous ^{137}Cs measurements have been used to calculate the ages of four historical tephra; three of these tephra were firmly chemically correlated (^{210}Pb dates:

AD 1962±2, 1922±4, and 1902±5 respectively; Arnaud et al., 2006; confirmed historical tephra: AD 1960, 1921-22, 1907; Bertrand et al., 2008a). These lead and tephra measurements were put into the Model 2 (A-E) to constrain the ages of the uppermost sediment. If they are removed from the model, older dates are returned in the late-Holocene and the model becomes less well-constrained. Only the reconstructed historical tephra ages are used in Model 1 (Bertrand, unpublished; Table 3.1).

3.2.1.2. Event correction

Out of the full 1122.0 cm sequence, there are 57.49 cm of tephra and 17.25 cm of turbidite deposits (74.74 cm instantaneous, non-pelagic deposits in total, comprised of tephra and turbidite deposits). Only the 17.25 cm of turbidite deposits were removed from Models 1, 2A and 2C, while all 74.74 cm of non-pelagic deposits (i.e., tephra units and turbidite deposits) were removed from Models 2B, 2D, and 2E. The removal of these deposits can influence the reconstructed age of tephra deposits and radiocarbon ages. This is because including tephra deposits in age models results in interpreting one or more large unit/s of instantaneous deposition/s as representative of longer time periods than they truly are. This results in disproportionately representing the ages of events by ascribing them dates which assume a type of continuous sedimentation. The use of event-corrected depths for age-depth modelling is thus highly preferable to a non-event corrected age-depth model (e.g., Bronk Ramsey 2009b).

Model 2 does not generate good model agreement indices when it is run as a non-event-corrected model (Model 2A; A_{model}: 2.1 %), or an event-corrected model (Model 2B; A_{model}: 2.5 %). Both Model 2A and Model 2B returned poor agreement indexes for the same five dates at 1025.5, (Poz-71092), 1012 (Poz-2215), 985.5 (OS-71091), 762 (Poz-1405), and 725.5 cm (OS-71090), but Model 2A (non-event-corrected) also returned poor agreement indices for the AD 1575 eruption of Osorno volcano (T4 in Bertrand et al., 2008b). When historical tephra is excluded, both Model 2A and 2B decrease in performance to 0.7 % agreement (A_{model}).

The reconstruction of tephra dates in an OxCal age model with agreement indices of <60 % is not appropriate, but the manual removal of radiocarbon dates (to increase model agreement) can result in age-models being less well-constrained and should be avoided if possible (Bronk Ramsey et al., 2009b). Outlier analysis applied in OxCal provides a solution for dates with poor agreement indices (and which bring the overall model agreement indices down) to be downweighted; this is preferable to removing poorly agreeing dates (Bronk Ramsey et al., 2009b).

3.2.1.3. Outlier modelling

Outlier analysis produces age-estimates which represent an average between a model in which the measurement was accepted and one in which it was rejected through the process of statistically downweighting ages (e.g., Bronk Ramsey, 2009b). Outlier analysis is not applied in Model 1. Two radiocarbon dates were manually removed due to inversions (725.5 and 1012 cm non-event corrected depths) in Model 1 (Bertrand, unpublished); the removal of outlying dates manually should involve careful consideration of the measurement process and sample context, or statistical analysis such as outlier modelling (e.g., Bronk Ramsey 2009b). In the case of Model 1, it is not clear why Bertrand et al. (2012) and Bertrand (unpublished) chose to remove these dates.

When outlier analysis is applied to the dates of Model 2A (with outlier analysis called Model 2C) and 2B (with outlier analysis called Model 2D) at 5 %, the models perform better, with only three dates poorly agreeing in the models: 1012 (Poz-2215), 985.5 (OS-71091), 725.5 cm (OS-71090). The A_{model} of these models of course remains low (i.e., <60 %), but the A_{model} performance can be ignored when outlier analysis is applied, since poorly constrained or inverted dates are downweighted in the model run (Bronk Ramsey, 2009b). The age-model with outlier detection is preferred since this permits the inclusion of radiocarbon dates which can be downweighted with no biased effects on the age-depth model itself, and increasing the robustness and model likelihood (Bronk Ramsey, 2009b).

3.2.1.4. Radiocarbon offsets

An average radiocarbon offset of -385 years (range: 232.6-522.2 years) has been found in Lago Puyehue using N/C ratios for AD 1870 sediments (short core PU-I; Bertrand et al., 2012; S. Bertrand, pers comms). Potential reservoir offsets at Lago Puyehue are thought to occur from variable inputs in terrestrial organic carbon during the Holocene which cover the lake watersheds (Bertrand et al., 2012). Lago Riñihue (located ~100 km north of Lago Puyehue) also reportedly has a radiocarbon offset. At Lago Riñihue, the offset is identified to be -580 years at AD 1575, identified by comparing varve dates, in addition to one radiocarbon date from the lake core against the AD 1575 turbidite from the Osorno eruption (Moernaut et al., 2017). Tephra from this turbidite is however, not chemically confirmed as being from Osorno volcano (Moernaut et al., 2017). In contrast, no reservoir effects have been identified in the AVZ (Stern et al., 2016).

To determine the effect that radiocarbon offsets may have on age-modelling data from Lago Puyehue, Model 2B (i.e., event-corrected, no outlier analysis) was modified and tested using a variable age offset calculated using C/N ratios (Bertrand, unpublished; Model 2E). This produced comparable ages to the model projected in the non-offset age-depth model (Model 2D). The use of C/N ratios to correct for radiocarbon reservoir effects has not been proven successful in numerous studies or different localities yet, and has only been utilised in Bertrand et al. (2012) and Bertrand (unpublished).

3.2.1.5. Age-depth model selection

Model 2D is selected as the most preferable age model for the Lago Puyehue sedimentary record as this model uses the globally preferred method of event-correction, in addition to outlier analysis and utilization of all available dates (i.e., historical tephra; Table 3.1; Figure 3.1). This model was created using appropriate parameters in OxCal 4.3 (Bronk Ramsey, 2009a) and can be compared with the sequence chronology with that of an existing age-depth model for Lago Puyehue, produced using CLAM 2.2 (Blaauw, 2010) by Bertrand (unpublished; Figure 1.9; Model 1).

In order to produce Model 2D, sixteen uncalibrated radiocarbon dates, three ^{210}Pb, and three historical tephra dates were inputted to OxCal in an event-corrected age-depth model using a *P_Sequence* and a variable *k* parameter set to 1, which allows OxCal to determine the optimal variability in sedimentation rate (Bronk Ramsey and Lee, 2013; see Chapter 2). Outliers were statistically determined and downweighted using the O*utlier_Model("General")* function to ensure that they did not negatively influence the refined calculated age. The outlier probability was set at 0.05, implying that there is a 5 % prior probability of the individual date being a statistical outlier, as per Bronk Ramsey (2009b). The ShCal13 calibration curve (Hogg et al., 2013) was used to calibrate radiocarbon ages on the basis that the sequence is located in the Southern hemisphere.

For the most part, the ages (probability ranges of individual modelled radiocarbon dates and tephra layers), of Model 2D are relatively comparable to those of Model 1 (Table 3.2, 3.3). For example, the reconstructed tephra age at 1117 cm depth (non-event-corrected; 1042.55 cm depth event corrected) in Model 1 is 15,734 to 15,250 cal yr BP while Model 2D returned ages of 15,883 to 15,256 cal yr BP (both: 2σ error; Supplementary Data S.1.3), and the modelled age of radiocarbon date OS-69044 is 15,287-14,896 cal yr BP in Model 1 and 15,557-15,092 cal yr BP in Model 2D (both: 2σ error; Table 3.2).

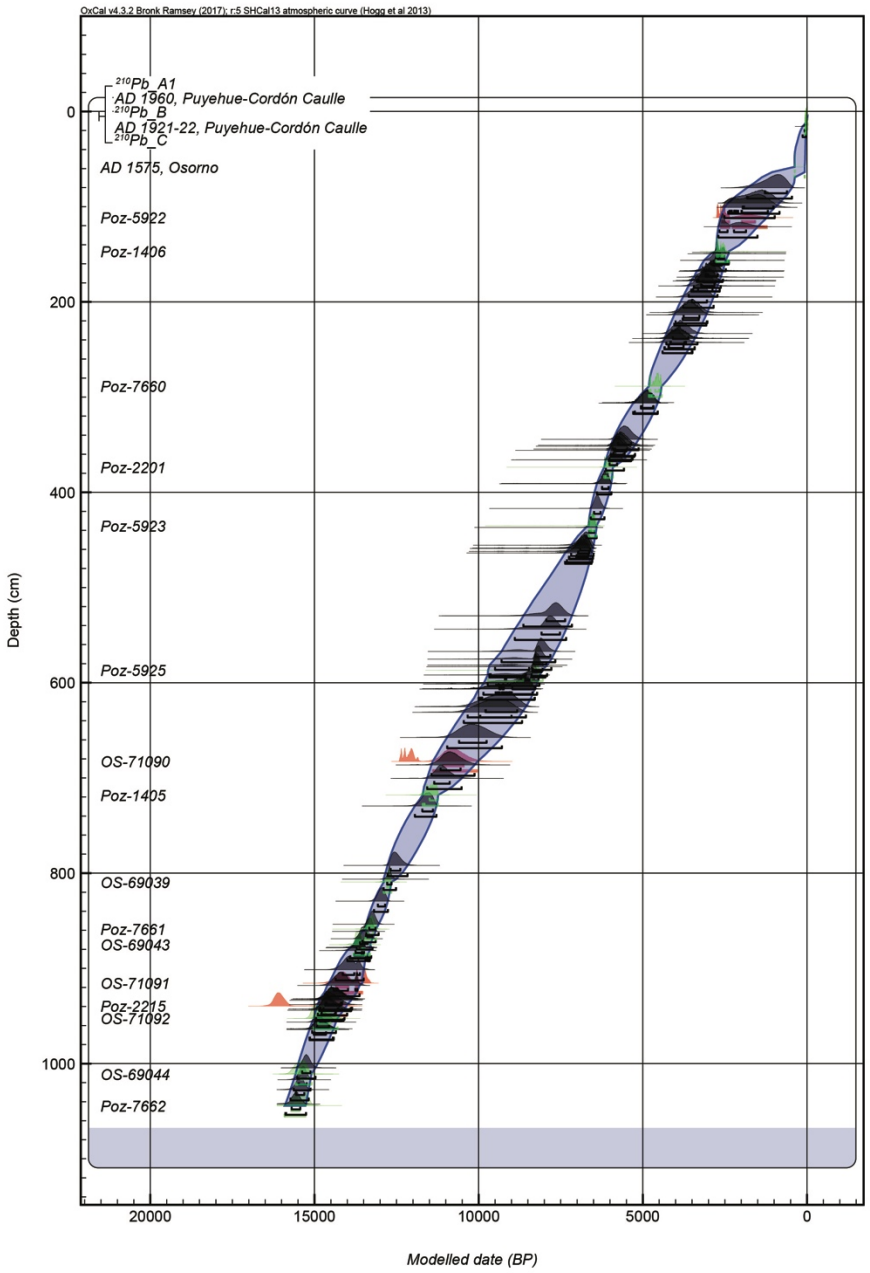


Figure 3.1. The OxCal age-depth model 2D based on calibrated radiocarbon dates, ^{210}Pb dates and historical tephra for the Lago Puyehue sequence which are analysed using outlier detection (General, 0.05). Dates which have been downweighted due to poor agreement are shown as red probability density functions, while those that agree well are shown in green. Black probability density functions represent the reconstructed dates for tephra deposits in the Lago Puyehue sequence. ^{210}Pb dates are from Arnaud et al. (2006). Radiocarbon and historical tephra dates are from Bertrand et al. (2008b) and Bertrand (unpublished).

Table 3.2. Table displaying radiocarbon data for both the selected OxCal (2D) and CLAM 2.2 age-depth model (1). Age offset is calculated after Bertrand et al. (2012) by Bertrand (unpublished); it is only used in Model 1 as per Table 3.1. EC=event corrected. Radiocarbon dates are from Bertrand et al. (2008b) and Bertrand (unpublished). *=ages that have poor agreement indices and have been downweighted in the model.

Non-EC depth (cm)	EC-depth (cm)	Radiocarbon Lab Number	^{14}C date (yr BP)	Error (1σ)	Age offset (yrs)	Model 2D modelled dates (cal yr BP; 2σ)	Model 1 modelled dates (cal yrsBP; 2σ)
120.5	111.4	Poz-5922	2570	35	480.9	1217-2638 *	1487-1919
156.5	146.9	Poz-1406	2590	40	379.1	2382-2767	2161-2534
306.5	288.6	Poz-7660	4110	40	370.3	4427-4813	4143-4483
400.5	373.55	Poz-2201	5300	40	444.3	5912-6177	5442-5645
463.75	435.1	Poz-5923	5760	40	298.6	6410-6647	6074-6264
627.75	586.9	Poz-5925	7450	50	522.2	8046-9712	7680-8078
725.5	682.55	OS-71090	10350	55	454.5	10031-11399 *	Removed
762.0	717.95	Poz-1405	10010	60	407.8	11231-11704	10723-11043
855.0	809.35	OS-69039	10900	75	NA	12659-12889	12522-12727
908.0	858.65	Poz-7661	11440	80	NA	13127-13445	13178-13406
925.0	875.15	OS-69043	11900	75	NA	13306-13804	13347-13602
985.5	915.35	OS-71091	11700	80	NA	13537-14559 *	13754-14119
1012.0	939.55	Poz-2215	13410	100	232.6	14025-14914 *	Removed
1025.5	952.65	OS-71092	12600	75	261.4	14299-15023	14172-14564
1085.0	1010.95	OS-69044	12950	95	NA	15092-15557	14896-15287
1119.0	1044.25	Poz-7662	12880	90	NA	15273-15908 *	15274-15763

One of the major differences between Model 1 and Model 2D is between ~11,000-4000 ^{14}C yr BP, whereby Model 2D returns older dates than Model 1 (Table 3.2). To determine which model is most accurate in its age-determination, we compare the dates of tephra in the Lago Puyehue sequence, confirmed using glass chemistry, to known ages represented in the literature. Many widespread tephra layers in the CLD are well-dated, and as such, comparing the reconstructed ages of chemically correlated units identified in the Lago Puyehue sequence provides a good method of investigating the model performance (Table 3.3; see Section 3.5 for details on regional marker horizons identified in the Lago Puyehue sedimentary sequence).

A tephra in Lago Puyehue at 632.7-633.6 cm depth (PUII_632) chemically correlates to the widespread Chaitén tephra called Cha1 (Section 3.4.1). The likely depositional age for Cha1 recorded in the literature is 10,105-9685 cal yr BP (Fontijn et al., 2016). The reconstructed depositional age for this eruption unit, PUII_632, in Model 2D is 9722-8147 cal yr BP, which means that the model is in chronological agreement with the date for the Cha1 unit. Model 1 (Bertrand, unpublished) estimates a depositional age of 8180-7769 cal yr BP for PUII_632, which suggests that Model 1 is underestimating the age. In both model 1 and 2D, the date at 725.5 cm depth (OS-71090) is excluded/downweighted and this likely accounts somewhat for the later than

expected age estimate – the age estimate of tephra preserved at 632.7 cm depth in Model 2B is 11,600-8,300 cal yr BP, for example.

Table 3.3. Dates for regional marker horizons as per identified from Model 1 and Model 2D, and as per identified in the literature. EC = event corrected. 1=Fontijn et al. (2016); 2=Singer et al. (2008). Dates for Models 1 and 2D calibrated using the SHCal13 calibration dataset (Hogg et al., 2013). Uncalibrated ages in Supplementary File S.5.

Depth in PUII sequence (cm; non-EC)	Regional marker horizon	VEI	Depth (cm; EC)	Model 1 (cal yr BP; 2σ)	Model 2D (cal yr BP; 2σ)	Date in literature for regional marker horizon (cal yr BP)
81.0-81.5	**Mil Hojas**	5	80.2-80.7	729-986	610-1286	672-1015 (1)
226.2-226.3	**PCC4**	4	211.1-211.2	3129-3496	3036-4002	2955-3264 (1)
632.7-633.6	**Cha1**	5	591.85-592.75	7769-8180	8147-9722	9685-10105 (1)
1036.5-1036.7	**PCC1**	4	963.45-963.65	14,300-14,688	14,417-15,148	10,295-10,455 (1); 10,470±150 (2); 11,500±1100-12,300±1900 (^{40}Ar/^{39}Ar; 2);

The PCC1 unit (known as the Pr1 unit in Singer et al. (2008)) has a wide range of ages attributed with it. One radiocarbon date from Singer et al. (2008) places the unit at 10,470±150 cal yr BP. However, ^{40}Ar/^{39}Ar dates from Singer et al. (2008) suggest a younger deposition of PCC1: 11.5±1.1 ka, 12.0±2.8 and 12.3±1.9 ka. The single radiocarbon date has been remodelled in Fontijn et al. (2016) to produce an age of 10,455-10,295 cal yr BP. It is possible that the age-depth models (2D and 1) perform poorly in the early Holocene, or that the tephra correlation produced relates to a different but chemically similar Puyehue-Cordón Caulle eruption to PCC1.

Overall, the widespread markers identified in the Lago Puyehue record correlate chronologically within error in Model 2D better than Model 1 (Table 3.3). In addition, Model 2D tackled outlying ages more thoroughly than Model 1 (e.g., Bronk Ramsey, 2009b). Model 1 used a manual removal technique to remove two outlying radiocarbon dates while Model 2D applied a non-biased model averaging approach through the use of Bayesian statistics which resulted in the downweighting of outlying dates, rather than the removal of them (Table 3.2; Bronk Ramsey, 2009b). Moreover, Model 1 did not account fully for the removal of event-layers in the sequence

(only turbidite layers were excluded) which can lead to interpreting one or more large units of instantaneous deposition as longer time periods than they are (e.g., Bronk Ramsey, 2009b). For these reasons, Model 2D is used in this study.

3.3. The tephrostratigraphy of Lago Puyehue

There are 79 visible tephra deposits in the 11.2 m long Lago Puyehue record (one more than identified by Bertrand et al. (2008b)); these deposits occur with varying thicknesses and contacts (Figures 3.2, 3.3). Many of the tephra units are thin (<0.3 cm in thickness), fine-medium ash (See Table 3.4 for an overview of the main characteristics of the tephra units). Compositional data (Section 3.4) confirms that many of these units are of basaltic/basaltic-andesitic affinity and therefore likely to originate from the predominantly mafic centres surrounding Lago Puyehue (Section 3.4; Table 3.4).

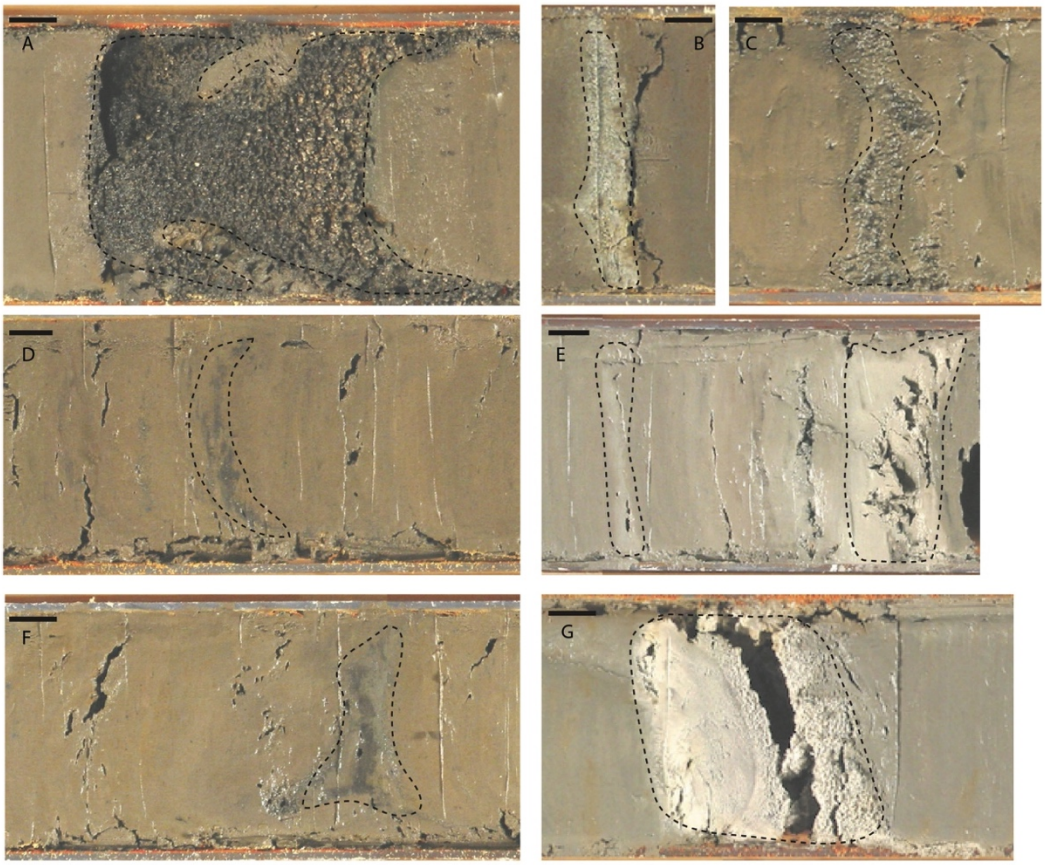


Figure 3.2. Tephra deposits (outlined) identified in the Lago Puyeue sequence (sequence has not been exposed; left hand side is core top). These deposits demonstrate the types of material identified in-situ; A) 495.6-502.9 cm (glass chemistry suggests it is likely from Antillanca or Mocho-Choschuenco volcanoes) is fining upward; B) 632.7-633.6 cm (Cha1 tephra from Chaitén volcano); C) 166.7-167.2 cm (indiscriminate unit likely from nearby centre); D) layer with diffuse boundary (insufficient chemistry to establish source); E) two primary tephra layers with unique compositions and both with sharp contacts at 1036.5-1036.7 (left layer; PCC1) and 1037.4-1037.7 cm (right layer; Puyehue-Cordón Caulle volcanic complex); F) layer with diffuse boundary 743.5-744.5 cm (insufficient chemistry to establish source); G) layer fining upwards with sharp contact at 899.5-903.0 cm depth (Calbuco volcano). Solid black line represents 1 cm in length.

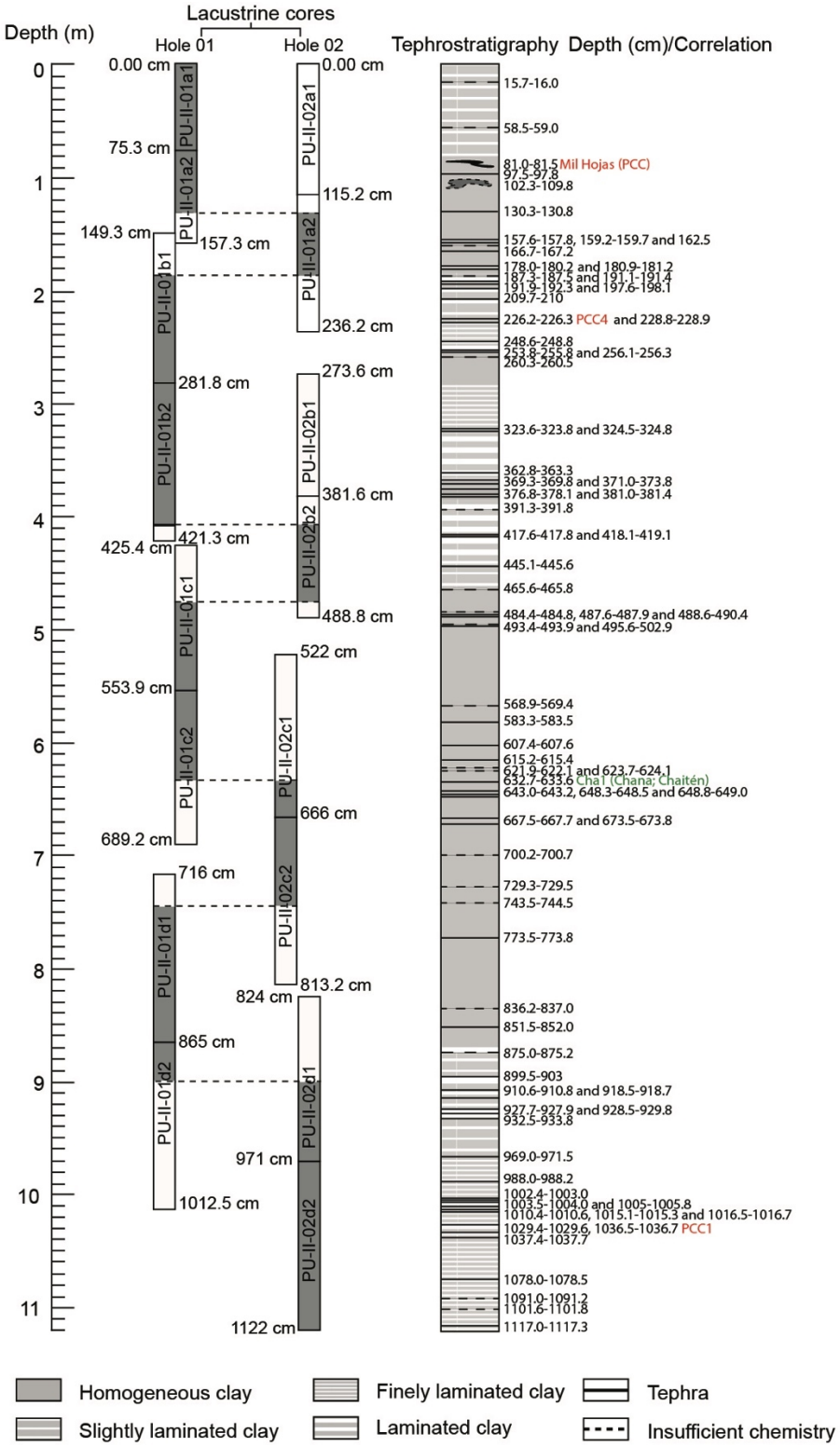


Figure 3.3. Schematic diagram of Lago Puyehue sedimentary record demonstrating the correlations between the 3-m-long sections from different boreholes, enabling the production of the composite sequence. The dark grey sections within 3-m-long sections represent the parts used to produce the composite log (middle). The composite log is drawn in accordance to macroscopic descriptions, including the tephrostratigraphy (this study; far right). Depths of tephra and regional marker horizons are labelled on far right. PCC=Puyehue-Cordón Caulle; Cha=Chaitén. After Bertrand et al. (2008b).

Many different types of glass shards have been identified in the tephra deposits in Lago Puyehue, from fluted glass shards to pumiceous and scoriaceous grains (Figure 3.4). While different types of glassy shards (platy, bubble-walled, cuspate, fluted) are often identified in the same tephra sample (e.g., Liu et al., 2016), it is less usual to identify two types of glass shards that represent two compositionally different tephra (e.g., scoria – mafic, and pumice – felsic). This typically indicates: i) a bimodal chemical composition caused by the tapping of magma from different reservoirs with different compositions, or magma mingling (e.g., Sparks et al., 1977; Laumonier et al., 2014), ii) a tephra deposit that has been contaminated with non-juvenile tephra (i.e., reworking), iii) two or more eruptions occurring simultaneously or close in time.

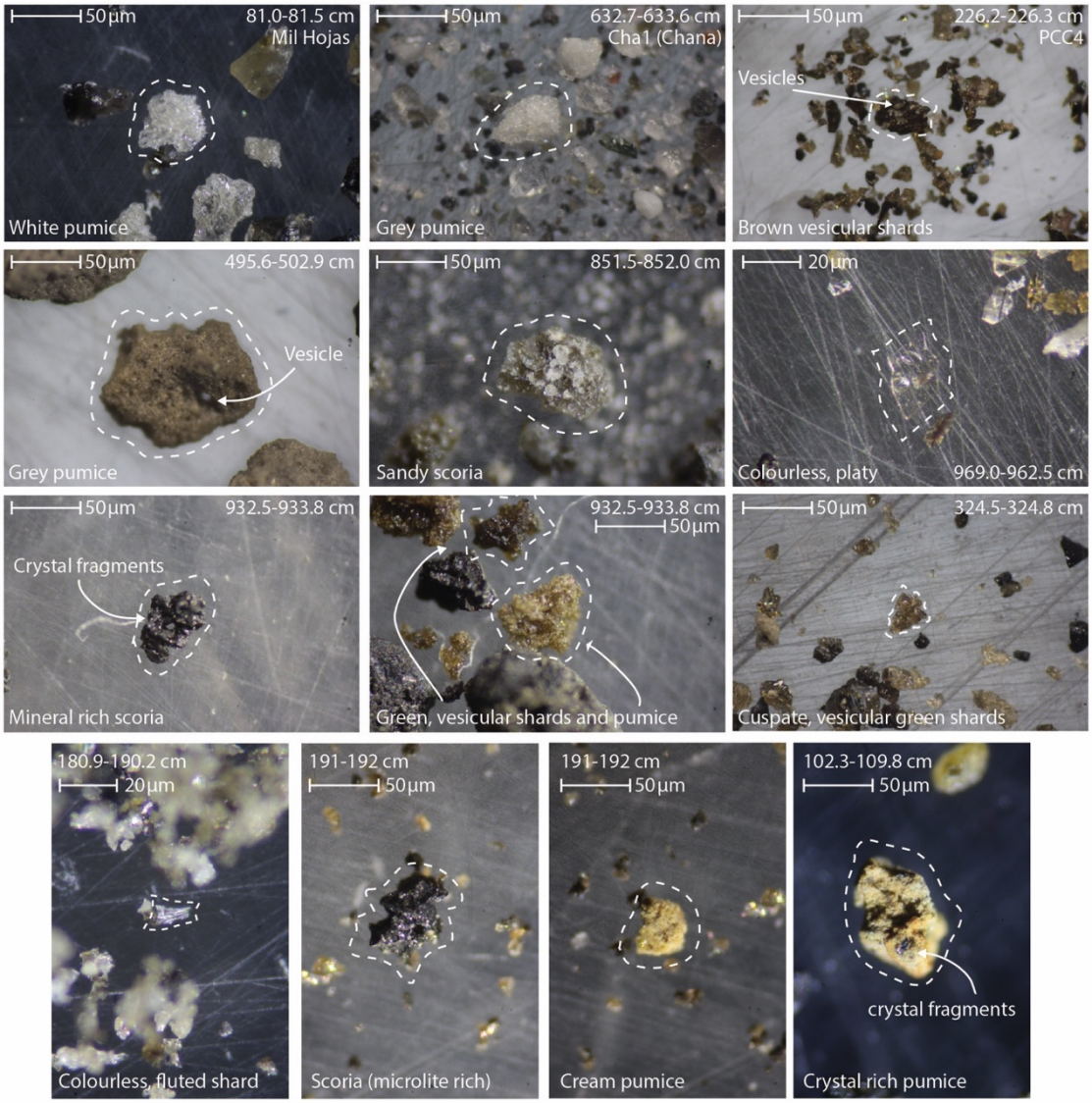


Figure 3.4. Photographs of the typical tephra morphologies preserved in the Lago Puyehue record. Individual scale bars are represented in each photograph. Morphologies include platy, vesicular, cuspate, pumice, and scoria, and include differing abundances of minerals. The depths and description of each tephra are included in each individual photograph, and each tephra is highlighted with a white dotted outline.

Table 3.4. Overview of all tephra deposits observed in the Lago Puyehue lacustrine record (PUII). Depth of tephra refers to the uppermost depth (top; cm); th refers to thickness in cm; description refers to the visual description of tephra deposit in situ; modelled age (cal yr BP; 95 % probability) is obtained from Model2D age-depth model (Section 2); glass description shapes can be identified in Figure 2.3; glass composition based on Total Alkali-Silica classification after Bas et al. (1986) and within this, the terminology is as follows: 'and' refers to tephra which has two separate end members, while 'to' refers to tephra which sits on an evolutionary trend; *n* refers to the number of chemical analyses obtained; * refers to regional marker horizon identified.

Depth (top; cm)	th (cm)	Description	Modelled age (cal yr BP; 2σ probability)	Glass description	Glass composition	*n*	FeO wt% (range)	K₂O wt% (range)	Correlation
15.7	0.3	medium brown ash	29-132	mineral-rich sample; some mineral-rich scoria	NA	*0*	No chemistry	(speculated to be AD1907 Rininahue Maar deposit in Bertrand 2008a; T3)	
58.5	0.5	medium brown ash	69-378	few grey pumice grains; predominantly scoria with detrital material	NA	*0*	No chemistry	(speculated to be AD1575 Osorno correlation in Bertrand et al., 2008a; T4)	
81 *	0.5	medium brown ash	458-1825	scoria with detrital material and fluted, colourless shards	rhyolite	*15*	3.73-4.46	2.62-2.95	PCC - Mil Hojas
97.5	0.3	fine brown ash	840-2402	pumice and glassy, green, vesicular shards	basaltic andesite	*18*	10.13-13.54	0.74-1.00	Indiscriminate unit likely from nearby centre
102.3	7.5	medium brown ash, fining upwards	982-2511	pumice and microphenocryst rich scoria	andesite	*3*	6.09-7.99	0.81-0.97	Insufficient chemistry
130.3	0.5	medium - coarse brown ash	1508-2699	Scoria with detrital material	andesite	*6*	6.26-8.45	0.91-1.24	Calbuco
157.6	0.2	medium brown ash	2381-2852	green microphenocryst rich, cuspate shards	basaltic andesite	*5*	10.78-11.61	0.61-1.11	Indiscriminate unit likely from nearby centre
159.2	0.5	fine brown ash	2385-2924	pumice and green, vesicular shards	basaltic andesite	*3*	8.73-11.19	1.01-1.25	Insufficient chemistry
166.7	0.5	medium brown ash	2476-3133	fluted colourless shards and pumice; scoria with detrital material	basaltic andesite to trachydacite	*19*	3.32-8.29	1.23-3.36	Indiscriminate unit likely from nearby centre
178	2.2	fine brown ash	2559-3308	cuspate/fluted colourless; light green/brown vesicular shards	basaltic andsite to trachydacite	*22*	3.43-8.68	1.32-3.51	Indiscriminate unit likely from nearby centre
180.9	0.3	fine brown ash	2575-3360	fluted colourless shards; light green vesicular shards	trachy-basalt to trachydacite	*22*	3.51-8.53	1.52-3.40	Indiscriminate unit likely from nearby centre
187.3	0.2	fine brown ash	2624-3444	green, microphenocryst rich shards	trachy-andesite	*3*	7.67-8.07	1.51-1.56	Insufficent chemistry
191.1	0.4	fine, light brown ash	2659-3521	pumice grains; scoria	basaltic andesite and dacite	*22*	4.53-10.17	0.89-2.67	Puyehue-Cordón Caulle
191.9	0.4		2663-3522						
197.6	0.5	very fine black ash	2728-3606	scoria and green, vesicular, cuspate shards; colourless platy shards	basaltic andesite and andesite	*7*	3.36-7.21	2.01-3.10	Puyehue-Cordón Caulle
209.7	0.3	fine brown ash	2845-3775	green/grey vesicular shards	basaltic andesite and dacite/rhyolite	*5*	4.00-12.12	0.76-2.85	Indiscriminate unit likely from nearby centre
226.2 *	0.1	very fine brown ash	3036-4002	pumice; brown, vesicular shards	dacite	*38*	4.47-5.58	2.32-2.73	PCC4
228.8	0.1	fine - medium black ash	3067-4039	pumice and green, vesicular shards	dacite	*11*	4.71-5.53	2.33-2.79	Puyehue-Cordón Caulle
248.6	0.2	fine - medium black ash	3337-4284	pumice and green, vesicular shards	basaltic andesite and dacite	*48*	4.42-12.02	0.60-2.80	Puyehue-Cordón Caulle

Depth (top; cm)	th (cm)	Description	Modelled age (cal yr BP; 2σ probability)	Glass description	Glass composition	*n*	FeO wt% (range)	K2O wt% (range)	Correlation
253.8	2	fine brown ash	3419-4334	pumice; colourless fluted shards; green-black vesicular shards	trachydacite and dacite	*65*	4.48-5.51	2.16-2.81	Puyehue-Cordón Caulle
256.1	0.2	fine brown ash	3420-4343	colourless fluted and vesicular shards; green, vesicular shards	dacite	*41*	4.63-5.50	2.26-2.76	Puyehue-Cordón Caulle
260.3	0.2	medium brown ash	3488-4399	colourless, cuspate shards with microphenocrysts; microphenocryst rich scoria	trachy-andesite	*2*	8.92-11.75	1.12-1.17	Insufficient chemistry
323.6	0.2	fine brown ash	4544-5244	grey microhpenocryst rich pumice; green, vesicular shards	dacite	*20*	4.92-6.40	1.57-2.93	Likely Puyehue-Cordón Caulle
324.5	0.3	fine brown ash	4550-5292	grey, microphenocryst rich pumice; green, cuspate and vesicular shards	dacite	*25*	4.69-6.19	1.85-3.95	Puyehue-Cordón Caulle
362.8	0.5	very fine black ash	5126-5905	yellow and green vesicular shards; some shards are fluted	trachydacite and dacite	*29*	5.03-6.1	1.9-2.78	Puyehue-Cordón Caulle
369.3	0.5	medium - coarse black ash	5237-5970	brown, scoria with detrital material	basalt and basaltic andesite	*9*	10.00-12.04	0.64-0.80	Indiscriminate unit likely from nearby centre
371	2.8	coarse brown ash	5258-5978	brown scoria	basaltic andesite	*16*	9.17-11.36	0.65-1.46	Indiscriminate unit likely from nearby centre
376.8	1.3	fine - medium brown ash	5309-6015	grey scoria	basaltic andesite	*20*	7.26-11.85	0.60-1.11	Indiscriminate unit likely from nearby centre
381	0.4	fine brown ash	5355-6036	green/grey cuspate/vesicular shards	basaltic andesite	*13*	7.92-11.01	0.78-1.19	Indiscriminate unit likely from nearby centre
391.3	0.8	fine - medium brown, crystal rich ash	5574-6125	crystal-rich scoria	basaltic andesite	*1*	NA	NA	Insufficient chemistry
417.6	0.2	medium brown ash with pumice lapilli	5958-6397	scoria with detrital material and pumice grains	basaltic andesite	*12*	10.05-11.01	0.76-0.94	Indiscriminate unit likely from nearby centre
418.1	1	medium - coarse ash with pumice	5963-6397	scoria with detrital material and pumice grains	basaltic andesite	*26*	8.02-12.71	0.59-0.89	Indiscriminate unit likely from nearby centre
445.1	0.5	medium brown ash with pumice	6169-6582	scoria and pumice grains	andesite	*10*	4.59-7.44	0.90-1.20	Llaima
465.6	0.2	medium - coarse brown ash	6407-6730	microphenocryst rich scoria	andesite	*2*	7.03-8.10	1.16-1.39	Insufficient chemistry
484.4	0.4	medium brown ash	6501-7183	scoria with crystal fragments	basaltic andesite	*2*	9.64-10.31	1.16-1.29	Insufficient chemistry
487.6	0.3	fine black ash with pumice	6519-7247	white pumice; green, vesicular glass; grey scoria	basaltic andesite to dacite	*4*	7.44-6.25	1.00-1.13	Indiscriminate unit likely from nearby centre
488.6	1.8	fine, black ash coarsening upwards to coarse black ash	6525-7248	light grey and darker grey scoria	basaltic andesite and andesite	*7*	6.08-9.57	0.80-1.77	Indiscriminate unit likely from nearby centre
493.4	0.5	coarse brown ash with pumice	6540-7310	pumice; scoria	trachydacite	*2*	5.72-6.14	2.23-2.33	Insufficient chemistry
495.6	7.3	fine brown ash with pumice lapilli; fining upwards	6561-7365	grey pumice grains; scoria	andesite to dacite	*16*	5.80-7.74	1.16-1.50	Indiscriminate unit likely from nearby centre
568.9	0.4	medium black ash	7160-8635	colourless and green vesicular shards	NA	*2*	5.38-7.53	1.32-1.57	Insufficient chemistry
583.3	0.2	fine black ash	7335-8898	vesicular and cuspate green shards	basaltic andesite and andesite	*5*	9.96-11.46	0.72-1.40	Unknown centre

Depth (top; cm)	th (cm)	Description	Modelled age (cal yr BP; 2σ probability)	Glass description	Glass composition	*n*	FeO wt% (range)	K_2O wt% (range)	Correlation
607.4	0.3	fine brown ash with pumice	7665-9302	predominantly minerals; pale green and colourless cuspate shards	basaltic andesite and andesite	*6*	9.86-12.97	0.90-1.28	Indiscriminate unit likely from nearby centre
615.2	0.2	very fine brown ash	7783-9502	large pale green cuspate/vesicular shards and small, cuspate, colourless shards	basaltic-andesite and rhyolite	*11*	1.50-11.87	0.81-3.12	Indiscriminate unit likely from nearby centre
621.9	0.2	fine brown ash	7913-9673	mineral rich scoria	NA	No chemistry	Insufficient chemistry		
623.7	0.4	medium - coarse brown ash with pumice	7968-9675	pumice; scoria	dacite	*2*	4.78-4.87	1.14-1.40	Insufficient chemistry
632.7 *	0.9	fine white ash with crystals present	8147-9722	pumice; colourless fluted and vesicular shards; microphenocryst rich scoria	rhyolite	*17*	1.19-1.45	3.09-3.47	Chaitén – Cha1
643	0.2	fine brown ash	8222-9854	colourless fluted and vesicular shards; green cuspate shards	basaltic andesite	*17*	10.85-12.58	0.88-1.13	Indiscriminate unit likely from nearby centre
648.3	0.2	very fine brown ash	8289-9976	microphenocryst rich pumice, green vesicular shards	basaltic andesite to rhyolite	*9*	1.25-12.61	0.95-3.65	Mafic composition is likely from indiscriminate and likely from nearby centres; felsic composition is likely from Chaitén
648.8	0.2		8297-10003						
667.5	0.2	very fine brown ash	8559-10335	scoria and cuspate, colourless shards	basaltic andesite to rhyolite	*14*	2.99-9.82	1.04-3.86	Puyehue-Cordón Caulle
673.5	0.2	very fine brown ash	8678-10453	grey pumice with mineral inclusions; green, vesicular shards	basaltic andesite to rhyolite	*12*	10.06-11.73	0.64-0.84	Indiscriminate unit likely from nearby centre
700.2	0.2	medium brown ash with pumice	9290-10959	grey pumice with mineral inclusions and crystal rich scoria	NA	No chemistry	Insufficient chemistry		
729.3	0.1	fine - medium brown ash	10123-11436	crystal rich scoria	NA	No chemistry	Insufficient chemistry		
743.5	1	fine brown ash	10517-11569	mineral rich scoria; light green, vesicular shards;	NA	*3*	9.09-10.26	1.12-1.25	Insufficient chemistry
773.5	0.3	fine beige ash	11286-11940	scoria and grey, microphenocryst rich pumice	basaltic andesite to rhyolite	*9*	3.25-11.01	1.04-3.45	Indiscriminate unit likely from nearby centre
836.2	0.8	fine brown ash	12163-12773	abundance of minerals, vesicular shards	NA	No chemistry	Insufficient chemistry		
851.5	0.5	fine brown ash	12515-12897	detrital material; brown vesicular shards	basaltic andesite	*5*	6.09-11.84	0.54-0.80	Caburgua-Huelemolle
875	0.2	fine brown ash	12765-13187	predominantly minerals; minimal cuspate colourless and green vesicular shards	NA	No chemistry	Insufficient chemistry		
899.5	3.5	fine beige ash	13046-13421	colourless pumice with sparse microphenocrysts	rhyodacite	*40*	2.45-3.20	1.27-1.59	Calbuco
910.6	0.3	medium - coarse black ash	13137-13543	green vesicular, cuspate shards	basaltic andesite	*7*	10.58-10.93	0.85-0.99	Indiscriminate unit likely from nearby centre
918.5	0.2	fine green-grey silty layer	13233-13714	colourless shards are cuspate and vesicular; green vesicular shards	basaltic andesite to andesite	*5*	8.14-10.51	0.90-1.81	Indiscriminate unit likely from nearby centre
927.7	0.2	fine - medium black ash	13273-13909	fluted and cuspate colourless shards; light green vesicular shards	andesite	*9*	8.04-9.90	1.28-2.24	Indiscriminate unit likely from nearby centre
928.5	1.3	fine beige ash	13309-13928	cuspate and vesicular green/yellow shards; grey vesicular shards; light grey pumice	basaltic andesite to dacite	*36*	6.17-9.88	1.18-2.12	Indiscriminate unit likely from nearby centre

Depth (top; cm)	th (cm)	Description	Modelled age (cal yr BP; 2σ probability)	Glass description	Glass composition	*n*	FeO wt% (range)	K2O wt% (range)	Correlation
932.5	1.3	medium - coarse brown ash	13315-13999	colourless, fluted shards; green vesicular shards and scoria	basaltic andesite to rhyolite	*42*	2.46-10.87	1.04-2.99	Indiscriminate unit likely from nearby centre
969	2.5	fine brown ash	13499-14354	colourless shards are fluted and platy; green, vesicular shards	basaltic andesite to andesite	*15*	8.66-10.77	1.13-1.79	Villarrica or Puyehue-Cordón Caulle
988	0.2	fine brown ash	13625-14609	few colourless cuspate shards, green vesicular shards	basaltic andesite to rhyolite	*5*	3.79-11.36	1.04-2.93	Puyehue-Cordón Caulle
1002.4	0.6	medium - fine black ash	13857-14841	black, vesicular scoria	basaltic andesite and andesite	*9*	8.33-10.10	1.07-1.46	Villarrica or Puyehue-Cordón Caulle
1003.5	0.5	fine black ash	13872-14851	green vesicular shards	basaltic andesite	*4*	9.41-10.37	1.13-1.40	Villarrica or Puyehue-Cordón Caulle
1005	0.8	fine black ash	13881-14852	green vesicular shards	basaltic andesite to andesite	*16*	8.30-11.22	0.72-1.52	Indiscriminate unit likely from nearby centre
1010.4	0.2	fine brown ash	14007-14898	fluted and vesicular colourless shards, green vesicular shards	basaltic andesite and rhyolite	*24*	2.69-11.42	0.69-3.08	Puyehue-Cordón Caulle
1015.1	0.2	fine brown ash with pumice	14086-14948	pumice with minerals; green, vesicular shards	basaltic andesite to rhyolite	*15*	4.39-11.27	0.59-2.66	Puyehue-Cordón Caulle
1016.5	0.2	medium black ash	14114-14956	few pumice grains; light green-grey vesicular shards	basaltic andesite to andesite	*18*	9.05-11.18	0.54-1.30	Villarrica or Puyehue-Cordón Caulle
1029.4	0.2	fine - medium black ash	14348-15071	grey pumice grains; light green and dark grey-black vesicular shards	basaltic andesite and rhyolite	*4*	4.49-12.11	0.89-2.83	Puyehue-Cordón Caulle
1036.5 *	0.2	fine black ash	14417-15148	colourless bubble walled/vesicular	rhyolite	*20*	3.95-4.72	2.68-2.92	PCC - PCCl
1037.4	0.3	fine brown ash	14420-15151	vesicular green shards	basaltic andesite and rhyolite	*13*	4.25-10.75	0.63-2.87	Puyehue-Cordón Caulle
1078	0.5	fine black ash	14971-15527	black/grey scoria	basaltic andesite	*14*	8.64-11.58	0.58-0.98	Caburgua-Huelemolle
1091	0.2	fine black ash	15122-15631	colourless vesicular shards; light green shards, vesicular and cuspate	NA	No chemistry	Insufficient chemistry		
1101.6	0.2	fine black ash	15177-15729	black, vesicular scoria	NA	*3*	9.92-10.91	0.98-1.60	Insufficient chemistry
1117	0.3	very fine black ash with pumice	15256-15908	minor amounts of cream-grey pumice grains; green, cuspate/vesicular shards	basaltic andesite	*23*	10.29-11.87	0.87-1.20	Caburgua-Huelemolle

3.3.1. The frequency of eruptive deposits in Lago Puyehue

The distribution of tephra layers (Figure 3.5) indicates that volcanic activity in the CLD, as recorded in Lago Puyehue, is mostly continuous through the Holocene (See Chapter 4 for further detailed discussion on event frequency using statistical analysis). There are, however, three periods of ~1 ky each during which there are no visible tephra recorded. These periods are (average ages):

- 4.40-3.48 cal ka BP (~0.95 ky duration between deposits 323.6 and 260.3 cm)
- 7.37-6.56 cal ka BP (~0.94 ky duration between deposits 568.9 and 495.6 cm)
- 11.94-11.29 cal ka BP (~0.86 ky duration between deposits 836.2 and 773.5 cm)

Most of the tephra units in the sequence are thin, with an average of 0.7 cm thickness, but a range of 0.1 to 7.5 cm. There are 13 units that are >1 cm thick in the Lago Puyehue sedimentary sequence. In the mid-Holocene (i.e., 4-8 ky), there are 18 tephra layers (based on average ages) which have an average thickness of 0.4 cm. During this period, there is a high abundance (n=5) of thick deposits; these are identified at 371.0, 376.8, 418.1, 488.6 and 495.6 cm depth and have thicknesses of 2.8, 1.2, 1.0, 1.8 and 7.3 cm, respectively.

There is a lack of large-magnitude silicic events recorded from Mocho-Choshuenco volcano during the mid-Holocene (Rawson et al., 2015, 2016; Section 3.6). In addition, Fontijn et al.'s (2016) study of regional volcanic activity indicates a general lack of widespread tephra markers representative of large, Plinian-style eruptions at this time. However, there are certainly some large, regional deposits preserved around this time, including Cha2 (Pumalin) and Puma Verde (ChaA1) from Chaitén volcano, which have been identified in Lago Teo (42°S; 72°W) and Lago Espejo (43°S; 71°W) at ~5500 cal yr BP and ~7600 cal yr BP, respectively (Alloway et al., 2017a; Fontijn et al., 2016; Moreno et al., 2015a). It is possible that numerous sites contain tephra units, and notably units from small events, during the mid-Holocene, but that these have not been able to be correlated yet as a consequence of complicated SVZ chemical compositions,

particularly from more mafic events (e.g., Shane, 2000). It is additionally possible, and must not be ruled out, that some of the units identified in the Lago Puyehue sequence are not primary in origin and rather reworked or overthickened as a consequence of the lake being an open body, and of close proximity to numerous volcanic centres; this could make it appear as though the mid-Holocene is more volcanically active than it truly is (Section 3.1).

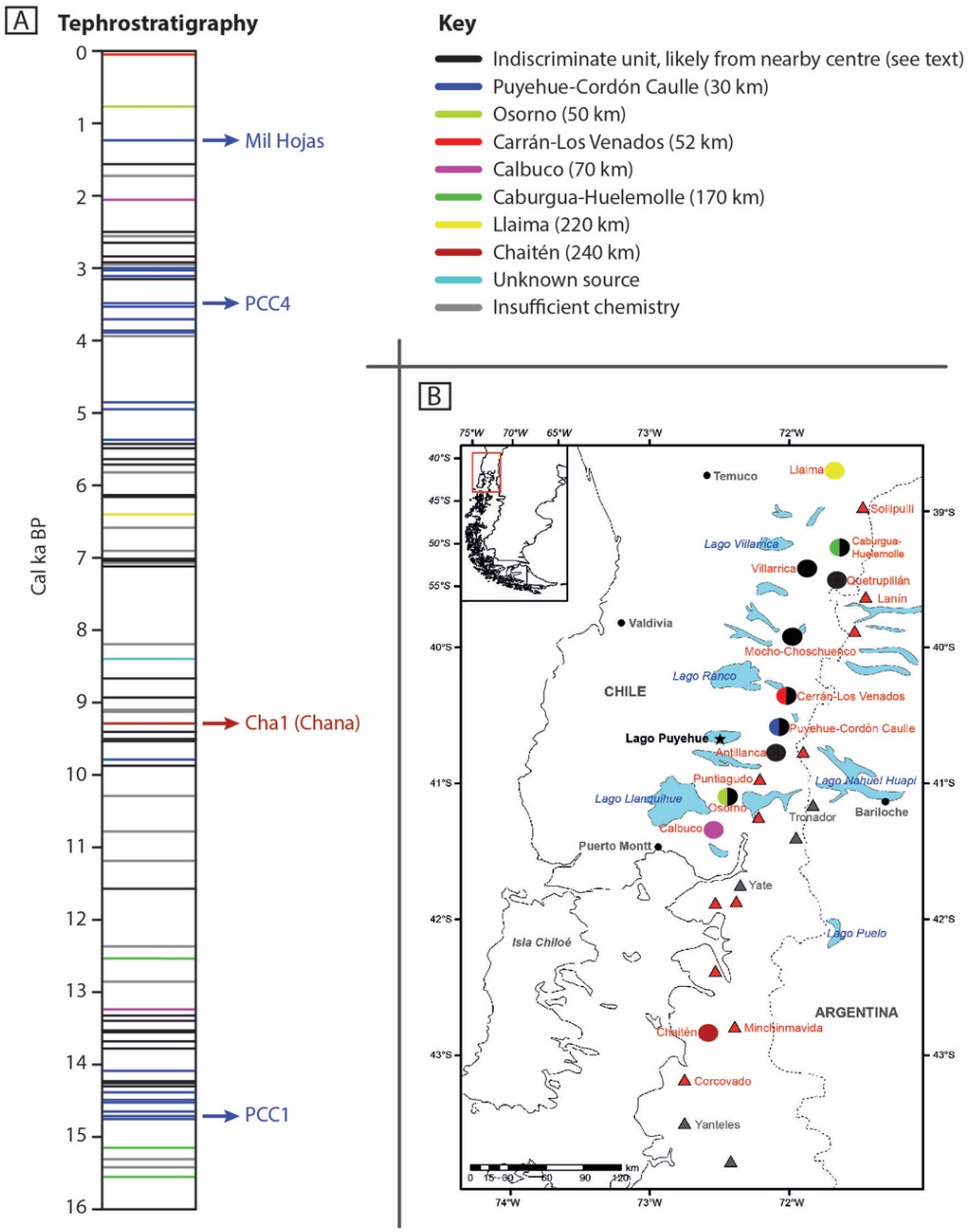


Figure 3.5. A) Tephrostratigraphy illustrating tephra horizons identified in Lago Puyehue by calibrated radiocarbon age (as per Model 2D; Section 3.2.1.5). Layers are marked by coloured lines which vary in accordance to their source composition; see key - top right. Identified regional marker horizons are labelled with arrows, their names, and in the appropriate colours to demark the volcanic source (see key; right). B) Map of the Chilean Lake District showing the location of volcanic centres active during the Quaternary. Centres that have produced deposits that are present in Lago Puyehue are demarked by a coloured circle which can be correlated to the key (above). Numerous centres have black circles, or partially black circles, as these are hypothesised to be sources of indiscriminate tephra frequently seen in in Lago Puyehue (nearby centres; Section 3.3.2). This illustrates the spatial range of eruptive deposits being preserved in the Puyehue record.

Figure 3.6 shows a frequency histogram of the temporal relationship of eruptive deposits preserved in the Lago Puyehue record. Binned dates (eruptions per ka) are plotted against number

of deposits identified (Figure 3.6). There is a statistically insignificant (R^2 value: 0.0055) trend (correlation coefficient) in eruptive activity through the Holocene and thus there is no linear relationship between eruptive activity and time. The highest frequency of events (*n*=12/ky) is seen between 3 and 4 cal kyr BP (Figure 3.6).

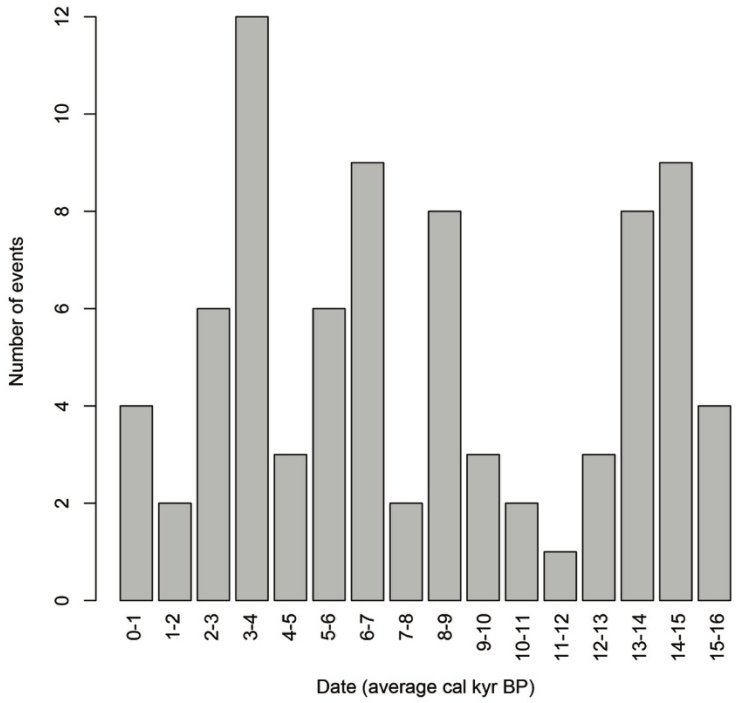


Figure 3.6. Frequency histogram representing the number of volcanic eruptions (deposits) preserved in the Lago Puyehue record as a function of time; each bar represents 1000 years. Dates for tephra deposits refer to those reproduced using Model 2D (see Section 3.2.1.5). The average of these eruptive dates have been used and they have been binned per ka to provide a single representative date per eruption in this figure.

3.4. The chemical composition of tephra deposits identified in the Lago Puyehue sedimentary sequence

This section describes and discusses the chemical composition of tephra deposits in the Lago Puyehue sedimentary sequence, including tentative correlations to source centres where possible. Reference should also be made to Table 3.4.

3.4.1. Contamination

As described in Section 2.1.1, tephra in Lago Puyehue may be preserved instantaneously after fluvial inwashing rather than by primary fallout over the lake (e.g., Bertrand et al., 2014), resulting in an enhanced preservation potential. However, this does also mean that there is potential for redeposition of tephra during non-eruptive periods via flooding, for example (e.g., McLean et al., 2018). The significance of this effect has been analysed by investigating the lacustrine sediment in the Lago Puyehue sedimentary sequence.

Three samples of lacustrine sediment at 292-293 (tephra above: 260.5 cm, tephra below: 323.6 cm), 781-782 (tephra above: 773.8 cm, tephra below: 836.2 cm), and 804-805 (tephra above: 773.8 cm, tephra below: 836.2) cm depth were investigated to determine the concentration of glass-shards in the background sediments. These samples were selected as there was significant portions of lacustrine sedimentation between tephra, allowing the best opportunity to investigate the possibility of tephra contamination. The samples were wet sieved at 25 μm and oven dried before being studied using binocular microscopy. The samples at 292 and 781 cm depth consisted of minerals and organics while the sample at 804 cm depth had minerals in addition to a very low abundance of coarse scoria fragments ~150 μm in size. The scoria grains were hand-picked and chemically analysed using EMPA (Table 3.5); these scoriaceous grains have a fairly homogeneous basaltic-andesite glass composition and are microphenocryst-rich (Figure 3.7).

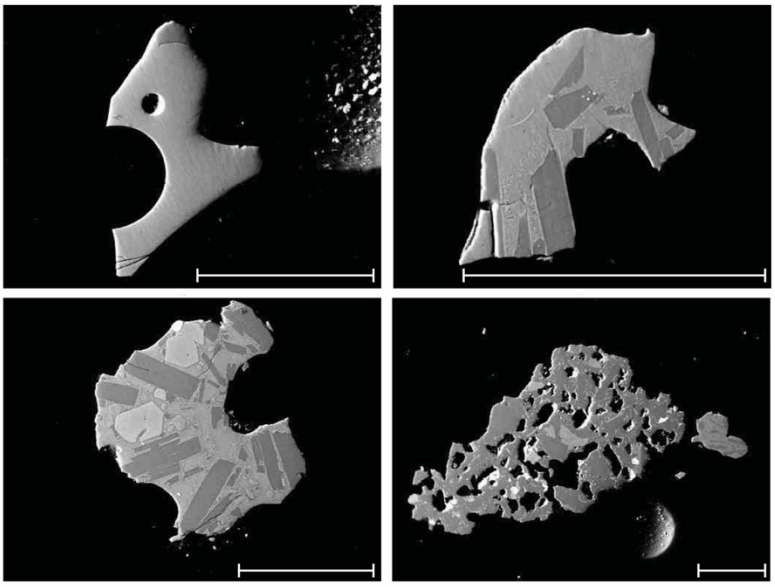


Figure 3.7. BSE images of basaltic andesite shards with microphenocrysts identified in Lago Puyehue sediment between 804 and 805 cm depth. Scale bars on bottom right of each figure represent 100 μm.

The appearance of this tephra may be due to reworking of another layer, or of inwashed scoriaceous material present in the lake's catchment. However, there is a large amount of sedimentation between the appearance of tephra in this contamination test at 804 cm, and the last visible tephra at 836.2 cm (insufficient chemical analyses to determine PUII_836 composition; Table 3.4). An alternative hypothesis is that the appearance of tephra at 804 cm reflects a tephra layer that is not thick enough to be visible to the naked eye (i.e., cryptotephra).

Table 3.5. Glass chemistry (normalised) for tephra identified in the pelagic (background) sediment at 804 cm depth. Total refers to analytical total.

Depth		SiO_2	TiO_2	Al_2O_3	FeO_t	MnO	MgO	CaO	Na_2O	K_2O	P_2O_5	Cl	Total
804 cm	avg	55.91	1.69	15.53	9.89	0.22	3.86	7.69	3.52	1.12	0.48	0.08	97.48
n=8	sd	1.25	0.36	2.10	1.82	0.05	0.64	0.70	0.30	0.27	0.11	0.02	1.94

The risk of chemical contamination between primary tephra units and possible background tephra is minimal given i) only one sample out of three had any presence of tephra, and ii) the presence of tephra in the lacustrine sample which did contain tephra (804 cm) was very sparse (i.e., low concentration). Given that mafic centres predominantly feed into the catchment, the likelihood of contamination by mafic tephra is considered greater than that of

contamination by felsic tephra, though it is respected that silicic-rich tephra can also contribute to contamination as they typically disperse widely and deposit thick units that can be reworked by wind (e.g., Zanchetta et al., 2018).

3.4.2. Heterogeneous deposits in Lago Puyehue

Fifteen tephra deposits in the sedimentary sequence have a bimodal composition (those at 1037, 1029, 1010, 1002, 615, 607, 583, 488, 369, 362, 253, 248, 209, 197, 191 cm depth) and 16 deposits have a heterogeneous composition, with a wide SiO_2 range (samples from 1015, 1005, 988, 969, 932, 928, 918, 773, 673, 667, 648, 495, 487, 180, 178, and 166 cm depth; Table 3.4). It is considered unlikely that contamination (i.e., of minerals or glass-shards from other layers) has influenced the results of the chemical analyses (See Section 3.4.1). Thus, the observed bimodalism/heterogeneity is hypothesised to most likely be caused by separate or poorly mixed magmas in the chambers at the time of the eruptions, as seen in Hudson tephra (Haberle and Lumley, 1998) and the NHT/PBN units from Antillanca volcano (Fontijn et al., 2016; Naranjo et al., 2017). Alternative causes for heterogeneous chemistry include i) the accidental analysis of mineral phases during EPMA (while all care is taken not to analyse minerals, and the chemical dataset is finally filtered for mineral presence, some partial mineral analyses may still be present), and ii) multiple eruptions occurring very closely in time; for example, tephra at 648 cm (10.16-8.95 cal ka BP) is heterogeneous and chemical analysis indicates that the more felsic component is derived from Chaitén while the more mafic component is derived from a non-correlatable centre which is likely close to Lago Puyehue.

The predominantly thin, bimodal/heterogeneous deposits identified in Lago Puyehue cannot easily be chemically fingerprinted to source because there are a high number of microphenocrysts present in the glass-shards, but it is speculated that they are sourced from nearby centres (e.g., Bertrand et al., 2014). These centres typically produce small-magnitude events that are silica-poor, but overall erupt a range of chemistries on different magnitudes, and as such their compositions are highly indistinct, making it challenging to fully discriminate to a

source origin (e.g., Puyehue-Cordón Caulle, Calbuco, Osorno, Antillanca, and possibly Mocho-Choschuenco, Carrán-Los Venados and Villarrica; Figures 1.3; 1.8; 3.8; Table 3.4). The chemical analysis of tephra layers identified in Lago Puyehue shows that 30 layers are likely from these aforementioned centres, in addition to a possible 15 that were unable to be analysed due a high abundance of microphenocrysts (Table 3.4; Figure 3.8). These 30 chemically analysed tephra layers typically have a mafic component (i.e., ~55 wt% SiO_2) but are not able to be easily correlated to sources due in large part to many of the samples being heterogeneous. Chemical heterogeneity (49.5-71.3 wt% SiO_2) has recently been observed in deposits from Melimoyu volcano, located in the SVZ, but is otherwise not widely reported in the region (e.g., Geoffroy et al., 2018).

Figure 3.8 (specifically A-C) shows that the chemical compositions of deposits from these centres identified in Lago Puyehue follow at least two distinct fractionation trends. Figure 3.8B shows two trends, with one of these changing abruptly. The onset of a new mineral phase fractionating can result in a sharp kink in the fractionation trend. Therefore, the abrupt adjustment in the fractionation trend observed in Figure 3.8B could indicate that there has been a change in the mineral assemblage being fractionated in the melt. Most deposits fall along one of two trends that plot in a straight line, identifiable in Figure 3.8A and 3.8C. This could indicate that the chemical variation observed in individual samples is caused by magma mixing; trace elemental analysis would likely provide further insight into this. Certainly in Figure 3.8C, there are at least three distinct trends in samples PUII_180, PUII_928/209 and PUII_495 which cannot be explained by fractionation alone. This indicates that there are at least three different volcanic sources for these groups of samples, or that different types of magma have been erupted across the complexes.

The use of TiO_2/CaO in Figure 3.8D indicates that some tephra deposits in Lago Puyehue are from Calbuco volcano or larger-than-characteristic eruptions from Villarrica volcano (~70 and 145 km south, respectively; Figure 3.8G/H). These are indicated by a number of deposits in Lago Puyehue having a high abundance of CaO (up to 11 wt%), which is comparable to the glass chemistry of Calbuco products (e.g., Watt et al., 2011; Fontijn et al., 2016; Rawson and Pyle,

unpublished), and recent products from Villarrica volcano (e.g., Van Daele et al., 2014). In the past 600 years, Villarrica has typically experienced small (VEI ~1-3) eruptions (Van Daele et al., 2014). These small eruptive deposits of mafic composition would, however, not be expected to reach Lago Puyehue based on previous investigations (e.g., Van Daele et al., 2014; Fontijn et al., 2016). Deposits from larger Villarrica eruptions include Chaimilla, Pucon Ignimbrite and Licán Ignimbrite (VEI 4, 5, 6; aged 3446-3091, 4044-3927, 16,877-16,549 cal yr BP respectively; Fontijn et al., 2016). These were dispersed north and radially and the current maximum observed distance of these large eruptions is still only 40 km (Silva Parejas et al., 2010; Costantini et al., 2011; Lohmar et al., 2012; Fontijn et al., 2016). However most of their studied deposits comprise deposits from Pyroclastic Density Currents (PDC), and very few associated tephra fall deposits from these units have been studied yet. It is therefore possible that some of the large known Villarrica deposits have an unidentified tephra fall component >40 km from source. In addition to possible source centres, Calbuco or Villarrica, the glass chemical dataset for Osorno volcano is small (and entirely within the range of Villarrica volcano), and given more research, this centre may well be a more likely candidate for many of these high-Ca deposits, as the centre is more proximal to Lago Puyehue (~50 km south).

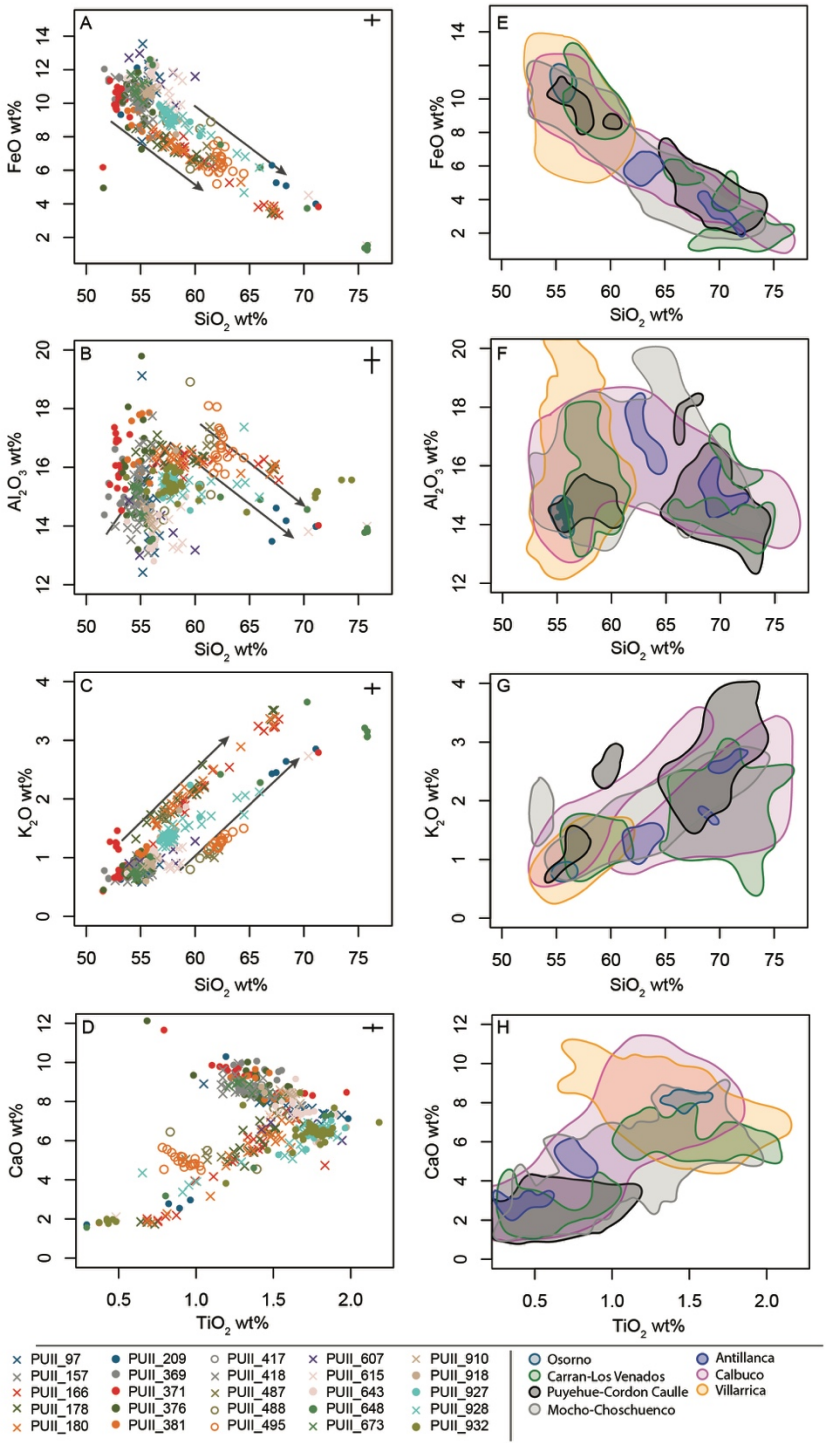


Figure 3.8. A-D: Glass chemistry of layers which have relatively indiscriminate chemical composition and are likely from nearby centres (Section 3.4.2). Chemical trends are identified on plots using arrows. Tephra can be identified by key at bottom left of figure; E-H: Chemical fields (glass-shard analysis only) of volcanic centres which produce deposits near-to Lago Puyehue. Colour relates to source; key at bottom right of figure. Error bars (top, right of A-D) represent 2 standard deviations of repeat analyses of the StHs6/80-G MPI-DING reference glass. Data from E-H is derived from Fontijn et al. (2016; Osorno, Carrán-Los Venados, Villarrica, Puyehue-Cordón Caulle, Calbuco); Rawson et al. (2015; Mocho-Choschuecno); this study (Antillanca, Puyehue-Cordón Caulle); Watt et al. (2011; Calbuco), and Rawson and Pyle (unpublished; Calbuco).

3.4.3. Llaima volcano (38°41' S; 71°43' W)

Llaima (~220 km north north-east from Lago Puyehue) is a composite stratovolcano that is characterised by large abundances of deposits which have a wide compositional range. Llaima has erupted at least two wide-spread deposits: i) the Curacautín ignimbrite, occurring as a two-phased event between ~14.4 and 13.0 cal ka BP and with a DRE of ~10.43 km^3 (after Lohmar et al., 2005, 2006), and ii) the Llaima pumice, occurring between 10.59 and 10.34 cal ka BP, which was a widespread fall with proximal PDC's and had an estimated eruptive volume of 4.7 km^3 (Fontijn et al., 2016).

One 0.5 cm thick andesitic deposit is identified in Lago Puyehue at 445.1 cm depth (PUII_445) which has an average SiO_2 and K_2O content of 61.01 wt% and 1.05 wt% respectively (Figure 3.9). While PUII_445 appears compositionally similar to deposits from Calbuco, and therefore this source cannot be fully ruled out, the unit has a lower abundance of FeO_t (~5.8 wt%) than Calbuco deposits typically do (cf. Watt et al., 2011). The unit also follows a different trend to Calbuco, which is more similar to the composition of deposits from Llaima volcano. The same is true for Al_2O_3 and SiO_2 contents. A tentative correlation to Llaima volcano is therefore suggested for PUII_445, which is deposited between 6.58 and 6.17 cal ka BP.

The ash specifically correlates chemically well with the Llaima Pumice scoria component as described in Fontijn et al. (2016), however the age does not correspond with this unit (~10.45 cal yr BP; Fontijn et al., 2016). None-the-less between ~12 and 4 ka, at least 19 tephra units were emplaced (unit V (V_a-V_t) in the terrestrial stratigraphy, above Llaima Pumice; see Schindlbeck et al. (2014) for full stratigraphy). During this time, the longest repose time was of 384 years (on the basis of proximal deposits in terrestrial stratigraphy) and the majority of deposits were basaltic-andesitic in composition (Schindlbeck et al., 2014). It is speculated that PUII_445 correlates to a deposit from Llaima volcano in unit V on the basis of age.

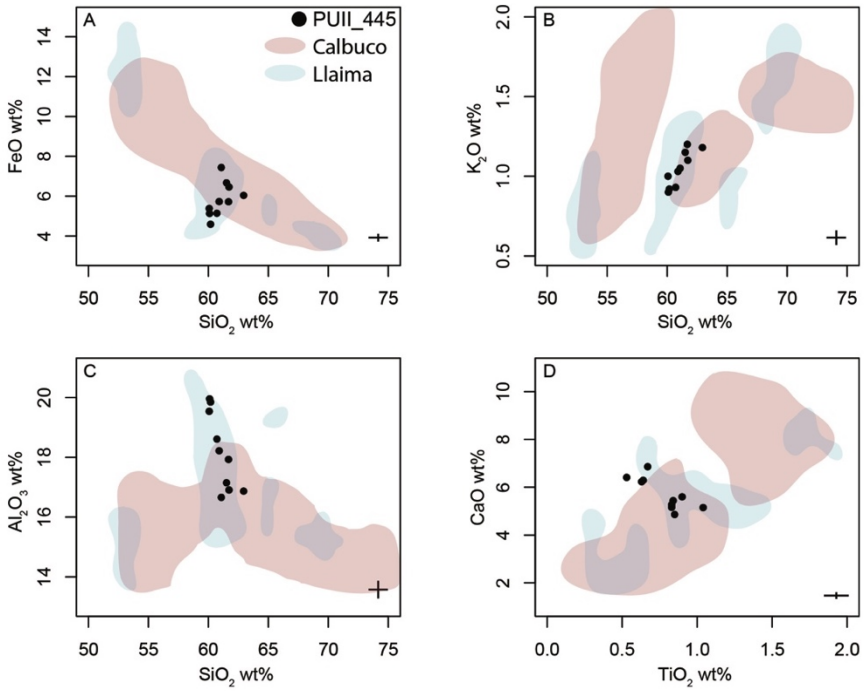


Figure 3.9. A-D: Glass chemistry of layer PUII_445 (key: top left) which has been correlated to Llaima volcano using glass-chemistry. Glass-chemical field data from Llaima (Llaima Pumice and Curacautin Ignimbrite) and Calbuco volcano from Watt et al. (2011), Fontijn et al. (2016) and Rawson and Pyle (unpublished). Error bars represent 2 standard deviations of repeat analyses of the StHs6/80-G MPI-DING reference glass.

3.4.4. Caburgua-Huelemolle (39°15' S; 71°42' W)

Caburgua-Huelemolle represents a group of 21 pyroclastic cones in eight volcanic centres: Caburgua, Huelemolle, La Barda, Relicura, Cañi, Redondo, Cordillera Cañi and San Jorge (Medina, 2016; 170 km north of Lago Puyehue). Relatively little is known about this group. However, two VEI 3-4 eruptions have been identified from Caburgua-Huelemolle, occurring between 10.38 and 10.31 cal ka BP (Fontijn et al., 2016). The erupted magmas of these centres are mafic, and the SiO_2 content of glass-shards from deposits from this group are ~53 wt% (Fontijn et al., 2016). The chemical signature of these deposits are similar to Villarrica and Puyehue-Cordón Caulle, but there are some distinctive characteristics. Caburgua-Huelemolle's location in the northern sector of the SVZ results in deposits which are typically relatively high in CaO (~8.5 wt%); centres located in the northern sector of the SVZ are likely to be more enriched in CaO than centres in the south of the SVZ due to their positioning above thickened crust and the subsequent continental crustal contamination that arises from this (Hickey et al.,

1986). Caburgua-Huelemolle deposits additionally often have higher K_2O contents relative to silica-poor deposits from Villarrica volcano (~1.1 vs. ~1.0 wt%).

Low abundance of SiO_2 (~53 wt%) in association with relatively high abundance of TiO_2 (1.42-2.03 wt%) and CaO (7.3-10.52 wt%) is identified in three deposits located at 1117.0-1117.3 cm (PUII_1117; 15.91-15.23 cal ka BP), 1078.0-1078.5 cm (PUII_1078; 15.53-14.97 cal ka BP) and 851.5-852.0 cm (PUII_851; 12.90-12.52 cal ka BP) depth (Figure 3.10). Based on these chemical traits, these deposits are speculated to be derived from the Caburgua-Huelemole cones. However, the deposits are older than those identified by Fontijn et al. (2016) and do not chronologically correlate with known eruptions from Caburgua-Huelemolle. This could point toward new occurrences of the deposits, or inaccurate tephra correlation; PUII_1117 remains the firmest chemically correlated unit of these three layers.

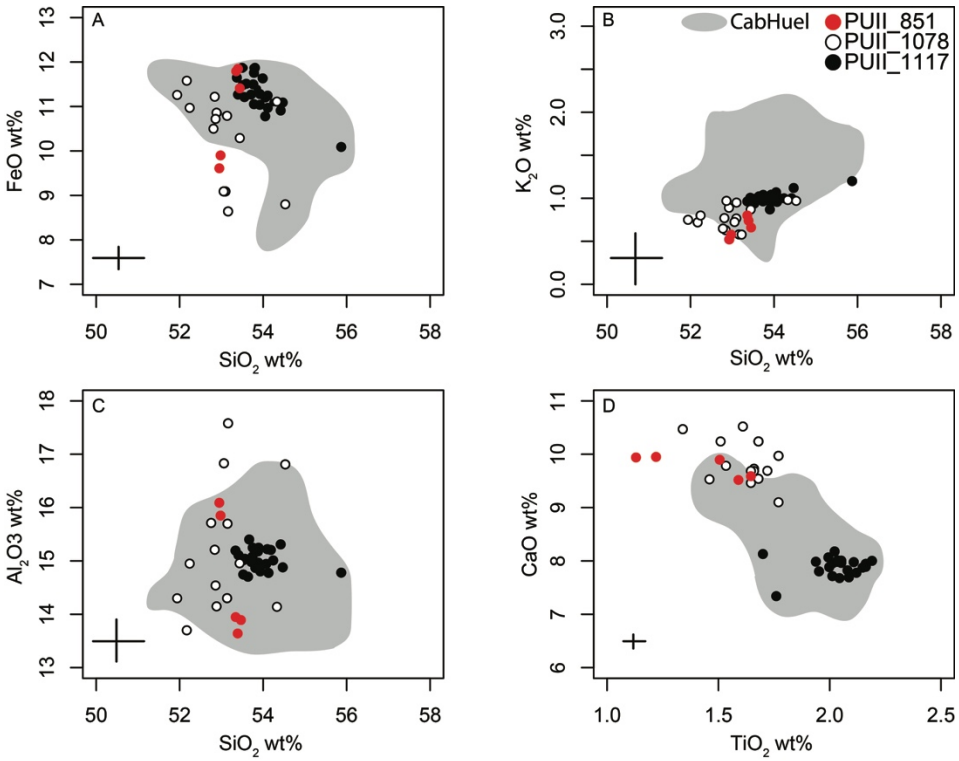


Figure 3.10. A-D: Glass chemistry of layers PUII_851, PUII_1078 and PUII_1117 (key: top right) which have been correlated to Caburgua-Huelemolle using glass chemistry. Glass-chemical field data from Caburgua-Huelemolle (CabHuel) volcano from Fontijn et al. (2016). Error bars represent 2 standard deviations of repeat analyses of the StHs6/80-G MPI-DING reference glass.

3.4.5. Puyehue-Cordón Caulle (40°35' S; 72°07' W)

Puyehue-Cordón Caulle is a frequently active volcanic complex and has experienced at least five VEI >4 explosive eruptions in the past, including PCC1, PCC2, Ranco pumice (all rhyolite), PCC4 (dacite), and Mil Hojas (rhyodacite). While deposits are typically homogeneous, the centre is capable of erupting a wide range of magma compositions (48-71 SiO_2 wt%; Lara and Moreno, 2006). Mafic products were erupted from Puyehue-Cordón Caulle during the early-Holocene (Lara et al., 2006) and have also been recorded in the heterogeneous Ranco Pumice (56-74 SiO_2 wt%; Fontijn et al., 2016). The three historical eruptions from Puyehue-Cordón Caulle in AD 2011, 1960 and 1921 were all rhyodacitic in composition. Because of this compositional variability, Puyehue-Cordón Caulle deposits have a relatively indistinguishable glass chemistry from other centres in the region, including for example, Villarrica and Mocho-Choschuenco. As already discussed, due to Villarrica's predominantly small-scale activity (e.g., Van Daele et al., 2014), and distance (~145 km) from Lago Puyehue, deposits from Puyehue-Cordón Caulle are more likely to be identified in the sequence than those from Villarrica.

Seventeen deposits from the Lago Puyehue sedimentary sequence are correlated tentatively to Puyehue-Cordón Caulle based on their chemical affinity (Table 3.4; Figure 3.11). These deposits are identified at 81.0, 191.1/191.9, 197.6, 226.2, 228.8, 248.6, 253.8, 256.1, 324.5, 362.8, 667.0, 988.0, 1010.4, 1015.1, 1029.4, 1036.5, and 1037 cm depth (see Section 3.5 for further information about 1036.5, 226.2, and 81 cm; Table 3.4). PUII_191 is a rhyodacite while other tephra correlated to Puyehue-Cordón Caulle are trachydacite and rhyolitic in composition overall (Table 3.4). Figure 3.11 shows the tephra deposits (excluding 1036.5, 226.2 and 81 cm; see Section 5) presented with the compositional fields for Puyehue-Cordón Caulle.

These eruptive deposits were identified by their different chemical characteristics. For example, tephra at 253.8 cm (2.0 cm thickness) was distinguished from Mocho-Choschuenco as it had greater amounts of FeO_t and lower amounts of Al_2O_3 than Mocho-Choshuenco deposits typically do, and was distinguished from Osorno and Villarrica volcanoes as it was more enriched in SiO_2 than deposits from these centres. In most cases, FeO_t was the greatest distinguishing chemical characteristic that indicated Puyehue-Cordón Caulle as the deposit source.

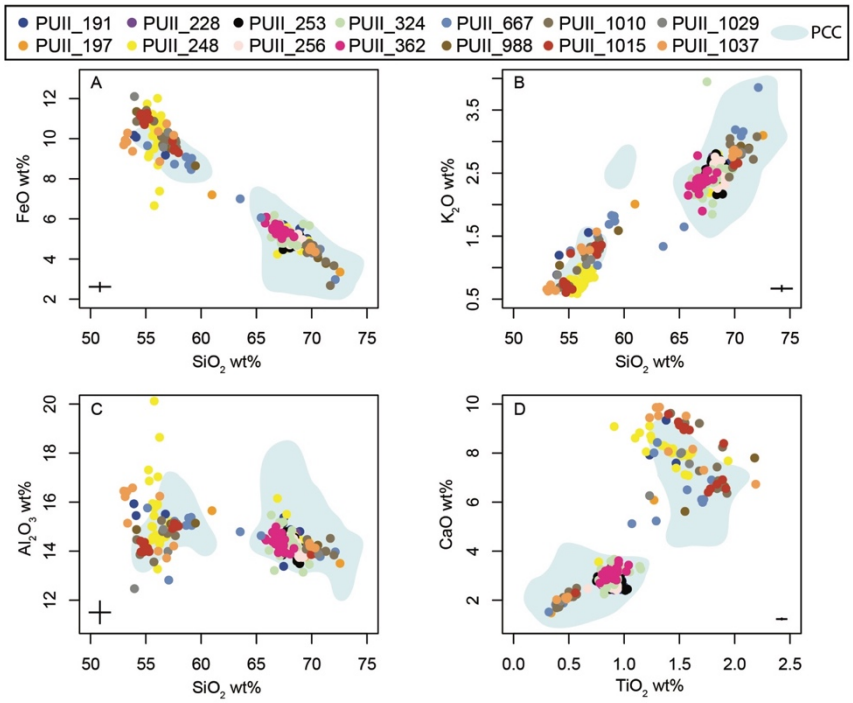


Figure 3.11. A-D: Glass chemistry of Puyehue tephra layers most likely associated with Puyehue-Cordón Caulle (key: top) on the basis of glass-shard chemistry. Glass-chemical field data from Puyehue-Cordón Caulle (PCC) volcano, from Fontijn et al. (2016). Error bars represent 2 standard deviations of repeat analyses of the StHs6/80-G MPI-DING reference glass.

3.4.6. Calbuco (41°19' S; 72°37' W)

The established stratigraphy for Calbuco volcano (~73 km distance from Lago Puyehue) indicates that the centre has been very active during the Holocene, with at least 14 locally dispersed eruptions including the 2015 eruption (see Watt et al., 2011 for pre-2015 stratigraphy). Activity at Calbuco increased during the early Holocene, with large explosive eruptions occurring with a periodicity of less than every 1 kyr (Watt et al., 2011). Proximal isopach mapping shows that deposits from the 2015 sub-Plinian VEI 4 eruption are preserved as far as 300 km, with 1 cm thick deposits as far north north-east as 55 km from the centre (e.g., Lago Rapunco; Castruccio et al., 2016; Van Eaton et al., 2016), and 0.1 cm thicknesses being preserved in the Lago Puyehue region, 70 km north from the centre (Van Eaton et al., 2016).

Deposits from this centre tend to be compositionally similar to others in the SVZ, and notably to Llaima as mentioned previously, making these predominantly andesitic deposits difficult to fingerprint. However, the overall chemical signature of the centre is generally well defined by having low K_2O values with respect to SiO_2, particularly in comparison to other SVZ

volcanoes. This is likely the result of higher degrees of partial melting (e.g., Crawford et al., 1989).

A 0.5 cm thick tephra identified in Lago Puyehue at 130.3 cm (PUII_130) has a chemical composition consistent with a Calbuco source. While it is compositionally similar to Llaima, the PUII_130 deposit is notably more depleted in TiO_2 (relative to SiO_2) than Llaima deposits (~1.0 vs. 1.3 wt%, respectively; Figure 3.12). PUII_130 was deposited between 2.70 and 1.51 cal ka BP, and it is hypothesised to correlate to the Calbuco tephra called Ca12 as identified in Watt et al. (2011; Figure 3.12), and which occurred between 1.8 and 1.4 cal ka BP (Watt et al., 2011).

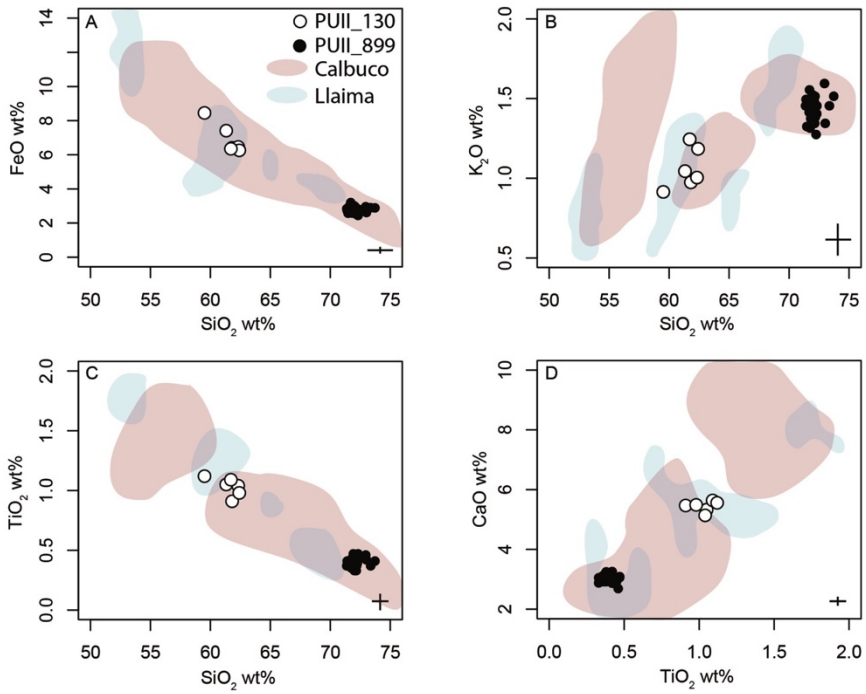


Figure 3.12. A-D: Glass chemistry of layers PUII_130 and PUII_899 (key: top left) which have been tentatively correlated to Calbuco using glass-chemistry. Glass-chemical field data from Calbuco volcano using data from Watt et al. (2011); Fontijn et al. (2016) and Rawson and Pyle (unpublished), and data from Llaima volcano using data from Fontijn et al. (2016). Error bars represent 2 standard deviations of repeat analyses of the StHs6/80-G MPI-DING reference glass.

The rhyodacitic tephra layer in Lago Puyehue at 899.5 cm depth (PUII_899; 13.42-13.05 cal ka BP; Figure 3.12) is also tentatively correlated to Calbuco based on its low K_2O and SiO_2 (1.43 and 72.05 wt%, respectively), but there are no contemporaneous tephra deposits known in the region (Figure 3.12). This correlation indicates that the volcano may have been active earlier in the Holocene than previously identified, with tephra being dispersed NNE at least ~70 km from

source. The thickness of this deposit is 3.5 cm. While this may indicate that the eruption was large, no quantitative eruptive size can be deduced since this layer has only been identified at a single site and units in Lago Puyehue may be prone to overthickening (Section 3.1; e.g., Dugmore et al., 2018; Weller et al., 2014). Further efforts should be made to attempt to identify this layer in other CLD archives.

3.4.7. Chaitén (42°49' S; 72°38' W)

Chaitén volcano (240 km south from Lago Puyehue) is located near to the forearc, and deposits are typically rich in SiO_2 (~75 %) and K_2O (~3.5 %); this may be the result of assimilation of granitoid basement (Watt et al., 2013b). A single and firm correlation to a widespread felsic deposit from Chaitén was identified in the Lago Puyehue record, and is discussed in Section 3.5.

3.5. Regional marker horizons

A regional marker horizon gives reference to a widespread tephra layer – these can be of any composition but are typically rhyolitic since deposits with this composition often result from Plinian eruptions that can widely disperse pumice and ash. More mafic tephra layers (e.g., basaltic andesite) are typically more complex to correlate over wide areas as they are less chemically distinct, and erupt more frequently with generally lower eruptive volumes (Shane, 2000). The value of regional marker horizons is outlined in Chapter 1. This section outlines and discusses the regional marker horizons identified in the Lago Puyehue sedimentary sequence.

3.5.1. Regional marker horizons in the Lago Puyehue sedimentary record

Four tephra layers in the Lago Puyehue sedimentary sequence have been correlated to previously documented widespread marker layers from large, explosive eruptions across the CLD. Using glass shard chemistry, three of these deposits have been correlated to the nearby volcanic complex Puyehue-Cordón Caulle (PCC1, PCC4, and Mil Hojas), located ~30 km away,

while one is from Chaitén volcano (Cha1), located ~240 km away. These isochrons are newly identified in the Lago Puyehue sequence and additional ages attributed to the layers offer scope to better constrain the chronologies of sedimentary archives across the region (Table 3.2; Figure 3.13). While these layers certainly appear to be firm correlations, it is still recommended that they be considered with caution given the complex nature of the chemical composition of SVZ deposits, and how frequently these centres erupt; the Mil Hojas and Cha1 layer are considered the strongest correlations in light of robust chronology, chemistry and prior knowledge of the deposits.

The Mil Hojas tephra layer is derived from Puyehue-Cordón Caulle and is described in detail in Naranjo et al. (2017). It is the largest known eruptive deposit (VEI 5) from a vent at Puyehue volcano (Fontijn et al., 2016; Naranjo et al., 2017). The unit is highly stratified in the terrestrial record and has significant grain size variations with sharp contacts between alternating layers of pale-beige to yellow pumice lapilli, and grey fine-coarse lithic-rich ash. These deposits are traceable up to 90 km east south-east from source in the terrestrial record (Naranjo et al., 2017). However, Mil Hojas deposits have also been identified in Lago Villarrica, 145 km north from source (Fontijn et al., 2016). The estimated volume of ejecta is 1.73 km^3 (Naranjo et al., 2017).

The age of the Mil Hojas deposit has been constrained using radiocarbon dating in other studies. Naranjo et al. (2017) reports ages of 1.11±0.07 cal ka BP (preferred age based on charcoal from base of deposit), and 0.84±0.11 cal ka BP (age based on charcoal from base of deposit). Fontijn et al. (2016) reports an age of 0.84±0.17 cal ka BP for the Mil Hojas deposit based on the regional age model (as per Fontijn et al., 2016; the reconstructed age is based on dates from individual core sequences).

A 0.5 cm thick, medium brown ash is located at 81 cm depth in the Lago Puyehue sedimentary record which has been chemically correlated to Mil Hojas (PUII_81). It was identified as T5 in Bertrand et al. (2008a), but it was not chemically analysed prior to this work. This tephra is composed predominantly of vesicular and fluted colourless shards but there are

also some scoria grains rich in microphenocrysts (there is detrital material present within the vesicles).

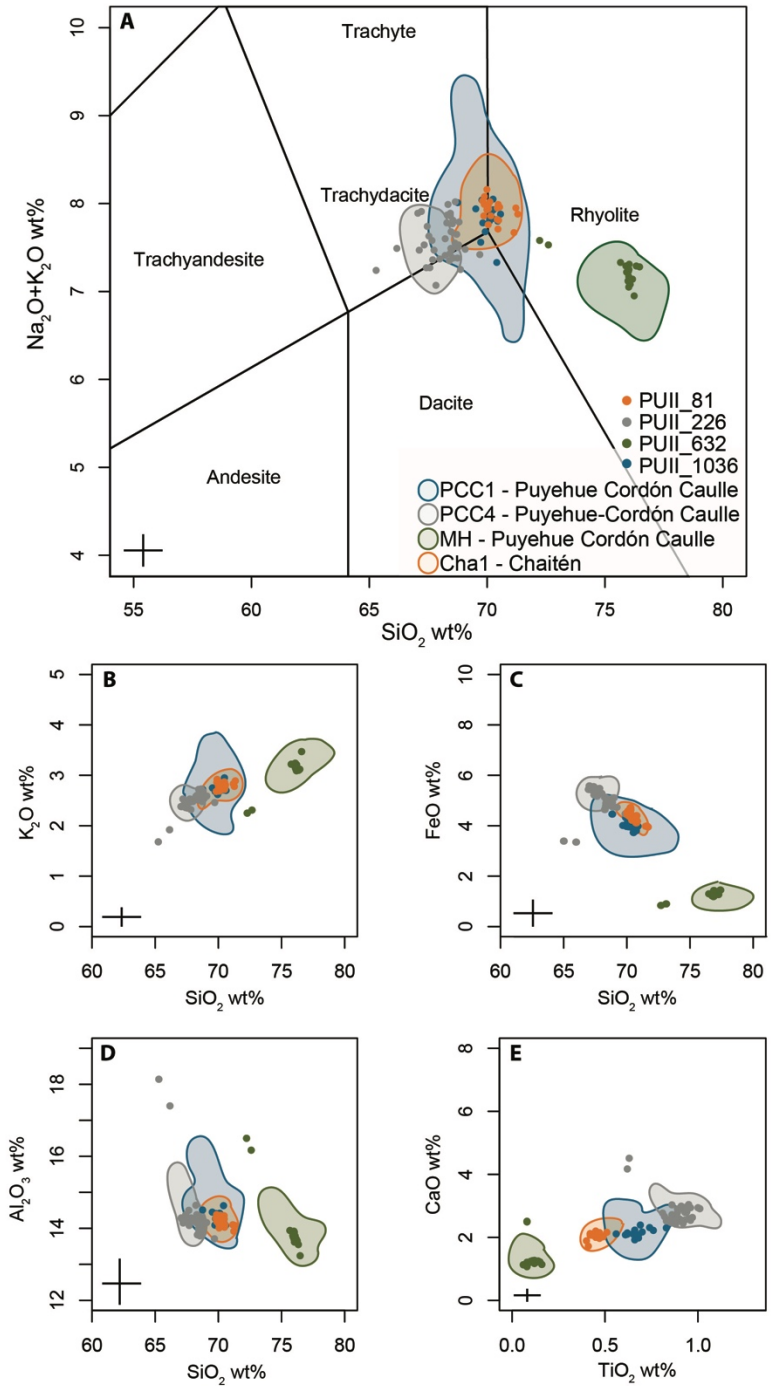


Figure 3.13. Glass chemistry of layers which have been identified as correlatable to regional marker horizons: PCC1, PCC4, Cha1 (Chana) and Mil Hojas (MH). Compositional fields for marker horizons are provided using data from Fontijn et al. (2016). Error bars represent 2 standard deviations of repeat analyses of the StHs6/80-G MPI-DING reference glass.

PUII_81 is a homogeneous rhyolite, and has an average SiO_2 content of 70.01 wt% which correlates well to the signature of the widespread marker horizon, Mil Hojas, originating from

the Puyehue-Cordón Caulle volcanic complex (Table 3.6, Figure 3.13). Unfortunately, the chemistry produced from this study cannot be compared to that from Naranjo et al. (2017) as they used bulk tephra analyses and the results of that are not comparable to individual glass-shard analysis (Chapter 1); Naranjo et al. (2017) obtained dacite chemistries for their Mil Hojas layers. Using the age-depth model from this study, PUII_81 is ascribed a date of 1.83-0.46 cal ka BP which correlates chronologically with other Mil Hojas layers (Fontijn et al., 2016; Naranjo et al., 2017).

Table 3.6. Glass chemistry (normalised) for tephra at 81 cm depth in PUII (this study), and glass chemistry for Mil Hojas regional marker horizon from Fontijn et al. (2016). Total refers to analytical total.

Unit		SiO_2	TiO_2	Al_2O_3	FeO_t	MnO	MgO	CaO	Na_2O	K_2O	P_2O_5	Cl	Total
PUII_81	avg	70.01	0.68	14.31	4.01	0.13	0.61	2.15	5.09	2.74	0.13	0.17	99.47
n=15	sd	0.45	0.07	0.16	0.18	0.03	0.08	0.13	0.19	0.08	0.03	0.03	0.56
Mil Hojas	avg	70.01	0.67	14.31	4.01	0.12	0.58	2.11	5.22	2.84	0.13	0.20	98.61
n=406	sd	0.54	0.06	0.25	0.21	0.04	0.07	0.17	0.29	0.16	0.03	0.02	0.83

There is very little known about the deposit from Puyehue-Cordón Caulle referred to as PCC4. There are no known terrestrial exposures of the deposit, and only one identification of the layer in Lago Calafquen (115 km from source) after work undertaken by Fontijn et al. (2016). The eruption producing this deposit is hypothesised to be ~VEI 4, but further identification of PCC4 deposits are needed to better constrain this. Based on the regional age model devised by Fontijn et al. (2016), the PCC4 eruption occurred between 3264 and 2955 cal yr BP.

A 0.1 cm thick tephra identified at 226.2 cm contains crystal-poor pumiceous grains, as well as brown, crystal-poor, vesicular shards. There is a limited amount of microlite inclusions in the glass. The homogeneous deposit identified in the Lago Puyehue sedimentary sequence is rhyodacitic and has an average SiO_2 content of 68.22 wt%. This layer chemically correlates well to the PCC4 tephra identified in Lago Calafquen (Fontijn et al, 2016; Table 3.7, Figure 3.13). It is dated between 3036 and 4002 cal yr BP in Lago Puyehue and therefore also correlates well chronologically.

Table 3.7. Glass chemistry (normalised) for sample from 226.2 cm depth (PUII_226; this study), the PCC4 regional marker horizon (as per Fontijn et al., 2016), and PCC4* which is the PCC4 sample from Fontijn et al. (2016), reanalysed in this study for inter-laboratory verification. Total refers to analytical total.

Unit		SiO_2	TiO_2	Al_2O_3	FeO_t	MnO	MgO	CaO	Na_2O	K_2O	P_2O_5	Cl	Total
PUII_226	avg	68.22	0.90	14.16	5.07	0.14	0.85	2.68	5.05	2.53	0.23	0.17	98.19
n=38	sd	0.59	0.05	0.20	0.27	0.06	0.09	0.18	0.20	0.09	0.03	0.04	1.96
PCC4	avg	67.68	0.93	14.37	5.36	0.16	0.90	2.89	4.99	2.46	0.26	0.16	99.00
n=43	sd	0.28	0.05	0.31	0.18	0.04	0.07	0.14	0.20	0.09	0.02	0.02	1.16
PCC4*	avg	67.40	0.93	14.29	5.39	0.16	0.93	2.89	5.14	2.45	0.26	0.15	99.02
n=43	sd	0.23	0.05	0.23	0.17	0.04	0.05	0.10	0.18	0.07	0.03	0.02	1.20

Cha1, from Chaitén volcano, is a widespread deposit from a VEI 5 eruption occurring between 10.11 and 9.69 cal ka BP (Fontijn et al., 2016). It produced 5.5 km^3 of aphyric rhyolitic (~75-76 SiO_2 wt%) tephra (Amigo et al., 2013; Fontijn et al., 2016; Watt et al., 2013b). Tephra was dispersed to the north and north-northeast of Chaitén (Naranjo and Stern, 2004; Amigo et al., 2013; Watt et al., 2013b; Fontijn et al., 2016), and has been identified up to 400 km from the source in Lago Espejo, Lago Villarrica and Laguna Las Ranas (Fontijn et al., 2016; Alloway et al., 2017a). The deposit can be observed as a ~70-cm thick pumice layer in outcrops around the volcano (e.g., the Mallines section ~25 km from the vent; Amigo et al., 2013).

At 632.7 cm depth in the Lago Puyehue sedimentary sequence, there is a 0.9 cm thick, fine white ash (PUII_632). This tephra is mineral-poor, and comprises predominantly microphenocryst-rich pumice, and colourless fluted and vesicular shards. There is a minor abundance of microphenocryst-rich scoria. The homogeneous deposit has a rhyolite chemistry (~76.05 wt% SiO_2) and it correlates well with the regional marker horizon, Cha1 from Chaitén (Table 3.8; Figure 3.13). The chronology from Lago Puyehue (Section 3.2.1.5) indicates it was most likely deposited between 9.72 and 8.15 cal ka BP, which is consistent with the previously known age.

Table 3.8. Glass chemistry (normalised) of the tephra at 632.7 cm depth (PUII_632), the Cha1 regional marker horizon as per Alloway et al. (2017a); Cha1[1]=Fontijn et al. (2016); Cha1[2]=Amigo et al. (2013). Total refers to analytical total.

Unit		SiO_2	TiO_2	Al_2O_3	FeO_t	MnO	MgO	CaO	Na_2O	K_2O	P_2O_5	Cl	Total
PUII_632	avg	76.05	0.11	13.72	1.30	0.06	0.21	1.21	3.99	3.19	0.06	0.09	94.70
n=17	sd	0.17	0.03	0.16	0.07	0.04	0.01	0.05	0.10	0.08	0.03	0.01	0.42
Cha1	avg	77.44	0.08	13.35	1.27	0.06	0.18	0.98	3.48	3.06	NA	NA	NA
n=16	sd	0.56	0.02	0.23	0.09	0.02	0.03	0.11	0.36	0.17	NA	NA	NA
Cha1[2]	avg	76.06	0.11	13.86	1.32	0.06	0.20	1.22	3.98	3.12	0.07	NA	95.34
n=71	sd	0.50	0.03	0.28	0.12	0.03	0.04	0.12	0.31	0.11	0.03	NA	1.15
Cha1[3]	avg	75.83	0.09	14.07	1.27	0.08	0.21	1.25	3.98	3.06	0.06	0.10	95.91
n=29	sd	0.26	0.04	0.13	0.07	0.03	0.02	0.05	0.331	0.08	0.02	0.01	1.67

A tephra unit from Puyehue-Cordón Caulle has been radiocarbon-dated using carbonate-cemented concretions from a varve record at Rio Fenix Chico to 10.47±0.15 ka (50 km east of Puyehue-Cordón Caulle; Kaplan et al., 2004). It is only identified in one location, on granitic moraine boulders, likely because it was deposited during/at the end of the Last Glacial Maximum and the tephra preservation is regionally poor because of scour (e.g., Fontijn et al., 2016). The tephra is weathered and comprises orange pumice lapilli, mostly altered to clay (Singer et al., 2008). Surrounding this unit, dacitic lavas have been identified and are referred to as Pr1; a range of $^{40}Ar/^{39}Ar$ dates (12.3±1.9, 12.0±2.8, and 11.5±1.1 ka) have been determined for Pr1 from 12.3 to 11.5 ka, indicating that during this period, sub-Plinian/Plinian activity was likely accompanied by phases of effusive activity (Singer et al., 2008), and this activity prevails to the present day. One radiocarbon date has been obtained, and returns a much younger age of 10.58-10.28 cal yr BP (calibrated using OxCal 4.3, ShCal13; 9310±45 yr BP; Singer et al., 2008). The Pr1 deposit of Singer et al. (2008) is suspected to be chemically indistinct from the better chemically characterised tephra called PCC1 in Fontijn et al. (2016) which has been calibrated to 10.46-10.30 cal ka BP on the basis of this previous radiocarbon date from Singer et al. (2008). This event is hypothesised to be medium sized (VEI 4) but currently only identified in medial-proximal sedimentary outcrops (Singer et al., 2008; Fontijn et al., 2016).

There is a 0.2 cm thick, fine black ash layer identified at 1036.5 cm depth in the Lago Puyehue sedimentary sequence which is composed of colourless, bubble walled and vesicular shards as well as a minority abundance of black, vesicular shards (PUII_1036). Chemical analysis shows that the deposit has a homogeneous rhyolitic composition, with an average SiO_2 content of 70.32 wt% (Table 3.9; Figure 3.13). As described, the chronology for this regional marker (PCC1) is relatively poorly constrained and based on both literary data of radiocarbon and $^{40}Ar/^{39}Ar$, may be between 12.3±1.9 ka (Singer et al., 2008) and 10.44±0.08 (Fontijn et al., 2016). It is considered, on the basis of chemistry, that the PUII_1036 layer is derived from Puyehue-Cordón Caulle and likely correlatable to the widespread marker horizon, PCC1 (Table 3.9, Figure 3.13). PUII_1036 is dated to 15.15-14.42 cal ka BP in this study. This is significantly older than the ages described in the literature (Singer et al., 2008; Fontijn et al., 2016).

Table 3.9. Glass chemistry (normalised) for tephra at 1036.5 cm depth, and glass chemistry for PCC1 regional marker horizon (Fontijn et al., 2016). Total refers to analytical total.

Unit		SiO_2	TiO_2	Al_2O_3	FeO_t	MnO	MgO	CaO	Na_2O	K_2O	P_2O_5	Cl	Total
PUII_1036.5	avg	70.32	0.45	14.18	4.32	0.15	0.34	2.05	5.13	2.79	0.08	0.18	98.65
n=20	sd	0.45	0.03	0.13	0.22	0.04	0.04	0.11	0.14	0.07	0.03	0.02	1.11
PCC1	avg	70.15	0.47	14.22	4.49	0.16	0.36	2.07	5.23	2.76	0.09	NA	98.78
n=59	sd	0.42	0.06	0.14	0.21	0.03	0.07	0.12	0.16	0.08	0.03	NA	0.74

At present, the chronologic data available for the PCC1 unit rests upon the Pr1 unit being comparable to the PCC1 unit. To truly confirm this tephra correlation, the Pr1 unit must be chemically analysed and compared to PCC1 and PUII_1036 as while this correlation is produced based on robust chemical data, it is important to remember that some volcanoes, such as Puyehue-Cordón Caulle, erupt compositionally similar products over time which can result in spurious correlations (e.g., Albert et al., 2012; Wastegård et al., 2013; Macleod and Davies, 2016; Cook et al., 2018).

3.6. Temporal variation in the composition and frequency of volcanic units identified in the Lago Puyehue sedimentary record

As described in Section 3.3, there is no long-term statistical significance in the temporal variability of event frequency through the Lago Puyehue sedimentary record. However, are there temporal changes in the chemical composition of deposits identified in the Lago Puyehue sedimentary record? Five phases can be broadly, and tentatively, identified in Figure 3.14, which show temporal changes in the tephra deposits of Lago Puyehue in terms of chemical composition, and mostly with regards to the deposits hetero/homogeneity.

Phase 1 can be observed at the onset of the record between ~16 and 15 cal ka BP. Phase 1 deposits are all homogeneous and are predominantly mafic; PUII_1117, PUII_1101 and PUII_1078 are basaltic andesites and have limited chemical variability (Table 3.4). Based on their composition, they are likely small-magnitude events which were limited in terms of their dispersal. These units are followed by **Phase 2**, which can be observed between ~15 and 7 cal ka BP, and which comprises of almost continually heterogeneous or bimodal units; the frequency of events appears to be lower between ~13 and 10 cal ka BP. **Phase 3**, between ~7 and 3.8 cal ka BP, is characterised by heterogeneous compositions; importantly though, the ranges of the compositions are less wide than observed in Phase 2, and there is an appearance of homogeneous dacitic events not seen before, as well as basaltic-andesite events. Similarly to Phase 2, **Phase 4** is typified by wide compositional ranges, with deposits being predominantly heterogeneous or bimodal between ~3.8 and ~2.6 cal ka BP. Finally, **Phase 5** is observed between ~2.6 cal ka BP and the present day; this is similar to Phase 3, and an increased abundance of homogeneous deposits is observed. These units are increasingly silica-rich.

It is difficult to compare this record of volcanism with others in southern South America. This is because the size (magnitude/VEI) of events preserved in Lago Puyehue is unknown and unable to be accurately reconstructed using deposit thickness. The record likely reflects mostly small magnitude (i.e., VEI <3) events from nearby centres. In Chile, small events (e.g., <0.3 km^3 volume) are typically under-sampled (Watt et al., 2013a). Studies such as Watt et al. (2013a), Rawson et al. (2015, 2016) and Fontijn et al. (2016) relate temporal changes in volcanic activity

(i.e., frequency, magnitude and composition) to climatic changes (i.e., ice-unloading). This is described in Chapter 1; in summary in areas where volcanism is driven by subduction, ice-unloading is thought to reduce stress and subsequently permit the release of stored magma which has had sufficient time to evolve through the dominant process of fractional crystallisation. This is thought to result in more silicic melts, and larger events at least at the onset of deglaciation (e.g., Watt et al., 2013a; Rawson et al., 2016; Kutterolf et al., 2019; Section 1.4). Watt et al. (2013a); Rawson et al. (2015, 2016), and Fontijn et al. (2016) related temporal changes in volcanic activity to climatic changes using datasets focussed predominantly on large events. For example, Rawson et al. (2015, 2016) presented volcanic data as identified in sedimentary outcrops, and the dataset may thus reflect some degree of preservation bias, with small events that are often more mafic being less well-preserved in sedimentary outcrops (e.g., Brown et al., 2014; Fontijn et al., 2014). Likewise, while Fontijn et al. (2016) investigated both small and large regional events, as identified in both continuous sedimentary archives (e.g., lacustrine settings) and terrestrial outcrops, the dataset used to compare climate and volcanic changes temporally utilised only relatively large (i.e., VEI 3+) events. This is perhaps a reason as to why the timing and description of the indicative phases do not correspond to temporal changes in volcanism as identified in the literature (e.g., Watt et al., 2013a; Rawson et al., 2015, 2016; Fontijn et al., 2016). However, because the Lago Puyehue record preserves different sized volcanic events (notably small) in the region, the record is excellent for studying systematic changes in chemical variability.

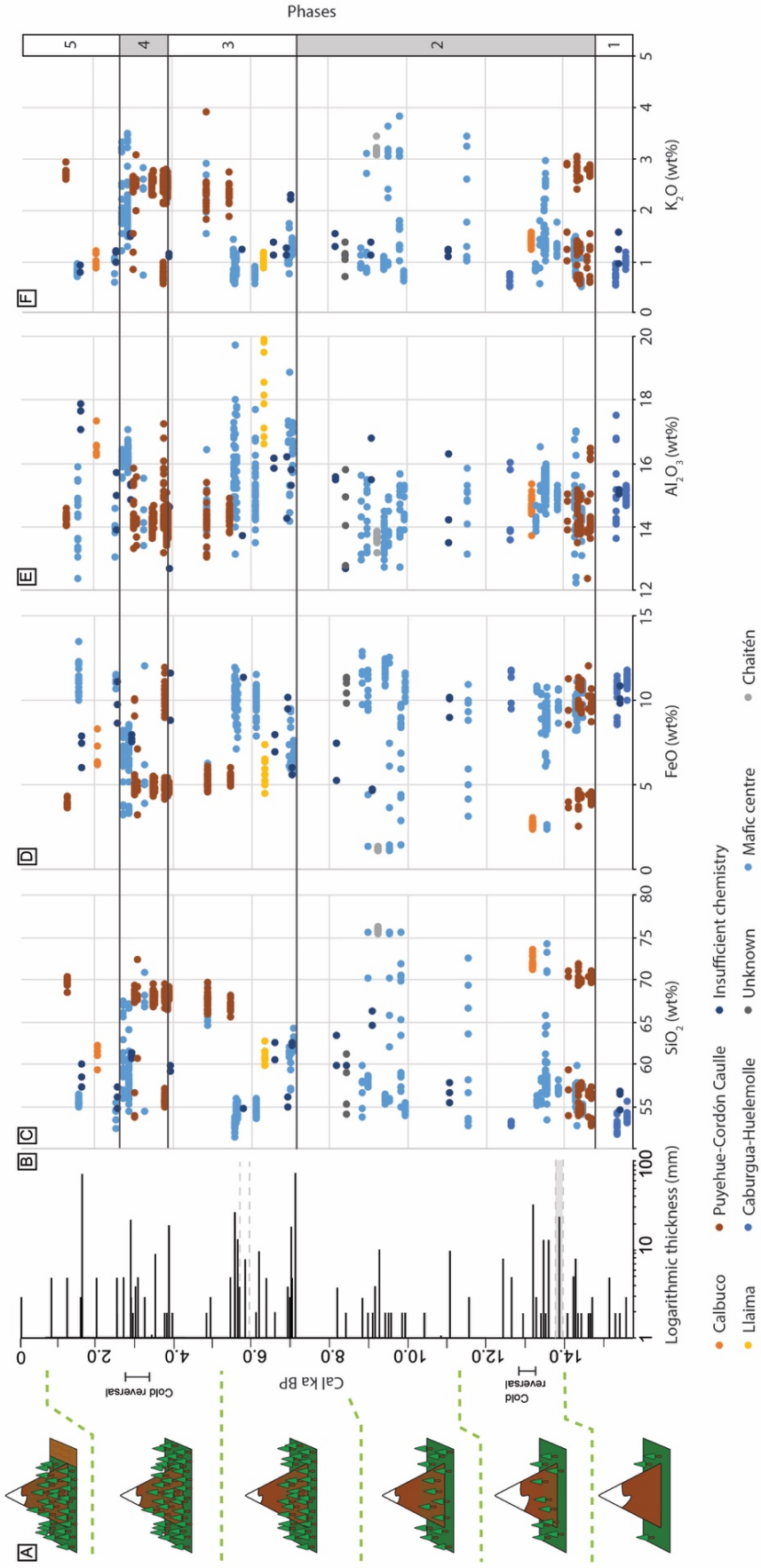


Figure 3.14. Illustration of the changes in tephra composition and frequency of eruptive deposits through time. A) Illustrative figures of past environment (Bertrand et al., 2008a; Vargas-Ramirez et al., 2008); B) Logarithmic thickness (mm) of tephra deposits; grey, dashed lines across figure represent turbidite layers, infilled line represents large turbidite layer (Bertrand, pers comms, 2016); C-F) glass-shard chemical analyses for elements, SiO_2, FeO_t, Al_2O_3 and K_2O respectively; phases are defined based on observed compositional changes, notably changes between more homogeneous (Phases 2 and 4) to more heterogeneous dominated deposits (Phases 1, 3, 5).

During the mid-Holocene, records of volcanism in Chile support a decline in eruptive activity (e.g., Watt et al., 2013a; Rawson et al., 2015, 2016; Fontijn et al., 2016;). For example, between 7.30 and 2.90 cal ka BP, Mocho-Choshuenco was erupting low abundances of basaltic-andesitic scoria (Rawson et al., 2015, 2016), and there is a general absence of large widespread silicic deposits regionally between 9.50 and 4.50 cal ka BP (Fontijn et al., 2016). However, in the Lago Puyehue record, between 6.30 and 5.24 cal ka BP, there is a clustering of six tephra units which have a mafic composition (and thus are considered likely small magnitude events); there is also an overall absence of any felsic deposits between 8.48 and 5.60 cal ka BP (Figure 3.14, 3.15). It is hypothesised on the one hand that the lack of identifiable silicic deposits at this time could be the result of erosion (and thus preservation bias), but since the record of regional volcanism presented in Fontijn et al. (2016) also includes lacustrine archives, which are less susceptible to erosion, this is less likely. It could thus be reflective of more frequently occurring (low explosivity) mafic volcanism during the mid-Holocene, between ~8 and 5 cal ka BP, or reworking and repeated or prolonged inwashing of the same event.

Using an eruption dataset of 121 deposits preserved in terrestrial outcrops and lake environments from volcanoes in Southern Chile from 26 volcanoes between Llaima to Hudson (38.7°S to 45.9°S), Watt et al. (2013b) noted that eruptive activity in Southern Chile declined between ~7.7 and 5.6 cal ka BP (7-5 ^{14}C ka BP) and ~10.1 cal ka BP (9 ^{14}C ka BP; both calibrated in this study using OxCal 4.3, ShCal13). These periods of repose observed across Southern Chile by Watt et al. (2013b) broadly correspond with at least one of the short periods of quiescence observed in Lago Puyehue at 7.37-6.56 cal yr BP, and possibly with revised age-constraints, a period of quiescence at 4.40-3.48 cal yr BP (Section 3.3.1). The lack of preserved deposits at Lago Puyehue at these times may therefore reflect a short paucity in eruptive activity as seen across the region. Using this same eruption dataset, Watt et al. (2013a) identified that regional volcanic activity increases in the late-Holocene, after a mid-Holocene decline in activity. The same relationship may not be evidenced in the Lago Puyehue sedimentary record because the record mostly reflects deposits originating from small eruptive events of local origin which are

typically under-represented in other records (notably soil-tephra alternations) due to their poor preservation and limited spatial abundance (e.g., Watt et al., 2013a).

A period of decline in the global solar irradiance between ~8.8 and 7.8 cal ka BP (8-7 ^{14}C ka BP; calibrated in this study using OxCal 4.3) is thought to have caused advances in the small glaciers of the CLD between 8.5 and 6.2 cal ka BP (Douglass et al., 2005; Markgraf et al., 2007). It is unclear whether these advances would be sufficient to increase the pressure on shallow crustal systems (and subsequently melt composition), but curiously this climatological shift occurs over both Phase 2 (~15-7 cal ka BP) and 3 (~7-3.8 cal ka BP), whereby heterogeneous/bimodal deposits (Phase 2) develop smaller compositional ranges (Phase 3; Figure 3.14). This chronological linkage is relatively weak because theories of solar forcing are overly not well proven and the timing of deglaciation across Chile is relatively poorly constrained (e.g., Moreno et al., 2015b; Bendle et al., 2017, 2019; García et al., 2019). But, assuming the chronological data is accurate, and these compositional changes occur during a period of decreased solar irradiance, it could be hypothesised that small-scale ice-development at volcanic centres prior to Phase 3 resulted in the pooling and storage of melt at (some) centres, which enabled more substantial magma mixing over longer time-scales and thus led to the production of deposits with more constrained chemical ranges than observed in Phase 2. Small changes in glacial-regime have affected volcanic behaviour in tectonic settings where decompression melting drives magmatism, such as Iceland, over very short (~600 year) timescales (cf. Swindles et al., 2018); there is currently insufficient evidence for small-scale glacial changes to influence volcanism in continental arc-settings, such as Chile.

It is possible that one of the largest periods of volcanic repose identified in Lago Puyehue, between 11.94 and 11.29 cal ka BP, is linked with climatological changes that caused small-scale glacial increases (Section 3.3.2; e.g., Swindles et al., 2018); palaeoclimate studies indicate that the Huelmo-Mascardi Cold Reversal (equivalent to the Antarctic Cold Event, and synonymous to the Younger Dryas in the northern hemisphere) occurred at a similar time to this (e.g., Massaferro et al., 2009 – 13.5-11.5 cal ka BP). However, a pollen study by Moreno and Videla (2016) places the cooling as having occurred between 15.5 and 13.0 cal ka BP, with only cold

and wet conditions identified until 11.6 cal ka BP. Such weak chronological constraints for the Huelmo-Mascardi Cold Reversal mean that it is difficult to relate very short-lived climatological changes to volcanic activity, such as Swindles et al. (2018) have done.

Other possible, and more plausible, explanations for the three periods of time when there is a lack of deposits identified in the Lago Puyehue sedimentary sequence (Section 3.3.2), include: i) eruptions are occurring, but deposits are not being preserved (this could be because of wind regime, or lack of ashfall onto Lago Puyehue and/or the Puyehue catchment); ii) eruptions are occurring but the abundance of ash is too fine/low to be preserved as a visible tephra layer and these are instead preserved as cryptotephra layers which are not studied here. It is unfortunately difficult to determine a singular cause of repose, particularly when many of the deposits are unable to be traced to source. Longer-term records with high-temporal resolution, such as Laguna Potrok Aike (Chapter 5), are therefore required to test this hypothesis further.

3.7. Conclusions

Through this work, a more detailed tephrostratigraphy has been produced for the Lago Puyehue sedimentary sequence which provides one of the most robust insights into the past frequency of eruptive activity for the Chilean Lake District to date. Using glass chemistry, correlations have additionally been made to four regional marker horizons: Mil Hojas, PCC4, and PCC1 from Puyehue-Cordón Caulle, and Cha1 from Chaitén.

As expected, this study identifies numerous mafic eruptions that are probably from surrounding centres: Puyehue-Cordón Caulle, Osorno, Antillanca, Mocho-Choschuenco, Carrán-Los Venados, Calbuco and possibly Villarrica. This work indicates that the centres in this region are highly active through the Holocene, and more research into the glass-shard chemistry of their proximal deposits is needed to enable better chemical distinction between these deposits with similar glass compositions – this is particularly needed for Osorno volcano and the Antillanca volcanic complex as there is a gap in knowledge.

There are three periods of time (4.40-3.48, 7.37-6.56, and 11.94-11.29 cal ka BP) during which no eruptive deposits are observed in the Lago Puyehue record, and there is an overall absence of silicic deposits between 8.48 and 5.60 cal ka BP. This corresponds with a decline in large explosive eruptions in other records in the CLD (e.g, Watt et al., 2013a; Rawson et al., 2016; Fontijn et al., 2016). However, long-term changes in the frequency of volcanic deposits identified through the Holocene in Lago Puyehue are statistically insignificant. While there are temporal changes in the composition of observed deposits, it is not possible to relate these to climatological changes, especially since this record only spans the postglacial period.

This study highlights new eruptive events hitherto unknown (e.g., Carbugua-Huelemolle between 15.90 and 15.26 cal ka BP, and Calbuco volcano between 13.42 and 13.05 cal ka BP). Further work undertaken using single-grain glass shard analysis via EPMA, and possibly trace elemental analysis where suitable, is required for tephra in other depositional environments to further constrain the timings of eruptions in the region and expand upon the regional tephrostratigraphy.

Chapter 4

Developing a better understanding of past eruptive frequency through the application of Kernel Density Estimations in OxCal

Abstract

Volcanic eruptions have the potential to cause devastating societal impacts, including loss of life. Understanding volcanic behaviour, such as the frequency of events, permits understanding of possible controlling mechanisms which is extremely useful for volcanic risk assessments. Typically, the analysis of temporal changes in past volcanic activity is undertaken through the examination of frequency histograms of eruptive occurrences, but this is unable to take into account temporal uncertainty and thus can covertly bias interpretations of event history. This chapter explores how temporal changes in volcanic eruption frequency can be illustrated by using Kernel Density Estimates (KDE) applied in Bayesian age-models. This method is powerful since it allows temporal changes in eruptive frequency to be investigated whilst considering the statistical uncertainty of eruptive ages which is something that cannot be achieved through traditional approaches investigating temporal changes in eruptive frequency. However, the output is strongly determined by the quality of the dataset used. Using data from 1) Lago Puyehue (sedimentary sequence) and Mocho-Choshuenco volcano in Chile, 2) Taupo Volcanic Centre (TVC) and the Okataina Volcanic Complex (OVC) in New Zealand, and 3) Mount Mazama and the region around Crater Lake, USA, to produce case studies, this chapter explores the usefulness of KDE applied to age models in OxCal 4.3 in order to rigorously investigate the frequency of volcanic eruptions preserved in the geological record.

4.1. Introduction

Volcanic eruptions can cause societal and economic disruption, as well as loss of human life (Brown et al., 2017). As global population continues to grow, the consequences of eruptions increase. Therefore, understanding past volcanic behaviour, including eruptive frequency and controlling mechanisms, is vital to better understand these threats. The impacts from large (e.g., VEI >5) volcanic events are typically more widespread and extensive than those derived from effusive events, such as lava flows or dome-forming events, notwithstanding some exceptional small-to-moderate historical events which have had devastating and widespread impacts such as Nevado del Ruiz in 1985 and Eyjafjallajökull in 2010, respectively. Risks from explosive events include: loss of livestock and crops as a consequence of widespread ashfall, depreciation of air quality, global temperature change, and disruption to air traffic; while the risks from effusive events typically include: reduction in air quality (associated with syn-eruption degassing), and destruction of infrastructure (e.g., Baxter et al., 1982; Brown et al., 2017).

Primarily, the style of eruption (i.e., explosive or effusive) is governed by magmatic properties and processes, including for example, magma composition, viscosity, volatile content, and conduit geometry because these control the rate of magma ascent, decompression and outgassing (cf. Cassidy et al., 2018 and references within). Volcanic activity has also been hypothesised to be controlled by external factors, including for example, sea-level changes (e.g., Crowley et al., 2015), ice-unloading (e.g., Sigvaldason et al., 1992; Jull and McKenzie, 1996; Maclennan et al., 2002; Jellinek et al., 2004; Rawson et al., 2016) and erosion (e.g., Sternai et al., 2016). In order to evaluate the influence of these internal and external factors on the frequency (and style) of activity, it is crucial to have complete and well-dated eruptive records.

Advances and developments in dating techniques have resulted in more precise event chronologies. Radiocarbon (^{14}C) measurements have improved due to better pre-treatment protocols (ABox-SC: Bird et al., 1999) and an improved calibration curve (IntCal13; Reimer et al., 2013; ShCal; Hogg et al., 2013); advances in mass spectrometry mean that $^{39}Ar/^{40}Ar$ methods can now routinely be applied for young (<100 ka) samples with small amounts of accumulated radiogenic Argon (e.g., Renne et al., 2010, 2011; Mark, 2011; Giaccio et al., 2017) and advances

in the identification and characterisation of volcanic ash layers in proximal and distal archives (e.g., Albert et al., 2012; Lane et al., 2013; Ponomareva et al., 2015; McLean et al., 2018) means that more complete records of volcanism can be obtained, and ages can be transferred between records (i.e., the principle of tephrochronology; Thorarinsson et al., 1959). These chronological constraints are now typically modelled using Bayesian methods to improve precision (e.g., BCal, Buck et al., 1999; CLAM, Blaauw, 2010; OxCal, Bronk Ramsey, 2009a), and can provide more robust constraints on the timing of past volcanic events.

Often, frequency histograms are used to analyse temporal changes in eruptive frequency (e.g., Schiff et al., 2008; Watt et al., 2013a; Damaschke et al., 2018). These typically have a specified bin-width of 500 or 1000 years for records spanning the Holocene, and datasets typically use the average or median age of the tephra deposit, and the abundance of tephra units observed in each bin. In some cases, a curve (e.g., a probability density function (PDF) or the annual deposition rate) is added to the histogram and this curve is often derived using the averaged depositional ages. The sliding-window technique has also been used to investigate frequency and compositional changes in volcanism (Paterne et al., 1990), and spectral analysis has been used in long-term datasets to investigate the relationship between volcanic activity and climate, including the effect of orbital forcing on volcanism (e.g., Schindlbeck et al., 2018; Kutterolf et al., 2019). All of these methods, however, do not fully take into account temporal uncertainty, which can be particularly large in long-term records due to (typically) increasing age-uncertainties with time, and therefore results can be covertly biased.

Kernel Density Estimation (KDE) is a frequentist approach (i.e., probability expressed as the limit of its relative frequency in a large number of trials), which allows for the visualisation of the shape of data without prejudice. KDE has previously been applied to data on eruptive frequency to investigate temporal variation (e.g., Matchan et al. 2016) but used in its basic form, KDE does not account for the statistical uncertainty of the event timings. To do this, the data needs to be analysed within a Markov Chain Monte Carlo (MCMC) simulated Bayesian framework; the application of KDE in an MCMC Bayesian framework using software such as OxCal permits both the visualisation of the shape of the data but additionally accounts for

statistical uncertainty in event timings and hence is an ideal method to study temporal variations of data (cf. Bronk Ramsey, 2017). The introduction of kernel density analysis within a Bayesian framework (OxCal 4.3; Bronk Ramsey, 2017) is a powerful tool and could be particularly useful for volcanologists and tephrochronologists seeking to better understand the clustering of volcanic eruptions and their potential controls. The application of this method requires precise eruption records, in which the event stratigraphy is well constrained.

Here, we apply Gaussian (normal-distribution) KDE within the OxCal radiocarbon calibration programme (Bronk Ramsey, 2009a) to age models from three different sites. Data are obtained from the literature and these sites are selected primarily because they have excellent eruptive records that span different time periods, in addition to numerous well-dated tephra units. Other possible case-studies for future work include Kamchatka and Iceland. These case-studies permit a better insight into past eruption frequency. The case studies are:

(1) the tephra record from the sediments of Lago Puyehue (Bertrand et al., 2008b; this study) and the eruption history of Mocho-Choshuenco volcano (Rawson et al., 2015). These Chilean records are high resolution, capturing events from multiple, and a single, volcano/es, respectively.

(2) the eruption history of the Taupo Volcanic Centre (TVC) and the Okataina Volcanic Complex (OVC) in New Zealand (Froggat and Lowe, 1990; Smith et al., 2005; Lowe et al., 2013). These represent a high resolution record, capturing mostly large-scale pyroclastic eruptions.

(3) the eruption history of Mount Mazama and the region around Crater Lake, USA (Bacon and Lanphere, 2006). This record represents a low resolution terrestrial record, capturing long-term eruptive cycles, including effusive volcanism at a single volcanic complex.

4.1.1. KDE statistical analysis

Like frequency histograms, KDE's create a visualisation of the shape of data. These are both non-parametric tests which mean that no prior assumptions are made about the distribution of the data. However, unlike a frequency histogram, KDE's generate a PDF (i.e., representation of the relative likelihood of the data) of random variables, producing data smoothing on the

population dataset (e.g., Parzen, 1962). How smooth (or peaky) the KDE is can be controlled by the bandwidth: if the bandwidth is too large, the structure of the data will be masked by an over-smoothed density estimate, while if it is too small, the structure and detail of the data will be over-exaggerated. Typically, Silverman's (1986) rule (i.e., the degree of smoothing applied to the kernel) is applied to datasets with a normal distribution. In most cases, this provides an appropriate bandwidth, but it should be considered the maximum choice when using multi-modal distributions as these may be easily over-smoothed.

The choice of bandwidth is mathematically determined by the OxCal model to optimise the level of smoothing in accordance to the modality of the dataset (Bronk Ramsey, 2017) and this inherently reduces user bias. While radiocarbon calibration applies a Bayesian approach, the KDE application within the OxCal programme is a frequentist approach. This combined statistical approach has been applied previously to estimate the kernel bandwidth in Zhang et al. (2006). Further detail is provided on the full KDE method and integration into OxCal 4.3 in Bronk Ramsey (2017).

4.2. Case studies: the application of KDE in OxCal and its relevance and importance to volcanology and tephrochronology

4.2.1. Lago Puyehue and Mocho-Choschuenco, southern South America

Here we apply KDE to data from two sites which are located very close to one another: Lago Puyehue (Bertrand et al., 2008b; Chapter 3) and Mocho-Choshuenco (Rawson et al., 2015). This will allow us to see whether there are notable differences in eruptive activity recorded from individual volcanoes (Mocho-Choshuenco), compared to records which preserve deposits representative of activity from multiple volcanoes (Lago Puyehue; Chapter 3). In theory, the Lago Puyehue and Mocho-Choshuenco records should represent similar trends to those identified in the regional study of volcanic activity by Fontijn et al. (2016) if climate (ice-unloading) is a modulator of volcanic frequency. However, since Lago Puyehue is hypothesised to preserve predominantly small events (VEI <3), and Mocho-Choshuenco medium-large events (VEI >3) there may be more variability in event frequency at Lago Puyehue than recorded in other archives.

4.2.1.1. An overview of activity in southern South America

The southern Andean volcanic arc is characterized by stratovolcanoes as well as fields of (monogenetic) basaltic-andesitic scoria cones. Several of the stratovolcanoes are the source of large explosive eruptions that have generated widespread tephra fall deposits (see Fontijn et al. 2014, for a review). Detailed analysis has been undertaken on tephra units identified in outcrops (e.g., Alloway et al., 2017a, b; Naranjo and Stern, 1998, 2004; Naranjo et al., 2017; Rawson et al., 2015; Stern, 2004, 2008; Stern et al., 2016), and recent efforts have focused on correlating the widespread tephra units identified in these outcrops to those identified in lacustrine and peat records using glass geochemistry (e.g., Weller et al., 2014, 2015, 2017, 2019; Fontijn et al., 2016; Del Carlo et al. 2018). The tephra layers are often well preserved in lacustrine and peat records as these represent low-energy environments that can preserve discrete layers from low-magnitude eruptions (e.g., Van Daele et al., 2014).

Recent dedicated studies on terrestrial (e.g., Stern et al., 2008; Rawson et al., 2016; Naranjo et al., 2017) and lacustrine (e.g., Van Daele et al., 2014; Weller et al., 2014, 2017) archives, and in some cases combining the two (e.g., ; Fontijn et al., 2016; Alloway et al., 2017a, b), has revealed a greater eruptive frequency at many volcanic centres in southern Chile than previously documented. Despite this there are still many centres for which there is limited knowledge about their eruptive history.

This study focusses on the Chilean Lake District (CLD; ~37-41°) in the Southern Volcanic Zone (SVZ; 33-47°S; Stern, 2004; Figure 1.8). Based on the abundance of tephra deposits in the Lago Puyehue record, Bertrand et al. (2008b) described the SVZ as being consistently active through the Holocene. Some volcanological assessments in this region have catalogued the abundance of tephra in various sedimentary archives and made inference to volcanic frequency (e.g., Watt et al., 2011; Fontijn et al., 2016; Rawson et al., 2016; Alloway et al., 2017a), but to date, none have analysed the frequency of tephra deposition using statistical measurements such as KDE in relation to the age (and associated uncertainty) of the events.

4.2.1.2. The Lago Puyehue and Mocho-Choschuenco record and background

Lago Puyehue (40°42'S; 72°27'W; Figure 1.8) represents one of the most complete records of volcanism for the postglacial period (15.5-0 ka) in southern South America as tephra layers from both small and large events are preserved. In particular, the analysis of moderate-magnitude eruptive events recorded in Lago Puyehue (e.g., the 2011 Cordón Caulle eruption; Bertrand et al. 2014) could provide invaluable insights into eruptive frequency hitherto unknown. This is because the deposits from such events are often not well-preserved or easily observed in terrestrial outcrops as a consequence of erosion, weathering and disturbance during soil development (e.g., Fontijn et al., 2014). The understanding of these moderate-sized events is critical because while the CLD is not densely populated, it is an important agricultural and touristic hub in southern Chile, and such eruptions thus have potential to cause widespread negative impact. This is evidenced by the 2011 eruption of Cordón Caulle (VEI ≤5; Elissondo et al., 2016) and the 2015 eruption of Calbuco volcano (VEI 4; Delgado et al., 2017). These particular eruptions had a significant impact on air quality, aviation, livestock, water and vegetation, including across the border in Argentina (e.g., Raga et al., 2013; Elissondo et al., 2016; Forte et al., 2018).

During the analysis of the frequency, magnitude and chemical variation of eruptive events in the CLD, Fontijn et al. (2016) identified a tripartite pattern of regional eruptive activity in the postglacial; Rawson et al. (2015, 2016) also identified this pattern after analysing postglacial tephra deposits from the Mocho-Choshuenco volcanic complex (39°55′S; 72°2′W; Figure 1.8) for frequency, magnitude and chemical variation (Figure 4.1). It is subsequently hypothesised that ice-unloading following deglaciation resulted in the release of large volumes of evolved melt that accumulated in the ice-loaded crust, and then the magmatic system moved into a different phase of activity that was dominated by smaller and more frequent events of less evolved magmas (cf. Rawson et al., 2016; Mocho-Choschuenco). The complex would have been glaciated during the Last Glacial Maximum (LGM), until ~18 ka (Moreno et al., 2015b). The complex is now considered to be one of the most hazardous in Chile's Southern Volcanic Zone

(Rawson et al., 2015), and has experienced mostly VEI 3 and 4 events, but also some VEI 5 eruptions (Enco, Pirehuieco and Neltume eruptions; Rawson et al., 2015). Here, we illustrate the usefulness of *KDE_Plot*, applied in OxCal 4.3, to present and detail changes in eruptive frequency.

4.2.1.3. Interpretation of Lago Puyehue and Mocho-Choshuenco KDE and its usefulness

The temporal distribution of eruptive deposits identified in Lago Puyehue is presented in Figure 4.1B as both a frequency histogram and a KDE. Whilst overall, the trend is similar between frequency histogram and KDE, the difference is notably that the frequency histogram is failing to accurately account for the statistical uncertainty of the ages of the volcanic events. The Lago Puyehue KDE in Figure 4.1B indicates that eruptive activity is not constant through the Holocene in the CLD, but rather that there are at least three periods of time when eruptive activity, as recorded in the lake sediments, is increased: 9-8, 6.5-5.5, 3.5-2.5 cal ka BP. Activity also appears to be temporally variable at Mocho-Choshuenco (Figure 4.1C); there are at least two periods of time during the event-history where there is increased activity, ~9.5-8.5 and ~1-0 cal ka BP, and this is broadly consistent with findings in Rawson et al. (2016). Notwithstanding the increase in tephra preserved between 3.5 and 2.5 cal ka BP at Lago Puyehue and at ~1-0 cal ka BP around Mocho Chochusenco, this is the opposite of the findings from the regional studies which identify limited volcanic activity during these times (cf. Fontijn et al., 2016).

In both the Lago Puyehue and Mocho-Choshuenco record (Figure 4.1B, 4.1C), there is an increase in eruptive activity at the start of the record. In the case of Lago Puyehue, this is between ~15 and 12.5 cal ka BP, and in the case of Mocho-Choshuenco this is at ~12.5 cal ka BP. Increases in eruptive frequency have previously been associated as a volcanic response to ice-unloading in the CLD after the LGM (Rawson et al., 2016; Figure 4.1A). At Mocho-Choshuenco, where the relationship between ice-unloading and increases in volcanic frequency has previously been reported, a lag of up to 5 kyr in volcanic response is recorded (Watt et al., 2013a; Rawson et al., 2016). While the timing of increased volcanic activity at Lago Puyehue

and Mocho-Choshuenco could possibly relate with ice-unloading (Figure 4.1A), both records are postglacial as a consequence of erosion during the deglaciation, and the absent synglacial period makes it difficult to determine whether there is a true postglacial increase in volcanic frequency. Additionally, any postglacial increase in the frequency of deposits is not particularly note-worthy on its own when considering the relationship between event-frequency and ice-unloading. Rawson et al. (2015) identified that at the onset of Holocene warming, there were a medium number of events, but that they are all large-magnitude and of highly silicic composition (Rawson et al., 2016). Thus, to truly investigate this relationship, further information including melt composition, and event magnitude, are required. Eruptive flux, for example, co-varies with the KDE plot of Mocho-Choshuenco (Figure 4.1C). Moreover, more records of individual volcanoes, as well as long high-resolution tephra records from continuous archives possibly unaffected by erosion, should be analysed to determine whether changes in volcanism are site-specific or regional.

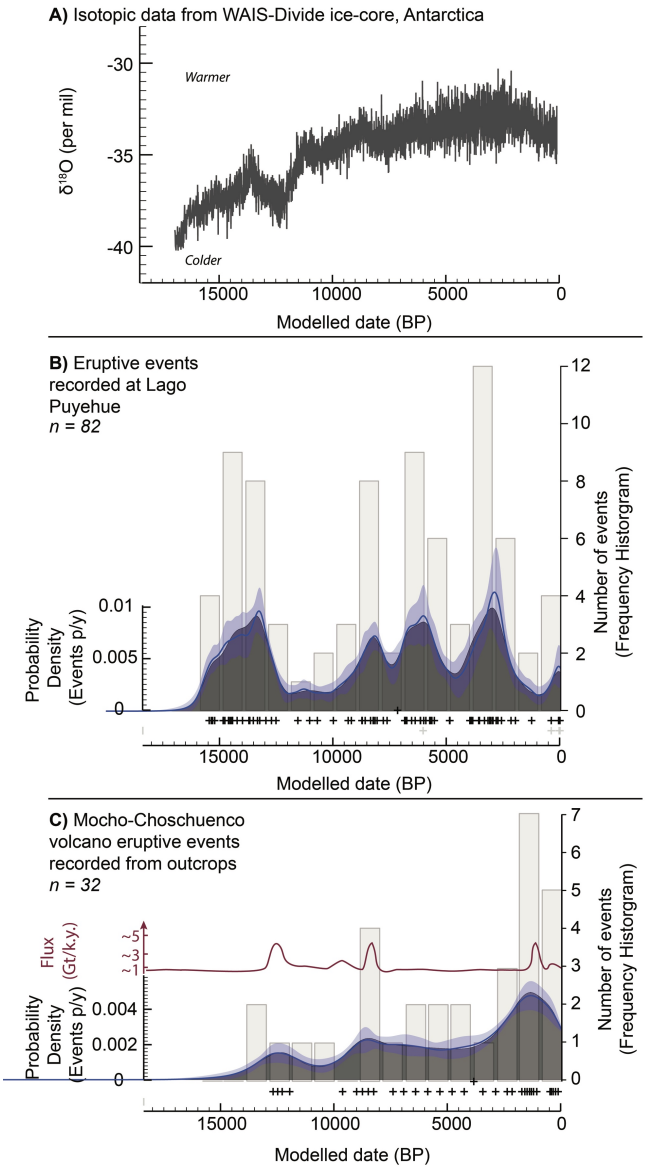


Figure 4.1. A) temporal changes in the abundance of Oxygen (per mil) in the WAIS-Divide ice core in Antarctica (after WAIS Members, 2013), with lower $\delta^{18}O$ values reflecting colder conditions. The chronology of the WAIS-Divide ice-core record is based on annual layer counts between 0 and 29.6 ka. B) The *KDE_Plot* of Lago Puyehue tephra data, showing temporal changes in eruptive frequency (combined view from multiple volcanoes in the region around Lago Puyehue), as well as the frequency histogram for comparison between KDE and traditional methodologies; the frequency histogram is composed using deposits grouped in bins of 1000 years and mean eruptive ages from the derived OxCal age model. C) As per B, but the plots illustrate activity from only Mocho-Choschuenco volcano, based on the identification of deposits in nearby outcrops. Comparing these records using their independent chronologies shows that temporal changes in eruption frequency at Lago Puyehue somewhat co-vary with the abundance of $\delta^{18}O$ values in the Epica Dome C Antarctic ice core. Eruptive flux is also presented for Mocho-Choshuenco volcano using data from Rawson et al. (2016); this was determined by summing eruptive masses into 0.5 ky bins using the deposit volumes and age probability distributions (as per Rawson et al., 2016; Section 2.6.3.1.). In all KDE figures (Figures 4.1, 4.4 and 4.5), the black crosses represent medians of the marginal posterior distributions of events from the KDE analyses, while grey crosses represent median values of the likelihood distributions from included dates. Snapshots of the KDE distribution generated during the MCMC process are represented by the solid blue line (average) and lighter blue band ($\pm 1\sigma$).

4.2.2. Taupo Volcanic Centre and Okataina Volcanic Complex, New Zealand

Here we apply KDE to data from Froggat and Lowe (1990), Smith et al. (2005) and Lowe et al. (2013). The data represents eruptive activity from 1) Taupo Volcanic Centre (TVC) and 2) Okataina Volcanic Complex (OVC), North Island, New Zealand, and comprises both dated and undated tephra deposits identified from Kaipo Bog and outcrops. Analysing this data in a *KDE_Plot* will allow us to see in great detail how these two different systems have behaved temporally.

4.2.2.1. An overview of activity in New Zealand

Subduction of the Pacific plate under the Indo-Australian plate gives rise to volcanism in New Zealand, and volcanic centres are predominantly located on the North Island. The eruption history of New Zealand's volcanoes over the last 50 ky is relatively well studied (e.g., Lowe and Hogg, 1986; Bebbington and Lai, 1996; Smith et al., 2005, 2006; Lowe et al., 2013).

The Taupo Volcanic Zone is a belt of centres that extends northeast from Tongariro National Park to White Island, through North Island, New Zealand (Healy, 1962; Figure 4.2). The Taupo Volcanic Zone has been active since 2 Ma, and during initial phases of volcanism, andesites were commonly erupted before a change to rhyolitic volcanism occurred (Wilson and Rowland, 2016). Between 1 My ago and the present day, $>10^4$ km^3 of rhyolitic magma has been erupted (Wilson et al., 1984).

The Taupo Volcanic Zone has been likened in size and longevity to the Yellowstone system in the USA, though the Taupo Volcanic Zone's events typically occur at shorter recurrence intervals, and with comparatively smaller eruptive volumes (Wilson et al., 1984). It is considered the most frequently active rhyolitic zone on Earth (Wilson, 1993), and is expressed mainly by six caldera volcanoes: Rotorua, OVC, Kapenga, Mangakino, Maroa, and TVC. Of these, the TVC and the OVC have been particularly active over the past 50 ky (Wilson et al., 1984; Figure 4.2).

The TVC and OVC have both experienced large, explosive events which have dispersed ash into distal archives. There have been at least 35 and 26 events from TVC and OVC over the past ~50,000 years, respectively (Froggat and Lowe, 1990; Smith et al., 2005; Lowe et al., 2013). Tephra from one of these explosive events, the Oruanui eruption from TVC, was recently identified in Antarctica, ~5,500 km distance from source, providing excellent cross-continental constraints (Dunbar et al., 2017). With the discovery of this new correlation, the age of the Oruanui tephra was remodelled using the SHCal13 calibration curve (Hogg et al., 2013) and refined to 25.58±0.03 cal ka BP (Dunbar et al., 2017).

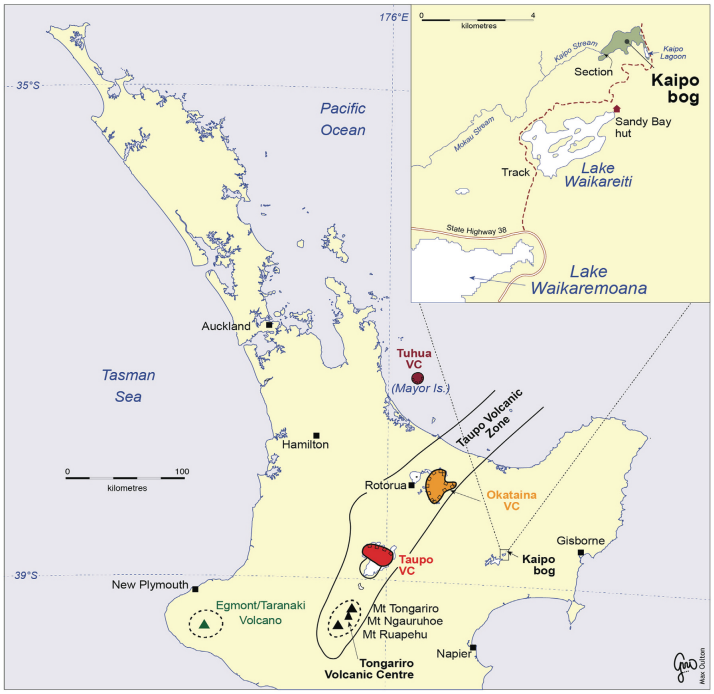


Figure 4.2. Map of central and northern North Island, New Zealand. Source volcanoes are listed – notably Taupo Volcanic Centre and Okataina Volcanic Centre. Inset shows locations of Kaipo bog and the tephra-peat section. Source: Lowe et al. (2013).

4.2.2.2. Records of TVC and OVC volcanism from Kaipo Bog and terrestrial outcrops

Deposits from the explosive events of TVC and OVC are well-preserved in terrestrial outcrops (e.g., Smith et al., 2005, 2006), and some sedimentary sequences, including Kaipo Bog (38°40′S; 177°10′E; Newnham and Lowe, 2000), situated in the Urewera National Park, North Island, New Zealand (Lowe and Hogg, 1986; Lowe et al., 2013; Figure 4.2). Kaipo Bog contains

a 4.4 m-long sedimentary archive that spans approximately ~17.8 ka cal BP. The record has 51 radiocarbon dates (Lowe et al., 2013) and contains 24 widespread tephra layers. Of these, 12 are rhyolitic deposits from the TVC and nine are rhyolitic deposits from the OVC; the remaining deposits come from the Tongariro, Egmont/Taranaki and Tuhua centres and are not considered here (Lowe et al., 2013). This tephra abundance compares with 35 and 23 silicic tephra units identified in the terrestrial record relating to TVC and OVC volcanism, respectively, over an approximately 50 ky period (Smith et al., 2005).

Analysis of tephra deposits from outcrops indicates that over the past 50 ky, there have been three phases of activity at the OVC; this has included a generalised decrease in eruption frequency toward the present day, but with increasing volume, notably from voluminous lavas and domes (Smith et al., 2005). The analysis of TVC deposits shows a decline in eruptive activity during the Last Glacial Maximum, but an increase in event frequency during the Holocene (Smith et al., 2005; Figure 4.3).

Temporal changes in eruptive frequency at OVC and TVC have not previously been statistically analysed. The use of KDE will allow new insights into changes in explosive volcanism in a long-term record, over the last glacial and Holocene.

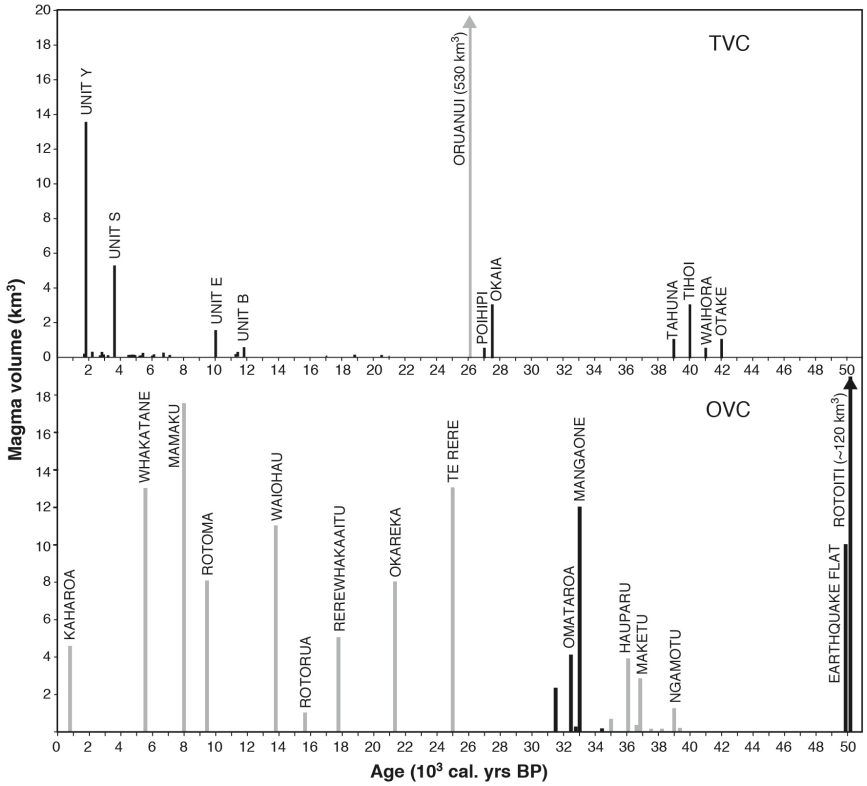


Figure 4.3. Volumes and ages of Taupo Volcanic Centre (TVC) and Okataina Volcanic Centre (OVC) highly-silicic-only volcanism. Dark grey represents eruptive subgroups. The Mangaone Subgroup (of the OVC) and pre-and post- 26.5 ka TVC eruption episode volumes are for pyroclastics only; any associated intra-caldera lavas (not exposed) are not included. Source: Smith et al. (2005).

4.2.2.3. Interpretation of TVC and OVC KDE and its usefulness

By looking at the scale of the probability densities in Figure 4.4, it is clear that the TVC is more frequently active than the OVC during the Late Quaternary. In agreement with Smith et al. (2005), there is a tripartite sequence of eruptive activity at the TVC (Figure 4.4B). In Figure 4.4B, these three increases in eruptive activity can be observed at ~46-40, ~28-24, and ~10-0 cal ka BP. There is a paucity in recognised events from TVC at ~40-28, and ~24-10 cal ka BP.

The same trends (i.e., tripartite pattern, with generalised increase in frequency of volcanism during the Holocene) are not identified at the OVC. The OVC is most active between ~33 and ~30 cal ka BP. A general decline in eruptive frequency is observed through the Late Quaternary from this point (i.e., ~30-0 cal ka BP). Based on the data obtained, activity at OVC is considerably lower than at the TVC. When the OVC is at its most active (~33 to ~30 cal ka BP),

the greatest number of events observed is ~0.7 eruptions per ky, and by comparison, when the TVC is at its most active, at ~6 cal ka BP, the greatest number of events observed is ~2.5 eruptions per ky (Figure 4.4).

The KDE only provides information on the likelihood of the volcanic event. However, volcanic frequency alone does not permit a solid understanding of volcanic behaviour; it is clear that additional data are required to identify factors which control event frequency, and as such eruptive flux data has been calculated for these well-studied centres and is presented in Figure 4.4 (Section 2.6.3.1). On the whole, eruptive flux covaries with increases in the probability density of eruptive frequency, particularly when there are several temporally disparate events (e.g., Figure 4.4B), but in instances where there are several, frequent volcanic events, eruptive flux can be more variable than the KDE (e.g., Figure 4.4A).

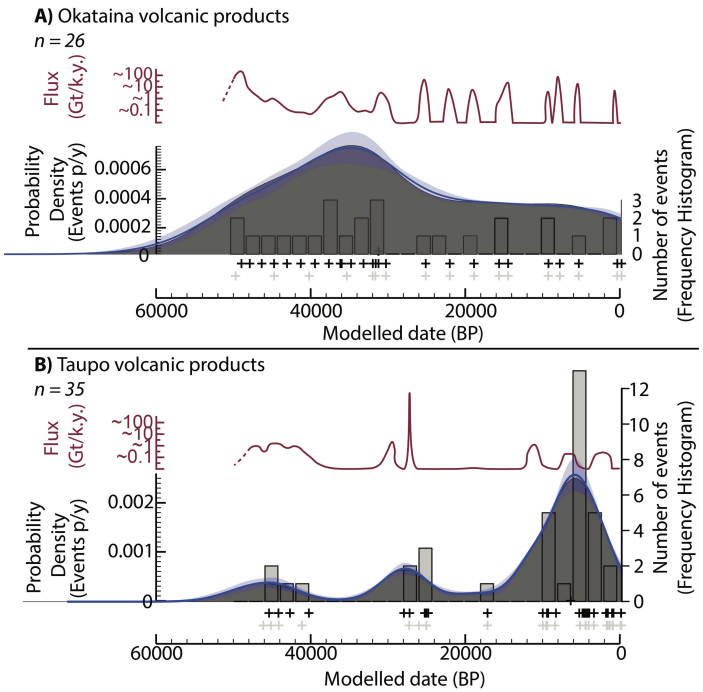


Figure 4.4. A and B) *KDE_Plot* of eruptive deposits from Okataina Volcanic Centre (OVC) and Taupo Volcanic Centre (TVC), respectively, as identified in Froggatt and Lowe (1990), Smith et al. (2005) and Lowe et al. (2013) between the present day and ~50 cal ka BP and remodelled in this study using OxCal 4.3 (Bronk Ramsey, 2009a). The frequency histograms are presented for comparison between KDE and traditional methodologies; the frequency histogram is composed using deposits grouped in bins of 2000 years and mean eruptive ages from the derived OxCal age model. Eruptive flux is also presented; this is determined by summing eruptive masses into 2 ky bins using the deposit volumes and age probability distributions (as per Rawson et al., 2016). Note that OVC and TVC are represented by different scales, with the TVC characterised by an order of magnitude higher probability than the OVC.

4.2.3. Mount Mazama and the Crater Lake region, Oregon, USA

Here we apply the *KDE_Plot* to tephra units identified in the Mount Mazama and Crater Lake region; many of these layers have been dated using $^{39}Ar/^{40}Ar$, providing good temporal constraints on this long record of volcanism, as described in Bacon and Lanphere (2006). The application of KDE to this dataset will enable a better understanding of the long eruption history of Mount Mazama and the Crater lake region, and how this may have changed temporally.

4.2.3.1. An overview of activity in the Mount Mazama and Crater Lake region

The Cascade arc is formed as a result of northeastward subduction of the Juan de Fuca and Gorda plates beneath the North American plate. Mount Mazama (45°N; 122°W) is located in an active zone of the Cascade arc where there are also numerous other smaller volcanoes that date back to 1901-1855 ka based on K-Ar dating (e.g., Bacon and Lanphere, 2006). The Mazama andesite-dacite edifice was built episodically between 420 and 35 ka, and during major edifice construction (0-80 ka), eruptive rates were ~0.8 km^3/ky in comparison to a baseline ~0.4 km^3/ky across the 420 ky period (Bacon and Lanphere, 2006). Andesite and dacite are observed in a 2:1 proportion at Mount Mazama and it is built on top of pre-Mazama rhyodacitic lavas (Bacon and Lanphere, 2006).

The region around the edifice preserves an exceptionally long record of varying types of volcanic deposits from Mount Mazama, with caldera wall exposures at Crater Lake providing unique insights into the growth and evolution of large arc volcanoes. Crater Lake lies within the caldera of Mount Mazama which was formed after a climactic VEI 7 eruption at ~7.7 cal ka BP (Hallett et al., 1997; Bacon and Lanphere, 2006), and post-caldera volcanism is dominated by andesitic lavas confined to the caldera (Bacon et al., 2002).

4.2.3.2. Records of volcanism from terrestrial outcrops in Mount Mazama and the Crater Lake region

Both Mount Mazama (45°N; 122°W) and the Crater Lake region have been extensively geologically mapped by Bacon et al. (2002) and Bacon and Lanphere (2006), and a suite of K-Ar and $^{40}Ar/^{39}Ar$ dates, in addition to three radiocarbon dates, place identified deposits in a more constrained chronological framework. The region has been occasionally glaciated, and K-Ar, $^{40}Ar/^{39}Ar$, and radiocarbon dating has helped to constrain the timing of these glaciations (Bacon and Lanphere, 2006). Fifty-eight deposits of effusive to explosive deposits have been identified and attributed to Mount Mazama volcanism, and nine deposits have been identified and attributed to pre-Mazama volcanism (Bacon and Lanphere, 2006). The ~7.7 cal ka BP climactic eruption of Mount Mazama dispersed ~50 km^3 of magma and left a 20-m-thick deposit across the surrounding region (e.g., Hallett et al., 1997; Bacon and Lanphere, 2006; Egan et al., 2015).

Extensive work constraining the long-term event chronology of Mount Mazama and the Crater Lake region by Bacon and Lanphere (2006) has permitted analysis of volcanic frequency for the past ~1.3 Ma. We use this long-term record documented by Bacon and Lanphere (2006), which is well-constrained but has low temporal resolution, to produce a KDE that illustrates temporal changes in Quaternary eruptive activity (Figure 4.5).

4.2.3.3. Interpretation of the Mount Mazama and Crater Lake KDE and its usefulness

The use of KDE and median summary statistics shows distinct temporal changes in volcanic activity at Mount Mazama and Crater Lake (Figure 4.5). There is very minimal data for the pre-Mazama volcanics (Figure 4.5A), with only nine deposits identified between 1275 and 435 ka, but a more comprehensive set of data for the Mount Mazama volcanics (i.e., >420-0 ka; Figure 4.5). These latter data suggest that activity increased over this time period, peaking at ~60 ka (Figure 4.5B). There are at least two periods of increased activity based on visual inspection of the KDE, i) between ~290 and ~250 ka, when the frequency is approximately 0.10 events per

ky, and ii) between ~60 and ~10 ka, during which time there are at least seven known (dated) events, and the frequency is approximately ~0.28 events per ky.

This data indicates a broadly similar eruptive frequency to that identified in Bacon and Lanphere (2006). However, it is important to note that the record, like other records of past volcanic activity, may be incomplete, or subject to preservation issues, as a result of blanketing pyroclastic deposits, (glacial) erosion and/or caldera collapse (e.g., Brown et al., 2014; Fontijn et al., 2014; McNamara et al., 2019). It is possible that the increasing trend in eruptive frequency toward the Holocene is therefore, at least in some part, a consequence of preservation and/or sampling bias rather than a true increase in activity toward the present day. It could also point toward long-term changes in tectonic regime (e.g., Caricchi et al., 2014).

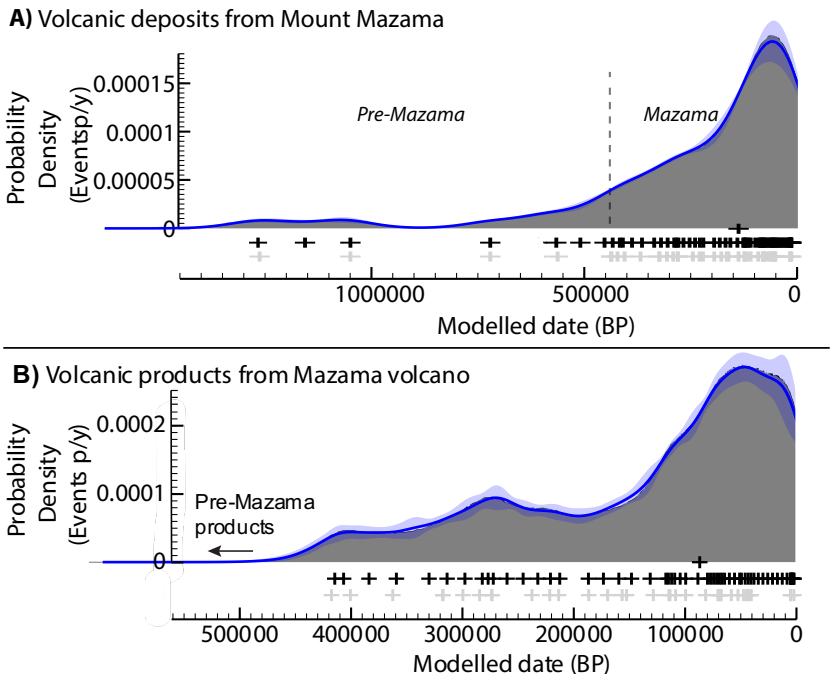


Figure 4.5. A) *KDE_Plots* of pre-Mazama and Mount Mazama eruptive deposits; the difference in these are marked onto the plot. The long-temporal nature of this record means variability in frequency is difficult to see in the Mazama products, and thus B) shows a *KDE_Plot* of Mount Mazama eruptive deposits only. The different types of volcanic deposits are defined in Section 2.6.4.6. Data are derived from Bacon and Lanphere (2006) and modelled in this study using OxCal 4.3 (Bronk Ramsey, 2009a).

4.3. Discussion and Conclusions

KDE has been applied to three case studies of differing spatial and temporal resolutions and has shown the usefulness of this statistical method in the analysis of the frequency of volcanic eruptions, while respecting the statistical spread of possible ages at which the eruptions could have occurred. While the application of KDE in a Bayesian framework is highly valuable in the analysis of temporal variability in eruptive activity, it is clearly identified that significantly more data is required before describing complex volcanological behaviour or inferring potential causal mechanisms. Additional data includes, for example, the magnitude of events and composition of deposits (e.g., Section 3.6).

In Section 4.2.1, Lago Puyehue and Mocho-Choshuenco are described. Lago Puyehue is a high resolution Holocene record and preserves predominantly small events (i.e., VEI <3); the terrestrial sequences surrounding Mocho-Choschuenco volcano preserves moderate to explosive events ranging from VEI 3-5. As such, both records permit a relatively complete record of postglacial activity. When we compare the KDE's of both records, we note that volcanic frequency is not synchronous, despite close proximity between sites (~85 km). Mocho-Choschuecno experiences heightened activity at least twice: at ~8.5 and ~1 cal ka BP, but three increases in the number of volcanic events is observed in the Lago Puyehue sedimentary record. Heightened activity is only synchronous between Mocho-Choshuenco and Lago Puyehue between ~9 and 8 cal ka BP. This likely reflects bias in the type of record since the KDE of Mocho-Choschuenco represents eruptive activity from one centre, while the KDE of Lago Puyehue represents activity from multiple centres in the CLD, and notably from Puyehue-Cordón Caulle located at ~30 km distance.

The relationship between volcanic activity and climate change (i.e., ice unloading) is often produced based on frequency data alone, or uses this data most heavily (e.g., Sigvaldason et al., 2002; Jellinek et al., 2004; Schindlbeck et al., 2018). However, as identified in Section 4.2.1, it is difficult to identify the existence of the relationship between volcanic activity and climate change based on frequency alone. Other parameters such as eruption magnitude, flux, and composition of deposits are essential for interpreting past volcanic behaviour. For example,

in Rawson et al. (2016), postglacial volcanism at Mocho-Choshuenco volcano was characterised by a tripartite sequence of events and called upon numerous strands of evidence including: frequency, magnitude, flux and composition. These variations were divided into phases: phase 1 (13.0-8.2 ka) was comprised of ~VEI 5 events of dacite and rhyolitic melts, with average eruptive frequencies of 1.9 eruptions ky; phase 2 (7.3-2.9 ka) was comprised of ~VEI 3 events of basaltic andesite melts, with average eruptive frequencies of 2.0 ky; while phase 3 (2.4-0 ka) was comprised of ~VEI 3-5 events with intermediate compositions, with average eruptive frequencies of 6.3 ky (Chapter 1). From these results, in the record of Mocho-Choshuenco, it is hypothesised that the high magnitude, evolved melts in phase 1 are a consequence of the accumulation and differentiation of melt during the glacial period, and their subsequent release after stress-changes associated with ice-unloading (Rawson et al., 2016). This is in agreement with expectations from Watt et al. (2013a), and findings from regional postglacial Chilean deposits in Fontijn et al. (2016) which also indicated similar trends to Rawson et al. (2016). Moreover, the relationship between deglaciation and volcanic activity would most robustly be analysed using records which span several glacial cycles, for example Laguna Potrok Aike (Kliem et al., 2013a; Wastegård et al., 2013; Chapter 5).

A high resolution record of the OVC and TVC explosive events from the present day to ~50 ka is produced using data from the Kaipo peat bog sequence and outcrops from North Island. When we compare the KDE's of these two records, we see that the TVC is considerably more active through the Late Quaternary than the OVC (Figure 4.4). The TVC is most frequently active at ~6 cal ka BP. By comparison, the OVC is most active at ~33 and 30 cal ka BP. The frequency of the events observed at OVC and TVC does not appear to be modified by preservation issues; we see decreasing and increasing frequency toward the present day at the OVC and TVC, respectively. The site was also not glaciated and thus not affected by glacial scour in ways in which Chile was, for example (e.g., Brown et al., 2014; Fontijn et al., 2014).

A comprehensive geological study by Bacon and Lanphere (2006) provided data of the pre-Mazama volcanics, spanning 1.2 My, and the Mazama eruptive history, spanning ~420 ky (Figure 4.5). While fine details on eruptive activity, and small volumetric events cannot be

observed, this data permits analysis of long-term evolutional trends of the Mazama system. The application of KDE to this data indicates that Mazama volcano was most active between ~60 and ~10 ka. There is a more generalised increase in volcanism between 120 ka and the present day, and this could possibly coincide with climatic changes, as described in Bacon and Lanphere (2006). However, there are likely preservation biases as older material is less likely to be preserved as a consequence of erosion, and this could partially explain why eruptive frequency increases toward the present day in some of the case studies (e.g., Brown et al., 2014; Fontijn et al., 2014).

Overall these case studies are important because they demonstrate that conventional methods for analysing volcanic event frequency can oversimplify temporal changes, and this may have implications for quantifying risk, the production of quality data for hazard assessments, and the attribution of causal mechanisms to volcanic frequency. Importantly, they clearly illustrate how different records may bias our understanding of eruptive frequency. For example, records that preserve moderate-to-large explosive events (i.e., VEI >3) may proffer an underestimation of activity in the region (e.g., Mocho-Choschuenco compared to Lago Puyehue; Figure 4.1), and records that span long time periods may have increased preservation issues, with more deposits being identified toward the present day than the past (e.g., Mazama; Figure 4.5).

OxCal's new KDE function provides a quick method of robustly analysing temporal changes and this can be useful for analysing the frequency of volcanic eruptions at a range of temporal and spatial resolutions, while respecting the statistical spread of possible ages at which the eruptions could have occurred. This is subsequently a powerful tool for volcanologists and those investigating volcanic hazard since it may illustrate trends in eruptive behaviour at centres, and better identifies controlling factors for volcanism. This tool, however, presents insufficient data (e.g., magnitude and compositional data) to permit for decisions to be made on the causal mechanisms of eruptive behaviour. The KDE will also only be as representative of the temporal distribution of deposits as the data inputted, and thus issues such as preservation artefacts and sampling bias should not be overlooked.

Chapter 5

Refining the Late Quaternary tephrochronology for southern South America using the Laguna Potrok Aike sedimentary record

This chapter has been modified after the peer-reviewed journal article in Quaternary Science Reviews: Smith et al. (2019).
DOI: https://doi.org/10.1016/j.quascirev.2019.06.001 (Supplementary File: S.6.2)

Abstract

This paper presents a detailed record of volcanism extending back to ~80 kyr BP for southern South America using the sediments of Laguna Potrok Aike (ICDP expedition 5022; Potrok Aike Maar Lake Sediment Archive Drilling Project - PASADO). Our analysis of tephra includes the morphology of glass, the mineral componentry, the abundance of glass-shards, lithics and minerals, and the composition of glass-shards in relation to the stratigraphy. Firstly, a reference database of glass compositions of known eruptions in the region was created to enable robust tephra correlations. This includes data published elsewhere, in addition to new glass-shard analyses of proximal tephra deposits from Hudson (eruption units H_1 and H_2), Aguilera (A_1), Reclus (R_1, $R_{2\text{-}3}$), Mt Burney (MB_1, MB_2, MB_x, MB_{1910}) and historical Lautaro/Viedma deposits. The analysis of the ninety-four tephra layers observed in the Laguna Potrok Aike sedimentary sequence reveals that twenty-five tephra deposits in the record are the result of primary fallout and are sourced from at least three different volcanoes in the Austral Andean Volcanic Zone (Mt Burney, Reclus, Lautaro/Viedma) and one in the southernmost Southern Volcanic Zone (Hudson). One new correlation to the widespread H_1 eruption from Hudson volcano at 8.7 (8.6-9.0) cal ka BP during the Quaternary is identified. The identification of sixty-five discrete deposits that were predominantly volcanic ashes (glass and minerals) with subtle characteristics of reworking (in addition to three likely reworked tephra, and one unknown layer) indicates that care must be taken in the analysis of both visible and invisible tephra layers to decipher their emplacement mechanisms.

5.1. Introduction

The nature and scale of past volcanism, and how this varies relative to external forcing, must be established in order to devise adequate hazard and risk assessments. This study focusses on the analysis of the lacustrine sediment record of Laguna Potrok Aike, in southern South America (Figure 5.1). This sediment sequence likely preserves tephra from explosive eruptions of the arc volcanoes in the southernmost sector of Chile. The postglacial eruptive history of these volcanoes has been derived by integrating proximal records with those preserved in other lacustrine records (e.g., Stern, 2008; Weller et al., 2018). However, due to issues in preservation, little is known about volcanism prior to deglaciation and following the Last Glacial Maximum (LGM; e.g., Fontijn et al., 2014). The sedimentary record of Laguna Potrok Aike is therefore ideal to investigate Late Quaternary volcanism as it lies downwind of major productive volcanic centres, was not glaciated during the last glacial period and thus provides an ~80 ky record of volcanism (Coronato et al., 2013; Gebhardt and Ohlendorf, 2019). Reconstructing a long-term record of volcanism from this region will additionally allow us to test the possible influence of external factors on volcanic activity; for example, the relationship between climate and volcanic activity (e.g., Rawson et al., 2016). Various studies have suggested that the removal of ice load after deglaciation affects the generation, storage and eruption of magma (e.g., Sigvaldason et al., 1992; Jellinek et al., 2004; Nowell et al., 2006; Watt et al., 2013a; Rawson et al., 2016; Chapter 1).

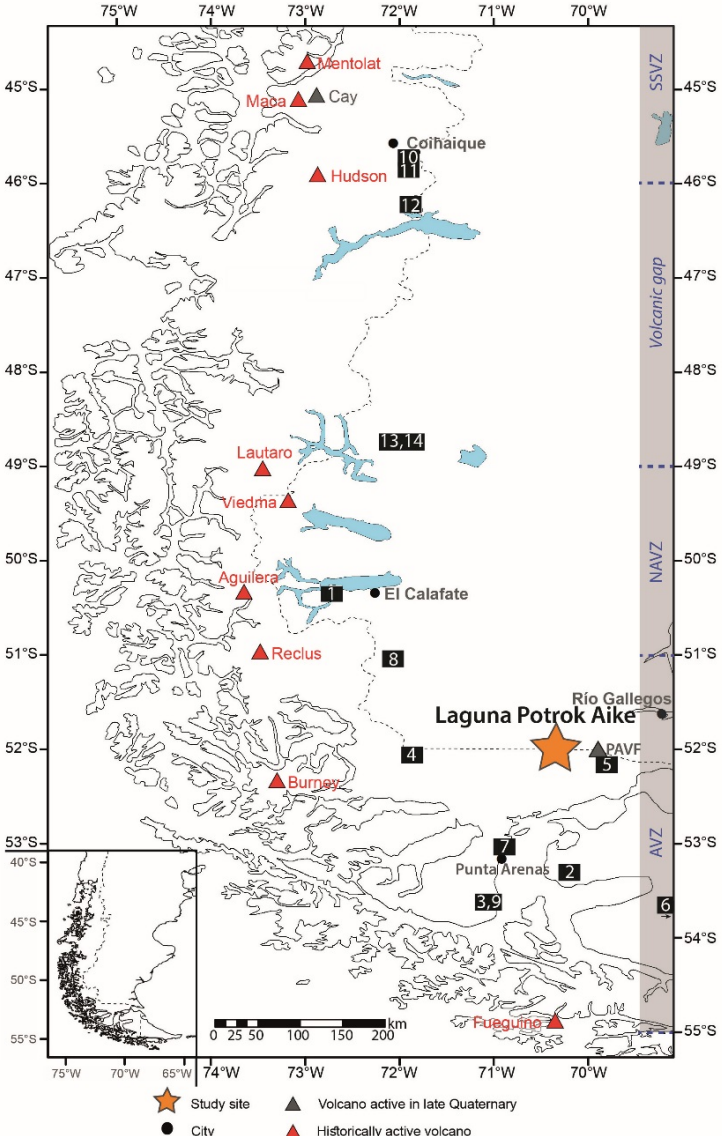


Figure 5.1. Map of southernmost South America with active volcanoes of the Austral and southernmost Southern Volcanic Zones. Star shows study site, Laguna Potrok Aike. White numbers in black boxes indicate the locations of terrestrial tephra samples (see Table 2.1). Abbreviations in blue text with grey shaded background to the right of map demark the volcanic zones; AVZ = Austral Volcanic Zone; NAVZ = northern Austral Volcanic Zone; SSVZ = southern Southern Volcanic Zone (as per Stern, 2004).

5.1.1. Records of volcanism in southernmost South America

Andean volcanoes are divided into zones, and this paper focuses on the Southern Southern Volcanic Zone (SSVZ; 41.5-46°S; Stern, 2004) where Hudson volcano is located, and the Austral Volcanic Zone (AVZ; 49-55°S; Stern, 2004; Figure 5.1). The AVZ contains several large and frequently active volcanoes, including Mt Burney, Reclus, Viedma, Lautaro and Aguilera, which are located ~200 km, ~250 km, ~350 km, ~390 km, ~300 km from Laguna Potrok

Aike, respectively. Several thick ash layers from these centres have been observed in sedimentary archives across southern South America, including H_1 from Hudson at 7.85-7.57 cal ka BP, R_1 from Reclus at 15.26-14.37 cal ka BP, MB_1 from Mt Burney at 9.95-8.85 cal ka BP, and A_1 from Aguilera at 3.34-3.07 cal ka BP (all dates from Stern, 2008).

There is a relatively good understanding of the large volcanic eruptions that have dispersed tephra widely across the southernmost part of South America during the Holocene (e.g., Naranjo and Stern, 2004; Stern, 2008; Wastegård et al., 2013; Weller et al., 2014, 2015, 2017, 2018; Stern et al., 2015; Del Carlo et al., 2018). However, beyond the Holocene, relatively little is known regarding the regional eruptive history. This is because long records of environmental change and terrestrial deposits are typically poorly preserved as a result of ice advance and retreat during the LGM, in addition to persistently strong westerly winds in the area which easily remove tephra from the landscape (e.g., Fontijn et al., 2014).

Further study of tephra deposits in the southern hemisphere could greatly improve the scope for correlating records over wide areas (including for example, South America and Antarctica). This would better refine the chronology of both climatic and volcanic events. Recent work demonstrates that tephra layers from southern Andean volcanoes exist far beyond South America. For example, a tephra from Sollipulli volcano (Alpehué pumice, So-A horizon) in the Chilean Lake District has been identified in sub-Antarctic South Georgia at ~3,000 km distance from the source (Oppedal et al., 2018), and widespread tephra layers from Mt. Burney (MB_1) and Reclus (R_1) volcanoes have been identified in the Falkland Islands (Monteath et al., 2019; both centres are ~950 km away). Koffman et al. (2017) have additionally investigated cryptotephra deposits found in surface snow and shallow firm samples from the West Antarctic Ice Sheet (WAIS) Divide Camp, Antarctica and correlated these to the AD 2011 Puyehue-Cordón Caulle eruption in Chile. Narcisi et al. (2012) have also produced correlations between Andean volcanic centres and ash identified in Antarctica, but some of these are brought into question by Del Carlo et al. (2018).

Bulk chemical analysis of southernmost South American tephra deposits is currently the most widely-used analytical method for characterising volcanic deposits and distinguishing source-localities (e.g., Stern, 2008; Weller et al., 2014, 2015, 2017). However, the analysis of volcanic ash deposits using individual chemical fingerprinting of glass-shards is increasingly recommended since it precludes the analysis of minerals, which can vary in abundance with distance from the vent (Tomlinson et al., 2015). In addition, the variation in melt composition is very sensitive to variations in crystallisation, which in particular varies between eruptive units, and data from bulk compositional analysis is not as effective as determining these often very subtle changes as individual glass-shard chemistry. As such, the chemistry of individual grains of glass provides the most accurate approach to fingerprint the composition of the deposit across wide areas and subsequently permits a robust source allocation and tephrocorrelations (e.g., Tomlinson et al., 2015; Fontijn et al., 2016; Del Carlo et al., 2018). For these reasons, the chemical fingerprinting of glass-shards from proximal deposits (Section 5.2.1) and the subsequent refinement of compositional fields has been undertaken to facilitate robust tephra correlations between volcanic centres and chemically analysed deposits from the Laguna Potrok Aike sedimentary archive (Tables 2.1, 5.1; Figure 5.2).

This study focuses on the volcanic deposits in the 106.09 metre-composite depth (m-cd) sediment sequence from site 2 of the ICDP expedition 5022 (5022-2CP) 'Potrok Aike Maar Lake Sediment Archive Drilling Project' (PASADO; Zolitschka et al., 2006). The site of Laguna Potrok Aike has not been covered by the Patagonian ice sheet during or after its Middle Pleistocene formation at ~0.77 Ma (Zolitschka et al., 2006). The sediment record recovered in the framework of the ICDP-PASADO mission spans the last ~80 ka, and therefore provides a record of part of the last glacial period and the Holocene (Gebhardt and Ohlendorf, 2019). It is subsequently the most comprehensive and longest record of volcanism in southern South America yet studied, offering the best opportunity to analyse regional volcanic activity during the Late Quaternary.

The tempo of activity and composition of the melts erupted may additionally provide insights into the relationship between ice-unloading and the occurrence of explosive volcanic activity (e.g., Huybers and Langmuir 2009; Watt et al., 2013a; Fontijn et al. 2016; Rawson et al. 2015, 2016). In areas where decompressional melting plays an important role in primary melt production, such as Iceland and mid-Ocean ridges, an increase in volcanic activity has been suggested as a result of deglaciation (e.g., Jull and McKenzie, 1996; Jellinek et al., 2004; Crowley et al., 2015). In continental arcs like the Andes, where primary magma production is less likely to be influenced by cycles of glaciation (e.g., Watt et al., 2013a), such cycles are thought to instead influence magma storage and residence time in the crust (e.g., Watt et al., 2013a; Rawson et al., 2016). This is based predominantly on the principle that the longer the melt sits in the crust, the more evolved it becomes because of fractional crystallisation (Watt et al., 2013a; Rawson et al., 2016).

Geochemical analysis of glass-shards in a high-resolution study using deposits from Mocho-Choschuenco volcano in the Chilean Lake District enabled the identification of three phases of post-glacial volcanic activity (Rawson et al., 2015, 2016). Here, relatively low frequency, large magnitude, silicic eruptions were recorded between one and five kyr after the termination of the last glaciation, during the first phase; the second phase comprised of medium-frequency, small-magnitude events of mafic composition; the final phase consisted of high-frequency events that varied in magnitude, and were predominantly of intermediate composition (Rawson et al., 2016). Rawson et al. (2016) hypothesised that significant changes in the eruption magnitude and composition of magmas at Mocho-Choshuenco are due to storage and release, which is most likely a response to changes in ice-overburden. This hypothesis can be better tested with synglacial records such as that from Laguna Potrok Aike.

5.1.2. Laguna Potrok Aike and previous tephra work

Laguna Potrok Aike (51°58’S; 70°23’W) is situated in the Pali Aike Volcanic Field (PAVF), related to back-arc volcanism of southern South America (Figure 5.1). The lake is

located downwind from the major productive centres of the SSVZ and AVZ, and thus Laguna Potrok Aike is an ideal site for the deposition of tephra from these centres (Wastegård et al., 2013).

During previous investigations of the Laguna Potrok Aike sedimentary record, 18 visible tephra layers were chemically characterised (Wastegård et al., 2013), allowing correlation between different sites due to identification of the MB_1 and R_1 tephra units. An increased abundance of tephra was identified between 72-38 and 25-19 cal ka BP (Wastegård et al., 2013; ages adjusted to reflect new age-model by Gebhardt and Ohlendorf, 2019). Not all of the identified tephra were chemically analysed in the previous study, and therefore we revisit the record to carry out more detailed analyses and increase the number of eruptions possibly recognised.

This new study significantly adds to prior research on the site and in the region as it:

1) provides new glass-chemistry for proximal deposits of the Austral Volcanic Zone, enabling more robust and compatible correlations to volcanic centres;

2) identifies five new primary ashfall (tephra) layers in the Potrok Aike record, providing a more complete regional tephra record for the region;

3) includes individual glass-shard geochemistry for each tephra layer in the Potrok Aike sequence with sufficiently large glass-shards;

4) identifies reworked ash layers, which provide insights into the palaeoenvironment for the last ~80 kyr, and

5) provides a dataset to test the relationship between tephra frequency and composition as well as changes in climate relating to ice-unloading.

5.2. Results

5.2.1. Glass chemical composition of proximal deposits

The commonly used bulk tephra (whole-rock) X-ray fluorescence method is not particularly appropriate for fingerprinting tephra and confirming correlations in tephrochronology. To resolve this issue, glass-shards from widespread regional markers (H_1, H_2,

MB_1, MB_2, R_1, and A_1) were analysed to produce a database of individual glass-shard major element chemistry (Tables 2.1, 5.1). Existing glass-chemical data for proximal samples by Del Carlo et al. (2018) and those affiliated to historical Lautaro and Viedma eruptions from Mayr et al. (2019) were additionally used for comparison (Figure 5.2).

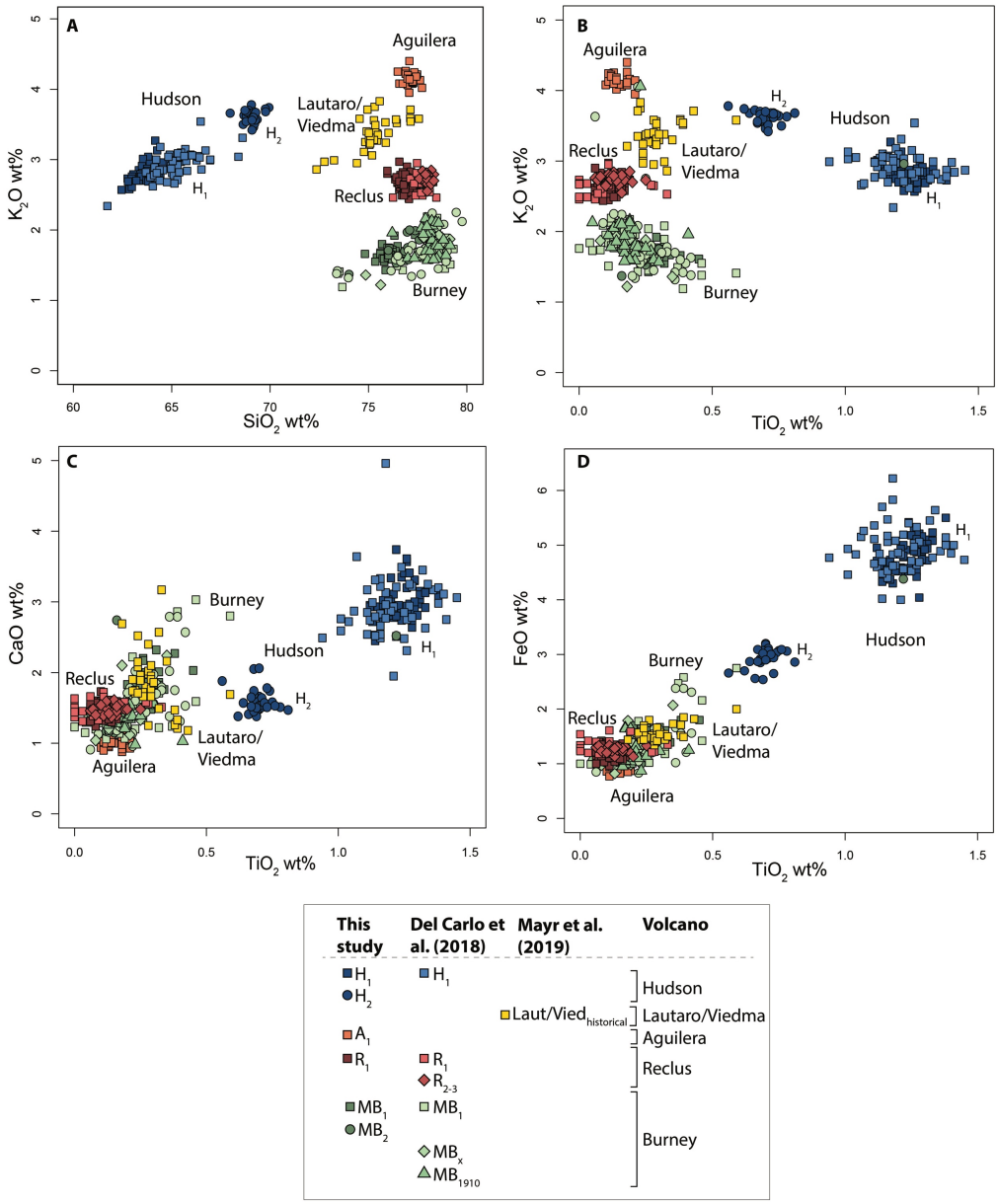


Figure 5.2. Glass-shard geochemistry from regional marker horizons, including new data from this study, from Del Carlo et al. (2018) and from Mayr et al. (2019); see key for details.

5.2.1.1. Hudson

Hudson volcano has had four large eruptions since the LGM, producing widespread tephra deposits in the Patagonia-Tierra del Fuego region: H_0 at 17.38 ± 0.12 cal ka BP (Bendle et al., 2017; Weller et al., 2014), H_1 at ~7.75 ka cal BP, H_2 at ~3.92 ka cal BP and AD 1991 (Stern, 2008). In this study, analysis was undertaken on H_1 and H_2 tephra samples from different sites (Table 2.1; Figure 5.1).

Hudson tephra deposits are compositionally typified by a relatively low silica content (62-69 wt% SiO_2 for H_1 and H_2 deposits) in comparison to products erupted by AVZ centres (Section 5.2.1.2-5.2.1.5; Table 5.1; Figure 5.2). The H_2 deposit has a silica content of ~69.02 SiO_2 wt% and is thus a trachyrhyolite; the H_2 deposit is enriched in Na_2O, with an average content of ~5.88 wt% and it also has an average K_2O content of ~3.62 wt%. The H_1 deposit has an average silica content of ~63.72 wt% and is thus a trachydacite. The H_1 deposit has high contents of FeO_t, MgO and CaO, with averages of 4.81 wt%, 1.49 wt%, and 3.02 wt%, respectively. The average K_2O content of the H_1 deposit is ~2.83 wt% (Table 5.1).

Table 5.1. Average glass-shard geochemistry for widespread eruptions normalised to 100 %[1] (all data is from this study, except Lautaro/Viedma reported by Mayr et al., 2019). Total represents analytical total (Supplementary File S.3.1).

Volcano	Marker	SiO_2	TiO_2	Al_2O_3	FeO_t	MnO	MgO	CaO	Na_2O	K_2O	P_2O_5	Cl	Total
Hudson	**H1**	***n=53***											
	avg	63.72	1.24	16.12	4.81	0.15	1.49	3.02	6.08	2.83	0.38	0.15	98.30
	stdev	0.58	0.06	0.19	0.30	0.05	0.14	0.26	0.18	0.13	0.05	0.04	1.75
	H2	***n=29***											
	avg	69.02	0.70	15.18	2.95	0.11	0.63	1.61	5.88	3.62	0.12	0.18	97.30
	stdev	0.35	0.05	0.20	0.16	0.05	0.08	0.17	0.22	0.08	0.03	0.03	1.98
Aguilera	**A1**	***n=24***											
	avg	77.12	0.15	12.62	0.98	0.03	0.17	1.01	3.57	4.14	0.02	0.19	97.53
	stdev	0.30	0.03	0.15	0.10	0.03	0.03	0.07	0.21	0.09	0.02	0.03	1.08
Burney	**MB1**	***n=52***											
	avg	76.07	0.28	13.09	1.56	0.04	0.37	1.84	4.79	1.68	0.05	0.23	96.39
	stdev	1.69	0.14	0.42	0.47	0.03	0.15	0.25	0.24	0.19	0.04	0.04	1.50
	MB2	***n=10***											
	avg	76.70	0.24	13.03	1.28	0.02	0.31	1.72	4.82	1.62	0.03	0.22	96.89
	stdev	1.14	0.04	0.76	0.14	0.02	0.24	0.37	0.23	0.11	0.03	0.06	2.53
Reclus	**R1**	***n=107***											
	avg	76.87	0.12	13.06	1.20	0.04	0.21	1.47	4.11	2.68	0.03	0.20	96.14
	stdev	0.27	0.03	0.19	0.10	0.04	0.02	0.12	0.17	0.19	0.02	0.03	1.41
Lautaro/ Viedma	**Historical**	***n=36***											
	avg	75.30	0.30	13.34	1.57	0.03	0.27	1.87	3.72	3.37	0.06	0.17	97.34
	stdev	1.08	0.08	0.72	0.14	0.03	0.08	0.43	0.28	0.23	0.05	0.04	1.64

[1] Analyses determined using wavelength dispersive electron microprobe analysis

5.2.1.2. Mt Burney

Mt Burney has had two volcanic eruptions that have emplaced widespread tephra across the Patagonia-Tierra del Fuego region: MB_1 and MB_2. The age of MB_1 is poorly constrained, with several different (but overlapping) dates in the literature, including 9.95-8.85 ka cal BP (Stern, 2008), 9.18-9.00 ka cal BP (Kilian et al., 2003) and 10.24-8.85 ka cal BP (Wastegård et al., 2013). MB_2 is deposited between 4.71 and 3.82 ka cal BP (Stern, 2008).

MB_1 and MB_2 are both rhyolitic and are chemically indistinct from one another, with combined averages of 76.17 wt% SiO_2; both layers are also potassium-poor, with combined

averages of 1.67 wt% K_2O. The potassium content of Mt Burney deposits is a distinct feature as it is significantly lower than that of tephra from other AVZ centres (Section 5.2.1.2-5.2.1.5; Table 5.1; Figure 5.2). In addition, Mt Burney deposits have higher sodium and magnesium contents than those of both Reclus and Lautaro/Viedma deposits with MB_1 deposits averaging 4.79 wt% Na_2O and 0.37 wt% MgO, and MB_2 deposits averaging 4.82 wt% Na_2O and 0.31 wt% MgO. As such these chemicals are useful indicators to characterise the Mt Burney source.

5.2.1.3. Reclus

The main widespread deposit documented for Reclus is the rhyolitic R_1 tephra unit at 14.76±0.18 ka cal BP (Stern et al., 2011). Two other tephra deposits with Reclus composition are identified in the Tierra del Fuego area (R_2 and R_3). These were deposited ~2.00 ka cal BP (Villa-Martínez and Moreno, 2007). Recent work by Del Carlo et al. (2018) have identified one of these units (i.e., R_2 or R_3) and provided a more precise age of <3.59-3.39 ka cal BP.

Deposits from Reclus are the most silica-enriched of all the deposits from AVZ centres; The SiO_2 content of R_1 deposits range between 75.96 and 77.79 wt%. The R_1 deposit contains on average 2.68 wt% K_2O (Table 5.1; Figure 5.2), which distinguishes it from deposits of other centres, such as Lautaro/Viedma. However, since glass analyses are only available for widespread Reclus deposits: R_1 and $R_{2\text{-}3}$ (LA-1B in Del Carlo et al., 2018), it is possible that the compositional field is not representative of all deposits from Reclus volcano.

5.2.1.4.Lautaro/Viedma

This study incorporates chemical data published by Mayr et al. (2019) who describe the chemistry of seven historical rhyolitic tephra layers in lake sediment cores ~40-60 km southeast of the Lautaro volcano. Based on geography and dating, Lautaro volcano is the most likely source of six of these tephras, and Viedma volcano the source of one (Mayr et al., 2019). The chemistry of these deposits are similar, and in i) the absence of other known widespread tephra deposits from these volcanoes, and ii) the inability to differentiate between them, we use the compositions

from Mayr et al. (2019) as a reference for Lautaro/Viedma chemistry. The chemistry of these deposits is similar to that of Reclus tephras, although Lautaro/Viedma deposits are more enriched in TiO_2 (~0.30 wt%) and K_2O (~3.37 wt%) than those from Reclus (~0.12 and ~2.68 wt%, respectively). There is only limited data from these two centres, and it is possible that other deposits may show greater compositional variability than what is shown in Figure 5.2.

5.2.1.5. Aguilera

There was one large, widespread eruption from Aguilera volcano, called A_1, between 3.34 and 3.07 ka cal BP (Stern, 2008). Tephra deposits >10 cm thick and >5 cm thick have been identified 80 km and 130 km east from the centre, respectively. The identification of these thick A_1 tephra deposits indicates an eruption volume greater than MB_2 (≥2.8 km^3) or the Hudson 1991 (≥3.6 km^3) eruptions (Stern, 2008). Other smaller eruptions of Aguilera volcano have been reported in the Holocene but their deposits have been less widely dispersed and they have only been identified in Torres del Paine, Chile and Lago Argentino. (e.g., Strelin and Malagnino, 2000; Stern, 2008). Further work is required to refine the dates and chemical signatures of these.

Aguilera deposits are characterised by a high potassium content, which ranges from 3.95 to 4.40 wt%. The A_1 tephra also has a high average SiO_2 content of 77.12 wt%. In contrast to other widespread AVZ tephra deposits, A_1 deposits have low contents of Al_2O_3, FeO_t and Na_2O, with averages of 12.62, 0.98 and 3.57 wt%, respectively. Sodium may be a useful tool for distinguishing tephra from NAVZ centres as it is particularly distinct when compared to the composition of other centres (Table 5.1), though caution should be taken since sodium is a mobile element that easily migrates with alteration.

5.2.2. Tephra units from Laguna Potrok Aike and their glass chemical composition

We identified 94 visible tephra deposits through the sedimentary sequence ranging in thickness from 0.1 to 35.5 cm (Figure 5.3); these predominantly had sharp bases separated by pelagic sediment, were light in colour and fine-grained. Seventy-nine of these deposits

were rhyolitic, one was rhyodacitic, and ten were trachydacitic; only four tephra layers could not be analysed due to low abundances of glass-shards. Variations in the major element glass composition of the Laguna Potrok Aike tephra allows these tephra units to be assigned to four broad groups that correspond to different volcanic sources; tephra was assigned to a group based on its dominant chemical composition (Figure 5.4). These compositional groups can also be used to identify reworked deposits as they often have heterogeneous compositions that span multiple groups atypical of a primary ashfall event.

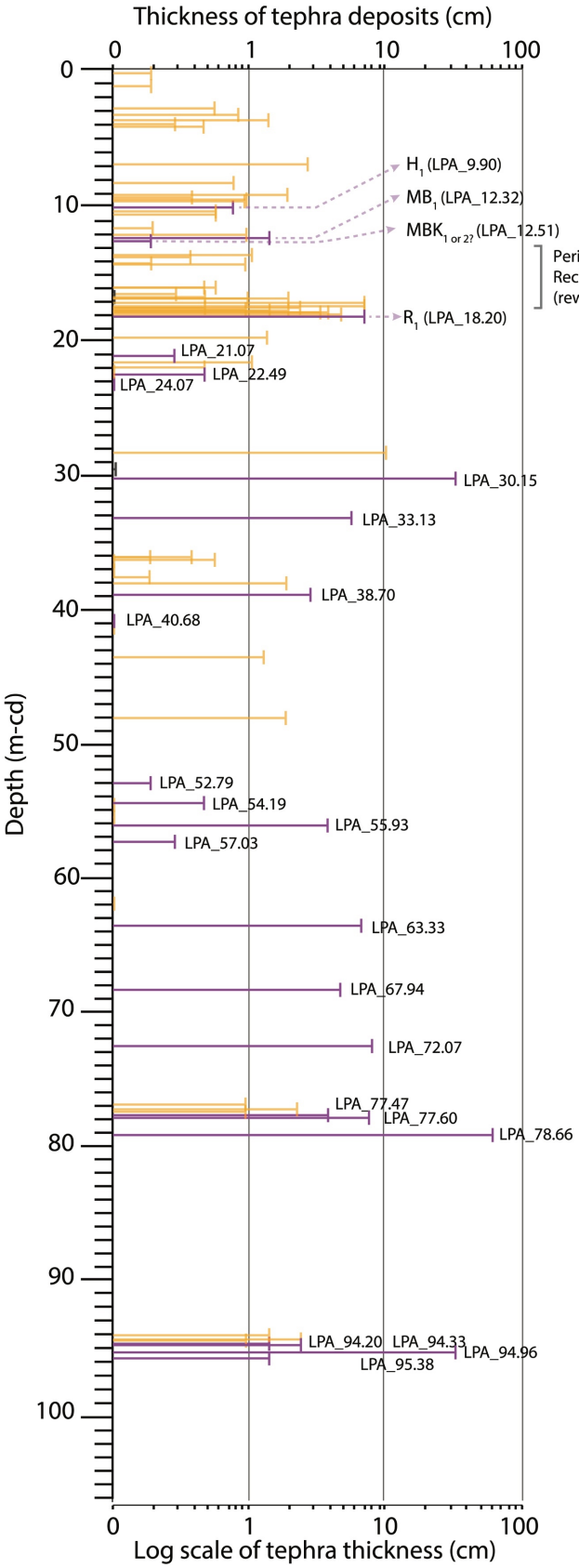


Figure 5.3. Logarithmic scale of tephra thicknesses, with primary (purple) and reworked (orange) tephra layers. Tephra labels are provided for primary layers only.

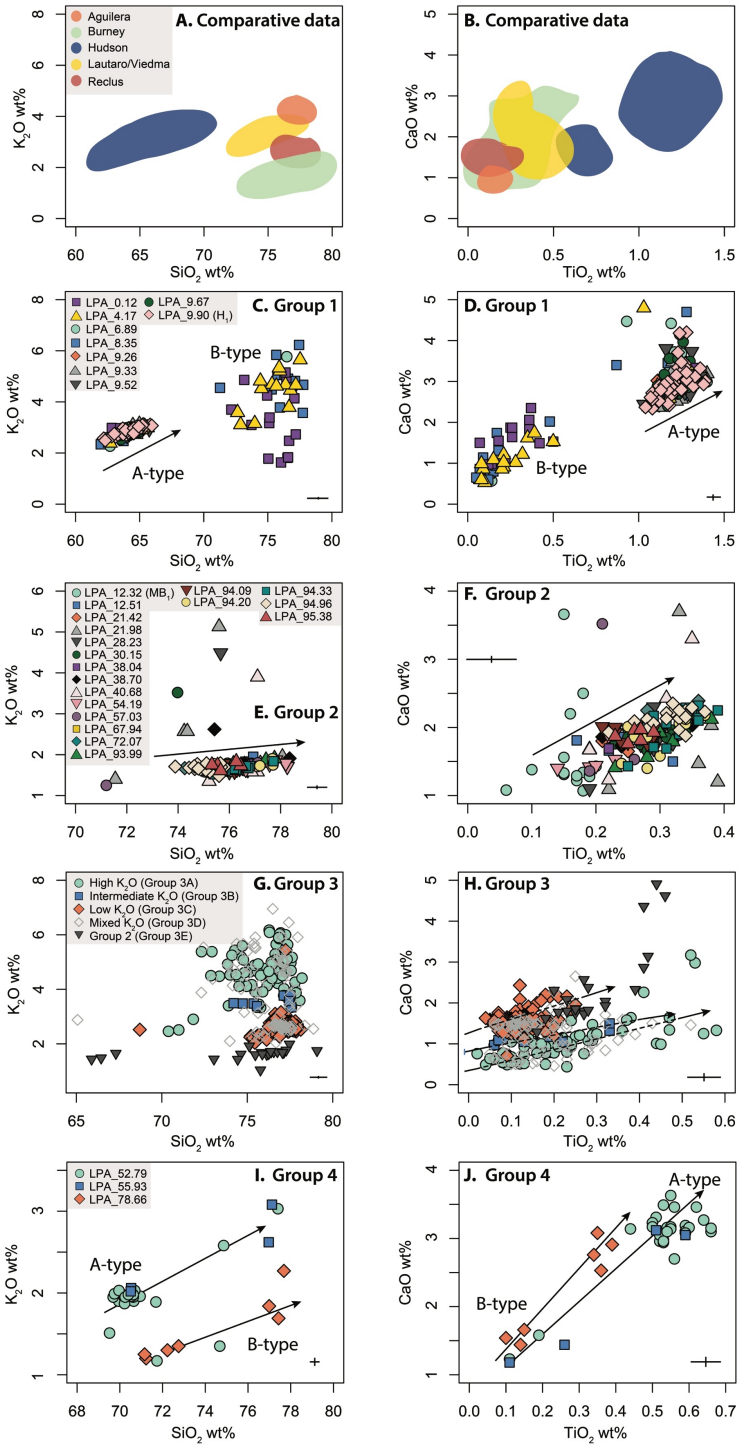


Figure 5.4. Variation diagrams of glass-chemical data for tephra identified in the Laguna Potrok Aike sedimentary sequence. Compositional trends are identified using black arrows. A-B) Compositional fields of widespread marker horizons extracted from the terrestrial realm (this study; Del Carlo et al., 2018); C-D) Group 1 tephra. Some of these deposits have two components (Group 1A from Hudson volcano and Group 1B from AVZ sources; see Section 4); E-F) Group 2 tephra (from Mt Burney); G-H) Group 3 tephra (from Reclus volcano and Austral Volcanic Zone centres); I-J) Group 4 tephra (from unknown centres). Error bars represent 2 standard deviations of repeated analyses of the StHs6/80-G MPI-DING reference glass. Note that axes are different in scale for each figure.

Based on tephra compositional and morphological information, 65 tephra deposits identified are considered to be reworked, three are potentially reworked, 25 are primary, and there is insufficient information for one tephra. Further detail on these deposits is provided in Section 5.5. Here the chemical compositions of both primary and reworked tephra are discussed.

5.2.2.1. Group 1 tephra

Group 1 includes nine tephra layers (LPA_0.12, 4.17, 6.89, 8.35, 9.26, 9.33, 9.52, 9.67, 9.90) that have been deposited between 8.4 and 0.08 ka cal BP. Tephra deposits belonging to this group are dark and medium grained (0.25–0.5 mm). Glass-shards forming tephra layers in this group are typically yellow or green in colour and have a vesicular or fluted morphology. Their free-crystal mineral assemblage is composed of plagioclase, quartz, orthopyroxene and minor hornblende.

The chemical composition of four deposits in Group 1 is heterogeneous and the group is subsequently sub-divided into A- and B-type tephra with B-type tephra reflecting heterogeneous compositions. Group 1A tephra can be identified by their trachydacitic affinities, with intermediate SiO_2 content (~64.22 wt%) and intermediate-high K_2O content (~2.84 wt%). Group 1A tephra has a high Al_2O_3 content, ranging from 15.50-18.06 wt%, and a high Na_2O content, ranging from 5.21-6.51 wt% (Table 5.2; Figure 5.4).

Table 5.2. Average and standard deviation of glass-shard chemistry for the different groups of tephra identified in the Laguna Potrok Aike sequence, including Groups 1 (A and B-type), 2, 3 (3A, 3B, 3C, 3D, 3E) and 4 (4A and 4B) (total *n*=1046). This data includes reworked and primary tephra chemistry. Tephra chemistry is normalised to 100 wt%. Total represents analytical total (See Supplementary File S.3.1).

Group		SiO_2	TiO_2	Al_2O_3	FeO_t	MnO	MgO	CaO	Na_2O	K_2O	P_2O_5	Cl	Total
Group 1	A-type	***n=182***											
	average	64.22	1.22	15.94	4.8	0.16	1.45	3.03	5.85	2.84	0.36	0.14	98.81
	stdev	0.77	0.08	0.3	0.32	0.05	0.23	0.42	0.25	0.15	0.05	0.03	1.25
	B-type	***n=41***											
	average	75.65	0.21	13.02	1.58	0.06	0.2	1.22	3.71	4.12	0.04	0.19	96.06
	stdev	1.58	0.13	0.65	0.5	0.04	0.15	0.47	0.61	1.15	0.04	0.04	1.83
Group 2		***n=150***											
	average	76.09	0.28	13.14	1.53	0.05	0.37	1.9	4.59	1.79	0.05	0.22	95.92
	stdev	1.09	0.06	0.56	0.24	0.04	0.08	0.41	0.33	0.46	0.03	0.04	1.8
Group 3	Group 3A	***n=77***											
	average	75.79	0.21	12.91	1.42	0.07	0.17	1.01	3.54	4.65	0.03	0.2	95.39
	stdev	1.63	0.13	0.63	0.56	0.04	0.13	0.47	0.52	0.81	0.03	0.05	1.11
	Group 3B	***n=11***											
	average	76.4	0.16	13.06	1.31	0.06	0.16	1.24	4.1	3.35	0.03	0.13	95.08
	stdev	1.21	0.1	0.22	0.59	0.03	0.06	0.21	0.28	0.37	0.02	0.08	1.23
	Group 3C	***n=475***											
	average	77.15	0.13	12.96	1.23	0.05	0.22	1.55	3.82	2.66	0.03	0.22	96.27
	stdev	0.57	0.05	0.23	0.20	0.04	0.04	0.14	0.30	0.17	0.02	0.09	2.69
	Group 3D	***n=101***											
	average	78.87	0.18	12.94	1.37	0.05	0.2	1.25	3.75	3.8	0.04	0.19	96.1
	stdev	65.07	0.13	0.59	0.49	0.04	0.14	0.44	0.61	1.27	0.04	0.04	1.76
	Group 3E	***n=23***											
	average	74.93	0.29	13.69	1.85	0.05	0.52	2.37	4.39	1.64	0.06	0.2	97.17
	stdev	3.54	0.09	1.36	0.8	0.03	0.46	0.99	0.58	0.19	0.06	0.06	1.69
Group 4	Group 4A	***n=31***											
	average	71.35	0.51	14.93	2.51	0.05	0.74	2.93	4.18	2.52	0.12	0.18	96.61
	stdev	2.27	0.14	0.87	0.58	0.04	0.22	0.64	0.40	0.38	0.05	0.03	1.94
	Group 4B	***n=7***											
	average	70.12	0.45	14.43	2.39	0.05	0.67	2.75	4.10	2.39	0.11	0.17	94.15
	stdev	3.01	0.12	1.13	0.74	0.06	0.21	0.70	0.44	0.40	0.55	0.02	1.54

5.2.2.2. Group 2 tephra

Group 2 tephra consists of 19 layers that occur between 12.32 m-cd and 95.39 m-cd (9.42 to 50.86 ka cal BP; LPA_12.32, 12.51, 21.42, 21.98, 28.23, 30.15, 38.04, 38.70, 40.68, 54.19, 57.03, 67.94, 72.07, 93.99, 94.09, 92.20, 94.33, 94.96, and 95.38). The deposits included in this group comprise colourless shards that have a fluted and vesicular morphology; the vesicle shape varies between circular and elongate. There are additionally white-grey pumice particles rich in dark micro-phenocryst inclusions in these deposits. Group 2 deposits are typically characterised by ~50 % glass-shards and a high abundance of minerals (~40 %). The mineral assemblage of Group 2 deposits is composed of plagioclase, orthopyroxene, olivine and hornblende with some tephra samples also having quartz.

The glass-chemical composition of Group 2 tephra is rhyolitic with low potassium (~1.79 K_2O wt%) and intermediate-high magnesium contents (~0.37 MgO wt%; Table 5.2; Figure 5.4). Group 2 tephra deposits have intermediate FeO_t contents, typically between 0.95 and 2.39 wt%, intermediate TiO_2 contents, typically between 0.06 and 0.39 wt%, and high Na_2O contents, typically between 2.43 and 5.19 wt%.

5.2.2.3. Group 3 tephra

Group 3 tephra consists of 47 tephra layers, which occur between 1.75 m-cd and 77.69 m-cd (1.3-63.1 ka cal BP) and are the most commonly identified tephra type (Table 5.2; Figure 5.4). Group 3 tephra predominantly consist of colourless glass shards with cuspate and fluted shard morphology. On occasion, grey pumice with microlite inclusions, as well as platy, colourless shards are also present. Tephra from this group usually have a mineral assemblage consisting of plagioclase, orthopyroxene, and occasionally olivine and hornblende. Very low abundances of biotite are observed in LPA_1.08, 2.56, and 63.33.

Group 3 tephra deposits are rhyolitic in composition and have quite variable potassium contents (~3.22 K_2O wt%; range: 1.04-6.95 K_2O wt%). Based on potassium content, Group 3 tephra are sub-classified into five groups: 3A) high, 3B) intermediate, 3C) low, 3D) mixed, and

3E) very low abundance potassium (in respect to the abundance of potassium identifiable in Group 3 tephra deposits). Group 3A, 3B and 3C have average K_2O contents of 4.64 wt% (*n=75*), 3.40 wt% (*n=16*), and 2.66 wt% (*n=475*), respectively. Group 3D shows a range between 2.04-6.95 wt% K_2O (*n=111*). There are some chemical outliers (Group 3E) amongst Group 3 tephra that are more comparable to Group 2 tephra compositions. Because of this, they are listed as Group 2 (Group 3E) chemistry in Figure 5.4 – these have a very low average potassium content of 1.63 wt% K_2O (range: 1.04-1.99 wt%; *n=27*).

The tephra layers in Group 3A are LPA_35.97, 36.04, 36.15, 42.00, 55.40, and 61.67; Group 3B layers are LPA_12.16 and 63.33; Group 3C layers are LPA_10.49, 10.59, 11.71, 16.11, 16.48, 16.78, 16.91, 16.92, 16.97, 17.19, 17.39, 17.55, 17.59, 17.62, 17.64, 17.65, 17.69, 17.75, 17.76, 17.79, 17.80, 17.85, 17.90, 18.03, 18.20, 77.04, 77.47, 77.61, and Group 3D layers are LPA_1.08, 13.62, 14.20. Group 3D/3E layers are, LPA_21.07, 2.56, 24.07, 37.55; Group 3C/3E layers are LPA_14.22, 16.04, Group 3A/3E layers are LPA_36.80, 43.46; Supplementary File S.3.2).

Titanium and calcium are useful to further differentiate the different sub-classifications of Group 3 tephra. Tephra in Group 3A have a low abundance of CaO (~1.01 wt%) and a relatively narrow range of TiO_2 (0.02-0.58 wt%). This contrasts with Group 3C, which has a higher abundance of CaO (~1.55 wt%) and a low abundance of TiO_2, with a mean of ~0.13 wt% and wider range of 0.04-0.91 wt%. The sample size of Group 3B is quite limited (*n=11*), but tephra in this group have similar calcium and titanium contents compared to those in Group 3A.

5.2.2.4. Group 4 tephra

Group 4 consists of 3 tephra layers observed at 52.79 m-cd (~40.8 ka cal BP), 55.93 m-cd (~44.6 ka cal BP), and 78.66 m-cd (~64.7 ka cal BP), respectively. Group 4 can be subdivided into two groups: 4A and 4B. Group 4A has, on average, slightly higher K_2O content than 4B (71.35 and 74.21 wt%, respectively).

Group 4A includes LPA_52.79 and LPA_55.93. LPA_52.79 is a 0.2 cm thick unit of grey/white pumice with dark microphenocryst inclusions and spherical vesicles. The mineral content is <10 % and comprises plagioclase, orthopyroxene, biotite, olivine and quartz. Accidental lithics are abundant in this sample at ~25 %. Chemically, it has an intermediate potassium content with respect to its silica content (~2.46 wt% K_2O and 70.99 wt% SiO_2). This chemical signature is not observed in any other group. TiO_2 (~0.53 wt%) and Al_2O_3 (~15.10 wt%) are relatively abundant. LPA_52.79 tephra chemistry follows similar K_2O/SiO_2 evolutionary trends to Group 3B tephra, but has different CaO/TiO_2 compositions (Table 5.2; Figure 5.4). LPA_55.93 is a 4 cm unit of white and colourless, crystal-poor, (spherical) vesicular and fluted shards. Glass-shard abundance is 85 %, while lithics and minerals comprise 15 % of the sample. Bottle-green orthopyroxene with Fe-Ti oxides, plagioclase, and hornblende form the mineral assemblage of this deposit. Chemically, LPA_55.93 is a rhyolite with a heterogeneous composition. The deposit has a SiO_2 range from 70.51 to 77.12 wt%.

Group 4B consists only of LPA_78.66, which is a ~63 cm thick cream-coloured unit that comprises white microphenocryst-poor pumice, and a minor abundance of vesicular and fluted colourless glass-shards. Overall, this unusually thick deposit is crystal-poor (<5 %), with only green orthopyroxene with Fe-Ti oxide inclusions and plagioclase. LPA_78.66 is chemically heterogeneous, with an SiO_2 content between 71.16 and 77.68 wt%, and a K_2O content between 1.70 and 2.77 wt%.

5.3. Interpretation and discussion

5.3.1. Chemical fingerprints and tephra correlations

In this section, tephra is correlated to source centres in the lowermost SVZ and AVZ on the basis of tephra chemistry. Tephra has been correlated to Hudson volcano, Mt. Burney, Reclus and NAVZ centres.

5.3.1.1. Hudson volcano

Group 1A tephra deposits (Figure 5.4C-D; Section 5.2.2.1) can be correlated with volcanism from Hudson volcano based on glass-shard geochemistry, and notably their intermediate silica content and intermediate-high potassium content (Figures 5.4C-D, 6; Section 5.2.2.1). Hudson volcano is located approximately 700 km from Laguna Potrok Aike. The widespread H_1 deposit from Hudson volcano was previously identified in the Laguna Potrok Aike record obtained for the SALSA campaign (Haberzettl et al., 2007). However, this chemically distinct tephra layer was never identified in the Laguna Potrok Aike record obtained for the PASADO campaign (Kliem et al., 2013b; Wastegård et al., 2013). The H_1 (LPA_9.90) deposit has now been identified as a coarse, 9.6 cm thick ash between 9.90 and 10.00 m-cd in the sediment sequence, and has a depositional age of 9.0-8.6 ka cal BP (Table 5.3; Figure 5.5). The age for this tephra from the Laguna Potrok Aike age model is somewhat older than most previously published ages for H_1 (Stern, 1992, 2008; Prieto et al., 2013; Naranjo and Stern, 1998) but does overlap with reported ages of 8.63-8.42 ka cal BP for this tephra from lake cores near Cochran, Chile, 150 km southeast of the volcano (Stern et al., 2016).

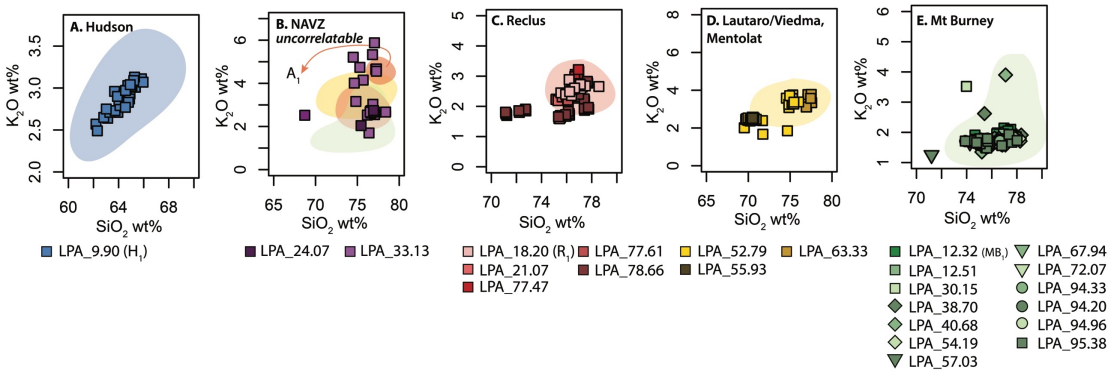


Figure 5.5. Variation diagrams of glass-chemical data for tephra deposited via primary ash-fall at individual centres identified in the Laguna Potrok Aike sedimentary sequence: A) Hudson; B) uncorrelatable deposits from the NAVZ; C) Reclus; D) Lautaro/Viedma or Mentolat; E) Mt Burney. Compositional fields of widespread marker horizons are extracted from the terrestrial realm (this study; Del Carlo et al., 2018; Mayr et al., 2019) and are represented using the same colours as for Figures 5.2 and 5.4.

After the deposition of this primary unit (stratigraphically up-core), there are five tephra layers with a Hudson affinity which are reworked, and two which are likely reworked (Figures

5.3, 5.6; Supplementary File S.3.2). These are identified by a dominance of rounded and sub-rounded minerals (Figure 2.3), a lack of glass coating on minerals (particularly on orthopyroxene), a decline in the overall abundance of glass-shards, an increase in the abundance of lithics, and in some cases, an increase in the abundance of organic material (e.g., Figure 5.7). Sedimentation rates vary during this period (e.g., Kliem et al., 2013b) and it is considered likely that the redeposition of tephra during the last ~8 ka cal BP is related to lake level changes that caused reworking of older sediments (Haberzettl et al. 2007; Anselmetti et al. 2009; Kliem et al., 2013a; Zolitschka et al. 2013; Section 5.5).

The analysis of individual deposits indicates that LPA_9.90 is the only primary tephra unit with a Hudson affinity in the Laguna Potrok Aike sedimentary record. Much of the up-core reworking shares the same tephra chemistry as the LPA_9.90 unit. However, there are four deposits with a larger compositional range (LPA_0.12, 4.17, 6.89, and 8.35). The Group 1 A-type composition of these deposits has Hudson affinity, but the occurrence of Group 1 B-type glass is more consistent with AVZ volcanism (Figure 5.4; Sections 5.2.2.1, 5.5). The heterogeneity in this glass chemistry is deemed to be further evidence of reworking.

The widespread and compositionally unique H_2 marker horizon, deposited ~3.92 ka cal yr BP (Naranjo and Stern, 1998), has not been identified in the Laguna Potrok Aike sedimentary record indicating limited possibility of other Hudson volcano sources for reworking than the LPA_9.90, H_1 unit.

5.3.1.2. Mt Burney

Group 2 tephra deposits (Figure 5.4E-F; Section 5.2.2.2) are associated with Mt Burney volcanism. There is little chemical variation between the Mt Burney proximal data and the layers that have been correlated to Mt Burney volcano in the Laguna Potrok Aike sedimentary sequence. Of the 19 layers identified, 13 are primary and six are reworked deposits (Tables 5.3; Figures 5.5, 5.8). This indicates that Mt Burney is possibly the most active volcanic centre in the AVZ through the Late Quaternary (Section 5.4).

Table 5.3. Average and standard deviation of glass-shard chemistry for the primary tephra layers identified in the Laguna Potrok Aike sedimentary sequence (this study; Supplementary Files S.3.1, S.3.2). Tephra chemistry is normalised to 100 % and analytical total is presented.

Tephra label and correlation		SiO_2	TiO_2	Al_2O_3	FeOt	MnO	MgO	CaO	Na_2O	K_2O	P_2O_5	Cl	Total
Hudson - H1													
LPA_9.90	avg	64.36	1.21	15.91	4.79	0.16	1.46	2.98	5.75	2.89	0.36	0.13	98.88
n=43	stdev	0.84	0.09	0.12	0.30	0.06	0.27	0.42	0.23	0.15	0.05	0.02	0.99
Mt Burney - MB1													
LPA_12.32	avg	77.11	0.16	12.86	1.08	0.04	0.26	1.56	4.68	1.97	0.04	0.23	95.49
n=17	stdev	0.75	0.03	0.19	0.10	0.03	0.02	0.65	0.15	0.08	0.03	0.02	2.28
Mt Burney - MBK1/2?													
LPA_12.51	avg	76.36	0.26	13.12	1.52	0.04	0.35	1.84	4.55	1.68	0.04	0.24	97.63
n=12	stdev	0.54	0.05	0.26	0.15	0.04	0.04	0.17	0.14	0.11	0.03	0.02	1.98
Reclus - R1													
LPA_18.20	avg	76.76	0.17	12.92	1.35	0.04	0.26	1.69	4.02	2.57	0.04	0.18	95.70
n=18	stdev	0.67	0.05	0.39	0.20	0.04	0.08	0.18	0.23	0.13	0.03	0.03	1.62
Reclus													
LPA_21.07	avg	75.58	0.22	13.52	1.67	0.06	0.32	2.10	4.15	2.19	0.04	0.14	98.34
n=7	stdev	0.28	0.05	0.22	0.09	0.05	0.05	0.09	0.26	0.26	0.02	0.03	2.50
Insufficient chemistry													
LPA_22.49													
NAVZ - Unknown													
LPA_24.07	avg	76.56	0.13	13.08	1.28	0.06	0.18	1.27	3.86	3.34	0.03	0.21	96.58
n=28	stdev	0.86	0.06	0.32	0.38	0.04	0.06	0.37	0.50	1.09	0.03	0.03	1.75
Mt Burney													
LPA_30.15	avg	76.13	0.28	12.97	1.57	0.03	0.38	1.85	4.62	1.87	0.04	0.24	95.59
n=12	stdev	0.79	0.04	0.25	0.28	0.04	0.04	0.10	0.31	0.52	0.02	0.04	1.07
NAVZ - Unknown													
LPA_33.13	avg	73.69	0.40	13.63	2.61	0.04	0.49	2.05	4.37	2.43	0.12	0.18	96.89
n=3	stdev	4.38	0.45	0.64	1.90	0.07	0.31	0.51	0.44	0.36	0.13	0.01	1.82
Mt Burney													
LPA_38.70	avg	76.47	0.26	13.20	1.46	0.08	0.33	1.83	4.15	1.96	0.05	0.23	95.27
n=5	stdev	1.14	0.05	0.41	0.10	0.06	0.03	0.13	0.97	0.38	0.02	0.05	1.61
Mt Burney													
LPA_40.68	avg	76.32	0.26	13.24	1.40	0.02	0.31	2.02	4.36	1.83	0.06	0.18	96.48
n=10	stdev	0.73	0.05	0.42	0.18	0.03	0.08	0.55	0.53	0.73	0.02	0.03	1.15
NAVZ - Lautaro/Viedma or Mentolat													
LPA_52.79	avg	70.99	0.53	15.10	2.59	0.05	0.77	3.03	4.18	2.46	0.13	0.18	96.97
n=27	stdev	1.80	0.12	0.63	0.47	0.04	0.18	0.51	0.42	0.33	0.04	0.03	1.63
Mt Burney													
LPA_54.19	avg	77.39	0.21	12.91	1.23	0.04	0.29	1.59	4.42	1.74	0.04	0.14	94.73
n=6	stdev	0.95	0.05	0.43	0.19	0.04	0.04	0.22	0.20	0.09	0.02	0.03	1.16
NAVZ - Lautaro/Viedma or Mentolat													
LPA_55.93	avg	73.78	0.37	13.79	1.97	0.03	0.49	2.20	4.17	2.94	0.07	0.18	94.84
n=4	stdev	3.77	0.22	1.45	1.00	0.02	0.32	1.03	0.25	0.50	0.06	0.04	2.44
Mt Burney													
LPA_57.03	avg	75.36	0.22	14.20	1.15	0.05	0.28	2.14	4.76	1.64	0.07	0.14	94.51
n=3	stdev	3.62	0.03	2.40	0.06	0.08	0.02	1.20	0.27	0.34	0.02	0.02	0.77
Lautaro/Viedma													
LPA_63.33	avg	77.32	0.09	13.04	0.81	0.04	0.11	1.09	3.91	3.51	0.01	0.06	94.90
n=5	stdev	0.28	0.03	0.23	0.12	0.02	0.04	0.09	0.08	0.29	0.01	0.02	0.55
Mt Burney													
LPA_67.94		75.68	0.33	13.02	1.86	0.07	0.43	2.00	4.67	1.64	0.06	0.24	96.04
n=1													

Tephra label and correlation		SiO_2	TiO_2	Al_2O_3	FeOt	MnO	MgO	CaO	Na_2O	K_2O	P_2O_5	Cl	Total
Mt Burney													
LPA_72.07	avg	74.71	0.32	13.65	1.88	0.04	0.53	2.32	4.64	1.64	0.06	0.21	97.37
n=2	stdev	0.64	0.05	0.05	0.05	0.01	0.09	0.09	0.23	0.05	0.02	0.01	0.59
Reclus													
LPA_77.47	avg	76.72	0.10	13.22	1.22	0.04	0.20	1.29	4.06	2.95	0.04	0.16	94.22
n=5	stdev	0.29	0.02	0.07	0.27	0.03	0.02	0.14	0.14	0.19	0.02	0.02	0.70
Reclus													
LPA_77.61	avg	76.78	0.14	13.21	1.26	0.08	0.23	1.59	4.02	2.48	0.03	0.18	94.32
n=5	stdev	0.41	0.01	0.07	0.22	0.06	0.07	0.17	0.13	0.25	0.03	0.01	0.61
Reclus													
LPA_78.66	avg	74.21	0.26	14.08	2.11	0.07	0.44	2.27	4.27	2.06	0.08	0.15	96.06
n=7	stdev	3.01	0.12	1.13	0.74	0.06	0.21	0.70	0.44	0.40	0.05	0.02	1.54
Mt Burney													
LPA_94.20	avg	76.23	0.30	12.91	1.59	0.06	0.40	1.92	4.62	1.69	0.05	0.22	96.39
n=13	stdev	0.91	0.04	0.46	0.23	0.05	0.05	0.28	0.18	0.09	0.02	0.03	1.39
Mt Burney													
LPA_94.33	avg	75.96	0.33	12.99	1.66	0.05	0.43	2.05	4.61	1.65	0.04	0.22	96.45
n=15	stdev	0.75	0.04	0.35	0.12	0.05	0.05	0.26	0.16	0.08	0.02	0.02	1.35
Mt Burney													
LPA_94.96	avg	75.02	0.31	13.53	1.73	0.05	0.46	2.13	4.80	1.67	0.06	0.24	95.48
n=18	stdev	0.51	0.04	0.20	0.14	0.04	0.04	0.13	0.18	0.08	0.02	0.01	1.45
Mt Burney													
LPA_95.38	avg	75.95	0.26	13.37	1.48	0.04	0.37	1.88	4.63	1.73	0.05	0.23	95.42
n=6	stdev	0.50	0.02	0.23	0.16	0.03	0.04	0.09	0.10	0.07	0.04	0.04	0.90

The most widespread unit, MB_1 (LPA_12.32), is additionally identified in the PASADO sequence as a 1.5 cm thick deposit between 12.32 and 12.34 m-cd, which corresponds to an age of 10.4-10.0 cal ka BP. This age is slightly older than that of Stern (2008) and Kilian et al. (2003) who report a depositional age for this widespread eruption of 9.5-8.9 cal ka BP and 9.6-9.0 cal ka BP, respectively. However, it overlaps with that of Del Carlo et al. (2018) who report ^{14}C ages of between 9299±65 and 7325±46 ^{14}C yr BP (10.64±0.10 and 8.10±0.06 cal ka BP).

Some studies (e.g., Kilian et al., 2003; Stern, 2008; Monteath et al., 2019) have reported Mt Burney-type tephra in the mid-Holocene. However, the largest of these, MB_2, is distributed well to the south, and we have not encountered any tephra layers after the deposition (up-core) of MB_1 in Laguna Potrok Aike with Mt Burney affinity. It is possible that Mt Burney tephra may be present as cryptotephra horizons (i.e., tephra not visible to the naked eye) rather than as visible tephra horizons. Cryptotephra was not analysed in this study because of the large number of visible and reworked tephra layers observed, which would result in a high background cryptotephra signal.

5.3.1.3. Reclus and NAVZ centres

The correlation of deposits to Reclus and individual NAVZ centres (Lautaro, Viedma, Aguilera) using major element glass compositions is difficult because they are compositionally similar to each other (e.g., Wastegård et al., 2013). While this study, in combination with Del Carlo et al. (2018), presents the most comprehensive glass-chemical dataset for proximal deposits in the southernmost part of South America, the dataset is still limited (Table 5.1; Figure 5.2). It has been suggested that trace elements should be used to further differentiate these (Wastegård et al., 2013; Del Carlo et al., 2018). However, glass-shards in NAVZ deposits are typically very small (~10-15 μm) and their trace elemental chemical characterisation is very challenging due to technical limitations of LA-ICP-MS (e.g., beam size; Tomlinson et al., 2010; Pearce, 2014). Future work should involve expanding this reference dataset because the compositional fields may be larger than shown at present, and they may overlap with one other as only the widespread eruptive deposits have been characterised. Correlations made to individual centres in the NAVZ should therefore be treated with caution, and suggested source volcanoes are simply the most likely event source based on our current knowledge of the chemical composition at each.

Group 3 tephra (Table 5.2; Figure 5.4G-H; Section 5.2.2.3) are representative of Reclus and NAVZ tephra. Aguilera, Lautaro and Reclus volcanoes can be sub-classified based on potassium, calcium and titanium contents (Tables 5.1, 5.2; Figure 5.4), and these are likely to correspond to the following sources: 3A-Aguilera (high K_2O), 3B-Lautaro (intermediate K_2O), 3C-Reclus (low K_2O), 3D-reworked (mixed K_2O), and 3E-outliers (very low K_2O) from Groups 3A-D that correspond best with Group 2 (Mt Burney) chemistry (Table 5.2; Figure 5.4G-H; Supplementary File S.3.2). The component of Group 1 labelled Type B is additionally most reflective of Group 3 tephra from the AVZ. These deposits have a very low average potassium content of 1.63 wt% K_2O (range: 1.04-1.99 wt%; n=27). Moreover, tephra layer LPA_78.66, of Group 4B is tentatively correlated to Reclus volcano (low K_2O; Group 3C; Figure 5.4G-H; Figure 5.5) because, while it does not plot on the known compositional field of Reclus, it lies on the

same compositional trend as other deposits from the centre. In addition, the chemistry of deposits in Group 4A correlate well with Lautaro/Viedma, or possibly Mentolat (Weller et al., 2019).

Some analyses in Group 3 (Figure 5.4G-H) are heterogeneous, and possess a mixed potassium content (Group 3D), while some analyses are outliers from Groups 3A-3D but possess the same trend and composition of Group 2 (Mt Burney) and thus are sub-categorised (Group 3E). Many of these layers are reworked based on analysis of their mineral assemblage and glass-shards, in addition to heterogeneous chemical composition which is atypical of AVZ tephra deposits. Of Group 3 deposits, six are primary, 38 are reworked, and one is likely reworked; reworked deposits are discussed in detail in Section 5.5 (Supplementary File S.3.2).

The sequence between 16.47 and 18.25 m-cd (~14.3 cal ka BP; Figure 5.6) is composed of multiple thick and persistently light beige, fine-grained tephra with little pelagic sediment in between. In Kliem et al. (2013a), the R_1 tephra was placed at the top of this sequence, at 16.78-16.79 m-cd (0.5 cm thickness). The tephra beneath were overlooked because they were considered as being part of a prolonged period of sedimentary reworking (e.g., Kliem et al., 2013a). However, no primary tephra deposit was identified which leaves no mechanistic explanation for the presence of subsequent (upper-core) tephra layers. In other words, reworked layers (particularly thick ones) are very unlikely to exist without the deposition of an initial primary tephra layer, and this is (often) thicker than any subsequent reworked layers. We therefore suggest the bottom tephra in this sequence at 18.20-18.25 m-cd (14.5-14.1 cal ka BP) to be the primary R_1, with the subsequent sequence representing its reworked facies (Figure 5.6).

Reclus volcano, located ~250 km northwest of Laguna Potrok Aike, deposited the large R_1 tephra horizon at 14.76 (±0.18) cal ka BP (date after Stern et al., 2011). Stern (2008) identified R_1 deposits in the terrestrial realm >10 cm thick, and >5 cm thick at 150 km and 350 km southeast of the volcano, respectively. The maximum observed thickness of R_1 was >40 cm, observed 90 km southeast from the volcano. Because the tephra thicknesses in lake environments are less affected by preservation issues than in their terrestrial counterparts (e.g., Fontijn et al., 2014) and the deposit had a south-south east dispersal, it is expected that the primary thickness of the R_1

deposit observed in Laguna Potrok Aike should be between 5 and 10 cm thick. As such, it is unlikely that the entire tephra-bearing sequence between 16.47 and 18.25 m-cd would correspond to R_1.

The visual and chemical analysis of numerous tephra layers in the sedimentary record between 16.47 and 18.25 m-cd (spanning a 4.0 ky year time period), indicates that the initial 5-cm-thick, diffuse, beige, Group 3C tephra layer deposited at 18.20-18.25 m-cd (~14.3 cal ka BP) most likely corresponds to the large and widespread R_1 tephra layer. Subsequent tephra above this (including the tephra labelled as R_1 by Kliem et al., 2013b and Wastegård et al., 2013) with the same glass composition are most likely reworked. The deposition of the 5-cm-thick R_1 tephra on unconsolidated sediment on relatively steep slopes near the edge of the lake could have caused the sediment to destabilise, and resulted in multiple reworked tephra layers with sediment in-between (see Section 5.5; Figure 5.6).

One tephra layer, LPA_63.33 (Group 3B; 43.4 cal ka BP) has a possible Lautaro/Viedma affinity based on comparisons to glass chemistry of proximal deposits from historical eruptions (Mayr et al., 2019). This possibly represents the first documentation of prehistoric Lautaro activity. Two tephra layers, LPA_52.79 and 55.93 (Group 4A; 34.2 and 35.6 cal ka BP, respectively) are also chemically similar to Lautaro/Viedma. However, these deposits of rhyolitic and rhyodacitic composition have a slightly lower silica and potassium abundance than the known Lautaro/Viedma compositional field for historical events (Section 5.2.1.4, Figures 5.2, 5.4, 5.5). The presence of olivine in LPA_52.79, lack of biotite in LPA_55.93, and the presence of accidental lithic clasts in both, typical of products associated with Mentolat volcanism (Weller et al., 2019), suggests that both layers could also possibly derive from eruptions of this volcano. We therefore tentatively attribute LPA_52.79 and LPA_55.93 to eruptions of either Lautaro/Viedma or Mentolat affinity, and require more proximal glass-shard chemical data from these centres to confirm their source.

Fifty-one deposits have a possible Reclus and/or NAVZ affinity (Group 3 and 4; Figure 5.4E-J; Supplementary File S.3.2). Most of these layers are reworked (41 = reworked; nine =

primary; one = likely reworked*;* Section 4.3). Of the nine primary tephra layers, one cannot be correlated to its source in the NAVZ (LPA_24.07), one is possibly correlated to Lautaro/Viedma (LPA_63.33), two are possibly correlated to Lautaro/Viedma or Mentolat (LPA_52.79 55.93), and five are correlated to Reclus (LPA_18.20 (=R_1), 21.07, 77.47, 77.61, 78.66). LPA_24.07 was deposited at 18.1 cal ka BP, and the potassium content has a large range of between 1.70 and 5.88 wt%, indicating that it could be from any centre in the NAVZ. LPA_33.13 is additionally considered to be a primary tephra; this unit has scarce chemical data associated with it and was therefore unable to be associate with a Group, but is likely of NAVZ affinity (Figure 5.3).

5.3.2. Temporal changes in volcanic activity

While there are some data on the frequency of eruptions in the CLD (e.g., Chaitén (Alloway et al., 2017), Villarrica and Llaima (Dzierma and Wehrmann, 2010), and Mocho-Choschuenco (Rawson et al., 2015)), relatively little is known about the frequency of eruptions from the Patagonia-Tierra del Fuego region, and particularly beyond the Holocene. This is predominantly due to a general lack of long-term records from this region.

Naranjo and Stern (1998) and Wastegård et al. (2013) report a lack of deposits from Hudson volcano in the early Holocene/Pleistocene, including proximally to the centre. However, Weller et al. (2014, 2015) identify Late Pleistocene and Early Holocene eruptions of Hudson, and Carel et al. (2011) noted an abundance of Hudson deposits through both the Pleistocene and the Holocene in a marine record located to the West of the volcano. Chemical analysis of tephra layers from Laguna Potrok Aike indicates that no Hudson tephra are preserved in the Lateglacial. The only primary Hudson tephra preserved in Laguna Potrok Aike is that of H_1 at 8.7 cal ka BP (Figure 5.5). The absence of primary Hudson tephra in the Laguna Potrok Aike sedimentary record possibly indicates that some of the eruptions identified by Weller et al. (2014) and Carel et al. (2011) were either smaller than H_1, and/or possibly that wind regime and intensity has changed through the Holocene, making Hudson deposition at Laguna Potrok Aike less likely (e.g., Saunders et al., 2018). The latter is plausible since another large and widespread Hudson

eruption, H_2 (4.00±0.05 cal ka BP) is not identified at Laguna Potrok Aike; H_2 had a more northeasterly dispersal than H_1 (Van Daele et al., 2016).

The greatest number of volcanic deposits in the Laguna Potrok Aike record are from Mt Burney (Figures 5.5, 5.8), indicating that it is one of the most active volcanic centres in the Late Quaternary. There are 13 primary tephra layers of Mt Burney affinity, and three of these are newly identified tephra layers (LPA_12.32, 12.51, 30.15, 38.70, 40.68, 54.19, 57.03, 67.94, 72.07, 94.20 94.33, 94.96, and 95.38). These tephras are deposited across the Quaternary, between 10.2 cal ka BP (LPA_12.32) and 72.1 ka BP (LPA_95.38). Gebhardt and Ohlendorf (2019) described the sediments between 93.34 and 95.44 m-cd as a debris flow deposit. Therefore, this section was excluded from age-modelling and the age determined across this part of the sedimentary sequence is the same (~72.1 ka BP). As such the ages of the tephra units identified within this section of the sedimentary sequence, LPA_94.20, 94.33, 94.96, and 95.38, are poorly constrained since they are intercalated within a debris flow. Based on factors mentioned in Section 2.3, these tephras are considered to be primary (Supplementary File S.3.2; see Section 5.5 for further information on reworking).

The longest interval without any recorded Mt Burney deposits (using average ages) is 12,740 years, between 52.6 ka (LPA_67.94) and 39.9 cal ka BP (LPA_57.03). The shortest interval is 200 years in the Holocene, between 10.2 cal ka BP (LPA_12.31) and 10.4 cal ka BP (LPA_12.51). Because Mt Burney is ~200 km from the site of Laguna Potrok Aike, it is most likely that the preserved tephra are from large, explosive events (i.e., Volcanic Explosivity Index (VEI) 5+; Newhall and Self, 1982). However, Mt Burney may well have experienced numerous smaller eruptions, which are less likely to travel sufficient distances to be preserved in the Laguna Potrok Aike sedimentary record. For example, four minor Holocene events from Mt Burney have been described by Kilian et al. (2003) and historical events have been described by Martinic (2008).

MB_1 (LPA_12.32; 10.0-10.4 cal ka BP) is preceded by a primary Mt Burney eruption only 200 years earlier, LPA_12.51 (Supplementary File S.3.2; Figure 5.3; 10.2-10.6 cal ka BP).

Both deposits are chemically comparable, but distinct enough to suggest they represent two different eruptive events. LPA_12.51 is only 0.2 cm thick, while LPA_12.32 is 1.5 cm thick. LPA_12.51 could correspond to the MBK1 or MBK2 (more likely) eruption described by Kilian et al. (2003; tephra sample names: CHK7/49-51, CHK7/15-17, respectively). Previously reported ages for MBK1 and MBK2 are >8.66±0.99 cal ka BP and >9.47±0.06 cal ka BP, respectively (Fontijn et al., 2014; Kilian et al., 2003). Similarly, Del Carlo et al. (2018) identified a 2.5 cm thick tephra (AR-1B) of Mt Burney affinity preceding the MB_1 unit by only 2 cm of peat deposition at Arroyo Robles (51°51'S; 70°25'W).

The 1.5 cm thick LPA_18.20 Reclus eruption, commonly known as R_1, is followed soon after by LPA_21.07. LPA_21.07 is a thin, 0.3 cm thick tephra deposited at 15.7 cal ka BP, which marks the first Reclus deposit after the LGM. There is a lack of identified Reclus affinity eruptions for 47.5 kyr until the identification of LPA_77.47, LPA_77.61 and LPA_78.66, which are considered to be primary units on the basis of factors outlined in Section 2.3 (Supplementary File S.3.2; See Section 5.5 for further information on reworking). It is likely that these three tephra layers were deposited relatively close to ~63.2 kyr, and that all represent very large eruptions, with LPA_78.66 being exceptionally large based on the tephra thickness (4, 8, ≥63 cm, respectively). Because much of the lithology has been classified as reworked beneath 76.50 m-cd, and is thus excluded from the age-model, it is difficult to determine the periodicity of Reclus volcanic eruptions from tephra deposits preserved in Laguna Potrok Aike (this particularly affects the determination of depositional ages for tephras from Reclus volcano identified in the lowermost sedimentary sequence). Given the thickness of the LPA_78.66 Reclus tephra in Laguna Potrok Aike (≥63 cm) at ~63.2 ka, it is likely that this unit is preserved in Antarctic and sub-Antarctic archives. The identification of this unit would be of great benefit to better understand the eruptive history of Reclus, and it could potentially allow age-transfer and the production of more robust chronologies in Antarctic and sub-Antarctic regions and thus further our understanding of Reclus event-history.

5.3.3. Reworking of tephra deposits

Sixty-five reworked and three likely reworked tephra layers were identified in the Laguna Potrok Aike record based on mineral componentry, glass-shard relative abundance, presence of organic and detrital material, and glass-shard morphology (Figure 5.7; Supplementary File S.3.2). As discussed, the tephra typically appears in the sequence as well-preserved, but after further inspection, is visibly reworked. In addition, there are often long periods of time and thick units of pelagic sedimentation between reworking events (Figures 5.6, 5.7). This strongly indicates that even visible layers that are seemingly well-preserved with distinct and sharp contacts can be reworked. If visible tephra layers can appear *in-situ* as pristine, but in fact are not, then this raises significant concerns regarding the analysis of cryptotephra (invisible ash layers) preserved in lithologies that appear to be undisturbed, for which the question of reworking is quite often overlooked. To overcome this issue in both visible and crypto-tephra studies, further respect should be given to the concept of tephra remobilisation, and detailed analysis should be undertaken on shard morphology and mineralogy, shard abundance and organic and detrital material through the entirety of the sequence.

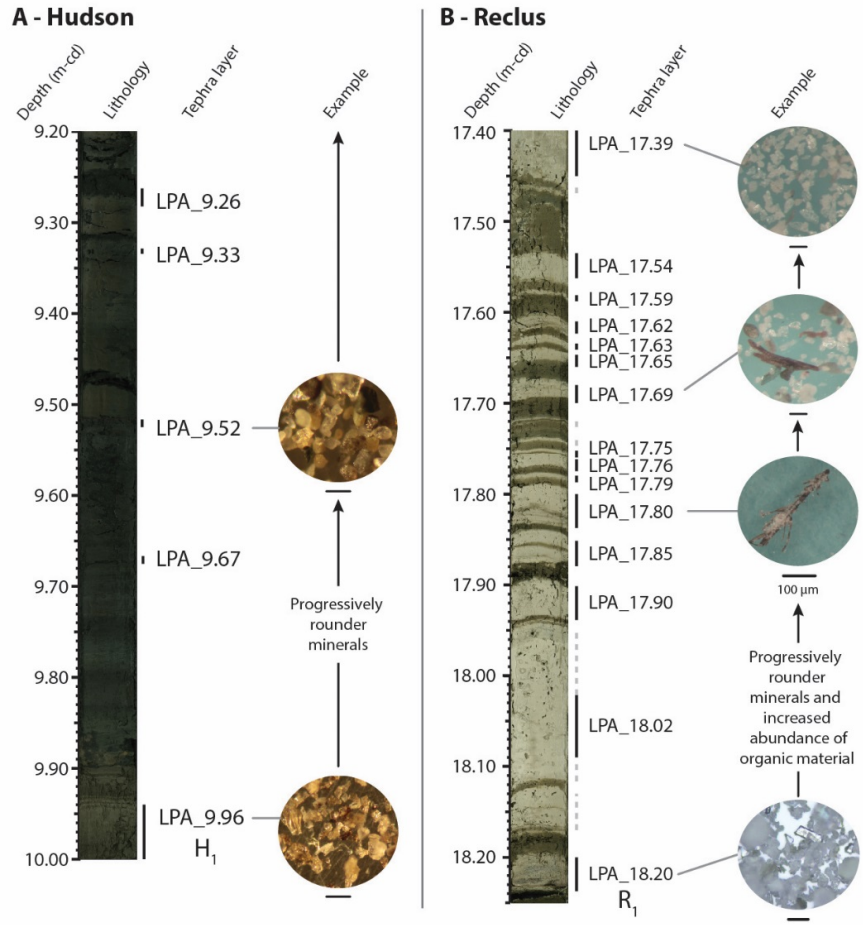


Figure 5.6. Illustration of reworked tephra deposits in the Laguna Potrok Aike sedimentary sequence. In both of these instances, an initial widespread tephra marker is succeeded by periods of pelagic sedimentation and further tephra layers. All tephra layers that are identified after the initial event have the same chemical composition as the first deposit, and analyses of the deposits indicate that these are reworked – notably by the increased appearance of rounded minerals, decreased abundance of glass-shards, and increased abundance of organic material. A) shows the H_1 (Hudson) event, and subsequent (up-core) identified tephra layers, all with Hudson compositions; B) shows the R_1 (Reclus) event, and subsequent (up-core) identified tephra layers, all with Reclus compositions. There are clear implications for the assumption that discrete visible tephra layers, or cryptotephra layers with a substantial amount of pelagic sediment between events, are the product of primary fallout. It is important to note that the sharp tephra boundaries observed in B) of the composite record are not seen in all core-sections.

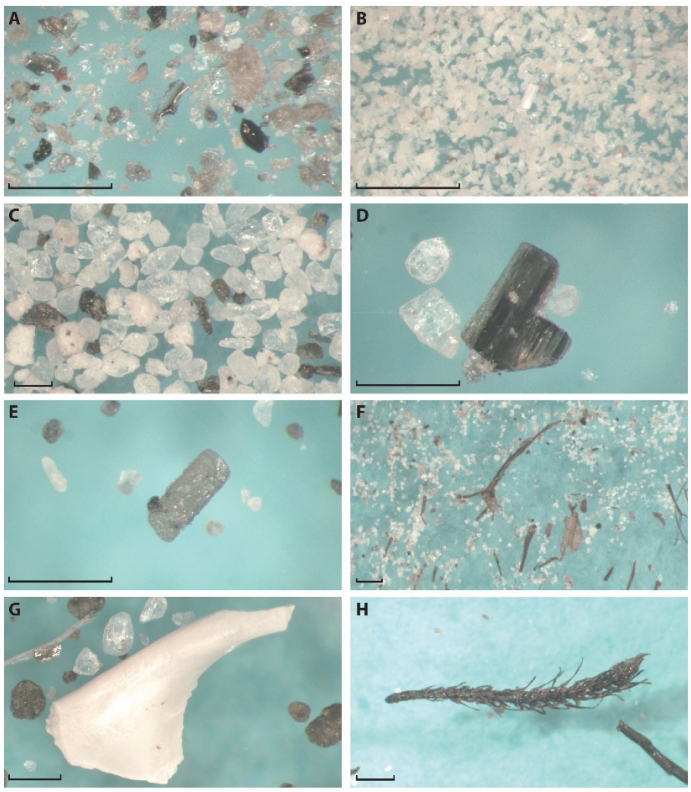


Figure 5.7. Images of volcaniclastic deposits illustrate diagnostic features of primary and reworked tephra. A-D represent distinguishing features of primary tephra deposits. E-H represent distinguishing features of reworked tephra deposits. A) Fluted and vesicular shards with minimal lithics or organics (LPA_9.90; Hudson volcano, H_1); B) High relative abundance (~95 %) of fluted glass shards (LPA_63.33; Lautaro/Viedma volcano); C) Low abundance of white grey pumice with high mineral abundance (~50 % relative abundance; LPA_12.32, Mt Burney; MB_1); D) Angular amphibole with clear 60° cleavage plane (LPA_12.32, Mt Burney; MB_1); E) sub-rounded orthopyroxene with some glass-coating and Fe-Ti oxide (left; LPA_4.17; Hudson volcano and Northern Austral Volcanic Zone (NAVZ) centres); F) high proportion of organic debris (15 % relative abundance of sample; LPA_16.04; Reclus volcano); G) gastropod shell fragment surrounded by rounded lithics and plagioclase (LPA_4.17; Hudson volcano and NAVZ centres); H) shoot of aquatic moss (sample is radiocarbon dated to 32.2 cal ka BP; LPA_47.86; insufficient chemical data to identify source). Scale bars (total lengths: 50 μm) are presented for individual photos in the bottom left corner.

In the case of Laguna Potrok Aike, reworked deposits are speculated to be caused predominantly by lake-basin slope instability, in addition to wind (aeolian reworking) and Quaternary lake level changes (Kliem et al., 2013b). Slope instability is possibly caused by sediment overburden on steep-sided slopes and can cause mass movement events such as debris flows or slides. Often material in debris flows is entirely disturbed (i.e., tephra unit and surrounding sediment is mixed). However, debris flows transport liquified matrix, as well as original sediment, and hence while the material in debris flows may be disturbed, slides are

additionally capable of preserving complete sections of the original sedimentary sequence. In some cases, this can include fully intact tephra units and the surrounding sedimentary matrix (e.g. Sauerbrey et al., 2013). This can therefore occasionally allow for identification of a primary tephra in a section of lithology that is classified as reworked (e.g., layers LPA_77.47, 77.61 and 78.66).

Debris flows become partially diluted during advancement. This allows sediment to be brought into suspension which in turn leads to lower density of the suspension, and the production of a turbid flow (i.e., turbidite) above the debris flow (Sauerbrey et al., 2013). Turbidites differ to debris flows as they typically deposit small-scale structures that are graded from coarse to fine, and are often overlain by a clay cap (Bouma, 1965). These clay caps often contain lightweight grains such as glass-shards and organic matter which are reworked from the initial slope destabilisation and movement. Turbidites, debris flows and slides are evidenced through the Laguna Potrok Aike sedimentary sequence (e.g., Kliem et al., 2013b). Similar sedimentary processes are observed in Lake El'gygytgyn, North-eastern Siberia (Juschus et al. 2009; cf. Sauerbrey et al., 2013). The presence of macrophytes, typically located at relatively shallow depth, in numerous samples demonstrates that tephra was moved rapidly to deeper parts of the lake, and is indicative of reworking produced by either sediment destabilisation or lake-level changes (e.g., Jouve et al., 2017).

Three Holocene tephra layers (LPA_11.71, 12.16, and 21.07) in the sequence are reworked but have no affiliated primary tephra unit. It is hypothesised that these tephra layers, and possibly others, were deposited by aeolian reworking. Here, we speculate that primary tephra was deposited away from the lake, and that these layers were resuspended via wind (notably the strong and dominating Southern Westerly Winds) very soon after or during deposition, resulting in (reworked) tephra layer formation in the Laguna Potrok Aike sedimentary sequence (e.g., Bertrand et al., 2014). This mechanism is particularly considered in the case of thin reworked units identified, and provides some explanation for the identification of rounded minerals and lack of glass-shard abundances in some layers.

The capability of already deposited tephra to be remobilised by wind was observed after the 1991 eruption of Hudson volcano (VEI 5), whereby strong winds caused ash to be remobilised and identified >1000 km from source, across Argentina and the western Atlantic Ocean (Wilson et al., 2011). Zanchetta et al. (2018) also documented aeolian redistribution of Lateglacial H_o tephra from Hudson volcano across Argentina, >400 km to the southeast of the main axis of the H_o tephra distribution. Fowler and Lopushinsky (1986) identified that even low wind speeds of 6-9 km h^{-1} (1.6-2.5 m s^{-1}) are capable of mobilising unconsolidated tephra; in the Pali Aike region, wind speeds are known to reach averages of 28.8 km h^{-1} (8 m s^{-1}; Ohlendorf et al. 2013), indicating the great potential for unconsolidated tephra to be remobilised by wind in the study region. Additionally, Monteath et al. (2019) has associated cryptotephra layers with heterogeneous chemistry from southern South America, identified in Hookers Point, Falkland Islands, as reworked by wind. They attributed temporal patterns of abundant reworked volcanic glass with changes in the position and/or strength of the Southern Westerly Winds (Monteath et al., 2019). Layers deposited by wind may provide scope to further understand the frequency of volcanic events, as well as dust influx from southernmost South America. However, owing to the high number of reworked layers in the Laguna Potrok Aike sedimentary record, reworked layers have been excluded from frequency analysis.

Reworked tephra layers are finally also thought to possibly result from lake-level changes which caused tephra mobilisation and erosion (e.g., Jouve et al., 2017). During the Holocene, South America experienced variable climatic conditions (e.g., Markgraf et al., 2003) which may have contributed to lake level changes, and certainly, Holocene palaeoshorelines have been identified for Laguna Potrok Aike (Haberzettl et al., 2007; Anselmetti et al., 2009; Kliem et al, 2013a). It is thus hypothesised that changes in lake levels are a suitable explanation for the repetitive reworking of tephra deposits between 8.7 cal ka BP and the present day. During the Lateglacial, lake level at Laguna Potrok Aike is thought to have been relatively stable (e.g., Haberzettl et al., 2007; Anselmetti et al., 2009; Zolitschka et al, 2013); the identification of

numerous reworked layers during this time period therefore indicates that other reworking processes (i.e., wind, lake basin instability) are more dominant at this time.

5.3.4. Changes in eruptive activity in relation to climate

There are limited records of long-term climate change in southern South America because of the advance and retreat of the Patagonian Ice Sheet (e.g., Fontijn et al., 2014). As such, Antarctic ice cores are thought to proffer the most representative record of climate change for the study region beyond the Lateglacial. The volcanic record from Laguna Potrok Aike is analysed with respect to climatological data derived from ice cores to determine if any relationship exists between volcanic activity and ice-unloading (Figure 5.8). This relationship has been discussed in Watt et al. (2013a) and Rawson et al. (2016) but in these studies only the Holocene is accounted for.

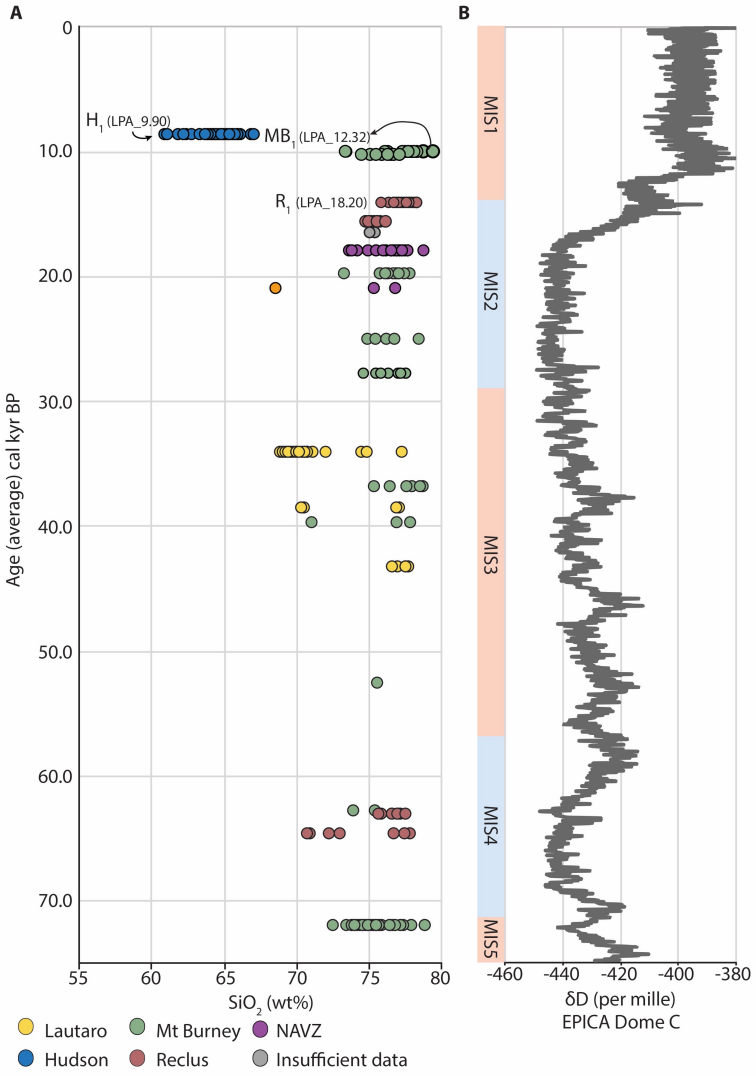


Figure 5.8. Plenary diagram for temporal changes in tephra chemistry. A) Tephra chemistry for primary (solid circles with black outline) deposits in the lake sequence – colours relate to the source of the deposit; See Supplementary File S.3.2 for further information; B) Deuterium (δD) data from Antarctic ice core Epica Dome C after Jouzel (2004). Marine Isotope Stages (MIS) are marked and reflect stadial/glacial (even numbers) and interstadial/interglacial (odd numbers) conditions (after Lisiecki and Raymo et al., 2005).

Ice sheets were particularly thick and extensive during MIS 4 (71-57 ka BP; Lisiecki and Raymo, 2005) in southern South America (Clapperton, 1994; Kaplan et al., 2008), and between ~65 and 43 ka BP (MIS3/MIS4), there was a decline in insolation at 40°S (Van Meerbeeck et al., 2009). This period coincides with a decline in eruptive activity recorded for Laguna Potrok Aike; between 62.9 and 43.4 cal ka BP (LPA_72.07 and 63.33, respectively) only one eruptive deposit is identified (LPA_67.94; Figure 5.8).

It is possible that the lack of volcanic deposits identified between 62.9 and 43.4 cal ka BP is a consequence of ice-overburden on volcanic centres, and that the effect of this ice-overburden inhibited eruptive activity (e.g., Jellinek et al., 2004; Watt et al., 2013a; Rawson et al., 2016). Alternatively, the lack of identified volcanic deposits in the lake during this time may reflect a lack of preserved (visible) deposits rather than a decline in overall volcanic activity, which may be caused for example, by different dominant wind directions. It is, however, difficult to speculate with no other long term records of such high resolution.

5.4. Conclusions

This detailed investigation of tephra preserved in the Laguna Potrok Aike sedimentary record provides the fullest account to date of eruptive activity in southern South America over the last 80 kyr.

- Correlations to source volcanoes are based on a newly established database of glass-geochemistry from proximal deposits of regionally distributed eruptions: A_1, R_1, MB_1, MB_2, H_1, and H_2, in addition to the tephra chemistry of widespread deposits described in Del Carlo et al. (2018) and Mayr et al. (2019). Three previously known regional marker horizons are now better chemically and chronologically characterised: H_1 (Hudson), identified in the PASADO record for the first time, has a depositional age of 9.0-8.6 cal ka BP; MB_1 has a depositional age of 10.4-10.0 cal ka BP, and R_1 has a depositional age of ~14.5-14.1 cal ka BP.
- We have built on previous tephra studies by Kliem et al. (2013b) and Wastegård et al. (2013). From this research we have identified nine new primary tephra layers. The chemical affinity of all layers from the Laguna Potrok Aike sedimentary record is presented for the first time.
- There are 94 visible tephra units preserved in the sedimentary sequence of Laguna Potrok Aike. Twenty-five of these have been emplaced by primary fallout, but 65

are reworked, three are likely reworked, and insufficient information is available for one layer. These reworked layers appear primary but have characteristic features of reworking based on microscopic and geochemical analysis. This strongly indicates that even well-preserved visible tephra in sedimentary archives may not be primary. As such, special care must be taken in the analysis of both visible, and (especially) invisible (crypto-) tephra layers to decipher their emplacement mechanisms; this includes visual inspection of the glass, and their chemical composition. In the case of invisible tephra in sediments which appear undisturbed, this should include a thorough study of changing shard morphological properties throughout the sequence to determine background changes from true eruptive events (e.g., McLean et al., 2018). The relocation of a widespread marker horizon in a sequence with numerous, very obvious visible tephra layers (Figures 5.6, 5.7) demonstrates that reworking of tephra is undoubtedly more prevalent in (at least) lacustrine records than currently appreciated. Further work should include the development of a standardised framework of glass-shard inspection for reworked deposits in different environments.

- There is a period of very low eruptive activity in the region recorded between 62.9 and 43.4 cal ka BP. At present it cannot be established whether this period reflects reduced eruptive activity or reduced preservation. As such, it is difficult to determine whether there is a relationship between climate and volcanism in this study region with only a single record.
- Further work should involve renewed efforts, using internationally recognised methods of tephra identification and analysis, to fingerprint these widespread marker horizons in extra-Andean records, including Antarctic ice-cores which are excellent archives of tephra on long time-scales. Such work would further inform on the scale of southern South American eruptive activity beyond the Lateglacial.

Chapter 6

Distal cryptotephra from southern South America in the Falkland Islands

Abstract

This chapter describes the chemical composition of cryptotephra isochrons and glass-shards identified in three peat sequences from the Falkland Islands (Islas Malvinas) which have limited chronological control: Poncho Hill Pass (51°36'S; 59°49'W), Stanley Common (51°42'S; 57°49'W) and Fox Bay (51°36'S; 59°49'W), and attempts to deduce the source affinity of the ash deposits. The chemical composition of cryptotephra samples confirms that the ash from Chilean volcanic events travel significant distances of ≥1,280 km via the dominant westerly wind regime, and are preserved as discrete layers in sedimentary environments. The R_1 (~14.30 cal kyr BP; Smith et al., 2019), H_1, and H_2 (~7.75 and 3.92 cal kyr BP, respectively; Weller et al., 2014) marker horizons from Reclus and Hudson volcanoes, respectively, were identified in the peat sequences. This is the first record of pre-historical Hudson ash in the Falkland Islands. In addition, the compositional fingerprinting of glass-shards have identified combinations of chemistries at the same location, including Aguilera (likely A_1) and Hudson volcano (H_2) which have depositional ages of ~3.20 cal kyr BP (Stern, 2008) and ~3.92 cal kyr BP (Weller et al., 2014), respectively, as well as Mt Burney (likely MB_2) and Hudson (H_2), which have depositional ages of ~3.82 (Stern, 2008) and ~3.92 cal kyr BP (Weller et al., 2014), respectively. These glass-shards are thought to be reworked, or reflective of events that were deposited closely in time (~hundreds of years) but they could also represent the first identification of a wider spread of H_1 chemistry than reported thus far. Three other samples of glass-shards were analysed and considered likely to be reworked based on their chemical heterogeneity and shard morphology. Potential mechanisms of reworking include the post-depositional movement of glass-shards through the porous peat microstructure, mass movement in the region, and wind-blown remobilisation.

6.1. Introduction

The identification and chemical correlation of widespread tephra layers in multiple records allows a more comprehensive understanding of the dispersal patterns of volcanic ash, but additionally facilitates the transfer of absolute ages across different records, and subsequently permits the ability to constrain the age/s of the event/s through Bayesian age modelling (Chapter 1; e.g., Bronk Ramsey et al., 2015; Fontijn et al., 2016). For example, Fontijn et al. (2016) established a regional-scale tephrochronology for the Chilean Lake District by chemically fingerprinting and correlating widespread tephra layers, and subsequently constraining the ages of these large explosive events. Such work may enable investigations into the timing of eruptive events (e.g., Rawson et al., 2016), and additionally allow for the analysis of spatio-temporal variability in past climate change (e.g., Lane et al., 2013). Expanding the existing regional-scale tephrochronology (Fontijn et al., 2016) into the lowermost Southern/Austral Volcanic Zone (SVZ/AVZ), and beyond, broadens the scope of such research.

The analysis of glass-shard abundance through a sedimentary sequence can provide insights into taphonomic, sedimentary, and geomorphological processes. When analysing sequential glass-shard abundance, cryptotephra that are entirely from primary fallout are typically marked by a discrete horizon of increased concentrations of glass-shards, indicative of rapid ash input, and surrounded by lower concentrations of background tephra (Figure 6.1A). However, when bioturbation, inwash, or migration of shards through a profile has occurred, smaller occurrences of the discrete horizon can move up/down the sequence (Figure 6.1B). Occasionally, records do not preserve well-defined glass-shard isochrons (e.g., Payne and Gehrels, 2010), and glass-shards are scattered down the profile (Figure 6.1C, D). Profiles such as Figure 6.1B/C/D can be caused by inlets (Pyne-O'Donnell, 2011), flood events (McLean et al., 2018) or perennial snow-beds trapping tephra, and subsequently melting at a later time (Davies et al., 2007). The glass-shard distribution profile has additionally been found to be different across a single lake basin in a tephra study of three lakes in the Scottish Inner Hebrides which investigated multiple lacustrine cores obtained from the same lake (Pyne-O'Donnell, 2011). Multiple cores from single sites or regions are therefore recommended in tephrostratigraphic studies by Boygle (1999) and

Pyne-O'Donnell (2011) but this is typically not feasible, and in which case bathymetric and seismic surveys can be used to detect optimal coring locations in sedimentary sequences (e.g., Moernaut et al., 2007, 2014).

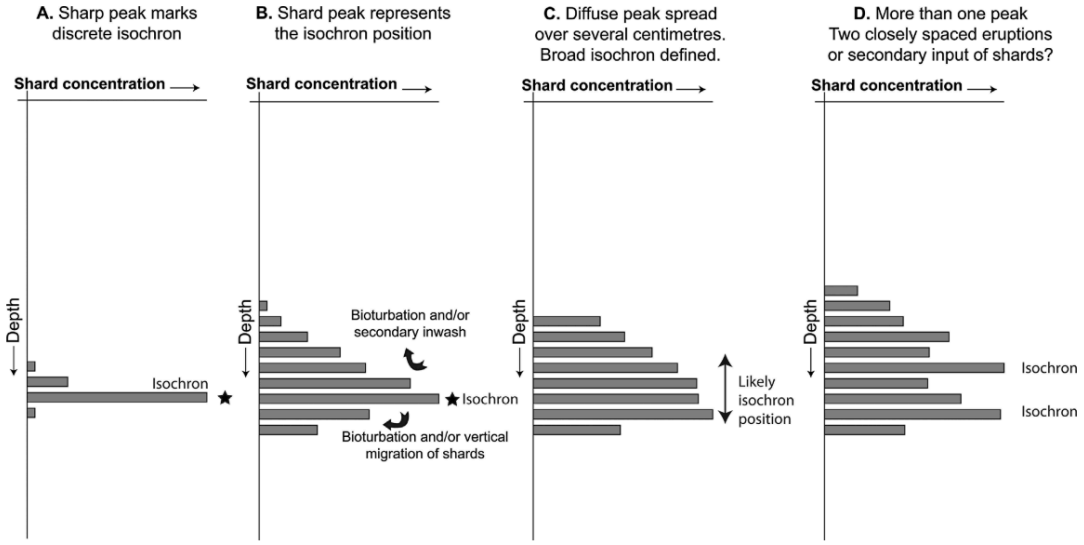


Figure 6.1. Schematic illustration of common shard distribution profiles that can be observed in cryptotephra deposits. Star represents likely primary ashfall. Source: Davies, 2015.

Peat profiles are generally excellent archives of environmental change and much like lacustrine sequences, preserve volcanic ash well (e.g., Langdon and Barber, 2004; Blundell et al., 2008; Langdon et al., 2012; Watson et al., 2016). However, taphonomic issues have been reported in them particularly because the microscopic structure can be porous and thus facilitate post-depositional movement through the sequence. An extreme example of this includes the observation of vertical movement of ash *c*. 220 cm from its primary origin in the Tenaghi Philippon peat record (Wulf et al., 2018). Typically though, ash mobility is not this extreme and in long records with high resolution cryptotephra analysis, unnoticeable. In a cryptotephra study on the taphonomy of volcanic ash in peatlands, Payne et al. (2005) identified that the majority of glass-shards from major events were retained in the top 1 cm of peat, but a small amount remobilised up to 6 cm depth; at a different site, Payne and Gehrels (2010) found a larger remobilisation distance of glass-shards of up to 15 cm through peat, and additionally identified both upward and downward movement of the glass-shards. The degree of movement is invariably

dependent on, or affected by, the accumulation rate of peat (the depth of glass-shard penetration being reduced as accumulation increases), the density and porosity of the peat, plant growth (Payne et al., 2005; Payne and Gehrels, 2010; Watson et al., 2015), and coring artefacts.

There are few Quaternary cryptotephra deposits from southern South America that have been identified in extra-Andean locations, notwithstanding the confirmed chemical correlations of Alpehue from Solipulli volcano (SVZ, Chile) in the South Georgia Islands (Oppedal et al., 2018), and MB_1 from Mt Burney, and R_1 from Reclus volcano (both: AVZ, Chile) in the Falkland Islands (Monteath et al., 2019). This is despite the fact that the region upwind is dominated by frequent and explosive volcanism, and there is also a dominant, strong westerly wind regime which makes it likely that discrete ash marker horizons from Andean volcanoes are preserved in distal locations such as the Falkland Islands and Antarctica (Chapter 1). The potential for widespread tephra dispersal from volcanoes along the Andes is demonstrated by historical events such as the 2011 eruption of Puyehue-Cordón Caulle. Ash from this event caused widespread disruption to air traffic in Australia and New Zealand, located ~7,500 km from source (Klüser et al., 2012), and has been identified on the Western Antarctic Ice Sheet ~4,600 km distance from the volcano (Koffman et al., 2017). The August 1991 eruption of Hudson volcano, ~1100 km distance from the Falkland Islands, additionally caused irritancies to people and livestock on the Islands (Holmes et al., 1999).

Cryptotephra from three vertical peat columns in the Falkland Islands, Poncho Hill Pass (51°36'S; 59°49'W), Stanley Common (51°42'S; 57°49'W) and Fox Bay (51°36'S; 59°49'W, were initially investigated by Hall et al. (2001) and Holmes et al. (1999; Section 1.6.3; Figure 1.15). Here, we reinvestigate extracted glass-shards from these sites, utilising all tephra samples that were prepared and able to be obtained, including background glass-shards and peaks (isochrons) with an overarching aim to determine what tephra are travelling long distances, and how these are preserved in extra-Andean sites (Section 2.2.1.3). Since these sequences currently have poor chronological control, these records cannot be used to enhance the regional tephrochronology presently, however, identifying isochrons would prove useful for further work in the region.

6.1.1. Site Background

While there is no published lithostratigraphy of the peat columns at the three sites, glass-shard distribution profiles have been established (Holmes et al., 1999; Hall et al., 200; Figure 6.2). Hall et al. (2001) linked the distribution of glass-shards in the profiles to the preservation potential of peat rather than changes in the frequency or source of volcanic activity (Hall et al., 2001; Figure 6.2). However, based on the distribution profiles (Figure 6.2), it is more likely that the profiles reflect the site-specific taphonomy of tephra in peat records, and the ability of shards to move through the profile (e.g., Payne and Gehrels, 2010; Davies, 2015; Figure 6.1).

The background glass-shard concentration at each site was different (Figure 6.2). Poncho Hill Pass has a low background concentration of ~5 % (relative abundance; Figure 6.2), and well-defined peaks at 82, 27, and 19 cm depth. Based on the analysis of glass-shard abundance (Figure 6.2; Holmes et al., 1999; Hall et al., 2001), it is likely that some increased concentrations around 20 cm depth in Poncho Hill Pass are derived from reworked tephra (e.g., Davies, 2015; Figure 6.1C; 6.2A). Stanley Common had a high glass-shard concentration throughout the entire sequence (~50 %; Figure 6.2B) which is indicative of continuous inputs of tephra and thus reworking; typically, such cryptotephra profiles would not be analysed in any detail beyond this. In contrast, Fox Bay had a low background glass-shard concentration (~10 %), with well-defined peaks in cryptotephra concentration at only two depths of the sequence (25-35 and 60-65 cm; ~50 %; Figure 6.2C). Samples were prepared for chemical analysis by Hall et al. (2001) and Holmes et al. (1999), and this was likely done in order to determine whether glass-shards present in background sediment were reworking of an isochron, or evidence of very low-concentration cryptic tephra being deposited over the islands (Section 2.2.1.3).

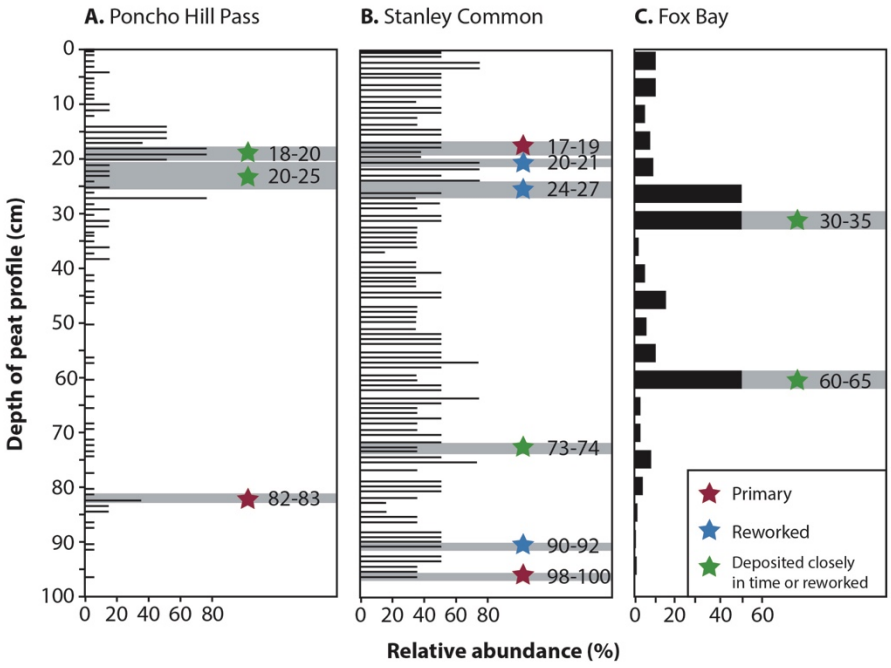


Figure 6.2. Distribution of volcanic glass-shards in the three peat bog localities: A) Poncho Hill Pass, B) Stanley Common, and C) Fox Bay. Shaded lines are points chemically analysed; stars represent samples that were chemically analysed in this study; numbers next to stars represent depth that the sample covers in centimetres. Cryptotephra at 30-35 and 60-65 cm in Fox Bay were previously chemically analysed by Hall et al. (2001). After: Hall et al. (2001); Holmes et al. (1999).

In Holmes et al. (1999) and Hall et al. (2001), the major element glass chemistry of two layers in Fox Bay (30-35 and 60-65 cm) were determined and compared with chemical analyses from the 1991 eruption of Hudson volcano. While tephra from Fox Bay at 30-35 and 60-65 cm did not correlate to the 1991 Hudson volcanic event, Hall et al. (2001) argued that the deposits were likely of Andean affinity since thick and visible units are prevalent in Chile and Argentina, while none are present in the Falkland Islands. They stated that further chemical analyses on proximal volcanic deposits was required to produce robust tephra correlations. Now there are data in recent publications (e.g., Stern, 2008; Weller et al., 2015; Fontijn et al., 2016; Del Carlo et al., 2018; Mayr et al., 2019; Smith et al., 2019) and within this thesis that provide sufficient chemical data of numerous Andean volcanic sources to permit correlations (e.g., Hudson, Aguilera, Lautaro/Viedma and Reclus volcano, and Mt Burney).

6.1.2. Chronological constraints

The chronology for the peat deposits studied by Holmes et al. (1999) and Hall et al. (2001) was not previously determined, although they reasonably assumed that the base of the deposits represent the onset of Holocene warming at ~15 cal kyr BP, and that the top represents the modern day (i.e., ~0 cal yr BP). The identification and correlation of known widespread tephra layers that have been dated in other locations may better inform on the chronology of these peat deposits.

6.2. Results and interpretation

6.2.1. Geochemical results and interpretation

As per Section 2.2.1.3, chemical analysis was undertaken on cryptotephra deposits from three sites in the Falkland Islands (Figure 6.2). The analysis was undertaken on pre-prepared glass-slides of volcanic ash, and in some instances this included background concentrations of glass-shards, while in others it included peaked concentrations. In this section, the morphological and chemical characteristics (Figure 6.3), including possible affiliation, are described. The discussion section details the hypothesised depositional nature of samples analysed in detail.

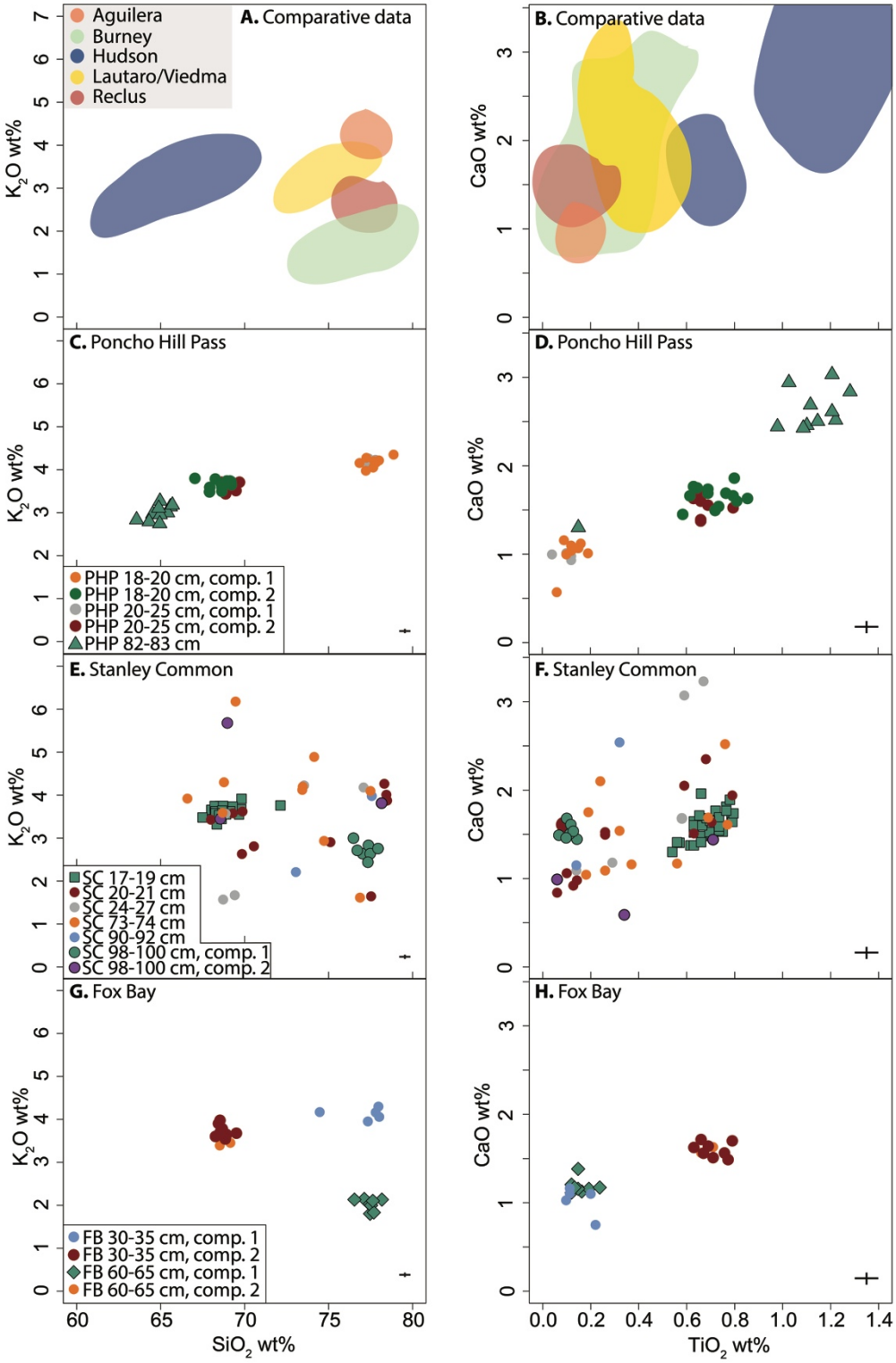


Figure 6.3. A-B) Chemical fields for Andean volcanic centres are based on chemical data from proximal deposits as per Chapter 5, Figure 5.4; Smith et al. (2019), and include: H_1, H_2, A_1, R_1, $R_{2\text{-}3}$, Lautaro/Viedma$_{historical}$, MB_1, MB_2, MB_x, MB_{1910}). Tephra chemistry of glass-shards in the three Falkland Island peat sites: C-D) Poncho Hill Pass (PHP), E-F) Stanley Common (SC), and G-H) Fox Bay (FB). Primary tephra deposits are represented by solid symbols with black outline. Error bars (bottom right) represent 2 standard deviations of repeat analysis of the StHs6/80-G MPI-DING reference glass.

6.2.1.1. Poncho Hill Pass

Two cryptotephra deposits with peaked concentrations in Poncho Hill Pass were chemically investigated at 18-20 and 82-83 cm depth (Table 6.1; Figures 6.2, 6.3). One analysis was undertaken on background concentrations of cryptotephra at 20-25 cm depth.

Table 6.1. Geochemical data for cryptotephra deposits identified in Poncho Hill Pass. Peak/Background shard concentrations of samples is specified. Total refers to analytical total.

Tephra label		SiO_2	TiO_2	Al_2O_3	FeO_t	MnO	MgO	CaO	Na_2O	K_2O	P_2O_5	Cl	Total
Poncho Hill Pass, 18-20 cm, Component One, peak													
Aguilera - reworked or deposited closely in time													
	Avg	77.74	0.12	12.33	0.87	0.03	0.15	1.01	3.36	4.17	0.03	0.19	95.23
n=9	stdev	0.38	0.04	0.10	0.09	0.04	0.04	0.17	0.21	0.07	0.02	0.02	1.97
Poncho Hill Pass, 18-20 cm, Component Two, peak													
Hudson (H_2) - reworked or deposited closely in time													
	Avg	68.47	0.72	15.54	2.85	0.11	0.64	1.64	6.09	3.65	0.11	0.18	98.81
n=13	Stdev	0.41	0.06	0.16	0.18	0.05	0.04	0.09	0.47	0.07	0.04	0.02	1.34
Poncho Hill Pass, 20-25 cm, Component One, background material													
Aguilera - reworked or deposited closely in time													
	Avg	77.58	0.10	12.40	0.91	0.03	0.15	0.99	3.42	4.20	0.02	0.20	97.45
n=3	Stdev	0.17	0.04	0.17	0.02	0.03	0.03	0.02	0.12	0.03	0.02	0.02	0.66
Poncho Hill Pass, 20-25 cm, Component Two, background material													
Hudson (H_2) - reworked or deposited closely in time													
	Avg	68.85	0.69	15.62	2.89	0.11	0.61	1.55	5.77	3.61	0.12	0.17	98.31
n=7	Stdev	0.27	0.04	0.30	0.19	0.04	0.03	0.08	0.17	0.08	0.03	0.02	1.98
Poncho Hill Pass, 82-83 cm, peak													
Hudson volcano (H_1) - primary													
	avg	64.80	1.14	16.28	4.39	0.15	1.25	2.65	5.75	2.95	0.27	0.15	99.08
n=10	stdev	0.42	0.07	0.21	0.38	0.04	0.11	0.20	0.48	0.25	0.09	0.04	0.99

6.2.1.1.1. 18-20 cm

The cryptotephra zone identified between 18 and 20 cm depth were up to 60 μm in size and had fluted, cuspate and vesicular morphologies; vesicles were predominantly elongate. Chemical analysis of the shards indicates that there are two components. Component One is rhyolitic and has an average SiO_2 and K_2O content between 77.74 and 4.17 wt%, respectively

(Table 6.1; Figure 6.3). Chemically, this unit corresponds well with Aguilera volcano. Based on our understanding of past large, explosive events, this unit would most likely represent the widespread A_1 event since this is the only recorded large event from Aguilera during the Holocene. Component Two is trachydacitic and has an average SiO_2 and K_2O content of 68.47 and 3.65 wt%, respectively (Table 6.1; Figure 6.3). Chemically, this unit corresponds well with Hudson volcano, and notably the widespread H_2 marker horizon.

6.2.1.1.2. 20-25 cm

Between 20 and 25 cm depth, the background tephra was investigated. In this sample, glass shards have a mixed morphology, and are platy, as well as vesicular (~5 % abundance each) and fluted (~90 % abundance). The glass-shards in this sediment are chemically similar to Poncho Hill Pass 18-20 cm, and there are two compositions identified. The composition of Component One is rhyolitic and deposits have an average SiO_2 and K_2O content of 77.58 and 4.20 wt%, respectively. Deposits from Component One correlate well with Aguilera volcano (likely A_1). Component Two is trachydacitic and deposits have an average SiO_2 and K_2O content of 68.85 and 3.61 wt%, respectively (Table 6.1; Figure 6.3). Component Two deposits correspond well with Hudson volcano (likely H_2).

6.2.1.1.3. 82-83 cm

Colourless glass-shards between 5 and 10 μm are identified at Poncho Hill Pass between 82 and 83 cm depth. These are fluted with mostly circular vesicles. The deposit is trachydacitic, and shards have an average K_2O and SiO_2 content of 2.95 wt% and 64.80 wt%, respectively. The average TiO_2 content of the sample is 1.14 wt% (Table 6.1; Figure 6.3). Overall, this homogeneous unit corresponds well to Hudson compositions, and notably to the widespread marker horizon, H_1, which was deposited ~7.75 cal ka BP (Weller et al., 2014).

6.2.1.2. Stanley Common

There are two cryptotephra deposits with peaked concentrations in Stanley Common that were geochemically investigated at 20-21 and 90-92 cm depth. Background cryptotephra was analysed in four sections of the sequence, at 17-19, 24-27, 73-74, and 98-100 cm depth (Figure 6.3).

Table 6.2. Geochemical data for cryptotephra deposits identified in Stanley Common. Peak/Background concentration of tephra is specified. Maximum and minimum values are shown instead of averages and standard deviations in the case of deposits which have a wide range of chemical values and cannot be divided into different components. Only normalised data is presented for the Stanley Common 90-92 cm sample as only two shards were analysed. Total refers to analytical total.

Tephra label		SiO_2	TiO_2	Al_2O_3	FeO_t	MnO	MgO	CaO	Na_2O	K_2O	P_2O_5	Cl	Total
Stanley Common, 17-19 cm, background material													
Hudson volcano (H_2) - primary													
	avg	68.82	0.69	15.72	2.82	0.10	0.63	1.61	5.68	3.64	0.11	0.18	98.20
n= 33	stdev	0.75	0.07	0.18	0.20	0.04	0.07	0.15	0.62	0.11	0.03	0.03	1.83
Stanley Common, 20-21 cm, peak													
Unknown source; numerous compositions - reworked													
	max	78.30	0.79	15.71	3.92	0.17	0.75	2.35	5.82	4.20	0.15	0.23	100.54
n= 12	min	67.99	0.06	12.09	0.88	0.00	0.01	0.84	2.87	1.64	0.00	0.17	93.27
Stanley Common, 24-27 cm, background material													
Unknown source; numerous compositions - reworked													
	max	77.08	0.67	15.57	3.28	0.14	0.92	3.23	5.94	4.21	0.15	0.36	97.49
n= 5	min	68.72	0.14	12.32	1.03	0.05	0.19	1.09	3.65	1.57	0.02	0.13	92.10
Stanley Common, 73-74, background material													
Numerous compositions - reworked or deposited closely in time													
	max	77.64	0.77	15.72	3.89	0.14	0.97	2.52	5.66	6.18	0.21	0.26	99.05
n= 11	min	66.59	0.18	12.46	0.85	0.00	0.14	0.96	2.71	1.62	0.02	0.13	93.12
Stanley Common, 90-92 cm, peak													
Unknown source - reworked													
	Anal. 1	77.57	0.14	12.43	1.08	0.07	0.15	1.15	3.16	3.98	0.05	0.21	93.80
n= 2	Anal. 2	73.05	0.32	14.29	2.13	0.13	0.59	2.54	4.48	2.21	0.08	0.19	101.06
Stanley Common, 98-100 cm, Component One, background material													
Reclus volcano (R_1) – likely primary													
	avg	77.20	0.11	12.93	1.11	0.04	0.21	1.53	3.99	2.75	0.03	0.21	94.92
n=7	stdev	0.45	0.02	0.17	0.08	0.05	0.02	0.08	0.41	0.17	0.03	0.04	1.82
Stanley Common, 98-100 cm, Component Two, background material													
Numerous compositions - reworked													
	max	78.09	0.71	15.15	3.23	0.21	0.53	1.44	6.43	5.68	0.14	0.49	93.46
n=3	min	68.55	0.06	12.45	0.77	0.00	0.11	0.59	3.50	3.45	0.02	0.17	92.24

6.2.1.2.1. 17-19 cm

The glass-shards from background material between 17 and 19 cm are vesicular and not well sorted: they vary in size from 10 to 100 μm and there is no noticeable clustering of specific sized glass-shards. The shards typically have a fluted or vesicular (circular) morphology. The glass-shards in this section of sediment are trachydacitic to rhyolitic in composition. Shards have an average K_2O and SiO_2 content of 3.64 wt%, and 68.82 wt%, respectively. The average TiO_2 content of the sample is 0.69 wt% (Table 6.2; Figure 6.3). Despite this section of sediment having a relatively low glass-shard abundance (~50 %; Figure 6.2), the composition of this unit is distinct and corresponds well to that of tephra from Hudson volcano, and notably the widespread marker horizon, H_2 which was deposited ~3.92 cal kyr BP (Weller et al., 2014).

6.2.1.2.2. 20-21 cm

This mineral-rich sample has a high concentration of glass-shards (~80 %), and colourless shards are up to 100 μm in size. Approximately 70 % of the glass-shards are fluted, but some have circular vesicles. This deposit is compositionally heterogeneous. The composition of K_2O in glass-shards from 20-21 cm range from 1.64 to 4.20 wt%, while the composition of SiO_2 in glass-shards from this depth range from 67.99 to 78.30 wt% (Table 6.2; Figure 6.3). The deposit is broadly affiliated with tephra from numerous Andean sources (including: Hudson (H_2), Aguilera and Lautaro volcano, and Mt Burney), and cannot be firmly correlated to any single source or event. It is thus clear that tephra from these sources are making it to the islands (distances of 1,280 km) but it is not possible to determine whether the heterogeneity is a consequence of taphonomy (i.e., reworking), or sedimentation rate (i.e., resolution).

6.2.1.2.3. 24-27 cm

Glass-shards in this section of sediment have elongated vesicles and are mostly ~5 μm in size. The background tephra is rhyolitic and has a wide compositional range. The K_2O content of glass shards has a range from 1.57 to 4.21 wt %, while the SiO_2 content ranges from 68.72 to 77.08 wt% (Table 6.2; Figure 6.3). The glass shards in this sample cannot be correlated to any

volcanic centre or event and are considered to be reworked background material. These layers could come from volcanic sources that have not yet been characterised accurately, including deposits identified on sub-Antarctic islands which share similar chemistry (e.g., Narcisi et al., 2005; Del Carlo et al., 2018).

6.2.1.2.4. 73-74 cm

There is a low abundance of glass-shards in this section of sediment and they are considered to be background material (~40 %; Figure 6.2). The glass-shards are rhyolitic and are predominantly fluted, or have circular vesicles. The composition of this deposit is heterogeneous, and is indicative of numerous sources, including Hudson volcano (H_2), Aguilera and an unknown source (Figure 6.3). The range of SiO_2 and K_2O observed is 66.59-77.64 wt%, and 1.62-6.18 wt%, respectively (Table 6.2). It is likely that these glass-shards are reworked from cryptic layers elsewhere in the core.

6.2.1.2.5. 90-92 cm

The rhyolitic tephra in this sample with peaked concentration (~50%) is both fluted and vesicular (circular vesicles). The SiO_2 content ranges from 73.05 to 77.57 wt%, and the K_2O content ranges from 2.21 to 3.98 wt% (Table 6.2; Figure 6.3). Only two chemical analyses were viable on the glass-shards of this deposit, and thus the dataset is not extensive; as yet the dataset is uncorrelatable, however, based on the chemical data obtained the deposit may have multiple sources.

6.2.1.2.6. 98-100 cm

The glass-shards in this sample, which are considered to be background material (~40 % relative abundance), are predominantly vesicular (elongate). Chemical analyses indicates that there are two components. Seventy percent of the analyses show a homogeneous composition with an average SiO_2 and K_2O content of 77.20 wt% and 2.75 wt%, respectively, and this is

referred to as Component One (Table 6.2; Figure 6.3). This is consistent with a Reclus origin, indicative that this is likely the R_1 tephra layer. It is hypothesised that this layer is primary in origin, but this layer could possibly be reworked, with the true isochron originating from below the sequence being analysed. The remaining 30 % of the analyses has heterogeneous chemistry with SiO_2 values ranging from 78.09 to 68.55 wt%, and K_2O values ranging from 3.45 to 5.68 wt%, and is referred to as Component Two (Table 6.2; Figure 6.3). These chemistries are consistent with Aguilera, Hudson and unknown volcanic compositions; these unknown compositions could come from sub-Antarctic centres (e.g., Narcisi et al., 2005; Del Carlo et al., 2018).

6.2.1.3. Fox Bay

Two peaks in shard concentrations at two positions within the Fox Bay peat core were chemically investigated (Table 6.3; Figure 6.3). These deposits were located at 30-35 cm and 60-65 cm depth.

Table 6.3. Geochemical data for cryptotephra deposits identified in Fox Bay. Peak/Background concentration of tephra is specified. Individual (normalised) data points are presented for Fox Bay 60-65 cm Component Two as only two shards were analysed. Total refers to analytical total.

Tephra label		SiO_2	TiO_2	Al_2O_3	FeO_t	MnO	MgO	CaO	Na_2O	K_2O	P_2O_5	Cl	Total
Fox Bay, 30-35 cm – Component One, peak													
Aguilera - reworked or deposited closely in time													
	avg	77.09	0.15	12.74	0.85	0.01	0.16	1.03	3.61	4.13	0.04	0.19	95.64
n=5	stdev	1.47	0.06	0.82	0.07	0.01	0.03	0.16	0.68	0.09	0.02	0.04	1.30
Fox Bay, 30-35 cm – Component Two, peak													
Hudson (H_2) - reworked or deposited closely in time													
	avg	68.77	0.71	15.50	2.83	0.14	0.66	1.60	5.76	3.71	0.14	0.18	97.34
n=8	stdev	0.26	0.06	0.17	0.14	0.03	0.05	0.07	0.24	0.10	0.02	0.02	2.32
Fox Bay, 60-65 cm - Component One, peak													
Mt Burney (likely MB_2) – reworked or deposited closely in time													
	avg	77.42	0.16	12.98	1.04	0.02	0.25	1.20	4.67	2.01	0.03	0.22	96.91
n=8	stdev	0.31	0.03	0.24	0.13	0.03	0.05	0.06	0.18	0.09	0.02	0.03	2.14
Fox Bay, 60-65 cm - Component Two, peak													
Hudson (H_2) - reworked or deposited closely in time													
	Analysis 1	68.64	0.66	15.62	2.85	0.14	0.63	1.59	6.11	3.49	0.08	0.20	98.91
n=2	Analysis 2	69.06	0.71	15.39	3.02	0.04	0.63	1.61	5.72	3.53	0.11	0.20	97.52

6.2.1.3.1. 30-35 cm

The glass-shards in this sample are fluted and vesicular with elongated vesicles. Shards are ~5-10 μm in size. Two chemical components are identified in this isochron; Component One is comprised of rhyolitic glass-shards which have an average SiO_2 and K_2O composition of 77.09 and 4.13 wt%, respectively. The chemical composition of Component One broadly corresponds to Aguilera volcano. Component Two is trachydacitic and glass-shards have an average SiO_2 and K_2O composition of 68.77 and 3.71 wt%, respectively (Table 6.3; Figure 6.3). The composition of Component Two correlates to Hudson volcano, and in particular, that of H_2. These events occurred at similar times (H_2: ~3.92 cal kyr BP (Weller et al., 2014); A_1: ~3.20 cal kyr BP (Stern, 2008)).

6.2.1.3.2. 60-65 cm

The glass-shards in this cryptotephra zone are fluted. Like Fox Bay 30-35 cm, two chemical compositions are identified. Component One is comprised of rhyolitic shards which have an SiO_2 and K_2O composition of 77.42 and 2.01 wt%, respectively. Component One correlates well with Mt Burney but because this centre has not experienced previous eruptions with distinct compositions, the event remains unknown. Component Two is comprised of trachydacitic shards which have a range of SiO_2 and K_2O of 68.64-69.06 and 3.49-3.53 wt%, respectively (there is a low number of analysis; *n*=2; Table 6.3; Figure 6.3). This component correlates well with Hudson volcano and notably the widespread marker horizon, H_2. Based on the identification of glass-shards with H_2 affinity, which have a depositional age of ~3.92 cal kyr BP (Weller et al., 2014), it is possible that the Mt Burney tephra relates to MB_2 which has a depositional age of ~3.82 cal yr BP (Stern, 2008). This would indicate that these 5 cm of peat accumulated over a period of ~100 years. However, the cryptotephra analysed between 30 and 35 cm contained ash from eruptions occurring between 4-3 cal kyr BP (H_2 and A_1). It is therefore unlikely that both this upper and lower unit of Fox Bay cryptotephra are preserved across an ~4-3 cal kyr BP time period. Thus, it could be that the earlier H_1 event, deposited ~7.75 cal kyr BP (Weller et al., 2014), has a wider compositional range than currently established by Del Carlo et al. (2018) and Smith et al. (2019) and that the cryptotephra preserved in Fox Bay at 60-65 cm instead represents the MB_1 (Component One) and H_1 event (Component Two), both of which were preserved ~8 cal kyr BP.

6.2.2. Chronology of Stanley Common

An age-depth model has been produced in OxCal 4.3 through the use of the ages of the two identified tephra layers in Stanley Common: R_1 (12,685±260 yr BP; Stern, 2008) at 98 cm, and H_2 (3670±70 yr BP; Naranjo and Stern, 1998) at 17 cm, and the relative stratigraphic position of the top (0 cm) and base (100 cm; Figure 6.4, Table 6.4). Though this model is poorly

constrained, we can determine that the approximate peat accumulation rate for the sequence is 150 years per cm (0.006 cm/y).

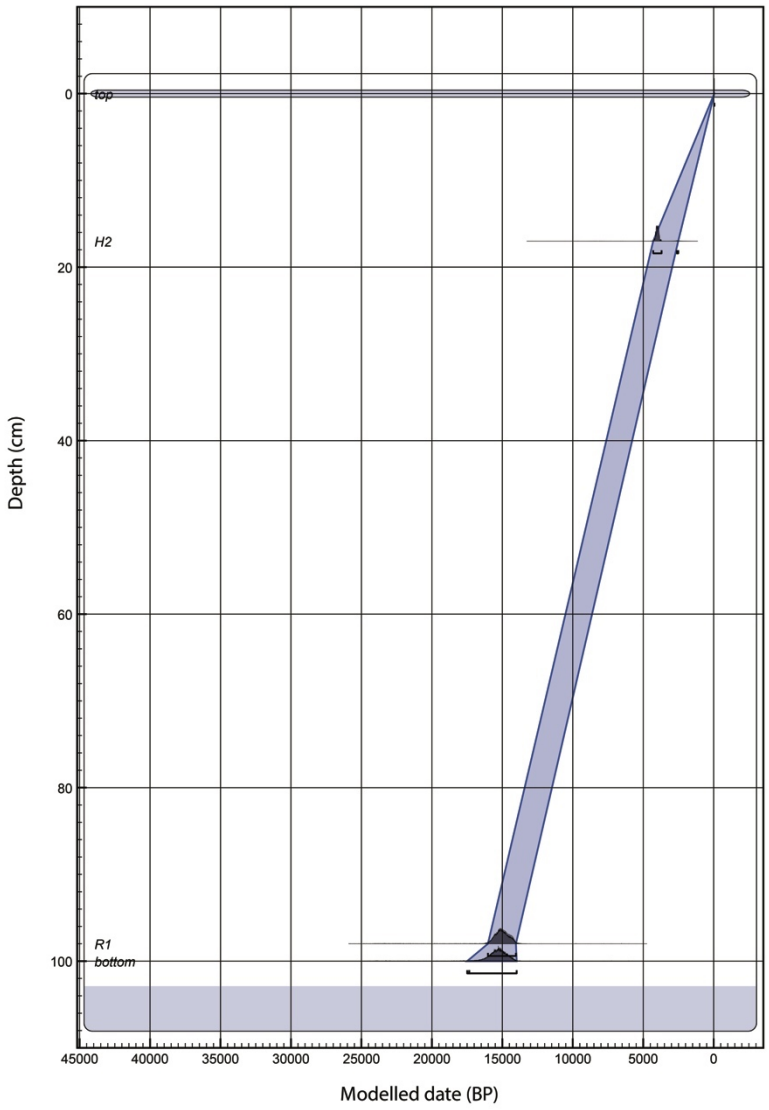


Figure 6.4. Age-depth model for Stanley Common, produced using tephra layers identified in the sequence, R_1 from Reclus volcano, and H_2 from Hudson volcano.

Table 6.4. Calibrated ages for the top/bottom of sequence, and widespread tephra units identified in the Stanley Common sequence

Depth (cm)	Age (from; cal yr BP)	Age (to; cal yr BP)
0 (Top)	AD 1994	AD 1995
17 (H_2, Hudson)	4237	2518
98 (R_1, Reclus)	16,023	14,038
100 (Bottom)	17,495	13,982

6.3. Discussion

The identification of pre-historical Andean ash in the Falkland Islands is unsurprising; volcanic ash from historical events in Chile are known to have been deposited as far South as Antarctica (e.g., 2011 Puyehue-Cordón Caulle ash reached the Western Antarctic Ice Sheet; Koffman et al., 2017). Pre-historical Andean ash has also been identified in the South Georgia Islands (widespread ash from Solipulli volcano; Oppedal et al., 2018), and most recently, in the Falkland Islands (widespread ash from Mt Burney including MB_1 and an unknown layer and R_1 from Reclus volcano; Monteath et al., 2019). In addition to the widespread ash layers identified at the Hookers Point site in the Falkland Islands by Monteath et al. (2019), a further five identified cryptotephra layers were identified which were considered to be reworked on the basis of their glass-shard morphologies and heterogeneous chemistries; these reworked tephra were attributed to post-depositional aeolian remobilisation, and site-specific taphonomic processes.

In this study which investigates both peaks of glass-shards and glass-shards in background sediment, we have identified three primary (Poncho Hill Pass 82-83 cm; Stanley Common 17-19, 98-100 cm), five possibly reworked or deposited closely in time (Poncho Hill Pass 18-20, 20-25 cm; Stanley Common 73-74 cm; Fox Bay 30-35, 60-65 cm) and three likely reworked (Stanley Common 20-21, 24-27, 90-92 cm) samples in three peat records, and all but three of these samples (Stanley Common 20-21, 24-27 and 90-92 cm depth) are of Andean affinity.

In this section, we discuss tephra deposition, including: i) how peat archives may affect the taphonomy of tephra and subsequently influence the isochronous horizons in this study, ii) how these widespread layers from Andean volcanoes may be reworked by wind from distal environments, and iii) why some tephra layers from the Andes may be preserved in distal records, and others not.

6.3.1. Primary tephra layers

At the sites investigated, three tephra samples are considered to be primary based on their homogeneous composition and shard morphologies. The identification of these tephra from large, explosive Chilean volcanic eruptions provides evidence for long-distance transport of Andean tephra to the Falkland Islands during the Late Quaternary (e.g., Monteath et al., 2019). These tephra are from Hudson (H_1 in Poncho Hill Pass at 82-83 cm depth, and H_2 in Stanley Common at 17-19 cm depth) and Reclus volcano (R_1 in Stanley Common at 98-100 cm depth; Figure 6.2); these centres are located ~1200 km, ~1000 km distance respectively to the Falkland Islands.

R_1 and MB_1 from Reclus volcano and Mt Burney, respectively, have been identified in the Falkland Islands previously by Monteath et al. (2019), however, the identification of deposits from Hudson volcano, H_1 and H_2, represents the first identification of Late Quaternary Hudson events in the Falkland Islands. It is unclear why Hudson tephra was not identified in Hookers Point, Falkland Islands by Monteath et al. (2019), but taphonomic processes are likely a dominant factor. Pyne-O'Donnell (2011) analysed multiple sedimentary sequences from single lakes and identified that lacustrine sedimentary archives can have variable glass-shard concentrations depending on the coring location, as a consequence of site-specific taphonomy. Pyne-O'Donnell (2011) and Boygle (1999) thus recommended that tephrostratigraphic studies be undertaken using multiple cores, as single-core studies may be a poor representation of the true tephrostratigraphy. In instances where this is not feasible, bathymetric and seismic surveys can be used to detect optimal coring locations in sedimentary sequences (e.g., Moernaut et al., 2007, 2014).

In this study, primary tephra isochrons were identified in cryptotephra samples that were representative of background material; for example R_1 and H_2 were identified in Stanley Common at 98-100 and 17-19 cm depth, with only 40 % relative abundance of glass-shards each. Using conventional methods, Monteath et al. (2019) did not analyse low concentration background samples. It is possible that a combination of site-specific taphonomy, depositional mechanism, and long-distance transport results in the requirement to analyse lower-than-expected glass-shard concentrations in some circumstances. Alternatively, the primary tephra identified in this study may actually represent a reworking of the widespread ash, and the real isochron is

stratigraphically lower in the sequence and has not been analysed or identified yet (e.g., The Y-2 layer in Wulf et al., 2018).

The age-depth model produced for Stanley Common, constrained by two tephra dates, H_2 and R_1, indicates a basal age of between 17.50-13.98 cal kyr BP which is in-line with Hall et al. (2001) and Holmes et al. (1999) who suggested that peat formed on the Falkland Islands at the end of the Last Glacial Maximum (Figure 6.3, Table 6.4). However, the cryptotephra identified near the base of Poncho Hill Pass peat, between 82 and 83 cm depth, corresponds to the primary deposition of the H_1 deposit from Hudson volcano, at ~8.8 cal kyr BP (Smith et al., 2019). This indicates that the chronological assumptions made by Hall et al. (2001) and Holmes et al. (1999) possibly do not hold true for all peat sequences on the Islands. Based on the presence of H_1 which is in close proximity to the basal sediment, the base of the Poncho Hill Pass peat formation is more likely some time shortly before this tephra was deposited.

6.3.2. Tephra remobilisation

6.3.2.1. Site-specific taphonomy

As described in Section 6.1, peat has previously been regarded by some as a poor archive for the study of cryptotephra since its microscopic structure is porous and this allows for the post-depositional movement of glass-shards both upward and downward through the sequence after, for example, sinking via gravity, vegetation growth, cutting and burning, altitude, weather, and peat accumulation (Figure 6.1C, D; e.g., Giles et al., 1999; Payne et al., 2005; Payne and Gehrels et al., 2010; Swindles et al., 2013; Watson et al., 2015).

It is thought that some of the samples analysed in this study are reworked. Similarly to Monteath et al. (2019), we identify numerous glass-shards in our three peat sequences that have mixed glass-shard morphologies and heterogeneous chemical compositions, indicative of reworking. Heterogeneous glass-compositions are atypical of tephra units from the AVZ and therefore may be attributed to reworking. However, it is also possible that the glass-shards have been chemically altered; the increased acidity of peat environments can alter the chemical

properties of glass-shards by causing cationic leaching or destruction of the glass' silica network (e.g., Thorseth et al., 1995; Hodder et al., 1990; Pollard et al., 2003; Blockley et al., 2005). Conversely, some of the tephra layers which may be reworked have two distinct chemical compositions; while these units may be reworked it is also possible that the resolution of the archive/sampling prohibits the identification of two discrete tephra units. It is considered that at least five cryptotephra layers/glass-shards may actually represent two eruptions occurring closely in time (notably H_2/A_1, and H_2/MB_2 or possibly H_1/MB_1). These cryptotephra units/glass-shards include samples from: Poncho Hill Pass 18-20, 20-25 cm, Stanley Common 73-74 cm, Fox Bay 30-35 cm and 60-65 cm depth (Tables 6.1-6.3; See Section 6.3.2.2 for further discussion).

The chemical analysis of likely reworked glass-shards identified in Stanley Common at 20-21, 90-92, and 24-27 cm does not permit any firm correlations to source affinity. The lack of identifiable source affinity and few clearly defined isochrons in the Stanley Common sequence is likely reflective of the fact that the shards are mostly derived from background material and likely/possibly reworked. Unknown source affinities could also possibly reflect association to non-Andean sources, including sub-Antarctic centres which share similar chemical characteristics (e.g., Narcisi et al., 2005; Del Carlo et al., 2018).

In a study by Wulf et al. (2018) on well-defined cryptotephra layers in the high-resolution Tenaghi Philippon peat core, several chemically heterogeneous layers were found to in fact be reworked visible tephra (notably from the Santorini Cape Riva/Y-2 and the Campanian Ignimbrite (CI)/Y-5). Wulf et al. (2018) noted that primary material from the Y-2 isochron had been displaced *c.* 58 cm up-core, and up to *c*. 220 cm down-core; this movement has been attributed to taphonomic processes causing lateral movement through the sequence and coring artefacts. Watson et al. (2015) additionally highlighted that reworking in peat environments can occur at different scales, both laterally and vertically, and can be caused by complex interactions which vary in different environmental conditions. As such, pinpointing a single causal mechanism for reworking in peat environments is difficult. While there are no visible tephra layers in the three sequences analysed in this study, it is possible that glass-shards

from high-concentration cryptic isochrons have been displaced, as per Figure 1.6C/D, and therefore appear as reworked layers.

There is limited research on the palaeoclimate of the Falkland Islands, but the region is not thought to have been completely glaciated (e.g., Clapperton, 1971; Barrow, 1978). The Islands therefore likely escaped the preservation issues that are so prevalent on the Andean mainland, such as glacial scour (Chapter 1; e.g., Fontijn et al., 2014). However, historic analysis on Falkland Island soils has identified high levels of soil erosion from overgrazing and burning (Wilson et al., 1993). Even on longer, Quaternary timescales, grain size analysis (e.g., size-sorting) has identified that natural soil erosion is a long-term issue. Throughout the Quaternary, soils have been emplaced by solifluction, translational landsliding and surface wash in mass-washing episodes (Clark et al., 1998). Such mass movement events in peat records are well known to lead to reworking of tephra (Swindles et al., 2013; Watson et al., 2015), and may provide a reasonable mechanism for the remobilisation of glass-shards identified.

While Monteath et al. (2019) have argued that a high abundance of reworked tephra in the Falkland Islands can be attributed to aeolian reworking and/or site specific taphonomic processes, the taphonomic issues surrounding peat sequences are little described in their study. On the basis of a large body of evidence that suggests glass-shards can be mobile in peat bogs (references within this chapter), we hypothesise that site-specific taphonomic processes likely play an integral role in the redeposition of cryptotephra in Falkland Island peat sites, and is a probable cause for at least some of the heterogeneous tephra chemistries identified in the three sequences investigated (notably tephras in Stanley Common at 20-21, 24-27, and 90-92 cm).

6.3.2.2. Aeolian reworking

Many of the reworked glass-shards in the three sequences analysed represent higher than background concentrations of tephra (e.g., Stanley Common 20-21 and 90-92 cm; Figure 6.1). It is possible that the relative abundances as per Holmes et al. (1999) and Hall et al. (2001) are not accurate (cryptotephra abundance measurements are typically undertaken using the more accurate

shards/g method these days), or that the glass-shards analysed represent deposition which occurred later than the primary ash-fall, via a different wind regime, and as such the primary event is not recorded at these sites.

Wind is well regarded as a plausible mechanism for remobilising and transporting ash over long distances (e.g., Malin et al., 1983; Scasso et al., 1994; Wilson et al., 2011; Pouget et al., 2014). Wulf et al. (2018) attributed some of the reworked CI tephra identified in the Tenaghi Philippon peat core to aeolian reworking. Similarly, Monteath et al. (2019) attributed much of the reworked, detrital glass-shards identified in Hookers Point, Falkland Islands to wind-blown remobilisation (reworking). Monteath et al. (2019) hypothesised that the location of the Falkland Islands beneath the central jet of the Southern Westerly Winds makes it ideally located to receive wind-blown ash from Andean sources. For example, these strong regional winds (Pali Aike wind speeds: 28.8 km h^{-1}; Ohlendorf et al. 2013) transported ash from the 1991 Hudson volcano eruption >1,000 km from Chile to the Falkland Islands (e.g., Scasso et al., 1994; Wilson et al., 2011). There are no visible ash layers reported on the Falkland Islands (Hall et al., 2001), but thick and visible ash layers are commonly reported across South America (e.g., Stern, 2008). Aeolian remobilisation from outcrops on the Andean mainland is thus a conceivable process for the redeposition of tephra in the Falkland Islands, after the time of primary deposition.

Discussion on the ability of ash to be remobilised via wind in Chile is provided in Chapter 5, and is therefore not repeated here. It is deemed a feasible cause for the identified reworked glass-shards in the sequences analysed in this Chapter (6).

6.3.2.3. Alternative explanations

Poncho Hill Pass 18-20 and 20-25 cm, Stanley Common 73-74 cm, and Fox Bay 30-35 cm samples have mixed chemical compositions representative of both Hudson volcano (notably H_2) and Aguilera volcano. H_2 was deposited ~3.92 cal kyr BP (Weller et al., 2014), and the only widespread tephra layer known from Aguilera volcano, A_1, was deposited ~3.20 cal kyr BP (Stern, 2008). The occurrence of glass-shards in the same sample with H_2 and Aguilera (possibly

A_1) affinity appear in three different sites, which indicates that these are likely primary rather than reworked isochrons.

A further cryptotephra peak analysed in Fox Bay at 60-65 cm depth also has mixed chemical composition; the glass shards are from Mt Burney and Hudson volcano, specifically the chemistry of the Hudson unit appears to relate to the H_2 event. If it is to be believed that this is the H_2 event then it is likely that the Mt Burney tephra, which is present in greater abundance than the Hudson component, represents MB_2 on the basis that both of these large, explosive events are thought to have taken place within ~100 years of one another; H_2 has a depositional age of ~3.92 cal kyr BP (Weller et al., 2014) and MB_2 has a depositional age of ~3.82 cal kyr BP (Stern, 2008). However, the ash layer above this in Fox Bay at 30-35 cm is related to Aguilera (likely A_1) and Hudson (H_2) which were deposited between ~3 and 4 cal kyr BP. Chronologically, the occurrence of all of these units occurring simultaneously, despite prolonged sediment preservation, is unlikely. It is therefore speculated that tephra from the H_1 event may have a broader chemical affinity than currently acknowledged and that the cryptotephra in Fox Bay between 60 and 65 cm depth may instead relate to H_1. Since the composition of past Mt Burney eruptions is not particularly unique for individual events, it is certainly possible that the cryptotephra of Mt Burney composition may relate to MB_1. Both of these events occurred ~8 cal ka BP.

Using the approximate peat accumulation rate derived from Stanley Common of ~150 years per 1 cm of sediment (Section 6.3.2), and ~100 years per 1 cm of sediment from Monteath et al. (2019; extrapolated from age-model), it is possible that the compositions of these tephra appear mixed simply because these tephra are deposited closely in time, rather than that they have been reworked. The chronological resolution of the peat archives, or sampling technique, may not be sufficient to differentiate between the tephra layers given how closely they are thought to have been deposited in time. However, given the ability for shards to move up and down peat cores (e.g., Payne and Gehrels, 2010; Wulf et al., 2018), it cannot be ruled out entirely that the layers have been reworked to some extent.

The stratigraphic positioning of MB_2 and H_2 is poorly understood, and the identification of these layers in continually deposited, high-temporal resolution archives could provide better stratigraphic and temporal constraints which would be beneficial to further constraining their eruptive ages and developing the regional tephrostratigraphy (e.g., Fontijn et al., 2016; Stern, 2008).

6.4. Conclusions

It is concluded that the following tephra sourced from southern South America are identified in the following sites in the Falkland Islands as primary isochrons:

- H_1 (Hudson volcano), in Poncho Hill Pass at 82-83 cm depth
- R_1 (Reclus volcano), in Stanley Common at 98-100 cm depth
- H_2 (Hudson volcano), in Stanley Common at 17-19 cm depth

These findings represent the first identification of pre-historical Hudson events in the Falkland Islands, the ash of which has travelled a distance of ~1280 km SE from source. They additionally highlight the potential of cryptotephra investigations in the Falkland Islands to expand upon the regional tephrostratigraphy of southern South America.

Three cryptotephra layers/glass-shards are considered likely to be reworked based on their chemical heterogeneity and shard morphology. Five cryptotephra layers/glass-shards are thought to either be reworked or represent events that were deposited closely in time. These tephra include combinations of compositions from Aguilera (likely A_1)/Hudson volcano (H_2) which have depositional ages of ~3.20 cal kyr BP (Stern, 2008) and ~3.92 cal kyr BP (Weller et al., 2014), respectively. Combinations of chemistry from Mt Burney and Hudson volcano have also been identified but it is not yet confirmed which past events they represent and it is possible that the H_1 eruptive unit has a wider compositional range than currently anticipated by Del Carlo et al. (2018) and Smith et al. (2019).

It is difficult to i) decipher the mechanisms that produced reworking (though this is thought to likely be related to taphonomic processes in association with peat environments, and/or aeolian reworking), and ii) determine whether events are deposited closely in time. To resolve this issue, archives with higher resolution chronologies should be sought in future research of Falkland Island tephra, including for example, well-dated or annually resolved lacustrine sequences. Such research would help to better constrain the ages of primary isochrons identified and offers excellent scope to expand upon the regional tephrostratigraphy of southern South America (e.g., Fontijn et al., 2016).

Chapter 7

Refining the age of large, explosive volcanic events in southern South America: development of southern South America's tephrochronological model using Bayesian age modelling

Abstract

Tephra from large, explosive Andean eruptions have been identified in numerous archives between 38 and 55°S, in Chile, Argentina, the Falkland Islands and the South Georgia Islands. This chapter outlines new and accurately calibrated age estimates for 49 of these large events, deposits of which are found in archives across these regions by using readily available published data; the associated ages of these units are subsequently modelled using the most modern and accurate radiocarbon calibrating techniques. This work has ultimately extended the regional tephrochronology of the Chilean Lake District (38-42°S; Fontijn et al., 2016). Many of the age estimates presented here for the eruptions are better constrained than previously published estimates (e.g., those of COR2, Lepue and Men_o), but some of the newly modelled age ranges for the eruptions are larger than previously reported (e.g., PCC1, Pucon, Chaimilla and PCC4). Possible reasons for more precise age-constraints include the identification and publication of new radiocarbon dates and the use of a more accurate age-modelling technique based solely on stratigraphic constraints. As a consequence of limited terrain accessibility, poor preservation, and limited volcanological research undertaken in the region, widespread correlations are currently lacking to enable numerous correlations between the southernmost Southern Volcanic Zone and surrounding volcanic regions (the Chilean Lake District, and the Austral Volcanic Zone), and future work to expand the regional tephrochronology could focus here. Because of its geographic proximity, widespread tephra from the AVZ offers significant potential to synchronise between Chilean and extra-Andean archives in the future.

7.1. Introduction

The lithostratigraphic identification and robust chemical analysis of tephra layers in numerous types of archives allows for the correlation of deposits between sites and subsequent usage as time-synchronous marker horizons. When found in multiple well-dated sites, the eruptive age of deposits can be refined by utilising surrounding chronological data, including for example, radiocarbon dates, and by analysing them with Bayesian statistics (e.g., Bronk Ramsey et al., 2015; Fontijn et al., 2016; i.e., tephrochronology). Occasionally, the timing of volcanic events can be determined through direct (absolute) radiometric measurements (e.g., $^{40}Ar/^{39}Ar$, $^{40}Ar/^{39}K$, $^{238}U/^{206}Pb$, $^{235}U/^{207}Pb$ or fission track dating) but it is often difficult to apply these techniques: in many cases the crystals are lacking in distal records, and some of the dating methods are most suitable for pre-Holocene deposits. More commonly, short-lived organic matter from sediment immediately underlying, overlying or from within the tephra unit is radiocarbon dated, and this offers an approximation of the eruptive date (e.g., Bronk Ramsey et al., 2015). Other indirect measurements (e.g., varved sediments) at distal sites can also be used to constrain the age of volcanic events.

The use of tephrochronology may allow for increased chronological control at sites that are less well-dated but have chemically-fingerprinted tephra layers, via the importation of the refined eruptive ages into the archive's age model (e.g., Blockley et al., 2012; Moernaut et al., 2014; Bronk Ramsey et al., 2015; Fontijn et al., 2016). This process is inherently important to analyse regional palaeoclimate (e.g., leads and lags in the climate system), archaeological, and geological archives within a precise chronological framework (e.g., Lane et al., 2012, 2013; Blockley et al., 2014; Bronk Ramsey et al., 2015; Fontijn et al., 2016). The analysis of well-constrained sequences of tephra deposits can additionally proffer a better understanding of temporal changes in eruptive behaviour, including frequency, style, magnitude and composition (Watt et al., 2013a; Rawson et al., 2015, 2016; Fontijn et al., 2016; Kutterolf et al., 2019; Schindlbeck et al., 2018).

Due to almost continuous sedimentation, volcanic ash deposits are exceptionally well preserved in lake and bog records in southernmost South America. These archives are critical for the detailed analysis of past volcanism in this region as they typically preserve deposits from both small and large events (e.g., Van Daele et al., 2014; Weller et al., 2014, 2015, 2017, 2018; Stern et al., 2015, 2016; Fontijn et al., 2016;). Complementary to analysis of these tephra records are those from terrestrial outcrops (soil-tephra formations). While these may be incomplete because of glacial scour caused by the retreat of ice at the end of the last glacial maximum at ~17.8 cal ka BP (Moreno et al. 2015b), in addition to difficulties in accessing sites and bias toward the preservation of larger events (e.g., Fontijn et al. 2014), they provide crucial extra information on the eruption, such as event magnitude (e.g., Watt et al., 2013a).

Detailed studies into past eruptive activity have been undertaken across the Southern Volcanic Zone (SVZ; 33-46°S; e.g., Watt et al. 2011; Fontijn et al., 2014, 2016) and Austral Volcanic Zone (AVZ; 49-55°S; e.g., Naranjo and Stern, 1998; Stern, 2008; Weller et al., 2018) in Chile and Argentina. The SVZ includes historically frequently active volcanoes that have for the most part have experienced relatively small events, such as Villarrica (e.g., Van Daele et al., 2014), and Llaima (e.g., Schindlbeck et al., 2014), as well as volcanoes which have experienced less-frequent, explosive Plinian and sub-Plinian eruptions, such as Puyehue-Cordón Caulle (e.g., Singer et al., 2008), Calbuco (e.g., López-Escobar, 1995), and Chaitén (Alloway et al., 2017a, b). Less is known about small eruptive events in the AVZ, but at least four large (> Volcanic Explosivity Index 5; VEI; Newhall and Self, 1982), explosive events have occurred during the postglacial, including those from Mount Burney, Reclus and Aguilera volcanoes (MB_2, MB_1, R_1, A_1; e.g., Naranjo and Stern, 1998; Kilian et al., 2003; Stern, 2008; Monteath et al., 2019).

Fontijn et al. (2014) presented a critical review of the previously known eruptive records of Southern Chilean and Argentinian volcanoes. A postglacial tephrochronological model of widespread deposits identified in the Chilean Lake District (38-42°S) was subsequently developed by Fontijn et al. (2016). Their work (Fontijn et al., 2016) outlined the chemical

composition of new and previously studied regional tephra layers, synchronised tephra correlations across multiple records, and integrated uncalibrated radiocarbon (^{14}C) and varve dates in a single Bayesian age-model (OxCal 4.2; Bronk Ramsey, 2009a) in order to constrain the depositional age of volcanic events. The model was comprised of integrated terrestrial and lacustrine sequences using a combined approach of event stratigraphy where known, and likely stratigraphic order, based on relative age, where absolute stratigraphic constraints were unknown (Fontijn et al., 2016). The phase-modelling technique employed permitted the estimation of the calibrated age of the widespread tephra units which is representative of the time of eruption, rather than the age of the sediment underneath or above the deposits as is common in many age-models (Fontijn et al., 2016).

The importance of combining data from both terrestrial outcrops and continuous sedimentary archives, in addition to relying on stratigraphy rather than solely on radiocarbon dates, is illustrated by the identification of the Llaima Pumice from Llaima volcano. This deposit had been radiocarbon dated to between 8.20±0.34 cal ka BP and 10.12±0.20 cal ka BP (cf. Fontijn et al., 2014), but the positive chemical identification of this layer in the VILLAR1 core from Lago Villarrica clearly places the Llaima Pumice stratigraphically between MC4 (11.96-10.57 cal ka BP; Neltume Pumice from Mocho-Choschuenco volcanic complex) and Cha1 (10.11-9.69 cal ka BP; Chaitén volcano). Using this stratigraphic information, Bayesian statistical analysis indicates that the Llaima Pumice was likely deposited at 10.45±0.13 cal ka BP, which is considerably earlier than radiocarbon date estimations for the unit (Fontijn et al., 2016).

Here we build upon the existing postglacial tephrochronological model for the Chilean Lake District as devised by Fontijn et al. (2016). We use a different approach to Fontijn et al. (2016), which is partly because of the vast difference in radiocarbon and stratigraphic ages derived from the Llaima Pumice (see above); this research is therefore based on event-stratigraphy only (i.e., events are not inserted into the age-model based on relative age where

absolute stratigraphic constraints are unknown). This highly accurate approach ensures that the age of deposits with an unknown depositional order are not artificially constrained.

The ages in this refined regional tephrochronology utilise a higher number of ^{14}C dates, and extend the latitudinal range of the study since it incorporates dates of widespread deposits identified in sites as far as the Falkland Islands (51°S), and notably also includes data for the southernmost part of the SSVZ (41.5-46°S) and the AVZ (49°S-55°S). The overall latitudinal range of this study is therefore 38-55°S. Overall, the production of this tephrochronological model constrains the eruptive ages of widespread and/or large explosive eruptions to produce improved age estimates. These age estimates can be used to enhance and develop other age-models where the same widespread tephra layers are identified. In addition, the tephrochronological model provides insights into regional-scale eruptive behaviour throughout the postglacial period.

7.2. Methodological background

The overall aim was to improve the constraints on the age of deposits. To achieve this, age data (^{14}C and varve dates) surrounding, or within, chemically established widespread tephra layers were compiled into a database (Supplementary File S.5.3). Phase models (Section 2.6; Supplementary File S.5.1) were used to order the events stratigraphically, as per Fontijn et al. (2016), in the Bayesian age-modelling programme OxCal 4.3 (Bronk Ramsey, 2009a). The ShCal13 (Hogg et al., 2013) calibration curve was used to calibrate the obtained radiocarbon ages and determine a most likely depositional or maximum/minimum age for the eruptive events. In all models, outlier analysis at 5 % (0.05) was applied, permitting the downweighing of ages which had poor model agreement (Bronk Ramsey et al., 2009a; Section 2.6). Fourteen individual phase models were produced using known event stratigraphies (i.e., relative order of events in stratigraphy) from different geographic sub-sectors which had the greatest proportion of chemically confirmed tephra units from large eruptions present in them; in some cases, the event stratigraphies of the sequence were modified to allow for the ages of other known tephra units to

be incorporated, in essence producing a composite stratigraphic sequence. This was done using the following criteria: the age of a tephra layer was transferred into another record if the tephra units above and below it were confirmed to be the same; in the instance that the tephra was the uppermost or lowermost unit in the sequence (e.g., Quet2 in CLD182 and VILLAR1), only the unit below or above had to be the same, respectively (e.g., 2011 PCC in CLD248 and CLD238/239; Table 7.1; Figure 7.1).

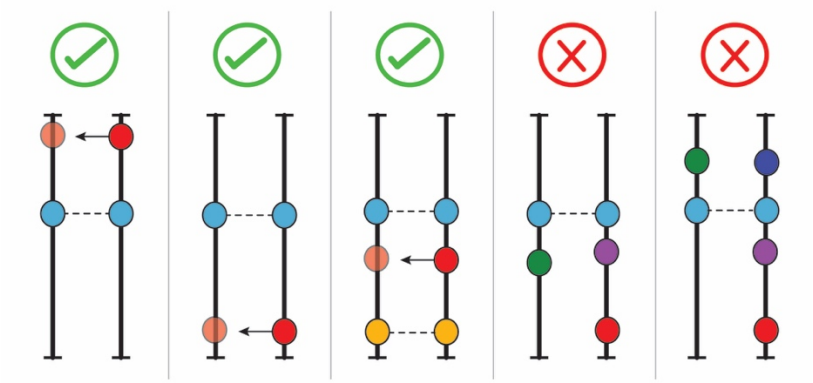


Figure 7.1. Schematic showing the criteria of acceptance for transferring ages of tephra into other sequences for age modelling. Each thick black line represents a physical stratigraphic sequence containing tephra (tephra layers are represented by coloured circles; tephra with the same composition have the same colour). Pale blue and yellow circles adjoined by dashed lines indicate tephra that is chemically correlated and identified in both sequences. Shaded red circles indicate a tephra (and affiliated ages) which were able to be transferred using the criteria, but these tephra represented by shaded red circles are not physically present in said sequence (see text). Green ticks at the top of logs indicate an age-transference is able to take place, while red crosses indicate one is not able to take place (see text).

The production of numerous age (phase) models representative of single/amalgamated stratigraphies resulted in the replication of likely dates for widespread tephra layers. Since any uncertainties of reconstructed and interpolated ages should be represented in final tephra ages (e.g., Bronk Ramsey et al., 2015), a single most likely age of the individual regional marker horizon was determined. To do this, the Priors of the modelled ages for the widespread marker layers as determined from the relevant event stratigraphic models were exported and then modelled using the *Combine()* function in OxCal 4.3 (Bronk Ramsey, 2009a).

All reconstructed ages are represented at 95.4 % confidence intervals, and for almost all tephra layers in the region, this work yields more precise composite age estimates using a more

accurate approach to age-modelling. There is insufficient tephra presence across the wide geographic area studied to understand the stratigraphic relationships between all the units, and incorporate these all into one composite regional tephrochronology, but the ages for these stratigraphically constrained layers are ordered in Table 7.2 by median age, providing a good likely representation of depositional order. The model is shown schematically in Figure 7.3.

Overall, this work has permitted new, accurate, timings of events based on stratigraphic constraints, and allows an analysis of the temporal and spatial distribution of large volcanic events. It is important to note that small events are not reflected in this study, and there is likely some degree of preservation bias as reported in Fontijn et al. (2014, and Brown et al., 2014) and this thesis. As a consequence, changes in the frequency of events will not be described.

Table 7.1: Table showing widespread tephra that were included in age models; **o** demarks tephra layer physically present in the sequence, while **x** demarks an imported tephra age based on the stratigraphic position relative to other records (as per Section 7.2). This table includes ages from the different age models for their respective sequences and lists the age-model by number, the name of the sequence used for the model, the sequence type (i.e., continuous sediment deposition or outcrop), latitude, as well as associated references for the particular sequence. This is marked against the widespread tephra layers, and source volcano (Figure 7.2). It additionally highlights whether the layer is identified in more than one sequence and therefore subject to the OxCal *Combine()* function to derive a single likely age determination (y=yes; n=no). References are: 1=Fontijn et al. (2016); 2=Wiemer et al. (2015); 3=Weller et al. (2017); 4=Amigo et al. (2013); 5=Alloway et al. (2017a); 6=Geoffroy et al. (2018); 7=Naranjo and Stern (2004); 8=Stern (2008); 9=Kilian et al. (2003); 10=This study.

Model Number		**1**	**2**	**3**	**4**	**5**	**6**	**7**	**8**	**9**	**10**	**11**	**12**	**13**	**14**	Tephra modelled in >1 sequence (either based on true presence or principles in Section 7.2.1; Figure 7.1) See Figure 7.3.
Sequence		**RIN2**	**CAL2 /3**	**VILLAR1**	**CLD248 and CLD238/ 239**	**CLD 154**	**CLD 168**	**L. Junco**	**L. Unco**	**Mallines**	**L. Espejo/ Pumalin- 3/Pumalin-2**	**Carretera Austral**	**170299-1 (Esquel) /T-20**	**L. Chandler**	**L. Potrok Aike**	
Latitude		40.2	39.5	39.3	40.6/40.7	40.2	39.5	44.3	45.3	42.5	43.1/42.6/42.6	44.1	44	52.8	51.6	
Outcrop (O) or continuous sediment (C)		O	O	C	O	O	O	C	C	O	C	O	O	C	C	
Reference		1	1	1, 2	1	1	1	3	3	4	5	6	7	8, 9	10	
Widespread tephra deposit	**Source Volcano**															
Llaima	Llaima			o												n
Alpehue	Sollipulli			o			x									y
CabHuel	Caburgua-Huelemolle			o												n
Pucon	Villarrica			o			o									y
Lican				o			o									y
Quet5	Quetrupillán			x			x									y
Puesco		o	o	o			o									y
Quet3				x			o									y

Model Number		**1**	**2**	**3**	**4**	**5**	**6**	**7**	**8**	**9**	**10**	**11**	**12**	**13**	**14**	Tephra modelled in >1 sequence (either based on true presence or principles in Section 7.2.1; Figure 7.1) See Figure 7.3.
Sequence		**RIN2**	**CAL2 /3**	**VILLAR1**	**CLD248 and CLD238/ 239**	**CLD 154**	**CLD 168**	**L. Junco**	**L. Unco**	**Mallines**	**L. Espejo/ Pumali n-3/Pumal in-2**	**Carretera Austral**	**170299-1 (Esquel) /T-20**	**L. Chandler**	**L. Potrok Aike**	
Latitude		40.2	39.5	39.3	40.6/40.7	40.2	39.5	44.3	45.3	42.5	43.1/42.6/42.6	44.1	44	52.8	51.6	
Outcrop (O) or continuous sediment (C)		O	O	C	O	O	O	C	C	O	C	O	O	C	C	
Reference		1	1	1, 2	1	1	1	3	3	4	5	6	7	8, 9	10	
Widespread tephra deposit	**Source Volcano**															
Quet2	Quetrupillán			**x**			**o**									y
Quet1				**x**			**o**									y
Achen Ñihue	Huanquihue Group	**o**														y
HUA1		**o**	**o**													n
MC23	Mocho-Choshuenco		**o**													n
MC18						**o**										n
MC15		**o**														n
MC4				**o**			**o**									y
2011 PCC					**x/o**											n
Mil Hojas		**o**	**o**		**o/x**											y
PCC4	Puyehue-Cordón Caulle	**o**	**o**													y
Ranco		**o**	**o**	**o**	**x/o**	**o**										y
PCC2		**x**	**o**	**o**												y
PCC1		**x**														n
Ant2	Antillanca Group				**o/o**											n
PBN					**o/o**											n
MIC2	Michinmahuida												**o/x**			n

Model Number		1	2	3	4	5	6	7	8	9	10	11	12	13	14	Tephra modelled in >1 sequence (either based on true presence or principles in Section 7.2.1; Figure 7.1) See Figure 7.3.
Sequence		**RIN2**	**CAL2/3**	**VILLAR1**	**CLD248 and CLD238/239**	**CLD 154**	**CLD 168**	**L. Junco**	**L. Unco**	**Mallines**	**L. Espejo/ Pumalin- 3/Pumalin-2**	**Carretera Austral**	**170299-1 (Esquel) /T-20**	**L. Chandler**	**L. Potrok Aike**	
Latitude		40.2	39.5	39.3	40.6/40.7	40.2	39.5	44.3	45.3	42.5	43.1/42.6/42.6	44.1	44	52.8	51.6	
Outcrop (O) or continuous sediment (C)		O	O	C	O	O	O	C	C	O	C	O	O	C	C	
Reference		1	1	1, 2	1	1	1	3	3	4	5	6	7	8, 9	10	
Widespread tephra deposit	**Source Volcano**															
MIC1	Michinmahuida									**o**			**o/x**			y
Lepue											**o/x/x**		**x/o**			y
VCha2008	Chaitén									**o**	**x/o/x**					n
Cha4 (Grande)											**x/x/o**					n
Cha3 (Vilcun)											**x/o/o**					n
Cha2 (Pumalin)										**o**	**o/o/o**					y
ChaA1 (Puma)											**x/o/x**					n
Cha1 (chana)				**o**												n
COR3	Corcovado												**o/o**			n
COR2													**o/o**			n
YAN1	Yanteles												**o/o**			n
Mel2 (MM-2)	Melimoyu							**o**				**o**				y
Mel1 (MM-1)												**o**				n
MEN-1	Mentolat							**o**								n
MEN1								**o**	**o**							y
MEN0									**o**							n
MAC1	Macá								**o**							n
H2	Hudson								**o**							n

Model Number		1	2	3	4	5	6	7	8	9	10	11	12	13	14	Tephra modelled in >1 sequence (either based on true presence or principles in Section 7.2.1; Figure 7.1) See Figure 7.3.
Sequence		**RIN2**	**CAL2 /3**	**VILLAR1**	**CLD248 and CLD238/ 239**	**CLD 154**	**CLD 168**	**L. Junco**	**L. Unco**	**Mallines**	**L. Espejo/ Pumalin- 3/Pumalin-2**	**Carretera Austral**	**170299-1 (Esquel) /T-20**	**L. Chandler**	**L. Potrok Aike**	
Latitude		40.2	39.5	39.3	40.6/40.7	40.2	39.5	44.3	45.3	42.5	43.1/42.6/42.6	44.1	44	52.8	51.6	
Outcrop (O) or continuous sediment (C)		O	O	C	O	O	O	C	C	O	C	O	O	C	C	
Reference		1	1	1, 2	1	1	1	3	3	4	5	6	7	8, 9	10	
Widespread tephra deposit	**Source Volcano**															
H0	Hudson								**o**							n
H1														**o**	**o**	y
A1	Aguilera													**o**		n
R1	Reclus														**o**	n
MB2	Mt. Burney													**o**		n
MB1														**o**	**o**	y

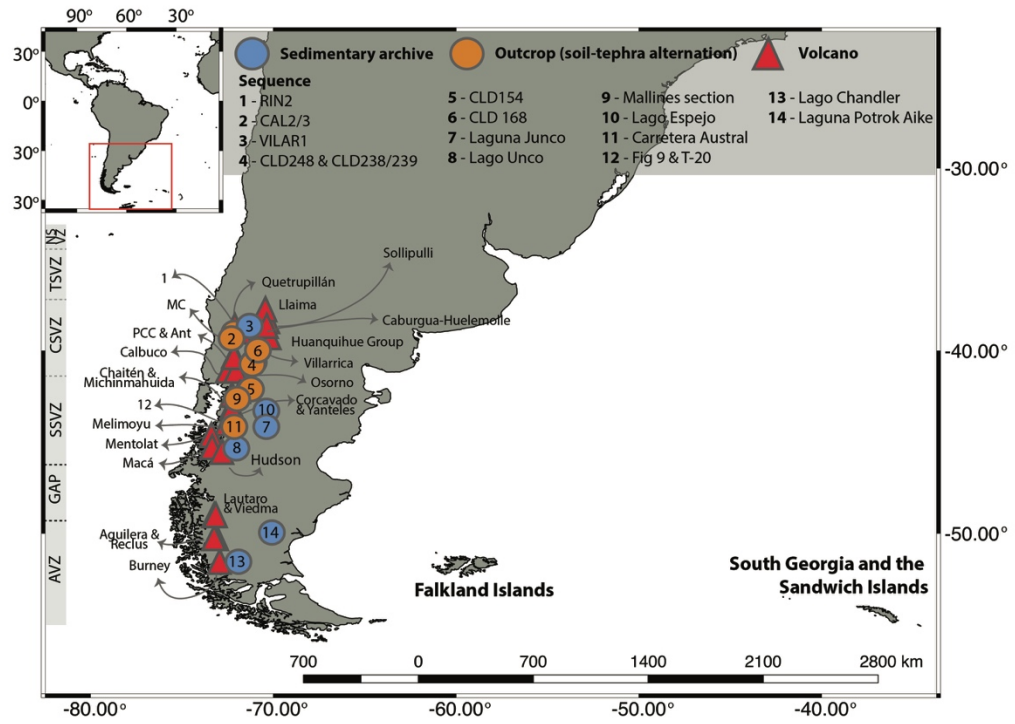


Figure 7.2. Map of southern South America and extra-Andean Islands (Falkland Islands and South Georgia and the Sandwich Islands). Circles represent the sedimentary (blue) or outcrop (orange) sequences used to inform the stratigraphic modelling as per Section 7.2; the number in the circle can be referenced to the sequence name in the Key at the top of the figure. Volcanic centres (triangles) which have had large, explosive events in the past are marked on this figure. NSVZ, TSVZ, CSVZ, SSVZ refers to Northern-, Transitional-, Central-, and Southern- Southern Volcanic Zone, respectively; GAP refers to the volcanic gap; AVZ refers to Austral Volcanic Zone. For further detail on the position of volcanic centres, see Figure 1.1. Radiocarbon dates used to inform modelling are obtained from numerous archives and are not shown here (Supplementary File S.5.3).

7.3. Results and discussion

This section describes the findings from the tephrochronological age-model from this study as per the volcanic region within the SVZ.

7.3.1. Eruptive dates from the Central-Southern SVZ

There are numerous reasons as to why this study may return likely depositional ages that differ from those presented in the literature. The most influential factor is likely that different age-modelling techniques have been implemented compared to previous investigations (Section 7.2). The identification and chemical correlation of units in numerous records can enable tighter chronological constraints (e.g., Bronk Ramsey, 2009a; Bronk Ramsey et al., 2015; Fontijn et al.,

2016). Unfortunately, there is a lack of physically overlapping units in the region; Fontijn et al. (2016) overcame this issue by inserting some tephra dates into their age-model on the basis of the units' estimated depositional age and likely relative stratigraphic position, rather than known exact stratigraphic position. This resulted in a single, long age-model for the CLD, and the implementation of these tephra dates within a larger framework enabled at least some of the poorly constrained tephra layers to be better resolved. For example, the PCC1 tephra was inserted into the Fontijn et al. (2016) age-model using estimated depositional age and likely relative stratigraphic position and was thus constrained by the Chaimilla unit (Villarrica volcano) and other tephra layers at the base. However, in this study, PCC1 is modelled at the base of the stratigraphic log, RIN2 (model 1; Table 7.1; Figure 7.3), and is not constrained by any previously deposited tephra; the PCC1 tephra has not been identified in a sequence where other widespread units are identified below (Singer et al., 2008; Fontijn et al., 2016). The PCC1 depositional age is also only determined by a single radiocarbon date (9310±45 ^{14}C (10,470±150 cal) yr BP; Singer et al., 2008). The combination of the PCC1 unit having few radiocarbon dates in the first instance, and also having limited stratigraphic constraints (i.e., no knowledge of what tephra is located below the PCC1 unit) is a likely cause for the difference in age determination in this model when compared to others. Here we identify an age of 8248-6950 (7237±453) cal yr BP for PCC1 compared to the reconstructed age of 10,455-10,295 (10,360±40) cal yr BP in Fontijn et al. (2016) which uses the ^{14}C age of Singer et al. (2008). It is considered that the modelling technique employed in this study, which is methodologically more accurate, but which subsequently has fewer stratigraphic constraints than Fontijn et al. (2016) as a consequence of only using known event-stratigraphy, has caused a potentially spuriously young age-estimation for PCC1, and that the PCC1 age from this study is likely too young.

Rawson et al. (2015) developed a well-constrained tephrostratigraphic framework for the Mocho-Choshuenco volcanic complex using numerous radiocarbon dates. Here, we can compare the dates obtained for large Mocho-Choshuenco eruptions as presented in both Rawson et al.

(2015), Fontijn et al. (2016), and this study. MC23 (Arauco) was reportedly deposited between 460-215 cal yr BP (Rawson et al., 2015), but here we identify a more tightly constrained eruptive date of 419-383 (399±8) cal yr BP. The age identified in this study is much more comparable with that identified by Fontijn et al. (2016), who modelled an age of 401-379 (390±5) cal yr BP. In both Fontijn et al. (2016) and this study, the age of MC23 is constrained by an age of 392 varve yr BP (Van Deale et al., 2014) in addition to a radiocarbon date of 376±35 ^{14}C yr BP (Rawson et al., 2015). The dates provided by Fontijn et al. (2016) and this study are more precise than Rawson et al. (2015) on the basis that the age model used by Rawson et al. (2015) does not include the varve date from Van Daele et al. (2014), which is a very precise time-marker for the deposition of the volcanic unit.

Other units from Mocho-Choshuenco described by Rawson et al. (2015), and that are also described here, are MC18 (Hua-Hum) and MC15 (Enco). The age estimate for MC18 is 1375-1155 cal yr BP in Rawson et al. (2015). In this study, we identify an age estimate of 1405-1130 (1296±68) cal yr BP for MC18 (Table 7.2). While the ages obtained for MC18 in this study and Rawson et al. (2015) are comparable, the ages are better constrained in Rawson et al. (2015; ranges of 220 years compared to 275 yrs in Rawson et al., 2015 and this study, respectively). This is possibly because Rawson et al. (2015) excluded one ^{14}C age (SUERC-51931; below tephra deposit) of 2831±35 ^{14}C yr BP. This uncalibrated age is older than other ages for the same deposit (Ch-3: 1420±80 ^{14}C yr BP; within tephra deposit, and SUERC-51922: 1509±37 ^{14}C yr BP; below tephra deposit). In this study, outlier analysis was used in order to downweigh anomalous ages (e.g., Bronk Ramsey et al., 2009b), while in Rawson et al. (2015) anomalous ages were removed from the age model despite the use of outlier analysis; the removal of outlying dates manually should involve careful consideration of the measurement process and sample context, but outlier analysis is preferable, and overall the manual removal of dates is not recommended (e.g., Bronk Ramsey et al., 2009b). It is likely that the manual removal of SUERC-51931 resulted in the identified age difference in MC18 between this study and Rawson et al. (2015).

MC15 in Rawson et al. (2015) is 1695-1465 cal yr BP, and in Fontijn et al. (2016) it is 1694-1475 (1587±58) cal yr BP. Here we identify ages of 1699-1584 (1652±30) cal yr BP for MC15 (Table 7.2). The ages for MC15 are better constrained in this study than in both Rawson et al. (2015) and Fontijn et al. (2016) (ranges of 230 and 219 yrs vs. 115 yrs in Rawson et al., 2015, Fontijn et al. 2016, and this study, respectively). This is likely a consequence of differences in the stratigraphic constraints applied in the radiocarbon age-model. The entire Mocho-Choshuenco stratigraphy presented by Rawson et al. (2015) is not (re-)modelled in this study because it investigates both medium-large events; this study instead provides well-constrained age estimates for only the identified widespread tephra units.

PCC4 from the Puyehue Cordón-Caulle volcanic complex (2816-2364; 2512±130 cal yr BP), HUA1 from the Huanquihue group (3877-2570; 3186±350 cal yr BP), and Quet3 from Quetrupillán volcano (13,947-13,291; 13,518±179 cal yr BP), all have wider errors than previously established age estimates by Fontijn et al. (2016), who calculated ages of 3.09±0.08, 4.12±0.04, and 12.61±0.03 cal kyr BP, respectively (Table 7.2). There are no terrestrial radiocarbon dates affiliated with these units, and thus the methods used by Fontijn et al. (2016; Section 7.1) permitted for the most-constrained age estimations.

Eruptive dates for deposits from Chaitén volcano are particularly better-constrained in this study than previously reported estimates (e.g., Amigo et al., 2013; Watt et al., 2013b; Fontijn et al., 2016; Alloway et al., 2017a). Weak age constraints were previously prevalent for Chaitén tephra for a number of reasons, including the fact that the ages of (likely) smaller, lesser-known events (e.g., Cha4, Cha3, ChaA1) do not have a large number of ^{14}C dates and the tephra are not widely dispersed. In addition, the available calibrated ages are not reported accurately (i.e., with no errors), and most often, modelled dates are not applied in a single comprehensive age model based on known stratigraphic constraints. The age of Cha4 (also referred to as Grande Tephra in Alloway et al., 2017a) was previously <0.85 cal kyr BP (Alloway et al., 2017a) but the new models constrain the age to 0.27±0.22 cal kyr BP; the 2008 Chaitén deposit (VCha2008) is

identified above this tephra (Table 7.1). Likewise, the age of Cha3 (also referred to as Vilcún Tephra in Alloway et al., 2017a) was previously ~0.85 cal kyr BP (Alloway et al., 2017a) and this new model constrains the age to 0.92-0.58 (0.73±0.10) cal kyr BP. ChaA1 (also referred to as Puma Verde in Alloway et al., 2017a) was initially reported by Amigo et al. (2013). It was subsequently mentioned by Moreno et al. (2015a), Fontijn et al. (2016) and Alloway et al. (2017a), but detailed information on this layer have been relatively scarce (chemistry, stratigraphy and age). New chemical data shows that two dates from Moreno et al. (2015a) surround the ChaA1 tephra layer, and these were used in this study to determine a well-constrained estimated eruption age of 7.91-7.60 (7.74±0.09) cal kyr BP for ChaA1 (Alloway et al., 2017a). This is considered to be in-line with the estimate of *c*. 8,000 cal years BP of Alloway et al. (2017a).

Cha1 (also referred to as Chana Tephra in Alloway et al., 2017a, b) from Chaitén volcano is now better constrained, with error ranges on the calibrated estimated date of deposition of ±71 years instead of between ±160 and ±100 years (Table 7.2). However, the actual age estimate obtained (9593-9328; 9492±71 cal yr BP) is slightly younger than numerous reported age estimates which range from 9.90±0.13 to 10.38±0.10 cal kyr BP (e.g., Watt et al., 2011; Amigo et al., 2013; Watt et al., 2015; Fontijn et al., 2016; Table 7.2). The new, lower age estimate is likely a reflection of seven new ^{14}C dates obtained from Alloway et al. (2017a). Four of these new radiocarbon dates are derived from within the tephra unit (as opposed to above/below). The new ^{14}C dates utilised a range from 8925±30 to 8465±30 ^{14}C yr BP (Alloway et al., 2017a) and this compares with previous ^{14}C data which was predominantly older, ranging from 9370±60 to 8770±45 ^{14}C yr BP (Amigo et al., 2013 and Naranjo and Stern, 2004, respectively).

7.3.2. Eruptive dates from the southernmost SSVZ

This work presents modelled and calibrated dates for the tephra from the southernmost part of the SSVZ (e.g., YAN1 from Yanteles volcano; COR3, COR2 from Corcovado volcano; MIC1, MIC2, Lepue from Michinmahuida; MEL2, MEL1 from Melimoyu; MAC1 from Macá,

and MEN1 from Mentolat; Figure 7.3). By presenting these schematically (Figure 7.3), we can see that these events likely occurred at a similar time to other large, explosive events (e.g., COR3 occurred at similar times to COR2, ChaA1, MEN1 and H_1; Table 7.2; Figure 7.3). Many of these SSVZ events are still poorly understood. They are relatively poorly chemically fingerprinted, partly because they have overlapping chemical compositions, but they are additionally not well-dated, with few ages associated with each unit. For example, there is only one date for COR2 and one date for COR3 and thus the likely depositional ages determined for these units (COR2: 8930-7740; 8387±363 cal yr BP; COR3: 7862-7675; 7744±57 cal yr BP; Table 7.2) rely heavily on the single radiocarbon date being accurate, and on unit's relative stratigraphic position against surrounding tephra which have more dates (e.g., Lepue and MIC1). Despite this, the dates derived for MIC2, MIC1, COR3, COR2, and Lepue are consistent with the calculated ages in the literature (within 2σ error; Table 7.1). YAN1 is slightly older than suggested dates in the literature, with a modelled depositional age of 11,627-11,263 cal yr BP in this study compared with ~11 cal kyr BP (based on two ^{14}C ages of 9560±60 (T-23) and 9190±130 (T-25) yr BP; Naranjo and Stern, 2004; Watt et al., 2013b).

The eruptive dates of deposits identified at the top or bottom of stratigraphic logs (i.e., those with only one stratigraphic constraint) appear more likely to differ from previously reported ages than those which have stratigraphic constraints both above and below. For example, MAC1 (3163-1373; 1810±615 cal yr BP), MIC2 (5984-3172; 5436±647 cal yr BP), and YAN1 (11,627-11,263; 11,413±100 cal yr BP) are identified at the top of Lago Unco (Weller et al., 2017), and top/bottom of 170299-1 (Esquel) and T-20 (Naranjo and Stern, 2004), respectively, and these appear older than those in the reported literature (Table 7.1; Figure 7.3). Comparatively, MEL1 (also referred to as MM-1 and La Junta; Geoffroy et al., 2018) is the lowermost tephra identified in the Carretera Austral outcrop (Geoffroy et al., 2018) and this study identified a depositional age of 2875-1772 (2584±358) cal yr BP which is younger than previous estimates of ~2.77 cal yr BP (Weller et al., 2019; no errors provided).

MEL2 (also referred to as MM-2 and Santa Ana; Geoffroy et al., 2018) is similar to MAC1, MIC2, YAN1 and MEL1 in that it is the uppermost tephra layer identified in the archive in which it is identified (Corretera Austral and Lago Junco) and thus the layer is not constrained from above. However, unlike the estimates for MAC1, MIC2, YAN1 and MEL1, the age for MEL2 derived from this study (1840-1716; 1772±42 cal yr BP) is approximately consistent with previous age-estimates for the tephra (~1.68 cal yr BP; Weller et al., 2019; no errors provided; Table 7.2). Alternative reasons for inconsistent age-estimates in the literature and this study include the possibility that reported ages are inaccurate. For example, Wils et al. (2018) have chemically and chronologically correlated a tephra in the Aysén Fjord, Chilean Patagonia, to MAC1, but the calibrated age for MAC1 appears to be reported incorrectly by Wils et al. (2018; note that the uncalibrated age used in this model of 1615±30 ^{14}C yr BP seems appropriate). Wils et al. (2018) describes the Naranjo and Stern (2004) age of MAC1 as already being calibrated, but it is not calibrated in the original Naranjo and Stern (2004) research paper, and it is not clear how Wils et al. (2018) calibrated the date, or to what timescale if so (e.g., SHCal13; Hogg et al., 2013). For example, the calibrated age for MAC1 (1.5-1.4 cal kyr BP; Wils et al., 2018) appears remarkably similar to the uncalibrated date of Naranjo and Stern (2004; <1.5±0.06 ^{14}C kyrs BP). The eruptive dates established for MIC1 and MEN1 are similar to previously reported calibrated dates (Table 7.2).

The estimated age of MEN-1 is 2534-1767 (2154±266) cal yr BP. This is significantly younger than previous modelled age estimates of 4.34 cal kyr BP by Weller et al. (2017; no errors provided; Table 7.2). Here it is thought that the phase-modelling method applied during age-modelling in this study has potentially resulted in an underestimation of the age-range. Two available ^{14}C dates from within the tephra deposit were identified for MEN-1: 3890±30 and 2510±30 ^{14}C yr BP (Mella et al., 2012). It is also thought that the calibrated age for MEN-1 determined by Weller et al. (2017) is too old, or not fully representative of the possible likely age; it is suspected that the calibrated age provided by Weller et al. (2017) is determined by crudely

calibrating the oldest available ^{14}C date of 3890±30 ^{14}C yr BP (of Mella et al., 2012) using CalPal Online (Danzeglocke, 2007), which uses an outdated calibration curve and is therefore inappropriate. Here, we have provided a more accurate modelled age, which includes error estimates as is standard protocol (e.g., Bronk Ramsey, 2008; Scott et al., 2007). Similarly, we have done this for another Mentolat eruption, MEN_0, whose published calibrated age previously had no error estimates (e.g., MEN_0 is dated to 15740±50 ^{14}C yr BP by de Porras et al., 2012, and MEN_0 is subsequently reported as ~18.67 cal kyr BP in Weller et al., 2018, 2019; Table 7.2).

Additional chronological research in the lowermost SSVZ, where each deposit only has one or a few radiocarbon dates associated with it, would help to refine the eruptive ages of volcanic deposits in the region. The identification of numerous volcanic units from Corcovado, Michinmahuida, Melimoyu, Macá, and Mentolat volcanoes indicates that these volcanoes are likely more active than currently anticipated (e.g., Naranjo and Stern, 2004; Weller et al., 2015, 2018, 2019; Fagel et al., 2017) and constraining their past eruptive activity is useful to better understand their behaviour and future hazards.

7.3.3. Eruptive dates from the AVZ

The estimated eruptive age of A_1 from Aguilera volcano in the AVZ is 3732-3394 (3555±89) cal yr BP and this indicates that the event occurred earlier than previously thought; Stern (2008) and Markgraf and Huber (2010) estimate an eruptive age of 3.18±0.14 cal kyr BP. A_1 is relatively well-dated compared to other widespread units and thus the difference in estimated age likely has little to do with this study using an age-model relying solely on event-stratigraphy (as per PCC4, HUA1, and Quet3). In the case of the A_1 unit, differences in the estimated age are thought to be firstly caused by the way boundaries have been used in OxCal 4.3 to derive the precise eruptive age rather than the age of the sediment under/above the tephra layer (after Fontijn et al., 2016). The majority of ^{14}C dates associated with A_1 are derived from below the tephra unit (five dates below, one date within, and one date above) and without using

the Bayesian age-modelling technique as this study does, the age is likely more heavily weighted to extreme values that represent a pre-eruptive age.

It is also here speculated that differences in A_1 age estimates can be derived from changes that have occurred in the calibration curve since publication. There is limited information in Stern (2008) with regard to how the radiocarbon data associated with A_1 was calibrated, but since the paper was published in 2008 we can confidently assume that the calibration was made using calibration curves that are now out of use (i.e., SHCal04 and IntCal04; McCormac, et al., 2004 and Reimer et al., 2004, as opposed to SHCal13, IntCal09 or IntCal13; Hogg et al., 2013 and Reimer et al., 2009, 2013). The most recently revised calibration curves (i.e., IntCal13; Reimer et al., 2013) notably have an increased abundance of tree-ring samples around the age of the A_1 tephra (111 German oak samples aged to 3660-3060 cal yr BP) which cause slight differences to the calibration curve at this time between IntCal09 and IntCal13 (Reimer et al., 2013) and which likely have contributed to a difference in the estimated timing of A_1 between this study, Stern (2008) and Markgraf and Huber (2010). It is therefore recommended to provide uncalibrated ages in addition to calibrated ages, so that they can be re-evaluated when calibration curves are updated.

The age of MB_1 from Mt Burney is 8820-8588 (8648±61) cal yr BP in this study. While relatively well constrained, this age is slightly younger than reported radiocarbon ages in the literature of 9949-8851 (9400±549; Stern, 2008; samples from terrestrial outcrops), 9175±111 to 9009±17 (Kilian et al., 2003; samples from peat sediment) and 10,200-9690 (9910; Mansilla et al., 2016; samples from peat sediment) cal yr BP. Two age-models were run which contained ages for the MB_1 unit (models 13 and 15; Table 7.1), and these ages were subsequently combined to produce one final age. In the modelling of the MB_1 ages, the OxCal programme recognised that radiocarbon samples obtained from 'above' the tephra (i.e., the most modern ages) were mostly outliers (in both age-models 13 - Lago Chandler - and 15 - Laguna Potrok Aike - only one sample out of five was not considered an outlier). None of the ages for the MB_1 unit obtained

from 'below the tephra' (i.e., the oldest ages) were identified as outlying. It is therefore curious as to why the age for the MB_1 unit in this study is younger than previously reported age estimates, when the age-models preferentially use the older available ^{14}C ages.

Stern et al. (2016) have reported that radiocarbon dates obtained from the organic material of lake and peat bogs appeared different for H_1 (Hudson volcano) samples. For example, Stern et al. (2016) identified that ages from lake cores averaged 7683±33 (median: 8440) ^{14}C yr BP, while bog deposits averaged 7084±23 (median: 7891) ^{14}C yr BP. Possible causal mechanisms for the variability in dates from different archives include (1) site-specific processes whereby variable inputs of carbon enter lake catchments from the soils covering the watersheds (e.g., Bertrand et al., 2012), (2) penetration of tephra into the lower parts of lakes where sediment can suspend (i.e., nepheloid layer; e.g., Moreno et al., 2015a), and (3) humic acid percolation and contamination (Stern et al., 2016). The identification of a systematic offset in multiple lake watersheds indicates that (1) is not a likely candidate (Stern et al., 2016). It is likely that this difference in radiocarbon dates extends beyond just the H_1 layer, and it is thus possible that the difference in the MB_1 depositional age is a consequence of smoothing out this difference better than previous studies since here we make use of all data in the literature. However, we do not note any difference in the overall calibrated age of the H_1 deposit, dated here as 7897-7706 (7757±36) cal yr BP, when compared to reported calibrated age estimates elsewhere (Table 7.2).

Table 7.2: Ages of widespread marker horizons identified in the Southern and Austral Volcanic Zone (S/AVZ) in order of median (cal yr BP) age from youngest to oldest, presented at 95.4% confidence. From the event-stratigraphy established from individual stratigraphic logs (Table 7.1), there are no inversions when ordered by median ages (this table) and thus this is considered to be the likely stratigraphic order of widespread eruptive events in Chile. Because many of the units are limited in terms of their dispersal distance and/or current identification, this data may not be fully reflective of the regional event-stratigraphy and further detailed analysis on multiple archives is recommended.

Unit	Modelled age (cal yr BP) From	Modelled age (cal yr BP) To	Mean (μ) cal yr BP	Stdev (σ) cal yr BP	Median cal yr BP	Date previously reported in the literature (cal kyr BP unless specified as uncalibrated)	Reference	Younger (<), older (>) or similar (-) age established than reported in the literature	Comments
Cha4 (Grande)	AD 1134	AD 2010	AD 1678	221	**AD 1677 (273 cal yr BP)**	<0.85	Alloway et al. (2017a)	-	
Achen Ñihue	421	355	387	19	**386**	0.36±0.005; 0.19±0.12; 359 varve years BP	Fontijn et al. (2016); Van Daele et al. (2014)	>	Only 1 date
MC23	419	383	399	8	**399**	0.39±0.005; 0.22-0.46	Fontijn et al. (2016); Rawson et al. (2015)	-	
Cha3 (Vilcún)	924	581	740	97	**732**	~0.85	Alloway et al. (2017a)	-	
MH	842	691	762	38	**759**	0.84±0.09; 1.03±0.05	Fontijn et al. (2016); Singer et al. (2008)	-	
MC18	1405	1130	1286	68	**1296**	1.17±0.09; 1.16-1.38	Fontijn et al. (2016); Rawson et al. (2015)	-	
MC15	1699	1584	1647	30	**1652**	1.58±0.06; 1.47-1.70	Fontijn et al. (2016); Rawson et al. (2015)	-	
Quet5	1831	1578	1726	73	**1739**	1.70±0.05	Fontijn et al. (2016)	-	
MEL2	1840	1716	1776	42	**1772**	<1.75±0.08 uncalibrated; ~1.68; 1.64	Naranjo and Stern (2004); Weller et al. (2019); Watt et al. (2013a)	-	
MAC1	3163	1373	2046	615	**1810**	1.4-1.5 reportedly calibrated; <1.5±0.06 uncalibrated	Wils et al. (2018); Naranjo and Stern (2004)	>	Only 2 dates; poorly constrained
Puesco	1917	1768	1854	36	**1859**	1.92±0.04; 1.5±0.08	Fontijn et al. (2016); Pavez (1997)	-	In combination: X-Test fails (7.8%; Acomb=22.2%; An=35.4%)
Ant2	1988	1790	1888	50	**1886**	1.85±0.04; >1.62±0.05; <1.89±0.05	Fontijn et al. (2016); Lara et al. (2006); Singer et al. (2008)	-	
MEN-1	2634	1767	2164	266	**2154**	2.51-3.89 uncalibrated; 4.34	Mella et al. (2012); Weller et al. (2017)	<<	< 2 dates; poorly constrained

Unit	Modelled age (cal yr BP) From	Modelled age (cal yr BP) To	Mean (μ) cal yr BP	Stdev (σ) cal yr BP	Median cal yr BP	Date previously reported in the literature (cal kyr BP unless specified as uncalibrated)	Reference	Younger (<), older (>) or similar (-) age established than reported in the literature	Comments
PBN	2299	2120	2222	47	**2228**	2.24±0.2; 2.16±0.09; 2.17±0.11; >2.17±0.09; >2.20±0.08; >2.22±0.06; >2.22±0.10; <2.42±0.09; <2.84±0.31; <3.11±0.08; <3.11±0.08; 2.83±0.08	Fontijn et al. (2016); Lara et al. (2006); Singer et al. (2008); Villarosa et al. (2006)	-	
PCC4	2816	2364	2547	130	**2512**	3.09±0.08	Fontijn et al. (2016)	<	no dates; poorly constrained
MEL1	2875	1772	2443	358	**2584**	<2.74 uncalibrated; <2.79 uncalibrated; ~2.77; 2.83	Naranjo and Stern (2004); Weller et al. (2019); Watt et al. (2013a)	>	2 dates
Alpehue	3060	2906	2994	38	**2996**	2.95±0.05; 2.93±0.09; 2.94±0.09; 2.98±0.08; 2.99±0.09	Fontijn et al. (2016); Naranjo et al. (1993)	-	
HUA1	3877	2570	3203	350	**3186**	4.12±0.04	Fontijn et al. (2016)	<<	no dates; poorly constrained
A1	3732	3394	3555	89	**3555**	3.18±0.14	Stern (2008); Markgraf and Huber (2010)	>	
Chaimilla	5440	3230	3949	646	**3711**	3.23±0.09; <3.35±0.06	Fontijn et al. (2016); Costantini et al. (2011)	>>	1 date; poorly constrained
H2	4155	3895	4024	65	**4024**	~3.95; 3.60 uncalibrated; 4.05-4.19	Fagel et al. (2017); Naranjo and Stern (2004); Van Daele et al. (2015)	-	
Pucon	4219	4012	4068	51	**4050**	3.97±0.03; 3.74±0.08; 3.82±0.10; 3.92±0.06; 3.95±0.09; 4.00±0.08; 4.00±0.08; 4.04±0.011; 4.09±0.13	Fontijn et al. (2016); Silva Parejas et al. (2010); Moreno and Clavero (2006)	-	
Ranco	4187	4046	4107	62	**4108**	4.35±0.16	Fontijn et al. (2016)	-	In combination: X-Test fails (9.5%; Acomb=1.5%; An=31.6%)
MB2	4375	3999	4183	101	**4180**	4.25±0.12; 4.21±0.09; 4.07-4.50	Killian et al. (2003); Stern (2008); Mansilla et al. (2018)	-	
Cha2 (Pumalin)	5173	4935	5045	58	**5040**	5.04-4.86	Watt et al. (2013a)	-	
MIC2	5984	3172	5213	647	**5436**	<3.82±0.70 uncalibrated; >1.84±0.07 uncalibrated; 4.21	Naranjo and Stern (2004); Watt et al. (2013a)	>>	no dates; poorly constrained. This unit is argued to be a correlative of Cha2 (i.e., from Chaitén volcano; e.g., Alloway et al., 2017; Watt et al., 2013). It has been modelled here for completeness, but further constraints could include replacing the MIC2 age in model 12 (170299-1 (Esquel)/T20) with available Cha2 ages
PCC2	6689	6514	6606	46	**6611**	6.42±0.82; 6.44±0.9; 6.9±1.6; >6.2±0.09; <6.66±0.09; <7.12±0.08	Fontijn et al. (2016); Singer et al. (2008)	-	

Unit	Modelled age (cal yr BP) From	Modelled age (cal yr BP) To	Mean (μ) cal yr BP	Stdev (σ) cal yr BP	Median cal yr BP	Date previously reported in the literature (cal kyr BP unless specified as uncalibrated)	Reference	Younger (<), older (>) or similar (-) age established than reported in the literature	Comments
MIC1	7231	5885	6830	326	**6944**	<6.35±0.06 uncalibrated; >5.12±0.08 uncalibrated; 7.29	Naranjo and Stern (2004); Watt et al. (2013a)	<	In combination: 2 dates; X-Test fails (3.8%; Acomb=30.8%; An=50.0%)
PCC1	8248	6950	7371	453	**7237**	10.36±0.04; 10.44±0.04	Fontijn et al. (2016); Singer et al. (2008)	<<	1 date; poorly constrained
MEN1	7667	7615	7640	13	**7641**	7.69; ~7.70	Stern (2016); Weller et al. (2019)	-	
COR3	7862	7675	7754	57	**7744**	<6.87±0.09 uncalibrated; 7.76	Naranjo and Stern (2004); Watt et al. (2013a)	-	
ChaA1	7909	7598	7751	86	**7749**	c. 8.00	Alloway et al. (2017a)	-	
H1	7897	7706	7761	36	**7757**	7.71-8.41; 7.65-7.49; 8.44 (lake); 7.89 (bog); 7.94–8.00; 7.75±0.10; ca. 8.50; 7.69–8.72	Killian et al. (2003); Björk et al. (2012); Stern (2008); McCulloch et al. (2017); Prieto et al. (2013); Unkel et al. (2010); Stern and Weller (2012)	-	
COR2	8930	7740	8355	363	**8387**	<7.98±0.13 uncalibrated; 8.82	Naranjo and Stern (2004); Watt et al. (2013a)	-	
MB1	8820	8588	8692	61	**8684**	8,851–9,949; 9009±17 to 9175±111; 9690–10,200 (9910)	Stern (2008); Kilian et al. (2003); Mansilla et al. (2016)	-	
Cha1 (Chana)	9593	9328	9475	71	**9492**	9.90±0.13; 9.91±0.14; 9.93±0.13; 9.97±0.16; <10.38±0.10	Fontijn et al. (2016); Watt et al. (2011); Amigo et al. (2013); Watt et al. (2015)	<	
YAN1	11,627	11,263	11,425	100	**11,413**	<9.56±0.06 uncalibrated; <9.19±1.3 uncalibrated; 9.70	Naranjo and Stern (2004); Watt et al. (2013)	<<	2 dates
CabHuel	10,600	10,335	10,474	66	**10,476**	10.38±0.04; 6.8-9.5	Fontijn et al. (2016)	-	
Llaima	10,675	10,409	10,545	67	**10,546**	10.45±0.07; 8.20±0.17; 9.85±0.16; 10.12±0.10	Fontijn et al. (2016); Naranjo and Moreno (1991); Naranjo and Moreno (2005)	-	

Unit	Modelled age (cal yr BP) From	Modelled age (cal yr BP) To	Mean (μ) cal yr BP	Stdev (σ) cal yr BP	Median cal yr BP	Date previously reported in the literature (cal kyr BP unless specified as uncalibrated)	Reference	Younger (<), older (>) or similar (-) age established than reported in the literature	Comments
Lepue	11,000	10,830	10,930	41	**10,937**	c. 11.00; 10.90	Alloway et al. (2017b); Moreno and Leon (2003); Abarzúa and Moreno (2008)	-	Previously refered to as COR1 in Naranjo and Stern (2004) and Watt et al. (2013); corrected in Alloway et al. (2018)
MC4	11,916	10,553	11,130	1329	**11,455**	11.40±0.4	Fontijn et al. (2016)	-	In combination test: X-Test fails (3.8%; Acomb=10.5%; An=50.0%)
Quet3	13,947	13,291	13,559	179	**13,518**	12.61±0.03	Fontijn et al. (2016)	>	no dates
Quet2	16,212	13,474	14,622	765	**14,463**	13.30±0.93	Fontijn et al. (2016)	-	
R1	14,995	14,695	14846	77	**14,849**	14.37-15.26; 14.5-15; 15.51–14.35	Stern (2008); Sagredo et al. (2011); McCulloch et al. (2005)	-	
Quet1	16,743	16,484	16620	65	**16627**	16.49±154	Fontijn et al. (2016)	-	
Lican	16,936	16,665	16,790	70	**16,783**	16.71±0.08; 16.56±0.17; 16.62±0.18; 16.63±0.13; 16.67±0.18; 16.69±0.18; 16.70±0.17; 16.79±0.14; 16.88±0.17; 16.91±0.18	Fontijn et al. (2016); Lohmar et al. (2007); Lohmar et al. (2012); Moreno and Clavero (2006)	-	
Ho	17,536	17,171	17,357	92	**17,361**	17.30-17.44; 17.38±0.12	Weller et al. (2014); Bendle et al. (2017)	-	
MENo	18,956	18,333	18,626	167	**18,615**	~18.67	Weller et al. (2018, 2019)	<	one date

7.3.4. Expansion of the tephrochronology

Here, we extend and expand the regional tephrochronology from 38-42°S, to 55°S (Figure 7.3). The identification of Andean tephra in archives including the Falkland Islands, and the South Georgia Islands illustrates the large spatial range that these deposits can be identified on. While logs for the Falkland Islands and South Georgia Islands were not analysed as independent age-models (Figure 7.3), some radiocarbon data associated with tephra layers in them were modelled in this study (e.g., Beta-193401, representative of MB_1 from Hookers Point in the Falkland Islands; Monteath et al., 2019).

Units currently chemically identified in the Falkland Islands include: MB_1 from Mt Burney (Monteath et al., 2019), R_1 from Reclus volcano (Monteath et al., 2019; Chapter 6), and H_1, and H_2 from Hudson volcano (Chapter 6). Based on our findings from Chapter 6, we tentatively suggest that the A_1 layer from Aguilera volcano is also likely well-preserved in archives in the Falkland Islands. All of these units are possibly identifiable as cryptic ash layers further afield, including extra-Andean locations such as the South Georgia and Sandwich Islands, and possibly the Antarctic peninsula and mainland. The Alpehue ash layer from Solipulli volcano (Oppedal et al., 2018) was recently identified in Diamond Bog in the South Georgia Islands (Figures 7.2, 7.3). The cryptic tephra layer could additionally be located further afield (e.g., Antarctica), albeit with likely smaller concentrations of ash. At present, there are no confirmed pre-historical tephrocorrelations identified between Andean centres and mainland Antarctica. While Narcisi et al. (2012) have correlated cryptic tephra in the TALDICE Antarctic ice core to widespread Andean ash layers (Chapter 1), these correlations have recently been disproven based on erroneous chemical correlations (e.g., Del Carlo et al., 2018). This tephrochronology (Figure 7.3) illustrates the scope of possible correlations both spatially and temporally, and can also highlight missing correlations. Further detailed chemical analysis on cryptotephra from Antarctic ice-cores is required to resolve this spatial gap.

There is a lot of potential in the S/AVZ to use tephra to correlate to known units and improve age models further. Numerous archives contain well-preserved tephra layers which are not yet chemically characterised for glass composition. For example, there are >50 tephra units in the sediments of Laguna El Trébol (41°S 04'12"S; 71°W 29'22"W; Tatur et al., 2002); 25 tephra units in Lago Mascardi (41°20'S; 71°34°W; Massaferro and Corley, 1998; Roman-Ross et al., 2002); 13 tephra units in Padre Laguna (41°21′34″S; 71°30′29″W; Iglesias et al., 2012); 11 tephra units in Lagunas Huala Hué (41°30′24″S; 71°30′32″W; Iglesias et al., 2012); and four tephra units in Mallín Fontanito (44.91°S; 71.57°W; Nanavati et al., 2019). These lakes are surrounded by numerous volcanoes, and extend back to a maximum of 18.3 cal kyr BP (Mallín Fontanito), and it is therefore likely that at least some large volcanic events are preserved in the records, and can be correlated across archives. Further to the South in the Patagonia-Tierra del Fuego region, the ash layers identified in records are often correlated principally based on chronology. For example, a peat record in Haberton (54°54′S) is thought to contain the H_1 deposit from Hudson volcano (Markgraf and Huber, 2010). Vega Ñandú (~51°0′S; 72°45′W) contains five tephra units which have been petrologically analysed, but three of the units are from the NAVZ and not associated with a firm a source centre, though are likely from Aguilera. A similar tephrostratigraphy is identified in nearby sediment cores from Lago Guanaco (unpublished), 12 km SW from Vega Ñandú (Villa-Martínez and Moreno, 2007). With new data from Smith et al. (2019; Chapter 5), a more firm correlation to an NAVZ source may be produced for Vega Ñandú and Lago Guanaco deposits, and possibly others in the region.

Additional identification and/or correlation of proximal deposits from relatively under-studied volcanic centres, such as Calbuco, Osorno, Chaitén, Yanteles, Macá, Cay, Mentolat, Corcovado, Michinmahuida, and Melimoyu would significantly enhance the regional tephrochronology; these volcanic centres have experienced large explosive events (e.g., Ca1-Ca13 from Calbuco volcano (Watt et al., 2013b), and Cha1-Cha4 from Chaitén volcano (Alloway et al., 2017a)), but not all of their tephra layers are widely identified. Reasons for the limited

identification of some ash layers could be because of limited dispersal, issues in tephra preservation (e.g., Brown et al., 2014; Fontijn et al., 2014), difficulties in chemical fingerprinting (e.g., centres in the SSVZ often have overlapping chemical compositions or high abundance of microphenocrysts, e.g., Fontijn et al., 2014; Geoffroy et al., 2018), and lack of study in the southern regions of the SSVZ and AVZ due to difficult to reach terrain/ice cover.

Tephra from southernmost SSVZ volcanoes may possibly be identified in other locations. For example, with further chemical analysis on tephra in the Alerce-6 section (located near to Los Alerces Parque Nacional, Argentina; 42°S; 71°W), the COR2 layer from Corcovado volcano may possibly be identifiable (Alloway et al., 2017b). In addition, three new layers were recently identified in Section 1 (road section W-887, located directly adjacent to Río Michimahuida; 43°S; 72°W): COR3-b, unk-2 and unk-1 (unk=unknown; Alloway et al., 2017b). COR3b is attributed to Corcovado volcanism but is not able to be correlated between other records, unk-1 is not able to be correlated and is from an unknown source (Alloway et al., 2017b). Unk-2 can however be traced back toward Michinmahuida due to its presence in both Pumalin-3 (10.3 km from Ruta 7-Termas El Amarillo road junction; 42°S; 72°W) and Section 13 (located South of Pumalin-3; 43°S; 72°W; Alloway et al., 2017b) in addition to Section 1. Recent efforts to understand the southernmost SSVZ volcanism are highlighting that these centres are more active than previously thought (e.g., Alloway et al., 2017a, b; Fagel et al., 2017; Stern, pers comms, Weller et al., 2019).

Further work on well-constrained stratigraphic logs could include the comparison of the palaeoenvironmental record; when based on independent time-scales, this allows for the testing of leads and lags in the climate system, and provides further insight into past atmospheric patterns (e.g., Björk et al., 1998; Lane et al., 2013; Blockley et al., 2014). For example, Lane et al. (2013) identified the widespread Vedde Ash as an isochronous marker in Kråkenes, Norway, and Meerfelder Maar, Germany, which allowed for the analysis of time-transgressive climate. Lane et al. (2013) further identified that palaeoclimate proxies showed climate reorganisation 100 years prior to the Vedde Ash deposition at Meerfelder Maar, but 20 years after the same Vedde Ash

layer at Kråkenes; this was associated with regional-scale atmospheric changes in the polar front. The regional tephrochronology of southern South America is currently not being used in this manner, but there is scope, particularly if cross-continental correlations (e.g., between south America and Antarctica) can be established.

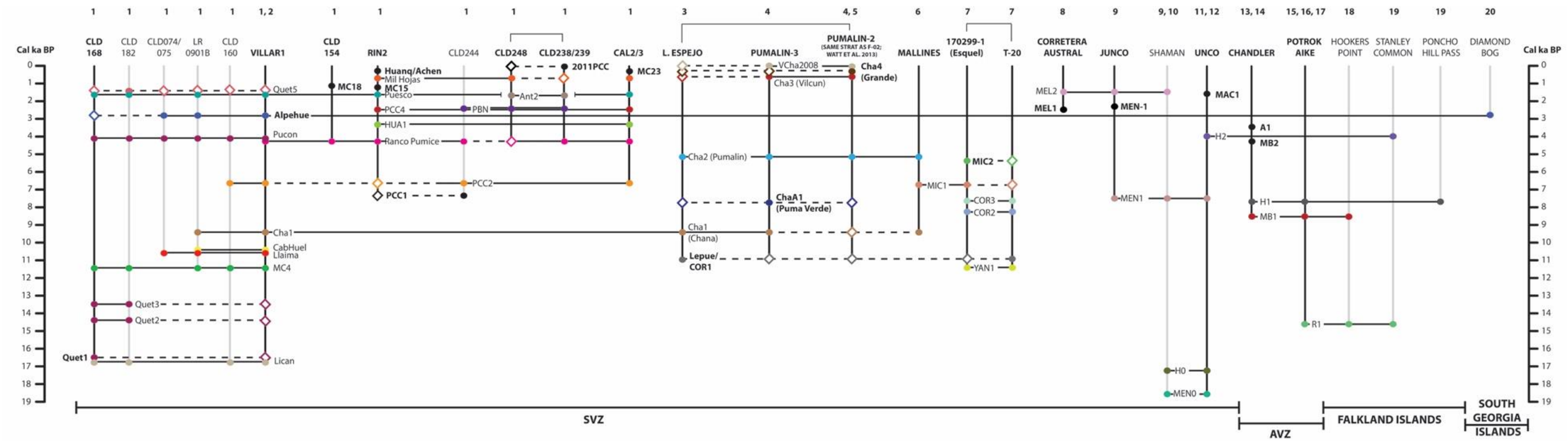


Figure 7.3: Schematic illustration of the synchronicity between sedimentary archives (logs) of widespread tephra deposits in southern Chile, Argentina, the Falkland Islands and the South Georgia Islands. Each log represents an individual lake sequence or terrestrial outcrop (Table 7.1). Black logs represent sequences whereby the stratigraphic ordering of the tephra units, and all associated ages identified in the literature, were modelled in OxCal 4.3; grey logs represent those which were not modelled; this was because the tephra identified did not supply any additional information when compared to other modelled logs. Tephra deposits are identified by circles; black circles represent tephra which is not identified in other sequences modelled in this study. Clear diamonds represent a tephra which has been assumed to likely exist in that sequence and in that position on the basis of the identification of the same tephra/s above and/or below in another log (i.e., a stratigraphically amalgamated layer represented as an X in Table 7.1); dashed lines also demark these presumed correlations. It is important to note that these logs do not represent the full spatial range that these tephra have been identified in, but provide a schematic illustration for the modelling process in this study, and also can be used to exemplify where correlations are currently spatially lacking (e.g., for Corcovado, Michimahuida, Mentolat and Macá volcanoes). Abbreviated names are: Ant = Antillanca, CabHuel = Caburgua-Huelemolle, Cha = Chaitén, COR = Corcovado, HUA = Huanquihue, H = Hudson, MAC = Macá, MB = Mount Burney, MC = Mocho-Choshuenco, MEN = Mentolat, MIC = Michimahuida, PBN = Playas Blancas Negras, PCC = Puyehue-Cordón Caulle, R = Reclus, YAN = Yanteles. References above log names are: 1=Fontijn et al. (2016); 2=Wiemer et al. (2015); 3=Weller et al. (2017a); 4=Alloway et al. (2017a); 5=Watt et al. (2013b); 6=Amigo et al. (2013); 7=Naranjo and Stern (2004); 8=Geoffroy et al. (2018); 9=Weller et al. (2017); 10=Stern et al. (2015); 11=Weller et al. (2014); 12=Weller et al. (2015); 13=Stern (2008); 14=Kilian et al. (2003); 15=Haberzettl et al. (2007); 16=Wastegård et al. (2013); 17=Smith et al. (2019); 18=Monteath et al. (2019); 19=See Chapter 6; 20=Oppedal et al. (2018).

7.4. Conclusions

New calibrated age estimates are determined for 49 large explosive volcanic eruptions from the SVZ and AVZ using readily available published data and the most modern radiocarbon calibrating techniques (e.g., OxCal 4.3; Bronk Ramsey 2009a, b). The fallout of these units have been identified in numerous archives between 38 and 55°S, in Chile, Argentina, Falkland Islands and the South Georgia Islands, and as such, this work extends the regional tephrochronology of the Chilean Lake District (38-42°S) that was developed by Fontijn et al. (2016). Some age-estimates are better constrained than published estimates. Notably, there are several calibrated age-estimates in the literature which do not have errors (e.g., COR2, Lepue, Men_o) and here we provide better age-constraints, including errors. However, other ash layers have wider errors attributed with their ages now, but their reconstructed age is formed using a more accurate approach (e.g., PCC1, Pucon, Chaimilla, PCC4). Possible reasons for variations between dates in the literature and this study include i) newly available data which has been taken into account, and ii) differing age-modelling techniques applied (e.g., stratigraphic constraints). Future work to develop the regional tephrochronology should focus on the southernmost SSVZ, where age-data for marker horizons and widespread correlations are currently lacking, in addition to the AVZ, where there is significant potential to synchronise between extra-Andean archives. The potential for this is shown by the correlations between ash from Andean centres and their identification in the Falkland Islands (e.g., Monteath et al., 2019; Chapter 6) as well as the South Georgia Islands (Oppedal et al., 2018).

Chapter 8
Discussion and summary

8.1. Discussion

Each results chapter has an individual discussion section, and thus this short chapter is designed to synthesise the results in view of the research questions set in Chapter 1, and in a wider context. In doing this, it is clear how the chapters relate to one another, and how the results presented throughout this thesis have advanced significantly our current understanding of Chilean volcanism in the Late Quaternary. I additionally outline what could be done in the future to advance on this novel work.

8.1.1. Aim 1: Identify widespread isochronous markers

In this thesis, numerous widespread marker horizons have been identified in the high-resolution, continuous sedimentary archives: Lago Puyehue (Chile), Laguna Potrok Aike (Argentina), Poncho Hill Pass, Stanley Common and Fox Bay (Falkland Islands). The identification of marker horizons in these sequences is useful to constrain the age of the widespread units, and to determine how far the volcanic products have travelled.

In the case of correlating volcanic layers identified in the Laguna Potrok Aike record to source volcanic centres in Chile, the construction of a database of the glass-shard compositions of past widespread AVZ deposits proved essential (Chapter 5). This database collated the limited suitable published glass-shard chemical data (Del Carlo et al., 2018; Mayr et al., 2019), in addition to significant amounts of newly obtained glass-shard chemical data from the proximal deposits of numerous widespread volcanic events of silicic (typically dacite-rhyolite) composition: H_1 (7.76±0.04 cal ka BP), H_2 (4.02±0.07 cal ka BP; Hudson volcano), A_1 (3.56±0.09 cal ka BP; Aguilera volcano), R_1 (14.85±0.08 cal ka BP; Reclus volcano), MB_1 (8.86±0.06 cal ka BP), MB_2 (4.18±0.10 cal ka BP; Mt Burney volcano; ages as per Chapter 7). While Del Carlo et

al. (2018) had already constructed a database, this did not include data from some major widespread events from the AVZ, and included only: H_1 (Hudson volcano), R_1, $R_{2\text{-}3}$ (<3385-3585 cal yr BP, cf. Del Carlo et al., 2018; Reclus volcano), MB_1, MB_x (older than MB_1; cf. Del Carlo et al., 2018), MB_{1910} (Mt Burney). Notably, the Del Carlo et al. (2018) database did not include tephra chemistry from deposits of Lautaro or Viedma volcanoes. Lautaro and Viedma volcanoes are ice-covered and their volcanic history and chemistry is very poorly understood, mostly because few samples have been collected due to difficulties accessing outcrops. Work from this thesis has enabled the chemical analysis of tephra from historical Lautaro and Viedma volcanic eruptions for the very first time, and these are presented in Mayr et al. (2019; Chapter 5; Supplementary File S.6.1.). This new database therefore contains the most comprehensive glass-chemical data for the AVZ and lowermost SVZ to date.

This comparative database has allowed for the identification of regional marker horizons in the Laguna Potrok Aike sedimentary sequence, including H_1 (Hudson volcano) and confirmation of the MB_2 (Mt Burney) and R_1 (Reclus volcano). It has also facilitated the correlation of numerous tephra units to source volcanoes; since these correlations provide one of the few insights into the volcanic activity that has occurred over that past 80 kyr in southern South America, this novel work resolves considerable gaps regarding understanding the past behaviour of Andean centres during the glacial period. From this, numerous previously unknown tephra layers have been identified, including those from Mt Burney and some pre-historical Lautaro units, and this has shed light on the history of AVZ centres. The work has additionally shown that there is no obvious evidence of systematic variations through time in glass-shard chemical composition. Additionally, the publication of this database means that it can continue to be used by others to confirm robust tephra correlations, and also be built upon with more tephra chemistry (Chapter 5; Smith et al., 2019; Supplementary File S.6.2.).

In the case of the Lago Puyehue record, many of the layers were unable to be correlated to a source, and this was because there was a dominance of silica-poor deposits that were rich in microphenocrysts which made chemical fingerprinting challenging. This was expected to be the case since the Lago Puyehue record was previously studied and thought to contain many deposits

from the predominantly mafic producing centres nearby, including: Puyehue-Cordón Caulle, Antillanca, Calbuco, Osorno and Mocho-Choshuenco. Despite these challenges, four correlations were successfully produced to widespread marker horizons, and these included the rhyolitic/rhyodacitic layers: Mil Hojas, PCC4 and PCC1 (Pr1) from Puyehue-Cordón Caulle volcanoes, and Cha1 from Chaitén volcano (Chapter 3).

Glass fingerprinting and correlating can be challenging (e.g., Chapters 1, 3, 5). For example, correlating more mafic deposits (e.g., basalts and basaltic andesites) can be incredibly difficult as these deposits are often rich in microphenocrysts and subject to post-depositional weathering (e.g., Alloway et al., 2017a; Fontijn et al., 2016). Correlating distal felsic deposits from frequently active volcanic centres can also be difficult, notably because some volcanoes erupt the same compositions during different events, and this can lead to mis-correlation or difficulties in calculating repose intervals (e.g., Ponomareva et al., 2015). In the future, it may prove useful to establish the source volcanoes of the compositionally similar Chilean deposits by analysing the mineral components (e.g., correlations based on Fe-Ti oxide composition at Mocho-Choshuenco volcano in Rawson et al., 2015), or by conducting trace-elemental analysis on glass shards (e.g., LA-ICP-MS; e.g., Albert et al., 2012, 2018). The latter may prove difficult, however, since the size of the beam required for trace-elemental analysis is routinely 20 μm (Tomlinson et al., 2010) and this is larger than the area of vitreous material available in many samples, and particularly so in i) microphenocryst-rich samples, and ii) in cryptotephra samples from extra-Andean locations where shard sizes are often 10 μm at their maximum extent.

Limitations induced by the sampling strategy meant that the layers in the Lago Puyehue sedimentary sequence were assumed to be primary in nature; of course, detailed characterisation of the tephra samples would have been ideal as they could have helped to establish whether any of the 79 visible tephra layers were reworked. For example, detailed observations and chemical analysis of the 94 tephra layers identified in the Laguna Potrok Aike record indicated that at least 65 visible layers which appeared to be primary were reworked (Chapter 5); similar techniques employed by McLean et al. (2018) led to the identification of numerous reworked glass-shards in cryptotephra studies of the Suigetsu Lake record. The thick units of reworked visible tephra

layers that were observed in Laguna Potrok Aike are not typically recorded in high-resolution lacustrine archives and strongly indicate that reworking should be considered more routinely in tephra analysis. This finding is important for any tephrochronologist and very much demonstrates a necessity to consider the depositional mode of tephras prior to reconstructing the records eruptive history; studies which explore the depositional nature of tephra deposits have been conducted by Bertrand et al. (2014), McLean et al. (2018) and McNamara et al. (2019), and these provide good examples of how to consider reworking in natural archives, including analyzing shard morphology, sediment size and organic content.

The reworked deposits identified in Laguna Potrok Aike were hypothesised to be redeposited through aeolian transport, as a result of the lakes positioning amongst strong prevailing westerly winds, and slumping within the steep-sided maar crater. These mechanisms for reworked tephra deposits have been proposed for various records (e.g., Gatti et al., 2013; Gudmundsdóttir et al., 2011). Reworking was also suspected for a number of the cryptotephra and glass-shards identified in peat profiles from the Falkland Islands which were analysed to meet the aim of producing extra-Andean correlations, and to establish how far deposits travel from Andean centres; in this instance, irrespective of their depositional mode, it is clear that tephras from the AVZ are capable of being transported long distances of ≥1,280 km from source (Chapter 6).

Reworking of tephra deposits is increasingly discussed or considered (e.g., Davies et al., 2007; Gudmundsdóttir et al., 2011; Smith et al., 2019; McLean et al., 2018; Monteath et al., 2019; Watson et al., 2015; Chapters 5, 6), but still, often, the depositional nature of units is overlooked, despite the fact that this can alter the determinations of: i) past eruption frequency, ii) robust tephra correlations (e.g., Cook et al., 2018; McLean et al., 2018; Wulf et al., 2018) and iii) accurate event-free depths for precise age-modelling (e.g., Bronk Ramsey, 2009a). The classification of reworked and primary tephra units in Laguna Potrok Aike was challenging because many of the tephra units appeared at first sight to be primary based on their in-situ appearance, however microscopic and glass-chemical inspection of these layers highlighted typical features of reworking (e.g., low abundance of glass-shards, high abundance of detrital and

organic matter and heterogeneous chemical composition, rounded minerals with minimal glass-coating). Future research in tephrochronology should include experimental tephra studies with a goal to fine-tune ways to identify or differentiate between reworked and primary tephra units for individual settings (e.g., lake/peat/terrestrial). For each setting, this could include, for example, guidance on the appearance of the tephra layer in-situ, typical quantities of glass-shards, organic and detrital matter present in visible/cryptotephra layers, and more prescriptive information on glass morphology and chemical analysis. Steps to begin outlining a framework for discriminating between reworked and primary cryptotephra or visible tephra layers have begun in Smith et al. (2019; Chapter 5; Supplementary Data S.6.2) and McLean et al. (2018), respectively. These could be advanced with experimental tephra studies which focus on how (historical) tephra layers of different composition and size are preserved in different localities and over different timescales (e.g., Cutler et al., 2018; Dugmore et al., 2018), in addition to how they are preserved in different sedimentary environments, where lake bathymetry, lake basin type, and sediment slope stability may affect deposition or preservation (e.g., Bertrand et al., 2014; McNamara et al., 2019).

To summarise, I have successfully met the aim of identifying widespread isochronous markers horizons through extensive chemical analysis of tephra deposits in both Laguna Potrok Aike, and Lago Puyehue. In the case of Lago Puyehue, the Cha1 tephra from Chaitén is identified. This unit was dispersed ~240 km to the lake. This VEI 5 unit is seen in other archives and observed at a maximum distance of ~400 km from the vent (Fontijn et al., 2016). Other tephras preserved in the Lago Puyehue sedimentary sequence are predominantly from nearby centres, and have travelled shorter distances of <100 km. Notably, the PCC1 (VEI 4), PCC4 (~VEI 4) and Mil Hojas (VEI 5) tephras of Puyehue-Cordón Caulle affinity, which are identified in Lago Puyehue, are dispersed ~30 km but have been identified as far as 50, 115, and 145 km from their source, respectively (Fontijn et al., 2016). Widespread layers in Laguna Potrok Aike include H_1, MB_1 and R_1. These layers are dispersed ~700, ~215, and ~260 km distance from their source location, respectively and are estimated to have erupted volumes of >18 km^3 (VEI 6), ≥2.8 km^3 >10 km^3, respectively (Dense Rock Equivalent; Naranjo and Stern, 1998; Stern, 2008). Importantly, I have identified the H_1, H_2 and R_1 layers as far as the Falkland Islands which

indicates that tephra from these explosive events are more widely dispersed than previously anticipated and have travelled up to 1,280 km via the dominant westerly wind regime. The A_1 and MB_2 tephra could also be identified with further research in this region (Chapter 5). These tephra identified in the Falkland Island records represent the identification of the furthest dispersed pre-historical AVZ tephras to date, notwithstanding the identification of MB_1 and R_1 in the Falkland Islands by Monteath et al. (2019).

8.1.2. Aim 2: Determine whether there is a relationship between eruption frequency and/or magma composition through time

Fontijn et al. (2016), Rawson et al. (2015, 2016) and Watt et al. (2013a) have investigated whether a relationship exists between eruption frequency and/or magma composition through time in Chile. These studies have identified variable amounts of change in the composition and magnitude of deposits temporally, and this is hypothesised to be a consequence of ice-unloading (Chapter 1). Rawson et al. (2015, 2016) investigated the chemical compositions of deposits from Mocho-Choshuenco volcano using terrestrial (soil-tephra) outcrops, while Fontijn et al. (2016) investigated the chemical compositions of deposits from different volcanoes across the Chilean Lake District using both terrestrial (soil-tephra) outcrops and lacustrine sequences. Results from these studies allowed Rawson et al. (2015, 2016) and Fontijn et al. (2016) to compare their postglacial datasets of ≥VEI 3 events, including data on composition and frequency, to the timing of major climate changes (i.e., ice unloading). Notably, Rawson et al. (2016) identified a tripartite pattern in volcanic behaviour which could be related to ice-unloading (Chapter 1; 3); Fontijn et al. (2016) identified similar trends, but to a lesser extent. Using regional data, Watt et al. (2013a) did not find a significant relationship between eruption frequency/composition.

The Lago Puyehue and Laguna Potrok Aike sedimentary records provide a novel perspective on the relationship between ice-unloading and volcanism. It was difficult to compare the postglacial record of Lago Puyehue with those in the literature. This is because the Lago Puyehue record preserves both small and large events, and reconstructing event-magnitude was not possible with sufficient accuracy since deposits were difficult to correlate to source, and the

distance that the deposit travelled was variable for many of the deposits, with the possibility of distances from the lake ranging between 30 and 240 km (Chapter 3). However, this research has identified that the postglacial sedimentary record of Lago Puyehue preserves predominantly small, heterogeneous-mafic volcanic events; there were no temporal changes in the frequency of deposits identified in the Lago Puyehue record, but small temporal differences in the heterogeneity of deposits were observed (Chapter 3).

At present, all of the studies investigating the relationship between ice-unloading and volcanic frequency/composition in Chile utilise postglacial records (at variable spatial and temporal resolution), which span a relatively short timescale (<15 ka), and therefore temporal variation identified in volcanic frequency and/or composition possibly has little to do with ice-unloading and is instead part of a longer-term pattern of volcanic activity (Chapter 1). The long synglacial record of Laguna Potrok Aike spans ~80 ka, and is therefore currently the only record in South America that permits the testing of the relationship between ice-unloading and volcanic activity (e.g., Watt et al., 2013a; Rawson et al., 2016). In this study (Chapter 5; Smith et al., 2019; Supplementary Data S.6.2), the abundance of volcanic deposits and their overall composition were found not to systematically vary in time. The distal (and mostly downwind) location of the lake relative to the source volcanoes means that it only preserves far-travelled deposits that are predominantly silica-rich and likely large-magnitude. The overwhelming presence of such tephra deposits throughout the last 80 ky, and so including during the last glacial period, is a significant finding since it contrasts with the idea that ice-overburden and subsequent unloading influences the composition of deposits and size of eruptions (e.g., Fontijn et al., 2016; Rawson et al., 2016). To investigate the relationship between volcanism and ice-unloading further, future studies could aim to identify synglacial sequences which contain proximal-medial deposits (which include smaller events of varying compositions) as well as large, predominantly silicic, events. Such sequences are, however, tremendously rare, and therefore synglacial records from the marine realm may prove useful for reconstructing past volcanism using tephra deposits (e.g., Carel et al., 2011).

Since event-frequency fails to show the magnitude of past events well, eruptive flux may be preferable to better demonstrate the size and scale of deposits; this can proportionally represent both large and small eruptions well. In Chapter 4, I quantified eruptive flux on very well investigated sequences which had sufficient data. Using data from OVC/TVC and Mocho-Choshuenco (Chapter 4), it is apparent that eruptive flux could be useful for considering the relationship between ice-unloading and volcanic activity (e.g., Jellinek et al., 2004; Rawson et al., 2016), however, the errors on determining eruptive flux are large (particularly for poorly preserved deposits). The findings of Chapter 3, 4 and 5 illustrate in particular that it is tremendously difficult to relate volcanic frequency and/or composition to climatic changes (or, ice unloading) without additional information, including for example, magnitude or eruptive flux (e.g., Rawson et al., 2016; Chapter 4). However, obtaining this information from lacustrine settings is particularly difficult since the thickness of tephra units may not always be representative of event magnitude due to overthickening, or as a consequence of the variable and often unknown source location of the deposits (e.g., McNamara et al., 2019; Moreno et al., 2015a). Statistical analysis has been used in other studies to investigate the link between volcanic activity and climate change, but again, such studies often fail to take into account additional information relating to volcanic behaviour including volcanic composition, magnitude and eruptive flux (e.g., Kutterolf et al., 2019; Paterne et al., 1990; Rawson et al., 2016; Schindlbeck et al., 2018). Statistically acknowledging the age-uncertainties attributed with the event-horizons is a crucial next step to answering such hypotheses, and while metadata on volcanic behaviour (e.g., magnitude and composition) cannot be inserted into OxCal at this present time, the ability to run KDE analysis in OxCal is a useful first step toward achieving these goals (Chapter 4).

8.1.3. Aim 3: Develop a well-defined chronicle of explosive events

The need to develop and expand upon the regional tephrochronology is derived mostly from the fact that the work in this thesis has spatially expanded upon the model by Fontijn et al. (2016) which was only for the Chilean Lake District (Chapters 3, 5, 6). Moreover, new tephra

layers and radiocarbon dates have been identified in the literature since the Fontijn et al. (2016) publication (e.g., Alloway et al., 2017a; Monteath et al., 2019). For example, newly published data now permits correlations between the Falkland Islands and Mt Burney (MB_1) and Reclus (R_1) volcanoes (Monteath et al., 2019). As a consequence, the regional tephrochronology has been extended through work in this thesis to as far southeast as the Falkland Islands. The work presented in this thesis (Chapter 7) ensures that the most refined eruptive ages are presented, and this is prudent to develop the most robust understanding of i) the timing of large, explosive Chilean events, ii) Chilean volcanic system dynamics and behaviour, and iii) eruption recurrence intervals in Chile (e.g., Papale, 2018).

In order to undertake this work, the most modern and accurate Bayesian statistical modelling techniques were used to determine eruptive ages for 49 events. Most of these ages are now better constrained than those identified in the literature. Instances where ages now have larger age-errors are mostly attributed to differences in age-modelling techniques between this study and others; this study utilises an event-stratigraphy only approach, rather than incorporating tephra units based on both relative age and stratigraphy. It is argued that the approach employed in this study (i.e., event-stratigraphy only) is the most accurate and robust approach to producing the regional tephrochronology, based on principles and guidance of Bronk Ramsey (2008, 2009a; Chapter 7).

The tephrochronology presented in Chapter 7 should not be used to discuss or highlight changes in the frequency of all volcanic events. This is because smaller events (i.e., VEI 1-3) are less likely to be well-preserved or preserved at all in the geological record; similarly larger events (i.e., VEI 3+) are more likely to be better preserved in long-term records (e.g., Brown et al., 2014; Kiyosugi et al., 2015; Papale, 2018). As with any chronicle of volcanic events, it is possible that there may be some inaccurate representation of the volcanic history as a consequence of such preservation and sampling bias, particularly with regards to the fact that centres in the SVZ/SSVZ are considered easier to access than those in the AVZ, and a subsequently greater proportion of tephrochronological research has been undertaken in the SVZ/SSVZ than the AVZ. In addition, deposits are likely to be better preserved toward the present day as they have had significantly

less time to erode (particularly in soil-tephra formations; e.g., Brown et al., 2014; Fontijn et al., 2014; Chapter 4). However, this tephrochronology, and the ages associated with deposits studied, provide the most accurate chronicle of explosive events to date. Where suitable, these well-constrained and accurate tephra dates can be imported into age-models to better refine them.

In time, the timing of these well-refined widespread volcanic events may lead to the use of tephra in investigating leading and/or lagging climate in Chile – this is something which is presently not being investigated. Notably, Lane et al. (2013) identified the widespread Vedde ash layer in two high-resolution sequences in Europe: Meerfelder Maar, Germany and Kråkenes, Norway. The rhyolitic component of the Vedde ash layer, from Iceland, was deposited at 12,121±114 cal yr BP (Greenland ice core age; Lane, 2013). It forms an ideal isochronous marker horizon to investigate the timing of climate change since its deposition is contemporaneous with the Northern hemispheric cooling event, the Younger Dryas (Lane et al., 2013). Lane et al. (2013) identified that cooling in Kråkenes occurred later than at Meerfelder Maar, on an order of 120 years, and attributed this to dynamic atmospheric responses. The temporal and proxy resolution of many Chilean archives is not sufficiently high enough to investigate such temporal variations in climate shifts, but with more data, higher-resolution records, and well-dated and chemically robust isochronous marker horizons that span both Chile, Argentina and extra-Andean locations, such investigations would be incredibly useful for further investigations into such time-transgressive climate shifts. Such work could even prove essential to the debate on the mechanisms of the bipolar seesaw and interhemispheric teleconnections (e.g., Bay et al., 2004; Cvijanovic et al., 2013; Pedro et al., 2018; Svensson et al., 2013).

8.2. Summary

- Small volcanic events (i.e., <VEI 3) are typically under-recorded in Chile, but the sedimentary record of Lago Puyehue has proffered unique insight into Holocene activity. Four widespread tephra layers have been identified (Mil Hojas, PCC4, and PCC1 from Puyehue-Cordón Caulle volcano, and Cha1 from Chaitén volcano) in the Lago Puyehue

record, and the study of the tephra units in the record have demonstrated that many of the likely small-moderate-magnitude events in Chile are chemically heterogeneous and frequently occurring.

- Applying volcanic data to KDE's in OxCal for the first time has allowed for a novel insight into temporal changes in eruptive frequency while accounting for age-uncertainties. These more accurate eruption timescales could also be coupled with additional information (e.g., melt composition, event magnitude, eruptive flux, and/or climate) to provide further insights into past volcanic behaviour.

- Laguna Potrok Aike preserves numerous ash layers which look primary in origin, but further analysis indicates that many of these are reworked. This highlights the need to conduct thorough investigations into the depositional nature of tephra units. Importantly, the identification and chemical fingerprinting of 94 volcanic ash layers through the 80 kyr record has permitted a unique insight into past volcanic behaviour in southern South America: notably, activity is continuous over this time period, and there is no obvious evidence to suggest variable frequencies before/after deglaciation.

- Tephra from numerous AVZ centres are capable of reaching the Falkland Islands; notwithstanding study limitations, it is likely that the first extra-Andean evidence of pre-historical Hudson (H_1, H_2) and Reclus (R_1) volcanism has been confirmed using glass compositions. It is also possible that Aguilera (likely A_1) and Mt Burney (MB_2) are preserved in peat records in the Falkland Islands, indicating excellent potential for distal tephrostratigraphic correlations and even possibly cross-continental correlations between Chile and Antarctica.

- The ages of 49 large, explosive events have been calculated using a novel event-stratigraphic approach and many eruptive dates are now better constrained than was previously the case. These more accurate and in some cases precise ages, provide better chronological constraints for the records in which they are preserved and are useful for volcanic hazard assessments.

Bibliography

Abarzúa, A. M. and Moreno, P. I. (2008). Changing fire regimes in the temperate rainforest region of southern Chile over the last 16,000 yr. *Quaternary Research*, 69: 62–71.

Albert, P. G., Tomlinson, E. L., Smith, V. C., Di Roberto, A., Todman, A., Rosi, M., Marani, M., Muller, W. and Menzies, M. A. (2012). Marine-continental tephra correlations: Volcanic glass geochemistry from the Marsili Basin and the Aeolian Islands, Southern Tyrrhenian Sea, Italy. *Journal of Volcanology and Geothermal Research*, 229–230: 74–94.

Albert, P. G., Smith, V. C., Suzuki, T., Tomlinson, E. L., Nakagawa, T., McLean, D., Yamada, M., Staff, R. A., Schlolaut, G., Takemura, K., Nagahashi, Y. and Kimura, J. I. (2018). Constraints on the frequency and dispersal of explosive eruptions at Sambe and Daisen volcanoes (South-West Japan Arc) from the distal Lake Suigetsu record (SG06 core). *Earth-Science Reviews*, 185: 1004–1028.

Alloway, B. V., Pearce, N. J. G., Moreno, P. I., Villarosa, G., Jara, I., De Pol-Holz, R. and Outes, V. (2017a). An 18,000 year-long eruptive record from Volcán Chaitén, northwestern Patagonia: Paleoenvironmental and hazard-assessment implications. *Quaternary Science Reviews* , 168: 151–181.

Alloway, B. V., Moreno, P. I., Pearce, N. J. G., De Pol-Holz, R., Henríquez, W. I., Pesce, O. H., Sagredo, E., Villarosa, G. and Outes, V. (2017b). Stratigraphy, age and correlation of Lepué Tephra: a widespread c. 11 000 cal a BP marker horizon sourced from the Chaitén Sector of southern Chile. *Journal of Quaternary Science*, 32: 795–829.

Amigo, Á., Lara, L. E. and Smith, V. C. (2013). Holocene record of large explosive eruptions from Chaitén and Michinmahuida Volcanoes, Chile. *Andean Geology*, 40: 227–248.

Anselmetti, F. S., Ariztegui, D., De Batist, M., Catalina Gebhardt, A., Haberzettl, T., Niessen, F., Ohlendorf, C. and Zolitschka, B. (2009). Environmental history of southern Patagonia unravelled by the seismic stratigraphy of Laguna Potrok Aike. *Sedimentology*, 56: 873–892.

Arnaud, F., Magand, O., Chapron, E., Bertrand, S. and Boe, X. (2006). Radionuclide dating (^{210}Pb, ^{137}Cs, ^{241}Am) of recent lake sediments in a highly active geodynamic setting (Lakes Puyehue and Icalma - Chilean Lake District). *Science of the Total Environment*, 366: 837–850.

Bacon, C. R., Gardner, J. V., Mayer, L. A., Buktenica, M. W., Dartnell, P., Ramsey, D. W. and Robinson, J. E. (2002). Morphology, volcanism, and mass wasting in Crater Lake, Oregon. *Geological Society of America Bulletin*, 114: 675–692.

Bacon, C. R. and Lanphere, M. A. (2006). Eruptive history and geochronology of Mount Mazama and the Crater Lake region, Oregon. *Bulletin of the Geological Society of America*, 118: 1331–1359.

Barrow, C. J. (1978). Postglacial Pollen Diagrams from South Georgia (Sub-Antarctic) and West Falkland Island (South Atlantic). *Journal of Biogeography*, 5: 251–274.

Bas, M., Maitre, R., Streckeisen, A. and Zanettin, B. (1986). A chemical classification of volcanic rocks based on the total alkali-silica diagram. *Journal of Petrology*, 27: 745–750.

Baxter, P. J., Bernstein, R. S., Fa, H., French, J. and Ing, R. (1982). Medical aspects of volcanic disasters: An outline of the hazards and emergancy response measures. *Disasters*, 6: 268–276.

Bay, R. C., Bramall, N. and Price, P. B. (2004). Bipolar correlation of volcanism with millennial climate change. *Proceedings of the National Academy of Sciences of the United States of America*, 101: 6341–6345.

Bebbington, M. and Lai, C. (1996). Statistical analysis of New Zealand volcanic occurrence data. *Journal of Volcanology and Geothermal Research*, 74: 101–110.

Bendle, J. M., Palmer, A. P., Thorndycraft, V. R. and Matthews, I. P. (2017). High-resolution chronology for deglaciation of the Patagonian Ice Sheet at Lago Buenos Aires (46.5°S) revealed through varve chronology and Bayesian age modelling. *Quaternary Science Reviews*, 177: 314–339.

Bendle, J. M., Palmer, A. P., Thorndycraft, V. R. and Matthews, I. P. (2019). Phased Patagonian Ice Sheet response to Southern Hemisphere atmospheric and oceanic warming between 18 and 17 ka. *Nature Scientific Reports*, 9: 1–9.

Bertrand, S., Charlet, F., Charlier, B., Renson, V. and Fagel, N. (2008a). Climate variability of southern Chile since the Last Glacial Maximum: A continuous sedimentological record from Lago Puyehue (40°S). *Journal of Paleolimnology*, 39: 179–195.

Bertrand, S., Castiaux, J. and Juvigné, E. (2008b). Tephrostratigraphy of the late glacial and Holocene sediments of Puyehue Lake (Southern Volcanic Zone, Chile, 40°S). *Quaternary Research*, 70: 343–357.

Bertrand, S., Araneda, A., Vargas, P., Jana, P., Sterken, M., Vargas-Ramirez, L., De Batist, M., Vyverman, W., Lepoint, G. and Urrutia, R. (2012). Using the N/C ratio to correct bulk radiocarbon ages from lake sediments: Insights from Chilean Patagonia. *Quaternary Geochronology*, 12: 23–29.

Bertrand, S., Daga, R., Bedert, R. and Fontijn, K. (2014). Deposition of the 2011-2012 Cordón Caulle tephra (Chile, 40°S) in lake sediments: Implications for tephrochronology and volcanology. *Journal of Geophysical Research: Earth Surface*, 119: 2555–2573.

Bird, M., Ayliffe, L., Fifield, L., Turney, C., Cresswell, R., Barrows, T. and David, B. (1999). Radiocarbon dating of 'old' charcoal using a wet oxidation stepped-combustion procedure. *Radiocarbon*, 41: 127–140.

Björck, S., Walker, M., Cwynar, L., Johnsen, S., Knudsen, K.-L., Lowe, J., Wohlfarth, B. and Members, I. (1998). An event stratigraphy for the Last Termination in the North Atlantic region based on the Greenland ice-core record: a proposal by the INTIMATE† group. *Journal of Quaternary Science*, 13: 283–292.

Blaauw, M. (2010). Methods and code for 'classical' age-modelling of radiocarbon sequences. *Quaternary Geochronology*, 5: 512–518.

Blaauw, M. and Christen, J. A. (2011). Flexible paleoclimate age-depth models using an autoregressive gamma process. *Bayesian Analysis*, 6: 457–474.

Blaauw, M., van Geel, B., Kristen, I., Plessen, B., Lyaruu, A., Engstrom, D. R., van der Plicht, J. and Verschuren, D. (2011). High-resolution ^{14}C dating of a 25,000-year lake-sediment record from equatorial East Africa. *Quaternary Science Reviews*, 30: 3043–3059.

Blampied, J., Barberon, V., Ghiglione, M., Leal, P. and Ramos, V. (2012). Disambiguation of the Nunatak Viedma: a basement block previously confused as a volcanic center. *Chilean Geological Congress*, 13th Antofagasta: 380–382.

Blockley, S. P. E., Pyne-O'Donnell, S. D. F., Lowe, J. J., Matthews, I. P., Stone, A., Pollard, A. M., Turney, C. S. M. and Molyneux, E. G. (2005). A new and less destructive laboratory procedure for the physical separation of distal glass tephra shards from sediments. *Quaternary Science Reviews*, 24: 1952–1960.

Blockley, S. P. E., Lane, C. S., Hardiman, M., Olander, S., Seierstad, I. K., Peder, J., Svensson, A., Lotter, A. F., Turney, C. S. M., Bronk Ramsey, C. and Members, I. (2012). Synchronisation of palaeoenvironmental records over the last 60,000 years, and an extended INTIMATE 1 event stratigraphy to 48,000 b2k. *Quaternary Science Reviews*, 36: 2–10.

Blockley, S. P. E., Bourne, A. J., Brauer, A., Davies, S. M., Hardiman, M., Harding, P. R., Lane, C. S., Macleod, A., Matthews, I. P., Donnell, S. D. F. P., Rasmussen, S. O., Wulf, S. and Zanchetta, G. (2014). Tephrochronology and the extended intimate (integration of ice-core, marine and terrestrial records) event stratigraphy 8-128 ka b2k. *Quaternary Science Reviews*, 106: 88–100.

Blundell, A., Charman, D. and Barber, K. (2008). Multiproxy late Holocene peat records from Ireland: towards a regional palaeoclimate curve. *Journal of Quaternary Science*, 23: 59–71.

Boës, X. and Fagel, N. (2008). Timing of the late glacial and Younger Dryas cold reversal in southern Chile varved sediments. *Journal of Paleolimnology*, 39: 267–281.

Bolender, D. J., Steinberg, J. M. and Diamata, B. N. (2011). Farmstead Relocation at the End of the Viking Age: Results of the Skagafjörður Archaeological Settlement Survey. *Archaeologica Islandica*, 9: 77–101.

Bouma, A. (1965). Sedimentary characteristics of samples collected from submarine canyons. *Marine Geology*, 3: 291–320.

Boygle, J. (1999). Variability of tephra in lake and catchment sediments, Svínavatn, Iceland. *Global and Planetary Change*, 21: 129–149.

Bronk Ramsey, C. (2008). Deposition models for chronological records. *Quaternary Science Reviews*, 27: 42–60.

Bronk Ramsey, C. (2009a). Bayesian Analysis of Radiocarbon Dates. *Radiocarbon*, 51: 337–360.

Bronk Ramsey, C. (2009b). Dealing with outliers and offsets in radiocarbon dating. *Radiocarbon*, 57: 217–235.

Bronk Ramsey, C. (2017). Methods for summarising radiocarbon datasets. *Radiocarbon*, 59 (6): 1809-1833.

Bronk Ramsey, C. and Lee, S. (2013). Recent and Planned Developments of the Program OxCal. *Radiocarbon*, 55: 720–730.

Bronk Ramsey, C., Albert, P. G., Blockley, S. P. E., Hardiman, M., Housley, R. A., Lane, C. S., Lee, S., Matthews, I. P., Smith, V. C. and Lowe, J. J. (2015). Improved age estimates for key Late Quaternary European tephra horizons in the RESET lattice. *Quaternary Science Reviews*, 118: 18–32.

Brown, S. K., Crosweller, H. S., Sparks, R. S. J., Cottrell, E., Deligne, N. I., Guerrero, N. O., Hobbs, L., Kiyosugi, K., Loughlin, S. C., Siebert, L. and Takarada, S. (2014). Characterisation of the Quaternary eruption record: analysis of the Large Magnitude Explosive Volcanic Eruptions (LaMEVE) database. *Journal of Applied Volcanology*, 3 (5): 1-22.

Brown, S. K., Jenkins, S. F., Sparks, R. S. J., Odbert, H. and Auker, M. R. (2017). Volcanic fatalities database: analysis of volcanic threat with distance and victim classification. *Journal of Applied Volcanology*, 6 (15): 1-20.

Buck, C., Christen, J. and James, G. (1999). *BCal: an on-line Bayesian radiocarbon calibration tool*. http://intarch.ac.uk/journal/issue7/buck_index.html. Last accessed 20-JUN-2019.

Buck, C. E. and Juarez, M. (2017). *Bayesian radiocarbon modelling for beginners*. http://arxiv.org/abs/1704.07141. Last accessed 25-JUN-2019.

Bursik, M. (1998). Tephra dispersal. In: *The Physics of Explosive Volcanic Eruptions*. Geological Society, London, Special Publications, 145: 115–144.

Buylaert, J.-P., Murray, A. S., Gebhardt, A. C., Sohbati, R., Ohlendorf, C., Thiel, C., Wastegård, S. and Zolitschka, B. (2013). Luminescence dating of the PASADO core 5022-1D from Laguna Potrok Aike (Argentina) using IRSL signals from feldspar. *Quaternary Science Reviews*, 71: 70–80.

Campos, H., Wladimir, S., Aguero, G., Parra, O. and Zuniga, Y. L. (1989). Estudios limnologicos en el Lago Puyehue (Chile): morfometria, factores fisicos y quimicos, plancton y productividad primaria. *Medio Ambiente*, 10: 36–53.

Carel, M., Siani, G. and Delpech, G. (2011). Tephrostratigraphy of a deep-sea sediment sequence off the south Chilean margin: New insight into the Hudson volcanic activity since the last glacial period. *Journal of Volcanology and Geothermal Research*, 208: 99–111.

Caricchi, L., Annen, C., Blundy, J., Simpson, G. and Pinel, V. (2014). Frequency and magnitude of volcanic eruptions controlled by magma injection and buoyancy. *Nature Geoscience*, 7: 126–130.

Cassidy, M., Manga, M., Cashman, K. and Bachmann, O. (2018). Controls on explosive-effusive volcanic eruption styles. *Nature Communications*, 9 (1): 2859.

Castruccio, A., Clavero, J., Segura, A., Samaniego, P., Roche, O., Le Pennec, J. L. and Droguett, B. (2016). Eruptive parameters and dynamics of the April 2015 sub-Plinian eruptions of Calbuco volcano (southern Chile). *Bulletin of Volcanology*, 78 (62), 1-19.

Chapron, E., Juvigné, E., Mulsow, S., Ariztegui, D., Magand, O., Bertrand, S., Pino, M. and Chapron, O. (2007). Recent clastic sedimentation processes in Lake Puyehue (Chilean Lake District, 40.5°S). *Sedimentary Geology*, 201: 365–385.

Charlet, F., De Batist, M., Chapron, E., Bertrand, S., Pino, M. and Urrutia, R. (2008). Seismic stratigraphy of Lago Puyehue (Chilean Lake District): New views on its deglacial and Holocene evolution. *Journal of Paleolimnology*, 39: 163–177.

Clapperton, C. M. (1971). Evidence of cirque glaciation in the Falkland Islands. *Journal of Glaciology*, 10: 121–125.

Clapperton, C. M. (1994). The quaternary glaciation of Chile: a review. *Revista Chilena de Historia Natural*, 67: 369–383.

Clark, R., Huber, U. M. and Wilson, P. (1998). Late Pleistocene sediments and environmental change at Plaza Creek, Falkland Islands, South Atlantic. *Journal of Quaternary Science*, 13: 95–105.

Cook, E., Davies, S. M., Guðmundsdóttir, E. R., Abbott, P. M. and Pearce, N. J. G. (2018). First identification and characterization of Borrobol-type tephra in the Greenland ice cores: new deposits and improved age estimates. *Journal of Quaternary Science*, 33: 212–224.

Coronato, A., Ercolano, B., Corbella, H. and Tiberi, P. (2013). Glacial, fluvial and volcanic landscape evolution in the Laguna Potrok Aike maar area, Southern Patagonia, Argentina. *Quaternary Science Reviews*, 71: 13–26.

Costantini, L., Pioli, L., Bonadonna, C., Clavero, J. and Longchamp, C. (2011). A Late Holocene explosive mafic eruption of Villarrica volcano, Southern Andes: The Chaimilla deposit. *Journal of Volcanology and Geothermal Research*, 200: 143–158.

Crawford, A., Falloon, T. and Green, D. (1989). Classification, petrogenesis and tectonic setting of boninites. In: A. Crawford (ed.) *Boninites and Related Rocks*. pp.2–49.

Crowley, J. W., Katz, R. F., Huybers, P., Langmuir, C. H. and Park, S. (2015). Glacial cycles drive variations in the production of oceanic crust. *Science*, 347: 1237–1240.

Cutler, N. A., Streeter, R. T., Marple, J., Shotter, L. R., Yeoh, J. S. and Dugmore, A. J. (2018). Tephra transformations: variable preservation of tephra layers from two well-studied eruptions. *Bulletin of Volcanology*, 80: 77.

Cvijanovic, I., Langen, P., Kaas, E. and Ditlevsen, P. (2013). Southward Intertropical Convergence Zone Shifts and Implications for an Atmospheric Bipolar Seesaw. *American Meteorological Society*, 26 (12): 4121–4137.

D'Orazio, M., Agostini, S., Mazzarini, F., Innocenti, F., Manetti, P., Haller, M. J. and Lahsen, A. (2000). The Pali Aike Volcanic Field, Patagonia: Slab-window magmatism near the tip of South America. *Tectonophysics*, 321: 407–427.

Daga, R., Ribeiro Guervara, S., Sánchez, M. L. and María, A. (2008). Source identification of volcanic ashes by geochemical analysis of well preserved lacustrine tephras in Nahuel Huapi National Park. *Applied Radiation and Isotopes*, 66: 1325–1336.

Damaschke, M., Cronin, S. J. and Bebbington, M. S. (2018). A volcanic event forecasting model for multiple tephra records, demonstrated on Mt. Taranaki, New Zealand. *Bulletin of Volcanology*, 80 (9): 1-14.

Danzeglocke, U. (2007). *CalPal Online v 1.5*. http://www.calpal-online.de/index.html. Last accessed 18-JUN-2019.

Davies, S. M., Elmquist, M., Bergman, J., Wohlfarth, B. and Hammarlund, D. (2007). Cryptotephra sedimentation processes within two lacustrine sequences from west central Sweden. *Holocene*, 17: 319–330.

Davies, S. M. (2015). Cryptotephras: The revolution in correlation and precision dating. *Journal of Quaternary Science*, 30: 114–130.

De Batist, M., Fagel, N., Loutre, M. F. and Chapron, E. (2008). A 17,900-year multi-proxy lacustrine record of Lago Puyehue (Chilean Lake District): Introduction. *Journal of Paleolimnology*, 39: 151–161.

de Porras, M. E., Maldonado, A., Abarzúa, A. M., Cárdenas, M. L., Francois, J. P., Martel-Cea, A., Stern, C. R., Méndez, C. and Reyes, O. (2012). Postglacial vegetation, fire and climate dynamics at Central Chilean Patagonia (Lake Shaman, 44°S). *Quaternary Science Reviews*, 50: 71–85.

Del Carlo, P., Di Roberto, A., D'Orazio, M., Petrelli, M., Angioletti, A., Zanchetta, G., Maggi, V., Daga, R., Nazzari, M. and Rocchi, S. (2018). Late Glacial-Holocene tephra from southern Patagonia and Tierra del Fuego (Argentina, Chile): A complete textural and geochemical fingerprinting for distal correlations in the Southern Hemisphere. *Quaternary Science Reviews*, 195: 153–170.

Delgado, F., Pritchard, M. E., Ebmeier, S., González, P. and Lara, L. (2017). Recent unrest (2002–2015) imaged by space geodesy at the highest risk Chilean volcanoes: Villarrica, Llaima, and Calbuco (Southern Andes). *Journal of Volcanology and Geothermal Research*, 344: 270–288.

Douglass, D., Singer, B., Kaplan, M., Ackert, R., Mickelson, D. and Caffee, M. (2005). Evidence of early Holocene glacial advances in southern South America from cosmogenic surface-exposure dating. *Geological Society of America Bulletin*, 33: 237–240.

Dugmore, A. (1989). Tephrochronology and UK Archaeology. *The Proceedings of Archaeological Sciences*: 242–250.

Dugmore, A., Streeter, R. and Cutler, N. (2018). The role of vegetation cover and slope angle in tephra layer preservation and implications for Quaternary tephrostratigraphy. *Palaeogeography, Palaeoclimatology, Palaeoecology*, 489: 105–116.

Dunbar, N. W., Iverson, N. A., Van Eaton, A. R., Sigl, M., Alloway, B. V., Kurbatov, A. V., Mastin, L. G., McConnell, J. R. and Wilson, C. J. N. (2017). New Zealand supereruption provides time marker for the Last Glacial Maximum in Antarctica. *Scientific Reports*, 7: 3–10.

Egan, J., Staff, R. and Blackford, J. (2015). A high-precision age estimate of the Holocene Plinian eruption of Mount Mazama, Oregon, USA. *Holocene*, 25: 1054–1067.

Elissondo, M., Baumann, V., Bonadonna, C., Pistolesi, M., Cioni, R., Bertagnini, A., Biass, S., Herrero, J. C. and Gonzalez, R. (2016). Chronology and impact of the 2011 Cordón Caulle eruption, Chile. *Natural Hazards and Earth System Sciences*, 16: 675–704.

Fagel, N., Alvarez, D., Namur, O., Devidal, J.-L., Nuttin, L., Schmidt, S., Jana, P., Torrejon, F., Bertrand, S., Araneda, A. and Urrutia, R. (2017). Lacustrine record of last millennia eruptions in Northern Chilean Patagonia (45–47°S). *The Holocene*. 27 (8): 1227-1251

Fontijn, K., Lachowycz, S. M., Rawson, H., Pyle, D. M., Mather, T. A., Naranjo, J. A. and Moreno-Roa, H. (2014). Late Quaternary tephrostratigraphy of southern Chile and Argentina. *Quaternary Science Reviews*, 89: 70–84.

Fontijn, K., Rawson, H., Van Daele, M., Moernaut, J., Abarzúa, A. M., Heirman, K., Bertrand, S., Pyle, D. M., Mather, T. A., De Batist, M., Naranjo, J.-A. and Moreno, H. (2016). Synchronisation of sedimentary records using tephra: A postglacial tephrochronological model for the Chilean Lake District. *Quaternary Science Reviews*, 137: 234–254.

Forte, P., Domínguez, L., Bonadonna, C., Gregg, C. E., Bran, D., Bird, D. and Castro, J. M. (2018). Ash resuspension related to the 2011–2012 Cordón Caulle eruption, Chile, in a rural community of Patagonia, Argentina. *Journal of Volcanology and Geothermal Research*, 350: 18–32.

Froggatt, P. C. and Gosson, G. J. (1982). Techniques for the preparation of tephra samples for mineral and chemical analysis and radiometric dating. *Department of Geology, Victoria University of Wellington*, 23: 1–2.

Froggatt, P. C. and Lowe, D. J. (1990). A review of late Quaternary silicic and some other tephra formations from New Zealand: their stratigraphy, nomenclature, distribution, volume, and age. *New Zealand Journal of Geology and Geophysics*, 33: 89–109.

García, J. L., Maldonado, A., De Porras, M. E., Delaunay, A. N., Reyes, O., Ebensperger, C. A., Binnie, S. A., Lüthgens, C. and Méndez, C. (2019). Early deglaciation and paleolake history of Río Cisnes Glacier, Patagonian Ice Sheet (44°S). *Quaternary Research*, 91: 194–217.

Gatti, E., Saidin, M., Talib, K., Rashidi, N., Gibbard, P. and Oppenheimer, C. (2013). Depositional processes of reworked tephra from the Late Pleistocene Youngest Toba Tuff deposits in the Lenggong Valley , Malaysia. *Quaternary Research*, 79: 228–241.

Gebhardt, A, C. and Ohlendorf, C. (2019). Revised Age Model for Composite Core 5022-2CP, Laguna Potrok Aike, Patagonia. *PANGEA*. https://doi.pangaea.de/10.1594/PANGAEA.901831.

Gee, M. A. M., Taylor, R. N., Thirlwall, M. F. and Murton, B. J. (1998). Glacioisostacy controls chemical and isotopic characteristics of tholeiites from the Reykjanes Peninsula, SW Iceland. *Earth and Planetary Science Letters*, 1–5: 9–13.

Geoffroy, C. A., Alloway, B. V., Amigo, À., Parada, M. A., Gutierrez, F., Castruccio, A., Pearce, N. J. G., Morgado, E. and Moreno, P. I. (2018). A widespread compositionally bimodal tephra sourced from Volcán Melimoyu (44°S, Northern Patagonian Andes): Insights into magmatic reservoir processes and opportunities for regional correlation. *Quaternary Science Reviews*, 200: 141–159.

Gerlach, D., Frey, F., Moreno-Roa, H. and López-Escobar, L. (1988). Recent volcanism in the Puyehue-Cordon Calle region, southern Andes, Chile (40.5°S): Petrogenesis of Evolved Lavas. *Journal of Petrology*, 29: 333–382.

Giaccio, B., Hajdas, I., Isaia, R., Deino, A. and Nomade, S. (2017). High-precision 14C and 40Ar/39Ar dating of the Campanian Ignimbrite (Y-5) reconciles the time-scales of climatic-cultural processes at 40 ka. *Scientific Reports*, 7: 1–10.

Giles, T. M., Newnham, R. M., Lowe, D. J. and Munro, A. J. (1999). Impact of tephra fall and environmental change: a 1000 year record from Matakana Island, Bay of Plenty, North Island, New Zealand. In: Firth. C., and McGuire, W. (eds) *Volcanoes in the Quaternary*. Geological Society, London, Special Publications. pp.11–26.

Gogorza, C. S. G., Irurzun, M. A., Sinito, A. M., Lisé-Pronovost, A., St-Onge, G., Haberzettl, T., Ohlendorf, C., Kastner, S. and Zolitschka, B. (2012). High-resolution paleomagnetic records from Laguna Potrok Aike (Patagonia, Argentina) for the last 16,000 years. *Geochemistry, Geophysics, Geosystems*, 13 (2): Q12Z37, 1-18.

Goldstein, J., Newbury, D., Echlin, P., Joy, D., Romig, J. A., Lyman, C., Fiori, C. and Lifshin, E. (1992). *Scanning Electron Microscopy and X-Ray Microanalysis - A Text for Biologists, Materials Scientists, and Geologists* (Second Edition). New York, London. pp. 1-820.

González-Ferrán, O. (1994). *Volcanes de Chile*. Santiago, Chile: Instituto Geográfico Militar. pp. 1-640.

Gudmundsdóttir, E. R., Eiríksson, J. and Larsen, G. (2011). Identification and definition of primary and reworked tephra in Late Glacial and Holocene marine shelf sediments off North Iceland. *Journal of Quaternary Science*, 26: 589–602.

Gutiérrez, F., Gioncada, A., González Ferran, O., Lahsen, A. and Mazzuoli, R. (2005). The Hudson Volcano and surrounding monogenetic centres (Chilean Patagonia): An example of volcanism associated with ridge-Trench collision environment. *Journal of Volcanology and Geothermal Research*, 145: 207–233.

Guyodo, Y. and Valet, J. (1999). Global changes in intensity of the Earth's magnetic field during the past 800 kyr. *Letters to Nature*, 399: 249–252.

Haberle, S. G. and Lumley, S. H. (1998). Age and origin of tephras recorded in postglacial lake sediments to the west of the southern Andes, 44°S to 47°S. *Journal of Volcanology and Geothermal Research*, 84: 239–256.

Haberzettl, T., Fey, M., Lücke, A., Maidana, N., Mayr, C., Ohlendorf, C., Schäbitz, F., Schleser, G. H., Wille, M. and Zolitschka, B. (2005). Climatically induced lake level changes during the last two millennia as reflected in sediments of Laguna Potrok Aike, southern Patagonia (Santa Cruz, Argentina). *Journal of Paleolimnology*, 33: 283–302.

Haberzettl, T., Corbella, H., Fey, M., Janssen, S., Lucke, A., Mayr, C., Ohlendorf, C., Schabitz, F., Schleser, G. H., Wille, M., Wulf, S. and Zolitschka, B. (2007). Lateglacial and Holocene wet-dry

cycles in southern Patagonia: chronology, sedimentology and geochemistry of a lacustrine record from Laguna Potrok Aike, Argentina. *The Holocene*, 17: 297–310.

Haberzettl, T., Kück, B., Wulf, S., Anselmetti, F., Ariztegui, D., Corbella, H., Fey, M., Janssen, S., Lücke, A., Mayr, C., Ohlendorf, C., Wille, M. and Zolitschka, B. (2008). Hydrological variability in southeastern Patagonia and explosive volcanic activity in the southern Andean Cordillera during Oxygen Isotope Stage 3 and the Holocene inferred from lake sediments of Laguna Potrok Aike, Argentina. *Palaeogeography, Palaeoclimatology, Palaeoecology*, 259: 213–229.

Haberzettl, T., Anselmetti, F. S., Bowen, S. W., Fey, M., Mayr, C., Zolitschka, B., Ariztegui, D., Mauz, B., Ohlendorf, C., Kastner, S., Lücke, A., Schäbitz, F. and Wille, M. (2009). Late Pleistocene dust deposition in the Patagonian steppe - extending and refining the paleoenvironmental and tephrochronological record from Laguna Potrok Aike back to 55 ka. *Quaternary Science Reviews*, 28: 2927–2939.

Hahn, A., Kliem, P., Oehlerich, M., Ohlendorf, C., Zolitschka, B. and The PASADO Science Team. (2014). Elemental composition of the Laguna Potrok Aike sediment sequence reveals paleoclimatic changes over the past 51 ka in southern Patagonia, Argentina. *Journal of Paleolimnology*, 52: 349–366.

Hall, V. A., Wilson, P. and Holmes, J. (2001). A preliminary tephra study of Holocene peats in the Falkland Islands. In: Juvigné, E., and Raynal, J-P. (eds) *Tephras: chronology and archaeology (Dossiers de l'Archäol-Logis)*. pp.39–44.

Hallett, D. J., Hills, L. V. and Clague, J. J. (1997). New accelerator mass spectrometry radiocarbon ages for the Mazama tephra layer from Kootenay National Park, British Columbia, Canada. *Canadian Journal of Earth Sciences*, 34: 1202–1209.

Haslett, J. and Parnell, A. (2008). A simple monotone process with application to radiocarbon-dated depth chronologies. *Journal of the Royal Statistical Society. Series C: Applied Statistics*, 57: 399–418.

Healy, J. (1962). Structure and Volcanism in the Taupo Volcanic Zone, New Zealand. In: Macdonald, G. A., and Kuno, H. (eds) *Geophysical Monograph Series*. pp. 151–157.

Hickey, R. L., Frey, F. A., Gerlach, D. C. and López-Escobar, L. (1986). Multiple sources for basaltic arc rocks from the southern volcanic zone of the Andes (34°–41°S): Trace element and isotopic evidence for contributions from subducted oceanic crust, mantle, and continental crust. *Journal of Geophysical Research*, 91: 5963.

Hodder, A. P. W., Green, B. E. and Lowe, D. J. (1990). A Two-Stage Model for the Formation of Clay Minerals from Tephra-Derived Volcanic Glass. *Clay Minerals*, 25: 313–327.

Hogg, A. G., Hua, Q., Blackwell, P. G., Niu, M., Buck, C. E., Guilderson, T. P., Heaton, T. J., Palmer, J. G., Reimer, P. J., Reimer, R. W., Turney, C. S. M. and Zimmerman, S. R. H. (2013). SHCal13 Southern Hemisphere Calibration, 0–50,000 Years cal BP. *Radiocarbon*, 55: 1889–1903.

Holmes, J., Hall, V. and Wilson, P. (1999). Volcanoes and peat bogs. *Geology Today*, 15: 60–63.

Huppert, H. E., Stephen, R., Sparks, J. and Turner, J. S. (1984). Some effects of viscosity on the dynamics of replenished magma chambers. *Journal of Geophysical Research*, 89: 6857–6877.

Huybers, P. and Langmuir, C. (2009). Feedback between deglaciation, volcanism, and atmospheric CO_2. *Earth and Planetary Science Letters*, 286: 479–491.

Iglesias, V., Whitlock, C., Martha, M., Villarosa, G. and Outes, V. (2012). Climate and local controls of long-term vegetation dynamics in northern Patagonia (Lat 41° S). *Quaternary Research*, 78: 502–512.

Jellinek, A. M., Manga, M. and Saar, M. O. (2004). Did melting glaciers cause volcanic eruptions in eastern California? Probing the mechanics of dike formation. *Journal of Geophysical Research B: Solid Earth*, 109: 1–10.

Jochum, K. P., Stoll, B., Herwig, K., Willbold, M., Hofmiann, A. W., Amini, M., Aarburg, S., Abouchami, W., Hellebrand, E., Mocek, B., Raczek, I., Stracke, A., Alard, O., Bouman, C., Becker, S., Dücking, M., Brätz, H., Klemd, R., De Bruin, D., Canil, D., Cornell, D., De Hoog, C. J., Dalpé, C., Danyushevshy, L., Eisenhauer, A., Gao, Y., Snow, J. E., Groschopf, N., Günther, D., Latkoczy, C., Guillong, M., Hauri, E. H., Höfer, H. E., Lahaye, Y., Horz, K., Jacob, D. E., Kasemann, S. A., Kent, A. J. R., Ludwig, T., Zack, T., Mason, P. R. D., Meixner, A., Rosner, M., Misawa, K., Nash, B. P., Pfänder, J., Premo, W. R., Sun, W. D., Tiepolo, M., Vannucci, R., Vennemann, T., Wayne, D. and Woodhead, J. D. (2006). MPI-DING reference glasses for in situ microanalysis: New reference values for element concentrations and isotope ratios. *Geochemistry, Geophysics, Geosystems*, 7. Q02008, 1-44, DOI:10.1029/2005GC001060.

Jouve, G., Francus, P., Lamoureux, S., Provencher-Nolet, L., Hahn, A., Haberzettl, T., Fortin, D. and Nuttin, L. (2013). Microsedimentological characterization using image analysis and μ-XRF as indicators of sedimentary processes and climate changes during Lateglacial at Laguna Potrok Aike, Santa Cruz, Argentina. *Quaternary Science Reviews*, 71: 191–204.

Jouve, G., Lisé-Pronovost, A., Francus, P. and De Coninck, A. S. (2017). Climatic influence of the latest Antarctic isotope maximum of the last glacial period (AIM4) on Southern Patagonia. *Palaeogeography, Palaeoclimatology, Palaeoecology*, 472: 33–50.

Jouzel, J. (2004). EPICA Dome C Ice Cores Deuterium Data. IGBP PAGES, World Data Center for Paleoclimatology, Data Contribution Series #2004-038. *NOAA/NGDC Paleoclimatology Program, Boulder CO, USA*. DOI: 10.3334/CDIAC/cli.007

Jull, M. and McKenzie, D. (1996). The effect of deglaciation on mantle melting beneath Iceland. *Journal of Geophysical Research*, 101: 21815-21828.

Juschus, O., Melles, M., Gebhardt, A. C. and Niessen, F. (2009). Late quaternary mass movement events in lake El'gygytgyn, north-eastern Siberia. *Sedimentology*, 56: 2155–2174.

Juvigné, E., Bertrand, S., Heuschen, B. and Tallier, E. (2008). Tephrostratigraphy of lake sediments located in an active geodynamic setting: Lessons from Lake Icalma (Chile, southern volcanic zone, 38°S). *Quaternaire*, 19 (2): 175-189

Kaplan, M. R., Ackert, R. P., Singer, B. S., Douglass, D. C. and Kurz, M. D. (2004). Cosmogenic nuclide chronology of millennial-scale glacial advances during O-isotope stage 2 in Patagonia. *Bulletin of the Geological Society of America*, 116: 308–321.

Kaplan, M. R., Moreno, P. I. and Rojas, M. (2008). Glacial dynamics in southernmost South America during marine isotope stage 5e to the Younger Dryas chron: a brief review with a focus on cosmogenic nuclide measurements. *Journal of Quaternary Science*, 23: 649–658.

Kilian, R., Hohner, M., Biester, H., Wallrabe-Adams, H. J. and Stern, C. R. (2003). Holocene peat and lake sediment tephra record from the southernmost Chilean Andes (53-55°S). *Revista geológica de Chile*, 30: 1–17.

Kiyosugi, K., Connor, C., Stephen, R., Sparks, J., Crosweller, H. S., Brown, S. K., Siebert, L., Wang, T. and Takarada, S. (2015). How many explosive eruptions are missing from the geologic record? Analysis of the quaternary record of large magnitude explosive eruptions in Japan. *Journal of Applied Volcanology*. 4 (17): 1-15.

Kliem, P., Buylaert, J. P., Hahn, a., Mayr, C., Murray, a. S., Ohlendorf, C., Veres, D., Wastegård, S. and Zolitschka, B. (2013a). Magnitude, geomorphologic response and climate links of lake level

oscillations at Laguna Potrok Aike, Patagonian steppe (Argentina). *Quaternary Science Reviews*, 71: 131–146.

Kliem, P., Enters, D., Hahn, A., Ohlendorf, C., Lisé-Pronovost, A., St-Onge, G., Wastegård, S. and Zolitschka, B. (2013b). Lithology, radiocarbon chronology and sedimentological interpretation of the lacustrine record from Laguna Potrok Aike, southern Patagonia. *Quaternary Science Reviews*, 71: 54–69.

Klüser, L., Erbertseder, T. and Meyer-Arnek, J. (2013). Observation of volcanic ash from Puyehue-Cordón Caulle with IASI. *Atmospheric Measurement Techniques Discussions*, 5: 4249–4283.

Koffman, B. G., Dowd, E. G., Osterberg, E. C., Ferris, D. G., Hartman, L. H., Wheatley, S. D., Kurbatov, A. V., Wong, G. J., Markle, B. R., Dunbar, N. W., Kreutz, K. J. and Yates, M. (2017). Rapid transport of ash and sulfate from the 2011 Puyehue-Cordón Caulle (Chile) eruption to West Antarctica. *Journal of Geophysical Research: Atmospheres*, 122: 8908–8920.

Kutterolf, S., Schindlbeck, J. c., Jegen, M., Freundt, A. and Straub, S. M. (2019). Milankovitch frequencies in tephra records at volcanic arcs: The relation of kyr-scale cyclic variations in volcanism to global climate changes. *Quaternary Science Reviews*, 204: 1–16.

Lane, C. S., Blockley, S. P. E., Lotter, A. F., Finsinger, W., Filippi, M. L. and Matthews, I. P. (2012). A regional tephrostratigraphic framework for central and southern European climate archives during the Last Glacial to Interglacial transition: comparisons north and south of the Alps. *Quaternary Science Reviews*, 36: 50–58.

Lane, C. S., Brauer, A., Blockley, S. P. E. and Dulski, P. (2013). Volcanic ash reveals time-transgressive abrupt climate change during the Younger Dryas. *Geology*, 41: 1251–1254.

Lane, C. S., Cullen, V. L., White, D., Bramham-Law, C. W. F. and Smith, V. C. (2014). Cryptotephra as a dating and correlation tool in archaeology. *Journal of Archaeological Science*, 42: 42–50.

Langdon, P. G. and Barber, K. E. (2004). Snapshots in time: precise correlations of peat-based proxy climate records in Scotland using mid-Holocene tephras. *The Holocene*, 141: 21–33.

Langdon, P. G., Brown, A. G., Caseldine, C. J., Blockley, S. P. E. and Stuijts, I. (2012). Regional climate change from peat stratigraphy for the mid- to late Holocene in central Ireland. *Quaternary International*, 268: 145–155.

Lara, L. and Moreno, H. (2006). Geología del Complejo Volcánico Puyehue-Cordón Caulle. *Servicio Nacional de Geología y Minería, Carta Geológica de Chile, Serie Geología Básica*, 99: 1 mapa escala 1:50.000.

Lara, L. E., Moreno, H., Naranjo, J. A., Matthews, S. and Párez de Arce, C. (2006). Magmatic evolution of the Puyehue-Cordón Caulle Volcanic Complex (40° S), Southern Andean Volcanic Zone: From shield to unusual rhyolitic fissure volcanism. *Journal of Volcanology and Geothermal Research*, 157: 343–366.

Laumonier, M., Scaillet, B., Pichavant, M., Champallier, R., Andujar, J. and Arbaret, L. (2014). On the conditions of magma mixing and its bearing on andesite production in the crust. *Nature Communications*, 5, 5607: 1-12.

Lisiecki, L. and Raymo, M. (2005). A Pliocene-Pleistocene stack of 57 globally distributed benthic $\delta^{18}O$ records. *Palaeoceanography*, 20, PA1003: 1-17.

Liu, E. J., Oliva, M., Antoniades, D., Giralt, S., Granados, I., Pla-Rabes, S., Toro, M. and Geyer, A. (2016). Expanding the tephrostratigraphical framework for the South Shetland Islands, Antarctica, by combining compositional and textural tephra characterisation. *Sedimentary Geology*, 340: 49–61.

Lohmar, S., Robin, C., Parada, M., Gourgaud, A., López-Escobar, L., Moreno, H. and Naranjo, J. (2005). The two major postglacial (13-14,000 BP) pyroclastic eruptions of Llaima and Villarrica volcanoes (Southern Andes): A comparison. In: *6th International Symposium on Andean Geodynamics (ISAG 2005, Barcelona), Extended Abstracts*. pp.442–445.

Lohmar, S., Parada, M. Á., Robin, C., Gerbe, M. C., Deniel, C., Gourgaud, A., López-Escobar, L., Moreno, H. and Naranjo, J. A. (2006). Origin of postglacial ¨Mafic¨ ignimbrites at Llaima and Villarrica volcanoes (Southern Andes, Chile): Assimilation of plutonics rocks as one of the triggering factors? *Simposio Sudamericano de Geología Isotópica (SSAGI)*, 5: 417–421.

Lohmar, S., Robin, C., Gourgaud, A., Clavero, J., Ángel Parada, M., Moreno, H., Ersoy, O., López-Escobar, L. and Naranjo, J. A. (2007). Evidence of magma water interaction during the 13,800 years BP explosive cycle of the Licán Ignimbrite, Villarrica volcano (southern Chile). *Revista Geologica de America Central*, 34: 233–247.

Lohmar, S., Parada, M., Gutiérrez, F., Robin, C. and Gerbe, M. C. (2012). Mineralogical and numerical approaches to establish the pre-eruptive conditions of the mafic Licán Ignimbrite, Villarrica Volcano (Chilean Southern Andes). *Journal of Volcanology and Geothermal Research*, 235–236: 55–69.

López-Escobar, L. and Moreno, H. (1981). Erupcion De 1979 Del Volcan Mirador, Andes Del Sur, 40° 21' S: Caracteristicas Geoquimicas De Las Lavas y Xenolitos Graniticos. *Andean Geology*, 8: 17–33.

López-Escobar, L., Parada, M., Hickey-Vargas, R., Frey, F., Kempton, P. and Moreno, H. (1995). Calbuco Volcano and minor eruptive centers distributed along the Liquiñe-Ofqui Fault Zone, Chile (41°-42°S): contrasting origin of andesitic and basaltic magma in the Southern Volcanic Zone of the Andes. *Contributions to Mineralogy and Petrology*, 119: 345–361.

Lowe, D. J. and Hogg, A. G. (1986). Tephrostratigraphy arid chronology of the Kaipo Lagoon, an 11,500 year-old montane peat bog in Urewera National Park, New Zealand. *Journal of the Royal Society of New Zealand*, 16: 25–41.

Lowe, D. J. (2011). Tephrochronology and its application: A review. *Quaternary Geochronology*, 6: 107–153.

Lowe, J., Barton, N., Blockley, S., Ramsey, C. B., Cullen, V. L., Davies, W., Gamble, C., Grant, K., Hardiman, M., Housley, R., Lane, C. S., Lee, S., Lewis, M., MacLeod, A., Menzies, M., Müller, W., Pollard, M., Price, C., Roberts, A. P., Rohling, E. J., Satow, C., Smith, V. C., Stringer, C. B., Tomlinson, E. L., White, D., Albert, P., Arienzo, I., Barker, G., Boric, D., Carandente, A., Civetta, L., Ferrier, C., Guadelli, J.-L., Karkanas, P., Koumouzelis, M., Müller, U. C., Orsi, G., Pross, J., Rosi, M., Shalamanov-Korobar, L., Sirakov, N. and Tzedakis, P. C. (2012). Volcanic ash layers illuminate the resilience of Neanderthals and early modern humans to natural hazards. *Proceedings of the National Academy of Sciences of the United States of America*, 109: 13532–7.

Lowe, D. J., Blaauw, M., Hogg, A. G. and Newnham, R. M. (2013). Ages of 24 widespread tephras erupted since 30,000 years ago in New Zealand, with re-evaluation of the timing and palaeoclimatic implications of the Lateglacial cool episode recorded at Kaipo bog. *Quaternary Science Reviews*, 74: 170–194.

Machida, H., Arai, F. (1982). Widespread late Quaternary tephras in Japan with special reference to archaeology. *The Quaternary Research*, 22: 133–148.

Maclennan, J., Jull, M., McKenzie, D., Slater, L. and Gronvold, K. (2002). The link between volcanism and deglaciation in Iceland. *Geochemistry Geophysics Geosystems*, 3: 1–25.

MacLeod, A. and Davies, S. M. (2016). Caution in cryptotephra correlation: resolving Lateglacial chemical controversies at Sluggan Bog, Northern Ireland. *Journal of Quaternary Science*, 31: 406–415.

Malin, M. C., Dzurisin, D. and Sharp, R. P. (1983). Stripping of Keanakakoi tephra on Kilauea volcano, Hawaii. *Geological Society of America Bulletin*, 94: 1148–1158.

Mansilla, C. A., McCulloch, R. D. and Morello, F. (2016). Palaeoenvironmental change in Southern Patagonia during the Lateglacial and Holocene: Implications for forest refugia and climate reconstructions. *Palaeogeography, Palaeoclimatology, Palaeoecology* , 447: 1–11.

Mansilla, C. A., McCulloch, R. D. and Morello, F. (2018). The vulnerability of the Nothofagus forest-steppe ecotone to climate change: Palaeoecological evidence from Tierra del Fuego (~53°S). *Palaeogeography, Palaeoclimatology, Palaeoecology*, 508: 59–70.

Mark, D. F., Stuart, F. M. and de Podesta, M. (2011). New high-precision measurements of the isotopic composition of atmospheric argon. *Geochimica et Cosmochimica Acta*, 75: 7494–7501.

Markgraf, V., Bradbury, J., Schwalb, A., Burns, S., Stern, C., Ariztegui, D., Gilli, A., Anselmetti, F., Stine, S. and Maidana, N. (2003). Holocene palaeoclimates of southern Patagonia: limnological and environmental history of Lago Cardiel, Argentina. *The Holocene*, 13 (4): 581-591.

Markgraf, V., Whitlock, C. and Haberle, S. (2007). Vegetation and fire history during the last 18,000 cal yr B.P. in southern Patagonia: Mallín Pollux, Coyhaique, Province Aisén (45°41′30″ S, 71°50′30″ W, 640 m elevation). *Palaeogeography, Palaeoclimatology, Palaeoecology*, 254: 492–507.

Markgraf, V. and Huber, U. M. (2010). Late and postglacial vegetation and fire history in Southern Patagonia and Tierra del Fuego. *Palaeogeography, Palaeoclimatology, Palaeoecology*, 297: 351–366.

Massaferro, J. and Corley, J. (1998). Environmental disturbance and chironomid palaeodiversity: 15 kyr BP of history at Lake Mascardi, Patagonia, Argentina. *Aquatic Conservation: Marine and Freshwater Ecosystems*, 8: 315–323.

Massaferro, J. (2009). Paleoecología: el uso de los quironómidos fósiles (Diptera: Chironomidae) en reconstrucciones paleoambientales durante el Cuaternario en la Patagonia. *Revista de la Sociedad Entomológica Argentina*, 68: 209–217.

Matchan, E. L., Joyce, E. B. and Phillips, D. (2016). A new 40Ar/39Ar eruption age for the Mount Widderin volcano, Newer Volcanic Province, Australia, with implications for eruption frequency in the region. *Australian Journal of Earth Sciences*, 63: 175–186.

Mayr, C., Lücke, A., Stichler, W., Trimborn, P., Ercolano, B., Oliva, G., Ohlendorf, C., Soto, J., Fey, M., Haberzettl, T., Janssen, S., Schäbitz, F., Schleser, G. H., Wille, M. and Zolitschka, B. (2007). Precipitation origin and evaporation of lakes in semi-arid Patagonia (Argentina) inferred from stable isotopes ($\delta^{18}O$, $\delta^{2}H$). *Journal of Hydrology*, 334: 53–63.

Mayr, C., Smith, R. E., García, M. L., Massaferro, J., Lücke, A., Dubois, N., Maidana, N. I., Meier, W. J.-H., Wissel, H. and Zolitschka, B. (2019). Historical eruptions of Lautaro Volcano and their impacts on lacustrine ecosystems in southern Argentina. *Journal of Paleolimnology*. http://link.springer.com/10.1007/s10933-019-00088-y.

Mazzarini, F. and D'Orazio, M. (2003). Spatial distribution of cones and satellite-detected lineaments in the Pali Aike Volcanic Field (southernmost Patagonia): Insights into the tectonic setting of a Neogene rift system. *Journal of Volcanology and Geothermal Research*, 125: 291–305.

McConnell, J. R., Aristarain, A. J., Banta, J. R., Edwards, P. R. and Simões, J. C. (2007). 20th-Century doubling in dust archived in an Antarctic Peninsula ice core parallels climate change and desertification in South America. *Proceedings of the National Academy of Sciences*, 104: 5743–5748.

McCormac, F., Hogg, A., Blackwell, P., Buck, C., Higham, T. and Reimer, P. (2004). SHCal04 southern hemisphere calibration, 0-11.0 cal kyr BP. *Radiocarbon*, 46: 1087–1092.

McCulloch, R. D., Bentley, M. J., Purves, R. S., Hulton, N. R. J., Sugden, D. E. and Clapperton, C. M. (2000). Climatic inferences from glacial and palaeoecological evidence at the last glacial termination, southern South America. *Journal of Quaternary Science*, 15: 409–417.

McCulloch, R. D., Fogwill, C. J., Sugden, D. E., Bentley, M. J. and Kubik, P. W. (2005). Chronology of the Last Glaciation in Central Strait of Magellan and Bahia Inutil, Southernmost South America. *Geografiska Annaler, Series A: Physical Geography* , 87: 289–312.

McCulloch, R. D., Torres, M. J. F., Goñalons, G. L. M., Barclay, R. and Mansilla, C. (2017). A Holocene record of environmental change from Río Zeballos, central Patagonia. *The Holocene*, 27: 941–950.

McLean, D., Albert, P. G., Nakagawa, T., Staff, R. A., Suzuki, T. and Smith, V. C. (2016). Identification of the Changbaishan 'Millennium' (B-Tm) eruption deposit in the Lake Suigetsu (SG06) sedimentary archive, Japan: Synchronisation of hemispheric-wide palaeoclimate archives. *Quaternary Science Reviews*, 150: 301–307.

McLean, D., Albert, P. G., Nakagawa, T., Suzuki, T., Staff, R. A., Yamada, K., Kitaba, I., Haraguchi, T., Kitagawa, J., SG14 Project Members, and Smith, V. C. (2018). Integrating the Holocene tephrostratigraphy for East Asia using a high-resolution cryptotephra study from Lake Suigetsu (SG14 core), central Japan. *Quaternary Science Reviews*, 183: 36–58.

McNamara, K., Rust, A. C., Cashman, Katharine, V., Castruccio, A. and Abarzúa, A. M. (2019). Comparison of lake and land tephra records from the 2015 eruption of Calbuco volcano, Chile. *Bulletin of Volcanology*, 81: 1–15.

Medina, E. (2016). *Petrologia y quimismo de los minerales del grupo de la espinela en lavas de los centros eruptivos menores Caburgua-Huelemolle*. Thesis submitted at Universidad De Chile Facultad De Ciencias Físicas Y Matemáticas Departamento De Geología. pp. 1-69.

Mella, M., Ramos, A., Kraus, S. and Duhart, P. (2012). Datos tefroestratigráficos de erupciones Holocenas del Volcán Mentolat, Andes del Sur (44º 40' S), Chile. In: *Actas, Congreso Geológico Chileno, No. 13, Antofagasta*.

WAIS Divide Project Members (2013). Onset of deglacial warming in West Antarctica driven by local orbital forcing. *Nature*, 500: 400–443.

Moernaut, J., De Batist, M., Charlet, F., Heirman, K., Chapron, E., Pino, M., Brümmer, R. and Urrutia, R. (2007). Giant earthquakes in South-Central Chile revealed by Holocene mass-wasting events in Lake Puyehue. *Sedimentary Geology*, 195: 239–256.

Moernaut, J., Van Daele, M., Heirman, K., Fontijn, K., Strasser, M., Pino, M., Urrutia, R. and De Batist, M. (2014). Lacustrine turbidites as a tool for quantitative earthquake reconstruction: New evidence for a variable rupture mode in south central Chile. *Journal of Geophysical Research*, 119: 1607–1633.

Moernaut, J., Van Daele, M., Strasser, M., Clare, M. A., Heirman, K., Viel, M., Cardenas, J., Kilian, R., Ladrón de Guevara, B., Pino, M., Urrutia, R. and De Batist, M. (2017). Lacustrine turbidites produced by surficial slope sediment remobilization: A mechanism for continuous and sensitive turbidite paleoseismic records. *Marine Geology*, 384: 159–176.

Monteath, A. J., Hughes, P. D. M. and Wastegård, S. (2019). Evidence for distal transport of reworked Andean tephra: Extending the cryptotephra framework from the Austral Volcanic Zone. 51: 64-71, *Quaternary Geochronology*.

Moreno, P. I. and Leon, A. (2003). Abrupt vegetation changes during the last glacial to Holocene transition in mid-latitude South America. *Journal of Quaternary Science*, 18: 787–800.

Moreno, H. R. and Clavero, C. R. (2006). Geología del Volcán Villarrica, Regiones de la Araucanía y de Los Lagos. In: *Carta Geol. Chile Ser. Geol. Basica 98*. SERNAGEOMIN, Santiago. pp.1–34.

Moreno, P. I., Alloway, B. V., Villarosa, G., Outes, V., Henríquez, W. I., Pol-Holz, R. De and Pearce, N. J. G. (2015a). A past-millennium maximum in postglacial activity from Volcán Chaitén, southern Chile. *Geology*, 43: 47–50.

Moreno, P. I., Roa, H. M. and Putnam, A. E. (2015b). Radiocarbon chronology of the last glacial maximum and its termination in northwestern Patagonia. *Quaternary Science Reviews*, 122: 233–249.

Moreno, P. I. and Videla, J. (2016). Centennial and millennial-scale hydroclimate changes in northwestern Patagonia since 16,000 yr BP. *Quaternary Science Reviews*, 149: 326–337.

Nanavati, W. P., Whitlock, C., Iglesias, V., Eugenia, M. and Porras, D. (2019). Postglacial vegetation, fire, and climate history along the eastern Andes, Argentina and Chile (lat. 41-55 S). *Quaternary Science Reviews*, 207: 145–160.

Naranjo, J. A. and Moreno, H. (1991). Actividad explosiva postglacial en el Volcán Llaima, Andes del Sur (38° 45'S). *Revista Geológica de Chile*, 18: 69–80.

Naranjo, J. A. and Stern, C. R. (1998). Holocene explosive activity of Hudson Volcano, southern Andes. *Bulletin of Volcanology*, 59: 291–306.

Naranjo, J. and Stern, C. (2004). Holocene tephrochronology of the southernmost part (42°30'-45°S) of the Andean Southern Volcanic Zone. *Revista Geologica de Chile*, 31: 225–240.

Naranjo, J. and Moreno, H. (2005). Geología del Volcan Llaima, Region de la Araucanía. In: Godoy, E., Marquardt, C R., Blanco, N. P. and Chile Servicio Nacional de Geología y Minería (eds) *Carta Geol. Chile Serie Geologia Basica 88*. SERNAGEOMIN, Santiago. pp. 1–34.

Naranjo, J. A., Singer, B. S., Jicha, B. R., Moreno, H. and Lara, L. E. (2017). Holocene tephra succession of Puyehue-Cordón Caulle and Antillanca/Casablanca volcanic complexes, southern Andes (40-41 °S). *Journal of Volcanology and Geothermal Research*, 332: 109–128.

Narcisi, B., Petit, J. R., Delmonte, B., Basile-Doelsch, I. and Maggi, V. (2005). Characteristics and sources of tephra layers in the EPICA-Dome C ice record (East Antarctica): Implications for past atmospheric circulation and ice core stratigraphic correlations. *Earth and Planetary Science Letters*, 239: 253–265.

Narcisi, B., Petit, J. R., Delmonte, B., Scarchilli, C. and Stenni, B. (2012). A 16,000-yr tephra framework for the Antarctic ice sheet: A contribution from the new Talos Dome core. *Quaternary Science Reviews*, 49: 52–63.

Newhall, C. G. and Self, S. (1982). The volcanic explosivity index (VEI): An estimate of explosive magnitude for historical volcanism. *Journal of Geophysical Research: Atmospheres*, 87: 1231–1238.

Newnham, R. M. and Lowe, D. J. (2000). Fine-resolution pollen record of late-glacial climate reversal from New Zealand. *Geology*, 28: 759–762.

Nowell, D. A. G., Jones, M. C. and Pyle, D. M. (2006). Episodic Quaternary volcanism in France and Germany. *Journal of Quaternary Science*, 21: 645–675.

Ohlendorf, C., Fey, M., Gebhardt, C., Haberzettl, T., Lücke, A., Mayr, C., Schäbitz, F., Wille, M. and Zolitschka, B. (2013). Mechanisms of lake-level change at Laguna Potrok Aike (Argentina) - insights from hydrological balance calculations. *Quaternary Science Reviews*, 71: 27–45.

Oppedal, L. T., van der Bilt, W. G. M., Balascio, N. L. and Bakke, J. (2018). Patagonian ash on sub-Antarctic South Georgia: expanding the tephrostratigraphy of southern South America into the Atlantic sector of the Southern Ocean. *Journal of Quaternary Science*, 33: 482–486.

Oppenheimer, C. (2003). Climatic, environmental and human con sequences of the largest known historic eruption: Tambora volcano (Indonesia) 1815. *Progress in Physical Geography*, 27: 230–259.

Papale, P. (2018). Global time-size distribution of volcanic eruptions on Earth. *Scientific Reports*, 8: 1–11.

Parzen, E. (1962). On Estimation of a Probability Density Function and Mode. *The Annals of Mathematical Statistics*, 33: 1065–1076.

Paterne, M., Labeyrie, J., Guichard, F., Mazaud, A. and Maitre, F. (1990). Fluctuations of the Campanian explosive volcanic activity (South Italy) during the past 190,000 years, as determined by marine tephrochronology. *Earth and Planetary Science Letters*, 98: 166–174.

Pavez, A. (1997). Geología e historia evolutiva del Complejo Volcánico Quetrupillán, Andes del Sur, 39.5ºS. In: *Congreso Geológico Chileno,* No. 8, Actas, Antofagasta. pp. 1443-1447

Payne, R. J., Kilfeather, A. A., Meer, J. J. M. Van Der and Blackford, J. J. (2005). Experiments on the taphonomy of tephra in peat. *Finnish Peatland Society,* 56 (4): 147–156.

Payne, R. and Gehrels, M. (2010). The formation of tephra layers in peatlands: An experimental approach. *Catena*, 81: 12–23.

Pearce, N. J. G. (2014). Towards a protocol for the trace element analysis of glass from rhyolitic shards in tephra deposits by laser ablation ICP-MS. *Journal of Quaternary Science*, 29: 627–640.

Pedro, J. B., Jochum, M., Buizert, C., He, F., Barker, S. and Rasmussen, S. O. (2018). Beyond the bipolar seesaw: Toward a process understanding of interhemispheric coupling. *Quaternary Science Reviews*, 192: 27–46.

Philippsen, B. (2013). The freshwater reservoir effect in radiocarbon dating. *Heritage Science*, 1: 1–19.

Pollard, A. M., Blockley, S. P. E. and Ward, K. R. (2003). Chemical alteration of tephra in the depositional environment: theoretical stability modelling. *Journal of Quaternary Science*, 18: 385–394.

Ponomareva, V., Portnyagin, M. and Davies, S. M. (2015). Tephra without Borders: Far-Reaching Clues into Past Explosive Eruptions. *Frontiers in Earth Science*, 3: 1–16.

Pouchou, J.-L. and Pichoir, F. (1991). Quantitative Analysis of Homogeneous or Stratified Microvolumes Applying the Model "PAP". In: *Electron Probe Quantitation*. Boston, MA: Springer US. pp. 31–75.

Pouderoux, H., Lamarche, G. and Proust, J. N. (2012). Building an 18 000-year-long paleo-earthquake record from detailed deep-sea turbidite characterisation in Poverty Bay, New Zealand. *Natural Hazards and Earth System Science*, 12: 2077–2101.

Pouget, S., Bursik, M. and Rogova, G. (2014). Tephra redeposition and mixing in a Late-glacial hillside basin determined by fusion of clustering analyses of glass-shard geochemistry. *Journal of Quaternary Science*, 29: 789–802.

Prieto, A., Stern, C. R. and Estévez, J. E. (2013). The peopling of the Fuego-Patagonian fjords by littoral hunter-gatherers after the mid-Holocene H1 eruption of Hudson Volcano. *Quaternary International*, 317: 3–13.

Pyle, D. M. (2000). Sizes of volcanic eruptions. In: H. Sigurdsson (ed.) *Encyclopedia of Volcanoes* (1st Edition). Academic Press, San Diego. pp.263–269.

Pyle, D. M., Ricketts, G. D., Margari, V., Andel, T. H. Van, Sinitsyn, A. A., Praslov, N. D. and Lisitsyn, S. (2006). Wide dispersal and deposition of distal tephra during the Pleistocene 'Campanian Ignimbrite/Y5' eruption, Italy. *Quaternary Science Reviews*, 25: 2713–2728.

Pyne-O'Donnell, S. (2011). The taphonomy of Last Glacial-Interglacial Transition (LGIT) distal volcanic ash in small Scottish lakes. *Boreas*, 40: 131–145.

Pyne-O'Donnell, S., Hughes, P., Froese, D., Jensen, B., Kuehn, S., Mallon, G., Amesbury, M., Charman, D., Daley, T., Loader, N., Mauquoy, D., Street-Perrott, F. A. and Woodman-Ralph, J. (2012). High-precision ultra-distal Holocene tephrochronology in North America. *Quaternary Science Reviews*, 52: 6–11.

Raga, G. B., Baumgardner, D., Ulke, A. G., Torres Brizuela, M. and Kucienska, B. (2013). The environmental impact of the Puyehue-Cordon Caulle 2011 volcanic eruption on Buenos Aires. *Natural Hazards and Earth System Sciences*, 13: 2319–2330.

Rawson, H., Naranjo, J. A., Smith, V. C., Fontijn, K., Pyle, D. M., Mather, T. A. and Moreno, H. (2015). The frequency and magnitude of post-glacial explosive eruptions at Volcán Mocho-Choshuenco, southern Chile. *Journal of Volcanology and Geothermal Research*, 299: 103–129.

Rawson, H., Pyle, D. M., Mather, T. A., Smith, V. C., Fontijn, K., Lachowycz, S. M. and Naranjo, J. A. (2016). The magmatic and eruptive response of arc volcanoes to deglaciation: Insights from southern Chile. *Geology*, 44: 251–254.

Recasens, C., Ariztegui, D., Gebhardt, C., Gogorza, C., Haberzettl, T., Hahn, a., Kliem, P., Lise-Pronovost, a., Lucke, a., Maidana, N., Mayr, C., Ohlendorf, C., Schabitz, F., St-Onge, G., Wille, M., Zolitschka, B. and Team, S. (2012). New insights into paleoenvironmental changes in Laguna Potrok Aike, southern Patagonia, since the Late Pleistocene: The PASADO multiproxy record. *The Holocene*, 22: 1323–1335.

Reed, S. (2005). *Electron Microprobe Analysis and Scanning Electron Microscopy in Geology* (Second Edition). Cambridge University Press. pp. 1-190.

Reimer, P. J., Baillie, M. G. L., Bard, E., Bayliss, A., Beck, J. W., Bertrand, C. J. H., Blackwell, P. G., Buck, C. E., Burr, G. S., Cutler, K. B., Damon, P. E., Edwards, R. L., Fairbanks, R. G., Friedrich, M., Guilderson, T. P., Hogg, A. G., Hughen, K. A. and Kromer, B. (2004). IntCal04 terrestrial radiocarbon age calibration, 0-26 cal kyr BP. *Radiocarbon*, 46: 1029–1058.

Reimer, PJ., Baillie, MGL., Bard, E., Bayliss, A., Beck, JW., Blackwell, PG., Bronk Ramsey, C., Buck, CE., Burr, GS., Edwards, RL., Friedrich, M., Gootes, PM., Guilderson, TP., Hajdas, I., Heaton, TJ., Hogg, AG., Hughen, KA., Kaiser, KF., Kromer, B., McCo, C. (2009). IntCal09 and Marine09 radiocarbon age calibration curves, 0-50,000 years cal BP. *Radiocarbon*, 51: 1111–1150.

Reimer, P. J., Bard, E., Bayliss, A., Beck, J. W., Blackwell, P. G., Ramsey, C. B., Buck, C. E., Cheng, H., Edwards, R. L., Friedrich, M., Grootes, P. M., Guilderson, T. P., Haflidason, H., Hajdas, I., Hatté, C., Heaton, T. J., Hoffmann, D. L., Hogg, A. G., Hughen, K. A., Kaiser, K. F., Kromer, B., Manning, S. W., Niu, M., Reimer, R. W., Richards, D. A., Scott, E. M., Southon, J. R., Staff, R. A., Turney, C. S. M. and van der Plicht, J. (2013). IntCal13 and Marine13 Radiocarbon Age Calibration Curves 0–50,000 Years cal BP. *Radiocarbon*, 55: 1869–1887.

Renne, P. R., Balco, G., Ludwig, K. R., Mundil, R. and Min, K. (2011). Response to the comment by W.H. Schwarz et al. on 'Joint determination of ^{40}K decay constants and ^{40}Ar*/ ^{40}K for the Fish Canyon sanidine standard, and improved accuracy for ^{40}Ar/ ^{39}Ar geochronology' by P.R. Renne et al. (2010). *Geochimica et Cosmochimica Acta*, 75: 5097–5100.

Renne, P. R., Mundil, R., Balco, G., Min, K. and Ludwig, K. R. (2010). Joint determination of ^{40}K decay constants and ^{40}Ar*/^{40}K for the Fish Canyon sanidine standard, and improved accuracy for ^{40}Ar/^{39}Ar geochronology. *Geochimica et Cosmochimica Acta*, 74: 5349–5367.

Roman-Ross, G., Depetris, P., Arribére, M., Ribeiro Guevara, S. and Cuello, G. (2002). Geochemical variability since the Late Pleistocene in Lake Mascardi sediments, northern Patagonia, Argentina. In: *Journal of South American Earth Sciences*, 15 (6): 657–667.

Rose, W. I. and Durant, A. J. (2011). Fate of volcanic ash: Aggregation and fallout. *Geology*, 39: 895–896.

Sagredo, E. A., Moreno, P. I., Villa-Martínez, R., Kaplan, M. R., Kubik, P. W. and Stern, C. R. (2011). Fluctuations of the Última Esperanza ice lobe (52°S), Chilean Patagonia, during the last glacial maximum and termination 1. *Geomorphology*, 125: 92–108.

Sauerbrey, M. A., Juschus, O., Gebhardt, A. C., Wennrich, V., Nowaczyk, N. R. and Melles, M. (2013). Mass movement deposits in the 3.6 Ma sediment record of Lake El'gygytgyn, Far East Russian Arctic. *Climate of the Past*, 9: 1949–1967.

Saunders, K. M., Roberts, S. J., Perren, B., Butz, C., Sime, L., Davies, S., Van Nieuwenhuyze, W., Grosjean, M. and Hodgson, D. A. (2018). Holocene dynamics of the Southern Hemisphere westerly winds and possible links to CO_2 outgassing. *Nature Geoscience*, 11: 650–655.

Scasso, R., Corbella, H. and Tiberi, P. (1994). Sedimentological analysis of the tephra from the 12-15 August 1991 eruption of Hudson volcano. *Bulletin of Volcanology*, 56: 121–132.

Schiff, C. J., Kaufman, D. S., Wallace, K. L., Werner, A., Ku, T. L. and Brown, T. A. (2008). Modeled tephra ages from lake sediments, base of Redoubt Volcano, Alaska. *Quaternary Geochronology*, 3: 56–67.

Schindlbeck, J. C., Freundt, A. and Kutterolf, S. (2014). Major changes in the post-glacial evolution of magmatic compositions and pre-eruptive conditions of Llaima Volcano, Andean Southern Volcanic Zone, Chile. *Bulletin of Volcanology*, 76: 1–22.

Schindlbeck, J. C., Jegen, M., Freundt, A., Kutterolf, S., Straub, S. M., Mleneck-Vautravers, M. J. and McManus, J. F. (2018). 100-kyr cyclicity in volcanic ash emplacement: Evidence from a 1.1 Myr tephra record from the NW Pacific. *Scientific Reports*, 8: 1–9.

Scott, E. M., Cook, G. T. and Naysmith, P. (2007). Error and uncertainty in radiocarbon measurements. *Radiocarbon*, 49: 427–440.

Shane, P. (2000). Tephrochronology: A New Zealand case study. *Earth Science Reviews*, 49: 223–259.

Siebert, L., Simkin, T. and Kimberly, P. (2010). *Volcanoes of the world: a regional directory, gazetteer, and chronology of volcanism during the last 10,000 years*. Smithsonian Institution, Washington, D.C, and the University of California Press, Berkeley. pp. 1-551

Sigvaldason, G., Annertz, K. and Nilsson, M. (1992). Effect of glacier loading/deloading on volcanism: postglacial volcanic production rate of the Dyngjufjöll area, central Iceland. *Bulletin of Volcanology*, 54: 385–392.

Sigvaldason, G. E. (2002). Volcanic and tectonic processes coinciding with glaciation and crustal rebound: An early Holocene rhyolitic eruption in the Dyngjufjöll volcanic centre and the formation of the Askja caldera, north Iceland. *Bulletin of Volcanology*, 64: 192–205.

Silva Parejas, C., Druitt, T. H., Robin, C., Moreno, H. and Naranjo, J. A. (2010). The Holocene Pucón eruption of Volcán Villarrica, Chile: Deposit architecture and eruption chronology. *Bulletin of Volcanology*, 72: 677–692.

Silverman, B. (1986). *Density estimation for statistics and data analysis* (First Edition). Chapman and Hall, New York. pp. 1-170.

Singer, B. S., Jicha, B. R., Harper, M. A., Naranjo, J. A., Lara, L. E. and Moreno-Roa, H. (2008). Eruptive history, geochronology, and magmatic evolution of the Puyehue-Cordón Caulle volcanic complex, Chile. *Geological Society of America Bulletin*, 120: 599–618.

Smith, V. C., Shane, P. and Nairn, I. A. (2005). Trends in rhyolite geochemistry, mineralogy, and magma storage during the last 50 kyr at Okataina and Taupo volcanic centres, Taupo Volcanic Zone, New Zealand. *Journal of Volcanology and Geothermal Research*, 148: 372–406.

Smith, V. C., Shane, P., Nairn, I. A. and Williams, C. M. (2006). Geochemistry and magmatic properties of eruption episodes from Haroharo linear vent zone, Okataina Volcanic Centre, New Zealand during the last 10 kyr. *Bulletin of Volcanology*, 69: 57–88.

Smith, R. E., Smith, V. C., Fontijn, K., Gebhardt, A. C., Wastegård, S., Zolitschka, B., Ohlendorf, C., Stern, C. R., and Mayr, C. (2019). Refining the Late Quaternary tephrochronology for southern South America using the Laguna Potrok Aike sedimentary record. *Quaternary Science Reviews*. https://doi.org/10.1016/j.quascirev.2019.06.001.

Sparks, S. R. J., Sigurdsson, H. and Wilson, L. (1977). Magma mixing: A mechanism for triggering acid explosive eruptions. *Nature*, 267: 315–318.

Sterken, M., Verleyen, E., Sabbe, K., Terryn, G., Charlet, F., Bertrand, S., Boes, X., Fagel, N., De Batist, M. and Vyverman, W. (2008). Late Quaternary climatic changes in southern Chile, as recorded in a diatom sequence of Lago Puyehue (40°40′ S). *Journal of Paleolimnology*, 39: 219–235.

Stern, C. R. (1990). Tephrochronology of Southernmost Patagonia. *National Geographic Research*, 6: 110–126.

Stern, C. R. (1992). Tefrocronologia de Magallanes: nuevos datos e implicaciones. *Anales del Insituto de la Patagonia*, 21: 129-141.

Stern, C. R. (2004). Active Andean volcanism: its geologic and tectonic setting. *Revista Geológica de Chile,* 31 (2): 1-51.

Stern, C. R. (2008). Holocene tephrochronology record of large explosive eruptions in the southernmost Patagonian Andes. *Bulletin of Volcanology*, 70: 435–454.

Stern, C. R., Moreno, P. I., Villa-Martínez, R., Sagredo, E. a, Prieto, A. and Labarca, R. (2011). Evolution of ice-dammed proglacial lakes in Última Esperanza, Chile: implications from the late-glacial R1 eruption of Reclús volcano, Andean Austral Volcanic Zone. *Andean Geology*, 38: 82–97.

Stern, C. and Weller, D. (2012). A Revised Age of 7430±250 ^{14}C yrs BP for the Very Large mid-Holocene Explosive H1 Eruption of the Hudson Volcano. *13th Chilean Geologic Congress, Antofagasta, Chile*: 6–8.

Stern, C., De Porras, M. E. and Maldonado, A. (2015). Tephrochronology of the upper Río Cisnes valley (44°S), southern Chile. *Andean Geology*, 42: 173–189.

Stern, C. R., Moreno, P. I., Sagredo, E. and Aravena, J. C. (2016). Holocene tephrochronology around Cochrane (~47° S), southern Chile. *Andean Geology*, 43: 1–19.

Sternai, P., Caricchi, L., Castelltort, S. and Champagnac, J.-D. (2016). Deglaciation and glacial erosion: a joint control on magma productivity by continental unloading. *Geophysical Research Letters*, 43: 1632–1641.

Strelin, J. A. and Malagnino, E. C. (2000). Late-glacial history of Lago Argentino, Argentina, and age of the Puerto Bandera Moraines. *Quaternary Research*, 54: 339–347.

Suárez, R. J., Ghiglione, M. C., Calderón, M., Sue, C., Martinod, J., Guillaume, B. and Rojo, D. (2019). The metamorphic rocks of the Nunatak Viedma in the Southern Patagonian Andes: Provenance sources and implications for the early Mesozoic Patagonia-Antarctic Peninsula connection. *Journal of South American Earth Sciences*, 90: 471–486.

Svensson, A., Bigler, M., Blunier, T., Clausen, H., Dahl-Jensen, D., Fischer, H., Fujita, S., Goto-Azuma, K., Johnsen, S., Kawamura, K., Kipfstuhl, S., Kohno, M., Parrenin, F., Popp, T., Rasmussen, S., Schwander, J., Seierstad, I., Severi, M., Steffensen, J., Udisti, R., Uemura, R., Vallelonga, P., Vinther, B., Wegner, A., Willhelms, F. and Winstrup, M. (2013). Direct linking of Greenland and Antarctic ice cores at the Toba. *Climate of the Past*, 9: 749–766.

Swindles, G. T., Galloway, J., Outram, Z., Schofield, J. E., Newton, A. J., Andrew, J., Church, M. J., Watson, E. J., Batt, C., Edwards, K. J., Turner, V. and Bashford, D. (2013). Re-deposited cryptotephra layers in Holocene peats linked to anthropogenic activity. *The Holocene*, 23: 1493–1501.

Swindles, G. T., Watson, E. J., Savov, I. P., Lawson, I. T., Schmidt, A., Hooper, A., Cooper, C. L., Connor, C. B., Gloor, M. and Carrivick, J. L. (2018). Climatic control on Icelandic volcanic activity during the mid-Holocene. *Geology*, 46: 47–50.

Terry, R, D. and Chilingar, G, V. (1955). Summary of 'Concerning some additional aids in studying sedimentary formations' by Shvestsov, M. S. *Journal of Sedimentary Petrology*, 25 (3): 229-234.

Thorarinsson, S., Einarsson, T. and Kjartansson, G. (1959). On the Geology and Geomorphology of Iceland. *Geografiska Annaler*, 41: 135–169.

Thorseth, I. H., Furnes, H. and Tumyr, O. (1995). Textural and chemical effects of bacterial activity on basaltic glass: an experimental approach. *Chemical Geology*, 119: 139–160.

Tomlinson, E. L., Thordarson, T., Müller, W., Thirlwall, M. and Menzies, M. A. (2010). Microanalysis of tephra by LA-ICP-MS - Strategies, advantages and limitations assessed using the Thorsmörk ignimbrite (Southern Iceland). *Chemical Geology*, 279: 73–89.

Tomlinson, E. L., Smith, V. C., Albert, P. G., Aydar, E., Civetta, L., Cioni, R., Çubukçu, E., Gertisser, R., Isaia, R., Menzies, M. A., Orsi, G., Rosi, M. and Zanchetta, G. (2015). The major and trace element glass compositions of the productive Mediterranean volcanic sources: tools for correlating distal tephra layers in and around Europe. *Quaternary Science Reviews*, 118: 48–66.

Trachsel, M. and Telford, R. J. (2017). All age–depth models are wrong, but are getting better. *Holocene*, 27: 860–869.

Tuffen, H. (2010). How will melting of ice affect volcanic hazards in the twenty-first century? *Philosophical Transactions of the Royal Society A: Mathematical, Physical and Engineering Sciences*, 368: 2535–2558.

Unkel, I., Fernandez, M., Björck, S., Ljung, K. and Wohlfarth, B. (2010). Records of environmental changes during the Holocene from Isla de los Estados (54.4 °S), southeastern Tierra del Fuego. *Global and Planetary Change*, 74: 99–113.

Van Daele, M., Moernaut, J., Silversmit, G., Schmidt, S., Fontijn, K., Heirman, K., Vandoorne, W., De Clercq, M., Van Acker, J., Wolff, C., Pino, M., Urrutia, R., Roberts, S. J., Vincze, L. and De Batist, M. (2014). The 600 yr eruptive history of Villarrica Volcano (Chile) revealed by annually laminated lake sediments. *Geological Society of America Bulletin*, 126: 481–498.

Van Daele, M., Moernaut, J., Doom, L., Boes, E., Fontijn, K., Heirman, K., Vandoorne, W., Hebbeln, D., Pino, M., Urrutia, R., Brümmer, R. and De Batist, M. (2015). A comparison of the sedimentary records of the 1960 and 2010 great Chilean earthquakes in 17 lakes: Implications for quantitative lacustrine palaeoseismology. *Sedimentology,* 62: 1466–1496.

Van Daele, M., Bertrand, S., Meyer, I., Moernaut, J., Vandoorne, W., Siani, G., Tanghe, N., Ghazoui, Z., Pino, M., Urrutia, R. and Batist, M. De (2016). Late Quaternary evolution of Lago Castor (Chile, 45.6°S): Timing of the deglaciation in northern Patagonia and evolution of the southern westerlies during the last 17 kyr. *Quaternary Science Reviews*, 133: 130–146.

Van Eaton, A., Amigo, Á., Bertin, D., Mastin, L., Giacosa, R., González, J., Valderrama, O., Fontijn, K. and Behnke, S. (2016). Volcanic lightning and plume behavior reveal evolving hazards during the April 2015 eruption of Calbuco volcano, Chile. *Geophysical Research Letters*, 43: 3563–3571.

Van Meerbeeck, C. J., Renssen, H. and Roche, D. M. (2009). How did Marine Isotope Stage 3 and Last Glacial Maximum climates differ? - Perspectives from equilibrium simulations. *Climate of the Past*, 5: 33–51.

Vargas-Ramirez, L., Roche, E., Gerrienne, P. and Hooghiemstra, H. (2008). A pollen-based record of late glacial-Holocene climatic variability in the southern lake district, Chile. *Journal of Paleolimnology*, 39: 197–217.

Villa-Martínez, R. and Moreno, P. I. (2007). Pollen evidence for variations in the southern margin of the westerly winds in SW Patagonia over the last 12,600 years. *Quaternary Research*, 68: 400–409.

Villarosa, G., Outes, V., Hajduk, A., Montero, E. C., Sellés, D., Fernández, M. and Crivelli, E. (2006). Explosive volcanism during the Holocene in the Upper Limay River Basin: The effects of ashfalls on human societies, Northern Patagonia, Argentina. *Quaternary International*, 158: 44–57.

Wagner, G. (1998). *Age Determination of Young Rocks and Artifacts: Physical and Chemical Clocks in Quaternary Geology and Archaeology*. pp. 1-467

Wastegård, S., Veres, D., Kliem, P., Hahn, a., Ohlendorf, C. and Zolitschka, B. (2013). Towards a late Quaternary tephrochronological framework for the southernmost part of South America - the Laguna Potrok Aike tephra record. *Quaternary Science Reviews*, 71: 81–90.

Watson, E. J., Swindles, G. T., Lawson, I. T. and Savov, I. P. (2015). Spatial variability of tephra and carbon accumulation in a Holocene peatland. *Quaternary Science Reviews*, 124: 248–264.

Watson, E. J., Swindles, G. T., Lawson, I. T. and Savov, I. P. (2016). Do peatlands or lakes provide the most comprehensive distal tephra records? *Quaternary Science Reviews*, 139: 110–128.

Watt, S. F. L., Pyle, D. M., Naranjo, J. A., Rosqvist, G., Mella, M., Mather, T. A. and Moreno, H. (2011). Holocene tephrochronology of the Hualaihue region (Andean southern volcanic zone, ~42° S), southern Chile. *Quaternary International*, 246: 324–343.

Watt, S. F. L., Pyle, D. M. and Mather, T. A. (2013a). The volcanic response to deglaciation: Evidence from glaciated arcs and a reassessment of global eruption records. *Earth-Science Reviews*, 122: 77–102.

Watt, S. F. L., Pyle, D. M. and Mather, T. A. (2013b). Evidence of mid- to late-Holocene explosive rhyolitic eruptions from Chaitén Volcano, Chile. *Andean Geology*, 40: 216–226.

Watt, S. F. L., Gilbert, J. S., Folch, A., Phillips, J. C. and Cai, X. M. (2015). An example of enhanced tephra deposition driven by topographically induced atmospheric turbulence. *Bulletin of Volcanology*, 77: 1–14.

Weller, D., Miranda, C. G., Moreno, P. I., Villa-Martínez, R. and Stern, C. R. (2014). The large late-glacial Ho eruption of the Hudson volcano, southern Chile. *Bulletin of Volcanology*, 76: 1–18.

Weller, D. J., Miranda, C. G., Moreno, P. I., Villa-Martínez, R. and Stern, C. R. (2015). Tephrochronology of the southernmost Andean Southern Volcanic Zone, Chile. *Bulletin of Volcanology*, 77: 1–24.

Weller, D. J., Porras, M. E. De and Maldonado, A. (2017). Holocene tephrochronology of the lower Río Cisnes valley, southern Chile. *Andean Geology*, 44: 229–248.

Weller, D., de Porras, M., Maldonado, A., Méndez, C. and Stern, C. (2018). New age controls on the tephrochronology of the southernmost Andean Southern Volcanic Zone, Chile. *Quaternary Research*, 91: 1–15.

Weller, D. J., Porras, M. E. De, Maldonado, A., Méndez, C. and Stern, C. R. (2019). Petrology, geochemistry, and correlation of tephra deposits from a large early-Holocene eruption of Mentolat volcano, southern Chile. *Journal of South American Earth Sciences*, 90: 282–295.

Welton, J. (2003). *SEM Petrology Atlas*. The American Association of Petroleum Geologists. pp 1-240.

Wiemer, G., Moernaut, J., Stark, N., Kempf, P., De Batist, M., Pino, M., Urrutia, R., de Guevara, B. L., Strasser, M. and Kopf, A. (2015). The role of sediment composition and behavior under dynamic loading conditions on slope failure initiation: a study of a subaqueous landslide in earthquake-prone South-Central Chile. *International Journal of Earth Sciences*, 104: 1439–1457.

Wils, K., Van Daele, M., Lastras, G., Kissel, C., Lamy, F. and Siani, G. (2018). Holocene Event Record of Aysén Fjord (Chilean Patagonia): An Interplay of Volcanic Eruptions and Crustal and Megathrust Earthquakes. *Journal of Geophysical Research: Solid Earth*, 123: 324–343.

Wilson, C. J. N., Rogan, A. M., Smith, I. E. M., Northey, D. J., Nairn, I. A. and Houghton, B. F. (1984). Caldera volcanoes of the Taupo volcanic zone, New Zealand. *Journal of Geophysical Research*, 89: 8463–8484.

Wilson, C. (1993). Stratigraphy, chronology, styles and dynamics of late Quaternary eruptions from Taupo volcano, New Zealand. *Philosophical Transactions of the Royal Society*, 343: 205–306.

Wilson, P., Clark, R., McAdam, J. H. and Cooper, E. A. (1993). Soil erosion in the Falkland Islands: an assessment. *Applied Geography*, 13: 329–352.

Wilson, T. M., Cole, J. W., Stewart, C., Cronin, S. J. and Johnston, D. M. (2011). Ash storms: Impacts of wind-remobilised volcanic ash on rural communities and agriculture following the 1991 Hudson eruption, southern Patagonia, Chile. *Bulletin of Volcanology*, 73: 223–239.

Wilson, C. J. N. and Rowland, J. V. (2016). The volcanic, magmatic and tectonic setting of the Taupo Volcanic Zone, New Zealand, reviewed from a geothermal perspective. *Geothermics*, 59: 168–187.

Wisner, B., Blaikie, P., Cannon, T. and Davis, I. (2003). Earthquakes, volcanoes and landslides. In: *At Risk: Natural Hazards, People's Vulnerability, and Disasters Chapter Eight: Earthquakes, volcanos and landslides* (Second Edition). Routledge, Taylor and Francis Group, London.

Woods, A. W. (1998). Observations and models of volcanic eruption columns. *Geological Society, London, Special Publications*, 145: 91–114.

Wulf, S., Hardiman, M. J., Staff, R. A., Koutsodendris, A., Appelt, O., Blockley, S. P. E., Lowe, J. J., Manning, C. J., Ottolini, L., Schmitt, A. K., Smith, V. C., Tomlinson, E. L., Vakhrameeva, P., Knipping, M., Kotthoff, U., Milner, A. M., Müller, U. C., Christanis, K., Kalaitzidis, S., Tzedakis, P. C., Schmiedl, G. and Pross, J. (2018). The marine isotope stage 1–5 cryptotephra record of Tenaghi Philippon, Greece: Towards a detailed tephrostratigraphic framework for the Eastern Mediterranean region. *Quaternary Science Reviews*, 186: 236–262.

Zanchetta, G., Ribolini, A., Ferrari, M., Bini, M., Isola, I., Lezzerini, M., Baroni, C., Salvatore, M. C., Pappalardo, M., Fucks, E. and Boretto, G. (2018). Geochemical characteristics of the infilling of ground wedges at puerto deseado (Santa Cruz, Argentina): Palaeoenvironmental and chronological implications. *Andean Geology*, 45: 130–144.

Zhang, X., King, M. L. and Hyndman, R. J. (2006). A Bayesian approach to bandwidth selection for multivariate kernel density estimation. *Computational Statistics and Data Analysis*, 50: 3009–3031.

Zolitschka, B., Schäbitz, F., Lücke, A., Corbella, H., Ercolano, B., Fey, M., Haberzettl, T., Janssen, S., Maidana, N., Mayr, C., Ohlendorf, C., Oliva, G., Paez, M. M., Schleser, G. H., Soto, J., Tiberi, P. and Wille, M. (2006). Crater lakes of the Pali Aike Volcanic Field as key sites for paleoclimatic and paleoecological reconstructions in southern Patagonia, Argentina. *Journal of South American Earth Sciences*, 21: 294–309.

Zolitschka, B., Anselmetti, F. S., Ariztegui, D., Corbella, H., Francus, P., Gebhardt, C., Hahn, A., Kliem, P., Lücke, A., Ohlendorf, C., Schäbitz, F. (2009). Deep Drilling at Laguna Potrok Aike, Argentina: Recovery of a Paleoclimate Record for the Last Glacial from the Southern Hemisphere. In: *Eos Trans. AGU 90 (52) Fall Meeting Abstract:* PP14A-10. p.1.

Zolitschka, B., Anselmetti, F., Ariztegui, D., Corbella, H., Francus, P., Lücke, A., Maidana, N. I., Ohlendorf, C., Schäbitz, F. and Wastegård, S. (2013). Environment and climate of the last 51,000 years - new insights from the Potrok Aike maar lake Sediment Archive Drilling prOject (PASADO). *Quaternary Science Reviews*, 71: 1–12.